SHRP-A-398

Stage 1 Validation of the Relationship Between Asphalt Properties and Asphalt-Aggregate Mix Performance

University of California at Berkeley
Oregon State University
Austin Research Engineers, Inc.
SWK Pavement Engineering

Strategic Highway Research Program
National Research Council
Washington, DC 1994

SHRP-A-398
ISBN 0-309-05814-7
Product No.: 1011, 1012

Program Manager: *Edward T. Harrigan*
Project Manager: *Rita B. Leahy*
Program Area Secretary: *Juliet Narsiah*
Production Editor: *Michael Jahr*

June 1994

key words:
aging
asphalt
binder
fatigue cracking
pavement deformation
performance
rutting
SHRP
specification
thermal cracking
validation
water sensitivity

Strategic Highway Research Program
National Research Council
2101 Constitution Avenue N.W.
Washington, DC 20418

(202) 334-3774

1.5M/NAP/694

Acknowledgments

The work described herein was supported by the Strategic Highway Research Program (SHRP). SHRP is a unit of the National Research Council that was authorized by section 128 of the Surface Transportation and Uniform Relocation Assistance Act of 1987.

Dr. R. G. Hicks, Oregon State University (OSU), and Mr. F. N. Finn, University of California at Berkeley (UCB), served as co-principal investigators. Individual researchers responsible for planning, executing, and interpreting results were:

- At UCB: Dr. A. A. Tayebali (fatigue), Dr. J. Sousa (permanent deformation and equipment development), Dr. J. Harvey (specimen preparation), and Dr. J. Deacon (fatigue and permanent deformation)
- At OSU: Dr. T. Vinson (thermal cracking), Dr. C. Bell (aging), and Dr. R. Terrel and Mr. T. Scholz (water sensitivity)
- At Austin Research Engineers: Mr. G. Paulsen, Mr. J. Coplantz, and Ms. M. Yapp
- At SWK: Dr. S. F. Brown and Mr. G. Rowe (fatigue, permanent deformation, and water sensitivity)
- At the U.S. Cold Regions Engineering Research Laboratory: Dr. V. Janoo (thermal cracking)

A number of students at UCB and OSU contributed significantly to the work. Without their assistance the work of the project would not have been completed: at UCB, Messrs. S. Alavi, E. Abi-Jaoude, P. Goodloe, P. Hendricks, T. Mills, R. Ng, B. Tsai, and K. A. S. Yapa; at OSU, Messrs. A. Al-Joaib, Y. Ab-Wahab, S. Al-Swailmi, J. Bea, M. Cristi, D. H. Jung, D. Sosnovske, A. Wieder, H. Zeng, Ms. W. Allen, and Ms. H. Kanerva.

The project consulting statistician was Mr. Lou Painter.

Mr. Greg Paulsen was responsible for assembling the draft from which this final report was prepared.

Contents

Page

List of Figures

Page

List of Tables

Page

Abstract

A primary objective for the Strategic Highway Research Program (SHRP) A-003A contract was to extend and verify (validate) the results obtained by other SHRP contractors on the performance-related characteristics of asphalt binders in paving mixes. This report specifically addresses validation of the following: (1) binder properties proposed by the A-002A contractor to predict asphalt-aggregate mix performance in terms of fatigue, permanent deformation, and thermal cracking; and (2) conditioning procedures that produce binder properties representative of those in a pavement immediately after construction (short-term) and after several years of service (long-term). While water-sensitivity requirements are not included in the binder specification, validation efforts in the water-sensitivity area are also described.

Materials used in the investigation included 8 to 16 asphalt binders and 2 to 4 aggregates obtained from the SHRP Materials Reference Library.

For fatigue, combinations of 8 asphalts and 2 aggregates were tested in the controlled-strain mode of loading using a flexural beam test device. For permanent deformation, two tests were used: (1) a wheel-tracking device operated by the University of Nottingham, and (2) a simple shear repeated-load test. With the wheel-tracking device, 16 asphalts and 2 aggregates were evaluated, while 9 asphalts and 2 aggregates were tested in simple shear. Thermal cracking was evaluated using the thermal stress restrained-specimen test, and combinations of 14 asphalts and 2 aggregates were tested. Aging studies included both short-term oven aging and three types of long-term aging (low-pressure oxidation and two types of oven aging) on combinations of 8 asphalts and 4 aggregates. Water-sensitivity testing included the use of the Environmental Conditioning System and two types of wet wheel-tracking devices on combinations of 8 asphalts and 4 aggregates. Results of all these tests and associated statistical analyses are described.

Overall, the findings are encouraging for the SHRP binder properties for thermal cracking and fatigue but are not very definitive for permanent deformation. Moreover, for aging and water sensitivity, the interaction between the asphalt and aggregate affects performance and underscores that these variables must be considered in the mix evaluation.

Executive Summary

Two of the major products emerging from the Strategic Highway Research Program (SHRP) Asphalt Program are the test methods and specifications for asphalt binders and asphalt-aggregate mixes. The binder tests and specifications were developed as part of SHRP Contract A-002A, conducted by Western Research Institute in Laramie, Wyoming, and The Pennsylvania State University. The mix tests were developed as a part of SHRP Project A-003A by the University of California at Berkeley (UCB) and Oregon State University (OSU). SWK Pavement Engineering in Nottingham, UK, and North Carolina State University also participated in the test development phase. The binder and mix tests and specifications address three primary modes of distress: fatigue, permanent deformation, and thermal cracking, as tempered by aging and moisture.

A critical element of the SHRP Asphalt Program was the validation of the proposed binder and mix tests using both laboratory and field data. Binder properties and tests were validated in parallel using both simulative laboratory tests and field performance data by the A-003A and A-005 contractors, respectively. Post-SHRP validation will be accomplished under the auspices of the Federal Highway Administration.

The discussion is limited to the validation of the A-002A binder tests and properties as they relate to the performance of asphalt-aggregate mixes. Specifically, the report addresses validation of the following:

1. Binder properties proposed by the A-002A contractor to predict asphalt-aggregate mix performance in terms of fatigue cracking, permanent deformation, and low-temperature cracking.

2. Aging procedures proposed by the A-002A contractor that produce binder properties representative of those in a pavement immediately after construction (short-term) and after several years of service (long-term).

In the SHRP binder specification, the following tests have been selected to characterize the binders:

1. *Dynamic shear rheometer*. This test is used to measure the rheological properties of the binder in terms of dynamic shear modulus (stiffness), G*, and phase angle, δ. In the SHRP binder specification, the parameter G* sin δ relates to fatigue cracking, and G*/sin δ relates to permanent deformation.

2. *Bending beam rheometer*. This test is used to measure the creep stiffness, S, of the asphalt at low temperatures and the slope of the creep stiffness versus loading time curve, m. In the SHRP binder specification, both these values relate to low-temperature cracking; m is also related to fatigue cracking.

3. *Direct tension test*. This test is used to measure the low-temperature failure properties of the binder. The failure strain at break is used as an indicator of the performance of mixes in cold environments.

4. *Aging*. The rolling thin-film oven test (RTFOT) has been selected as the preferred method to represent binder aging during the construction process, or short-term aging. Permanent deformation is evaluated using RTFOT-aged binders. Fatigue and thermal cracking are evaluated using binders that have been subjected to long-term oxidative aging using the pressure-aging vessel (PAV).

5. *Water sensitivity*. There is no binder test proposed for evaluating water sensitivity. It has been concluded that the water-sensitivity test for asphalt-aggregate mixes is more appropriate as it relates to field performance.

All materials used in the validation effort were obtained from the SHRP Materials Reference Library. Eight to 16 asphalt binders were employed for the various studies. Two aggregates were employed for fatigue, permanent deformation, and thermal cracking studies. For fatigue and thermal cracking, aggregate characteristics are less significant than the asphalt properties. For permanent deformation, time and material constraints precluded the testing of more than 2 aggregates in spite of the universally recognized effect that aggregate has on mix resistance to rutting. Four aggregates were used for the aging and water-sensitivity studies because of the dominant effect of the aggregate.

Fatigue

For fatigue, combinations of eight asphalts and two aggregates were tested with a flexural beam test device developed at UCB. All tests were conducted on prismatic specimens (5 cm × 6.25 cm × 37.5 cm) in the controlled-strain mode at 20°C using a sinusoidal loading at a frequency of 10 Hz.

All asphalt-aggregate mixes were prepared at a fixed asphalt content near the optimum determined by the Caltrans mix design procedure (ASTM D-1560, D-1561). Mixes were prepared by rolling-wheel compaction to produce specimens with target air-void contents of 4 and 7 percent.

A full-factorial experiment was designed to allow all main factors and two-factor interactions to be tested. The factorial matrix consisted of 8 asphalts, 2 aggregates, 2 air-void contents, and 2 strain levels, resulting in a total of 64 cells. Each cell had 2 replicates to allow for estimation of experimental error, resulting in a total of 128 flexural fatigue tests.

Response variables included the following: (1) initial flexural stiffness measured at the 50th load cycle; (2) fatigue life in terms of the number of load cycles corresponding to a 50 percent reduction in flexural stiffness; and (3) total dissipated energy (i.e., the summation of dissipated energy per cycle until a 50 percent reduction in flexural stiffness).

Binder properties provided by A-002A included complex shear modulus (G*), phase angle (δ), storage modulus (G′, which is equal to G* cos δ), loss modulus (G″, which is equal to G* sin δ), and loss tangent (tan δ, which is equal to G″/G′).

G* sin δ includes the viscous component of asphalt binder stiffness. The A-002A contractor hypothesized that G* sin δ relates to the accumulation of dissipated energy during repetitive loading. Therefore, it should also relate to the dissipated energy parameter measured in asphalt-aggregate mixes by the flexural beam fatigue test. Both parameters include terms for stiffness and phase angle. Dissipated energy for a single load cycle in the flexural beam fatigue test is equal to $\pi\varepsilon_i^2 S_i^*$ sin ϕ_i. Note that the phase angles δ and ϕ_i are equal; however, for purposes of notation, δ is used for the phase angle of the binder, and ϕ_i for the phase angle of the mix.

A-002A binder properties are based on materials aged by the thin-film oven test (TFOT) to simulate short-term aging during the construction process. The binders used in this study were aged and the properties calculated for conditions different from those required in the SHRP binder specification for fatigue evaluation. This was done to more closely represent the properties of the binder in the asphalt-aggregate mixes tested in the fatigue validation effort. The specification calls for aging binder specimens in the PAV to simulate long-term aging effects and then testing them at a loading frequency of 10 rad/sec. Asphalt-aggregate mixes were subjected to short-term aging (4 hr at 135°C), but not long-term aging, and tested at a loading frequency of 10 Hz. In spite of this minor modification from the binder aging and testing protocols, there is excellent correlation between the values of G* sin δ after PAV aging and after TFOT aging. Thus, it is expected that the conclusions drawn from this study would not change significantly if asphalt binder properties had been determined in accordance with the A-002A testing protocol.

Comprehensive statistical analysis revealed that comparisons of flexural stiffness, fatigue life, or dissipated energy to all binder properties (G* sin δ, G*, G′) were equally strong. For example, an inverse relationship between mix fatigue life and binder stiffness as measured by G* sin δ was obtained that exhibited a coefficient of determination (R^2) of 0.88.

Asphalt binder properties were compared with fatigue life estimates for "hypothetical" pavements constructed with various asphalts. Fatigue life estimates were made for two hypothetical structural sections by calculating the maximum principal tensile strain (using the computer program ELSYM5; Federal Highway Administration 1985) at the bottom of the asphalt-concrete layer and then calculating the corresponding fatigue life from the tensile strain using the relationship between fatigue life and tensile strain for a given mix.

In general, the relationship between G* sin δ and predicted pavement fatigue life was much weaker than that observed with the lab testing; linear regression produced R^2 values of 0.21 to 0.38. More important, however, is that the *direction* of the trend was opposite to that

observed in the laboratory flexural fatigue analysis; in this analysis, *predicted fatigue life generally increased as binder stiffness increased.*

In summary, the conclusions with respect to the A-002A binder tests and properties for fatigue are as follows:

1. G *sin δ, G*, and G′ all result in equivalent correlations with mix fatigue response. Hence, one may conclude that the effect of the sin δ term of G* sin δ is negligible, and any of these terms could be used in the SHRP binder specification. However, the effect of sin δ may still be important for modified asphalts.

2. The relationships of the binder specification property G* sin δ to mix flexural stiffness and fatigue life were very strong. The relationship to dissipated energy was significantly weaker.

3. In the prediction of fatigue cracking in pavement structures, it appears that asphalt binder properties are again important but pavement structure effects may be equally or more important. In fact, pavement structure effects may influence fatigue cracking so much that the relationship between G* sin δ and pavement fatigue life is reversed as the thickness of the asphalt-concrete layer changes. Although the study performed by A-003A to evaluate these effects has some limitations, it identifies an issue worthy of further study. If further evaluation confirms that the direction of the relationship between G* sin δ and pavement fatigue life depends on the pavement structure, the binder specification will need to include provisions for pavement structure effects.

4. Overall, asphalt binder properties play a critical role in the fatigue response of asphalt-aggregate mixes. However, other mix characteristics, such as air-void content and aggregate characteristics, can also significantly affect fatigue response. Therefore, asphalt binder properties alone may not provide reliable enough estimates of fatigue cracking in pavements. In critical design situations (unusual traffic volume or loading conditions, modified materials), asphalt-aggregate mix fatigue testing should be conducted to increase the reliability of estimates of pavement fatigue cracking.

Permanent Deformation

The relationship between binder properties and permanent deformation response of asphalt-aggregate mixes was evaluated using the wheel-tracking device at the University of Nottingham and a shear device developed at UCB as part of the SHRP-sponsored research.

Wheel-tracking tests were performed by SWK Pavement Engineering Ltd. at the University of Nottingham. A wheel, fitted with a solid rubber tire, passes over the top of a cylindrical core specimen 200 mm in diameter at a frequency of approximately 3 Hz. Wheel-tracking tests

were conducted at 40°C, and each test was run for a duration of 5000 load passes (approximately 2 hr). The wheel passes are not made continuously (i.e. the lever are has to pick up the wheel and return it for unidirectional loading) hence the length of time is longer than what one would calculate. Tests were performed with an applied load of approximately 620 N. The contact area of the tire measured 850 mm^2, which gives a corresponding contact stress of approximately 730 kPa.

Two rutting parameters were measured from the wheel-tracking test data: normalized rut rate and total rut depth. The normalized rut rate is the rate of increase in rut depth (in millimeters per hour) between 2000 and 4000 load passes divided by the contact stress of the wheel. The total rut depth is the average rut depth (in millimeters) at the end of the test (i.e., after 5000 passes). SWK staff considered rut rate a more reliable indicator of permanent deformation performance because it is less likely to be affected by "initial start-up errors" and, perhaps, additional compaction of the specimen during the initial stages of the test.

A full-factorial experiment was designed to allow all main factors and two-factor interactions to be tested. The factorial matrix consisted of 16 asphalts, 2 aggregates, and 2 air-void contents, resulting in a total of 64 cells. All mixes were prepared at a fixed asphalt content near the optimum determined by the Caltrans mix design procedure (ASTM D-1560, D-1561). Mixes were prepared by rolling-wheel compaction to produce specimens with target air-void contents of 4 and 7 percent.

Binder properties provided by the A-002A contractor were measured from dynamic mechanical analysis and included the following: complex shear modulus (G*), phase angle (δ), storage modulus (G′), loss modulus (G″), and loss tangent (tan δ).

The SHRP binder specification requires a minimum value of 2 kPa for $G^*/\sin\delta$ for any RTFOT-aged binder when tested at 10 rad/sec at the specified temperature.

The binders and asphalt-aggregate mixes used in this study were subjected to similar aging and testing conditions. Asphalt binders were aged according to the RTFOT to simulate the short-term aging effects of the construction process. Asphalt-aggregate mixes were also subjected to short-term aging; after mixing, they were placed in an oven at 135°C for 4 hr. Asphalt binder properties were calculated for 40°C, and mixes were tested at that temperature. Binder properties were calculated at a loading frequency of 10 rad/sec (1.6 Hz). Mixes were tested at a loading frequency of 20 rad/sec (3.2 Hz). Considering that binder properties are logarithmic functions of loading time, the difference in loading rates is not substantial.

The results of this study suggest that $G^*/\sin\delta$ is not a reliable predictor of potential rutting. Aggregate and air-void characteristics appear to have more influence on the rutting response of asphalt-aggregate mixes than does the asphalt binder. However, there are several considerations that temper this conclusion, including (1) repeatability of the wheel-tracking test; (2) temperature effects, since tests were conducted at 40°C, while the minimum specification temperature is 45°C; and (3) small size of the loaded area relative to the aggregate size.

Binder properties were also compared with the permanent deformation response of asphalt-aggregate mix specimens subjected to repetitive simple shear loading under controlled conditions in the laboratory, since the test simulates shear stress conditions believed to be the primary cause of permanent deformation in asphalt-concrete pavements.

Specimen conditioning, compaction, and target air-void contents were as reported in the wheel-tracking validation effort. All shear testing was conducted on cylindrical specimens 152 mm in diameter by 51 mm high. A full-factorial experiment was designed to allow all main factors and two-factor interactions to be evaluated. The factorial matrix consisted of 9 asphalts, 2 aggregates, and 2 air-void contents, resulting in a total of 36 cells. Each cell had only 1 replicate, for a total of 36 tests for each shear test condition. Thus, a total of 72 shear test results were analyzed. Since no replicates were provided, the three-factor interaction of asphalt source, aggregate source, and air-void content was used as an estimate of experimental error.

The response variables were as follows: load cycles to 2 percent strain ($N_{2\%}$ = number of shear load cycles at which the asphalt-aggregate mix specimen exhibits 2 percent cumulative permanent shear strain), and cumulative permanent shear strain ($\Sigma\gamma_p$ = cumulative permanent shear strain after a constant number of load cycles).

Half the specimens in this study were tested under *constant height* (CH) conditions and the other half under *field state of stress* (FS) conditions. The CH shear test is sensitive to elastic and viscous characteristics of the asphalt binder, and it also measures the effect of dilatancy. The FS shear test incorporated loading conditions thought to represent the state of stress occurring in an asphalt-concrete layer near the edge of a tire.

Overall, the results of this study indicate that binder properties can affect the shear response of asphalt-aggregate mixes. However, aggregate characteristics can be equally or more significant. Specific findings from this study include the following:

1. Better relationships between asphalt binder properties and mix shear response ($N_{2\%}$ or $\Sigma\gamma_p$) were observed for mixes tested under CH conditions than for mixes tested under FS conditions.

2. Although the relationships between binder properties and mix shear response are generally weak, it appears that any binder property ($G^*/\sin\delta$, G^*, or G'') can be used to estimate mix shear response with the same degree of reliability (poor). Thus, the significance of the $\sin\delta$ term in $G^*/\sin\delta$ is questionable, although it may have a greater effect with modified binders.

3. The strongest relationship between asphalt binder properties and mix shear response was observed for mixes containing RH aggregate compacted to 7 percent air voids. This suggests that when a mix has low interparticle friction, the influence of asphalt binder properties becomes more significant. Aggregate RD was a quarried product that was 100 percent crushed; RH was a partially crushed river gravel that would be expected to provide less

interparticle friction than RD. The difference underscores the influence of aggregate characteristics on permanent deformation.

Results of the permanent deformation validation effort indicate that the influence of asphalt is highly dependent on the conditions to which the mix is subjected. Analysis of variance showed that the effect of asphalt type was significant but that its influence was small compared with the influence of aggregate type and air-void content, especially when the mix was tested at lower temperatures (e.g., 40°C) or was subjected to states of stress that amplified the aggregate influence (e.g., FS shear test).

The correlations between $G^*/\sin \delta$ and the various measures of permanent deformation response were generally poor. The weakness of the correlations results partly from the dominant effect of aggregate characteristics on permanent deformation response. However, if mix characteristics are such that interparticle friction is low (e.g., RH aggregate and 7 percent air voids) and the mix is subjected to harsh environmental and loading conditions (e.g., 60°C and CH shear test), the influence of the binder becomes more readily apparent. When aggregate characteristics or compaction conditions are expected to produce a mix susceptible to permanent deformation, it is important to select an asphalt that can overcome these deficiencies. It appears that the value of $G^*/\sin \delta$ may be used to screen binders that will provide inferior performance in such cases.

The results of these studies underscore the importance of mix testing, in addition to binder testing, for evaluation of permanent deformation in pavements. Although the mix tests used in these validation efforts are only estimates of the permanent deformation response that would actually occur in a pavement, the general conclusions presented here are expected to hold when future studies compare binder properties with permanent deformation response of mixes measured from larger-scale wheel-tracking tests and actual pavement performance.

Thermal Cracking

The A-002A ranking for resistance to thermal cracking is based on the limiting stiffness temperature and the ultimate strain at failure. The limiting stiffness temperature is estimated on the basis of a stiffness value of 200 MPa at a loading time of 2 hr in the bending beam rheometer. The ultimate strain at failure is estimated at -26°C and a loading time of 2 hr in the direct tension test. The experiment design for this task was developed to relate fundamental properties of asphalt cement (suggested by the A-002A contractor) to the thermal cracking characteristics of asphalt-concrete mixes, as measured by the thermal stress restrained-specimen test (TSRST).

The experiment design included 14 asphalt cements and 2 aggregates. Two degrees of aging and 2 air-void contents were employed, leading to a $14 \times 2 \times 2 \times 2$ fully replicated factorial design.

Before compaction, the loose mix was subjected to short-term oven aging (STOA) for 4 hr at 135°C. Following STOA, the mix was compacted using kneading compaction. Some of the

specimens were also subjected to long-term oven aging (LTOA) for 5 days at 85°C. The TSRST was performed on prismatic specimens (5 × 5 × 25 cm) at a cooling rate of 10°C/hr. For each specimen, the fracture temperature and strength were determined.

Based on the results obtained, the following conclusions are appropriate:

1. The repeatability of the TSRST is estimated as *good* for fracture temperature and *reasonable* for fracture strength.

2. Asphalt type, aggregate type, degree of aging, and air-void content are major factors that substantially affect the thermal cracking characteristics of asphalt-concrete mixes. Interactions between mix properties are considered to have a minor effect.

3. Asphalt type, degree of aging, air-void content, and the interaction between asphalt and degree of aging are significant factors for the fracture temperature. Fracture temperature was higher for long-term aged mixes. Fracture temperature is most affected by asphalt type and degree of aging; it is also affected by air-void content, though to a much lesser extent.

4. Asphalt type, aggregate type, air-void content, and the interaction between aggregate type and degree of aging are significant factors for the fracture strength. Fracture strength is highly influenced by air-void content and aggregate type. Fracture strength was greater for mixes with lower air-void contents than for mixes with higher air-voids contents and also greater for mixes with RH aggregate than for those with RC aggregate. Asphalt type and the interaction between aggregate type and degree of aging have a minor influence on fracture strength. The effect of degree of aging on fracture strength is inconclusive.

5. Fracture temperature was highly correlated to A-002A low-temperature index test results, specifically the temperature at limiting stiffness, the m value, and the ultimate strain at failure.

6. The penetration of asphalt cement at 15°C is also a good indicator of the thermal cracking characteristics of asphalt-concrete mixtures. Fracture temperature was highly correlated to penetration at 15°C. The fracture temperature was lower for mixes with softer asphalt cements. Fraass brittle point of asphalt cement also provided a good indication of the low-temperature cracking characteristics of asphalt-concrete mixes.

Aging

In the proposed binder specification, there is no direct provision for evaluating asphalt durability other than the effect of aging (short- or long-term) on binder properties to control

fatigue, permanent deformation, and thermal cracking. Fatigue and thermal cracking are controlled on binders that are long-term aged in the PAV, while rutting is controlled on binders that are short-term aged (using the RTFOT).

Tests on 32 different mixes (8 binders and 4 aggregates) were performed in this phase of the validation effort. The mixes were evaluated after both short- and long-term aging and the stiffness ratios compared with stiffness (viscosity) ratios of the neat binders, the intent being to determine whether binder tests alone are adequate to predict the durability of asphalt-aggregate mixes.

The procedure developed for short-term aging involves heating the loose mix in a forced-draft oven for 4 hr at 135°C. This treatment simulates the aging of the mixture during the construction process while it is uncompacted. Two procedures, LTOA and low-pressure oxidation (LPO), were developed for long-term aging of the compacted mix. Both approaches were found to be appropriate. The effects of aging were evaluated by resilient modulus at 25°C using both the diametral (indirect tension) and triaxial compression modes of testing (ASTM D-4123 and D-3497, respectively).

From the study the following conclusions were drawn:

1. The aging of asphalt-aggregate mixes is influenced by both asphalt type and aggregate type.

2. Aging of the asphalt alone and subsequent testing does not appear to be adequate to predict mix performance because of the apparent mitigating effect aggregate has on aging.

3. The aging of certain asphalts is strongly mitigated by some aggregates but not by others. This effect appears to be related to the strength of the chemical bonding (adhesion) between asphalt and aggregate.

4. The short-term aging procedure results in a twofold increase in resilient modulus. For a particular aggregate, there is not a statistically significant difference in the aging of certain asphalts. The eight asphalts investigated typically fell into three groups: those with high, medium, and low aging susceptibility.

5. The long-term aging methods produce somewhat different rankings of aging susceptibility compared with the short-term aging procedure and with each other. This is partially attributable to variability in the materials, aging process, and testing. However, it appears that the short-term aging procedure cannot be used to predict the effects of long-term aging.

6. The LPO long-term aging procedure causes the most aging and least variability in the rankings of aging susceptibility relative to the short-term rankings.

Water Sensitivity

An accelerated rutting test using the Laboratory Central Des Ponts Et Chaussées (LCPC) rutting tester (here called the OSU wheel tracker) was selected as the primary method to evaluate water sensitivity. However, tests on the same mixes were also conducted using the wheel-rutting tester at SWK/University of Nottingham (here called the SWK/UN wheel tracker) and with the Environmental Conditioning System (ECS) developed at OSU. Each test procedure results in a different failure mechanism, but all tests can be used to evaluate the water sensitivity of asphalt-aggregate mixes. The test program included 8 asphalts and 4 aggregates, for 32 mix combinations.

Specimens for all three test programs were prepared by rolling-wheel compaction from mixes that had undergone STOA. The beams required for the OSU and SWK/UN wheel trackers and the cores required for the ECS testing were all obtained by dry sawing or coring.

Changes in specimen stiffness were determined in the ECS during four conditioning cycles: three hot and one cold. Rutting was observed in the OSU wheel tracker up to 5000 passes after the specimens had been subjected to a conditioning procedure similar to that used for the ECS specimens. Specimens were tested in the SWK/UN equipment for up to 7 days (about 500,000 passes). The wheel passes are not made continuously (i.e., the lever arm has to pick up the wheel and return it for unidirectional loading), hence the length of time is longer than what one would calculate. The data from each of the test programs were analyzed statistically as described below.

ECS Test Results

The method of least squares, fitting a linear model, was used to analyze the results obtained after each conditioning cycle (i.e., after one, two, three, and four cycles of conditioning). Initially, a model was used in which ECS resilient modulus ratio was related to all the following variables: asphalt type, aggregate type, air-void content, water permeability, air permeability, initial water permeability, initial modulus, and asphalt-aggregate interaction. With each iteration, the least significant variable was removed. The final model that best represents the effect of asphalt type, initial modulus, and asphalt-aggregate interaction yielded an R^2 of 0.89. The most important observation from this analysis was that asphalt-aggregate interaction is highly significant (i.e., the susceptibility of an aggregate type depends the asphalt type and vice versa).

OSU Wheel Tracking Test Results

A similar analysis of the OSU wheel-tracking test results was undertaken to investigate the significance of asphalt type, aggregate type, air-void content, stripping rate, and asphalt-aggregate interaction on rut depth developed at 5000 wheel passes. The analysis revealed that aggregate-asphalt interaction had no effect. It did show, however, very high correlation between rut depth and stripping rate, asphalt type, aggregate type, and air-void content.

SWK/UN Wheel Tracking Test Results

The statistical analysis of the SWK/UN wheel-tracking tests used a Bayesian "survival analysis." The SWK/UN wheel-tracking data were tested to determine the probability that the time to failure would be less than or equal to some reasonable value (in this case 7 days of testing). This analysis method allows the ranking of asphalt and aggregate type while giving some importance to the air-void content of the test specimen provided it is greater than 8 percent (i.e., air-void contents greater than 8 percent diminished the probability of the specimen surviving beyond 7 days). This analysis indicated that asphalts AAM and AAK and aggregates RC and RD performed the best, while asphalts AAC and AAG and aggregate RJ performed the worst.

The following conclusions were drawn from the study:

1. Performance ranking of mixes by asphalt type or aggregate type alone cannot be done for the ECS test results because of the significant interaction between asphalt and aggregate. Water sensitivity in the ECS is significant for asphalt-aggregate combinations.

2. The OSU wheel-tracking test results indicate that the RJ aggregate is a good performer, the RC aggregate is a poor performer, and the RD and RH aggregates are intermediate performers in terms of rut resistance. The SWK/UN wheel-tracking test results indicate that the RC and RD aggregates are good performers (with practically no difference between the two), the RH aggregate is an intermediate performer, and the RJ aggregate is a poor performer. The significant differences between the results of the two test methods may possibly be attributed to the differences in testing methods, test apparatus, specimen size, environment during testing, and other factors. However, the results of the SWK/UN wheel-tracking test appear to generally validate the predictions from the net adsorption test results (A-003B), while those of the OSU wheel-tracking test do not. Thus, it would appear that the OSU wheel- tracking test may not be appropriate for evaluating aggregate type as it pertains to water sensitivity.

Conclusions

Overall, the findings to date relative to the SHRP binder specifications are encouraging for fatigue and thermal cracking, but less so for permanent deformation. No specific properties have been associated with aging and water sensitivity in the SHRP binder specification. The specifications do stipulate, however, that tests for rheological properties will be made with tank, short-term aging, or long-term aging, depending on performance requirements. The results of the A-003A research indicate that asphalt properties, as well as aggregate properties, will influence the effects of both aging and water sensitivity, underscoring that these effects should be evaluated in the asphalt-aggregate mix to be confident of their effects on pavement performance.

1

Introduction

Background

A primary objective for Strategic Highway Research Program (SHRP) Project A-003A was to extend and verify the results obtained by other SHRP asphalt contractors (A-002A, A-003B) on the performance-related characteristics of asphalt binders in paving mixes. Another important objective was to develop test methods suitable for standardization that can be used by the highway industry, both government and private agencies, to measure fundamental material properties that can be used in prediction models of pavement performance related to fatigue, permanent deformation, and thermal cracking. The test methods were to incorporate procedures to consider the effects of aging and water sensitivity so that the laboratory-measured properties would be representative of long-term in-place pavement properties. This report will emphasize the first objective, referred to as the Stage I validation effort. A companion report titled *Accelerated Performance Tests for Asphalt-Aggregate Mixes - Test Selection and Validation* covers the work performed on mixes and results obtained toward the second objective (University of California at Berkeley [UCB] et al. 1993).

Additional validation efforts have been conducted and are planned. For example, the Stage II validation of the binder properties was accomplished at Texas A&M as part of SHRP Contract A-005. Post-SHRP validation is also planned using SPS-9 pavement sections being constructed as part of the long-term pavement performance program managed by the Federal Highway Administration. The general approach in the validation effort is illustrated in Figure 1.1.

The purpose of SHRP Project A-002A was to develop binder tests that measure the fundamental, performance-related chemical and physical properties of original (virgin), short-term aged, and long-term aged asphalt. These tests were developed at the Western Research Institute in Laramie, Wyoming, and at Pennsylvania State University. Physical properties from binder tests have been proposed for use in the SHRP asphalt binder specifications. Their relationship to asphalt-aggregate mix performance was evaluated by simulative tests performed by A-003A and reported here.

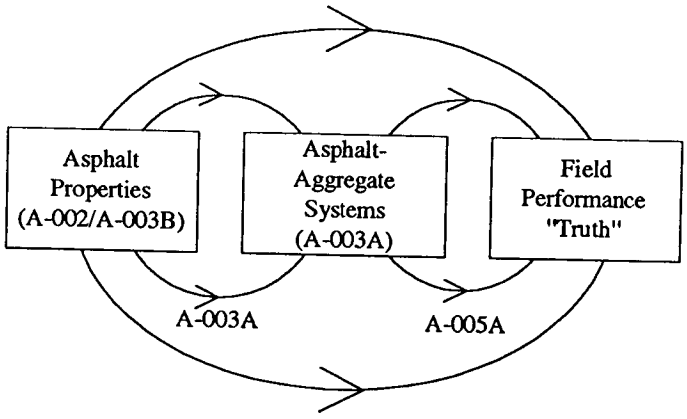

Figure 1.1. General approach used in validation effort

Evaluating the relationship between asphalt-aggregate mix properties and field pavement performance, as well as setting specification limits for mixes, was part of SHRP A-005.

Objectives

The objective of the investigation was to validate the findings and recommendations of the A-002A contractor with regard to the relationship of asphalt properties to the performance of asphalt-aggregate mixes. Asphalts and aggregates representative of those available throughout the United States were used in this effort. Sources and types of materials were selected by SHRP and the A-001 contractor. Asphalt properties related to fatigue, permanent deformation, and thermal cracking are identified in the SHRP binder specification (see Table 1.1),[1] and these properties were to be evaluated with various amounts of aging appropriate to the specific performance parameter. Water sensitivity has not been included in the specification, since the dominant factor influencing exposure to water is the character of the aggregate.[2] Nevertheless, the results of all A-003A validation efforts, including those related to aging and water sensitivity, are summarized in this report.

[1]The binder specification shown in Table 1.1 was that available at the time that the validation efforts here were conducted. Changes have been made in the binder specifications, as shown in Table 1.2, but the validation efforts are directed to the characteristics shown in Table 1.1.

[2]Work accomplished at Auburn University (SHRP Project A-003B, 1991), resulted in information that suggested that the net adsorption test relates to adhesion failures in asphalt-aggregate mixes.

Table 1.1. SHRP binder specification, version 7G, June 6, 1992

Performance grade	PG1-		PG2-					PG3-					PG4-	
	4	5	1	2	3	4	5	1	2	3	4	5	1	2
Avg. of 7-day max pavement temp, (°C[a])	<45		<55					<65					<75	
Min, Pavement Service Temp, °C	>-30	>-40	>0	>-10	>-20	>-30	>-40	>0	>-10	>-20	>-30	>-40	>0	>-10
Original Binder														
Flash point temp, ASTM D-92 min, (°C)	230													
Viscosity, ASTM D-4402 (Brookfield):[b] max. 2000 cSt Test temp, (°C)	165													
Dynamic Shear, SHRP B-003: G*/sin δ, min. 1.0 kPa Test temp. at 10 rad/sec (°C)	45		55					65					75	
Rolling Thin-Film Oven Test (ASTM D-2872) Residue[c]														
Mass loss, max. %	1.00													
Dynamic Shear, SHRP B-003: G*/sin δ, min. 2.0 kPa Test temp. at 10 rad/sec (°C)	45		55					65					75	
Pressure-Aging Vessel Residue (SHRP B-005)														
PAV aging temp. (°C)	90		100					100					110	
Dynamic shear, SHRP B-003: G*sin δ, max, 3000 kPa Test temp. at 10 rad/sec, (°C)	10	5	30	25	20	15	10	35	30	25	20	15	40	35
Creep stiffness, SHRP B-002:[d] S, at 60 sec, max, 200 MPa m value, min. 0.35 Test temp at 60 sec, (°C)	-20	-30	10	0	-10	-20	-30	10	0	-10	-20	-30	10	0
Direct tension, SHRP B-006: Failure strain, 1.0% Test temp. at 1.0 mm/min (°C)	-20	-30	10	0	-10	-20	-30	10	0	-10	-20	-30	10	0

Notes:

- Tenderness is related to the values of G*/sin δ before and after RTFOT.
- Rutting is related to the value of G*/sin δ after RTFOT.
- Fatigue is related to the value of G* sin δ and direct tension strain to failure after PAV.
- Thermal cracking is related to S, m, and direct tension strain to failure after PAV.
- Rheological type is controlled by m.

[a]Pavement temperatures were determined from air temperatures by the algorithm contained in SUPERPAVE program.
[b]For reporting purposes, measurement was also obtained at 145°C. AASHTO T 202 (ASTM D-2171) may be used in lieu of ASTM D-4402; however, ASTM D-4402 is considered reference method. Values measured at two temperatures were used to develop viscosity-temperature profile.
[c]TFOT AASHTO T 179 (ASTM D-1754) may be used in lieu of AASHTO T 240 (ASTM D-2872).
[d]S is stiffness after 60 sec loading time, and m is the slope of the log stiffness versus log time curve at 60 sec loading time.

Table 1.2. SHRP performance graded asphalt binder specification, May 1993

Performance Grade:	**PG 52[a]**	**PF 58**	**PG 64**	**PG 70**
Pavement Temperature (°C):[a]	**-10 -16 -22 -28 -34 -40 -46**	**-16 -22 -28 -34 -40**	**-16 -22 -28 -34 -40**	**-16 -22 -28**
	Original Binder			
Flash point, AASHTO T 48 min: (°C)	230			
Viscosity, ASTM D-4402:[b] Max. 3 pa•s Test temp. (°C)	135			
Dynamic shear, SHRP B-003:[c] G*/sin δ, min. 1.0 kPa Test temp. at 10 rad/sec (°C)	52	58	64	70
Physical hardening index[d], h	Report			
	Rolling Thin-Film Oven Residue (AASHTO T 240)			
Mass Loss, max. (%)	1.00			
Dynamic shear, SHRP B-003: G*/sin δ, min. 2.2 kPa Test temp. at 10 rad/sec (°C)	52	58	64	70

Table 1.2 (continued). SHRP performance graded asphalt binder specification, May 1993

Performance Grade:	PG 52[a]	PF 58	PG 64	PG 70
Pavement Temperature (°C):[a]	**-10 -16 -22 -28 -34 -40 -46**	**-16 -22 -28 -34 -40**	**-16 -22 -28 -34 -40**	**-16 -22 -28**
	Original Binder			
PAV aging temperature (°C)	90	100	100	100(110,90)[e]
Dynamic shear, SHRP B-003: G*/sin δ, max. 5000 kPa Test temp. at 10 rad/sec (°C)	24 22 19 16 13 10 7	25 22 19 16 13	28 25 22 19 16	34 31 28 25
Creep stiffness, SHRP B-002:[f] S, max. 300,000 kPa m value, min. 0.30 Test temp. at 60 sec (°C)	0 -6 -12 -18 -24 -30 -36	-6 -12 -18 -24 -30	-6 -12 -18 -24 -30	0 -6 -12 -18
Direct tension, SHRP B-004:[f] Failure strain, min. 1.0% Test temp. at 1.0 mm/min, (°C)	0 -6 -12 -18 -24 -30 -36	-6 -12 -18 -24 -30	-6 -12 -18 -24 -30	0 -6 -12 -18

[a]Pavement temperatures are estimated air temperature using an algorithm contained in SUPERPAVE software program or may be provided by the specifying agency.

[b]This requirement may be waived at the discretion of the specifying agency if the supplier warrants that the asphalt binder can be adequately pumped and mixed at temperatures that meet all applicable safety standards.

[c]For quality control of unmodified asphalts cement production, measurement of the viscosity of the original asphalt may be substituted for dynamic shear measurements of G*/sin δ at test temperatures at which the asphalt S in Newtonian fluid (generally above 55°C). Any suitable standard means of viscosity measurement may be used, including capillary or rotational viscometry.

[d]They physical hardening index h accounts for physical hardening and is calculated by $h = \left(\frac{S_{24}}{S_1}\right)^{\frac{M_1}{M_{24}}}$ where 1 and 24 indicates hours of conditioning of the tank asphalt. Conditioning and testing are conducted at the designated test temperature. Values should be calculated and reported. S is the creep stiffness at 60 sec loading time and m is the slope of the log creep stiffness versus log time curve after 60 sec loading time.

[e]The PAV aging temperature is 100°C, except in desert climates, where it is 100°, and in Alaska and Canada, where it is 90°C.

[f]If the creep stiffness is below 300,000 kPa, the direct tension test is not required. If the cree stiffness is between 300,000 and 600,000 kPa, the direct tension failure strain requirement can be used in lieu of the creep stiffness requirement. The m value requirement must be satisfied in both cases.

The specific objectives of this report are to provide information that:

1. Validates the ability of asphalt properties proposed by the A-002A contractor to predict asphalt-aggregate mix performance—specifically, fatigue, permanent deformation, and thermal cracking

2. Validates the ability of the aging procedures proposed by the A-002A contractor for asphalt to correlate with the aging tendencies of the asphalt-aggregate mix for both short-term (immediately after construction) and long-term (beyond 3 years) aging conditions

3. Validates the ability of the net adsorption test proposed by the A-003B contractor to predict moisture damage (stripping) in asphalt-aggregate mixes

4. Ranks the relative asphalt or aggregate performance for the mixes tested for each type of pavement distress

Organization of Report

Chapter 2 presents the study approach and describes the test methods and materials used. Chapters 3 through 7 summarize the results of the validation efforts that were accomplished as part of Task D.2 of the A-003A contract. Chapter 8 presents the conclusions and recommendations that resulted from this research investigation.

2

Validation of Binder Properties

Approach

To validate the proposed binder properties and to develop limits for the binder specifications, a two-stage validation effort was planned, as shown in Figure 2.1. Stage I validation, a part of Strategic Highway Research Program (SHRP) Project A-003A, consisted of performing laboratory tests that simulate pavement field conditions. Stage II validation, performed as part of SHRP Project A-005, was based primarily on sampling and testing in situ pavement materials and comparing their properties with in-service pavement performance. This activity is also closely related to the long-term pavement performance program of SHRP. The results of both these efforts are being used to develop the final binder specifications.

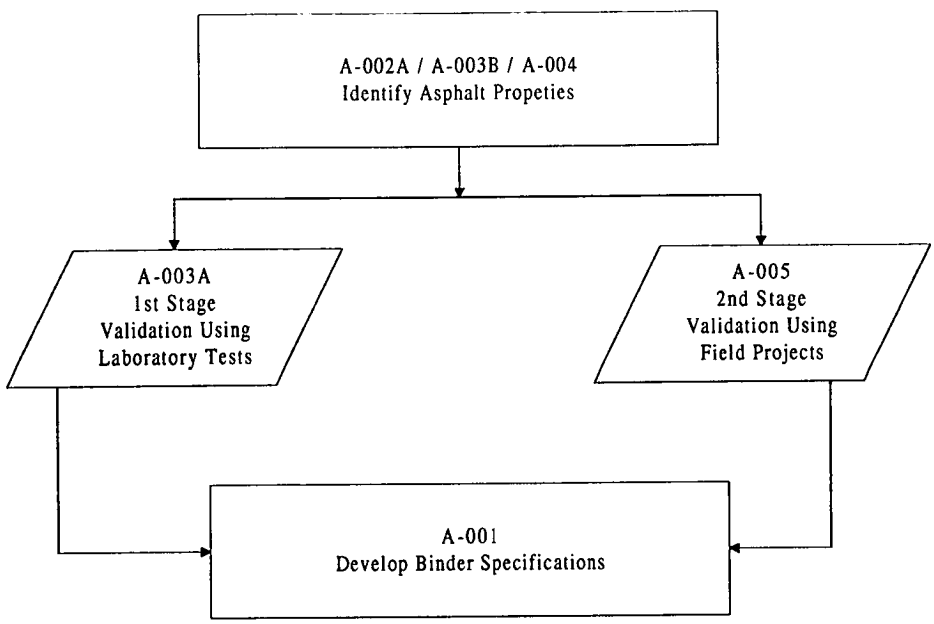

Figure 2.1. General approach used to validate binder tests and specifications

With the completion of the SHRP program, additional validation will be provided from the Special Pavement Studies 9 (SPS-9) pavement test sections. Construction of the pavements began in 1992 and is expected to continue over the next few years. These test sections should provide valuable information that can be used to adjust or modify the resulting binder specifications.

Proposed Binder Tests and Properties

The following tests and associated properties were selected by A-001/SHRP to characterize the fundamental properties of the neat asphalt. Note that the properties selected corresponded to SHRP binder specification 7G dated June 6, 1992 (Table 1.1).

1. *Dynamic shear rheometer.* The instrument is used to measure the rheological properties in terms of dynamic shear modulus (stiffness), G*, and phase angle, δ, of the asphalt binder. In the SHRP binder specification, the parameter G* sin δ relates to fatigue cracking, and G*/sin δ relates to permanent deformation.

2. *Bending beam rheometer.* This instrument is used to measure the low-temperature stiffness of the asphalt binder. From this test it is possible to determine the creep stiffness (S) at 60 sec loading time. By combining information from the dynamic shear rheometer and the bending beam rheometer, it is possible to develop a master curve for log (reduced) time versus log stiffness from which the m value used for thermal cracking is determined. The m value is the slope of the log stiffness versus log time curve in the low-temperature region of the master curve.

3. *Direct tension test.* This test is used to measure the failure strain of the asphalt binder tested at low temperatures. In the SHRP binder specification, the failure strain value relates to thermal cracking.

4. *Aging tests.* The rolling thin-film oven test (RTFOT) has been selected as the preferred method to simulate binder aging during the construction process, or short-term aging. Permanent deformation is evaluated using binders that have received short-term aging. Fatigue and thermal cracking are evaluated using binders that have been subjected to long-term oxidative aging using the PAV.

5. *Water sensitivity.* There is no binder test proposed for evaluating water-sensitivity. It has been concluded that a water-sensitivity test performed on asphalt-aggregate mixes is more appropriate, since such a test would appear to be more closely related to field performance. Hence, the net absorption test developed by A-003B has been used to evaluate asphalt-aggregate combinations as a compatibility test.

Stage I—Validation Tests

The mix tests selected for use in the initial validation efforts both closely simulate field conditions and were available for use in the validation effort. Included were the following:

1. *Fatigue.* The flexural beam test developed at the University of California Berkeley (UCB) was used (Figure 2.2). All tests were conducted on prismatic specimens 51 x 64 x 381 mm in a controlled-strain mode at 20°C using a sinusoidal loading at a frequency of 10 Hz. Flexural stiffness, fatigue life, and total dissipated energy at failure were recorded in this test. Specimens were prepared using the UCB rolling-wheel compactor.

2. *Permanent deformation.* A wheel-tracking device developed originally by the Transport and Road Research Laboratory, UK, and situated at the University of Nottingham (Figure 2.3) was used for this effort. Specimens 200 mm in diameter were cored from slabs prepared using the UCB rolling-wheel compactor. All tests were performed at a test temperature of 40°C using a wheel load of 620 N. The rate of deformation development and rut depths were measured at regular intervals during the test.

   The repetitive shear test developed at UCB also was used in the permanent deformation validation effort (Figure 2.4). Specimens 150 mm in diameter by 50 mm high were cored from slabs prepared with the UCB rolling-wheel compactor. All tests were performed at 60°C. Specimens were subjected to a combination of repetitive shear and normal stresses and constant confining stress; shear strain as a function of load cycles was measured.

3. *Thermal cracking.* The thermal stress restrained-specimen test (TSRST) developed at Oregon State University (OSU) was used for this investigation (Figures 2.5 and 2.6). All mixes were prepared using kneading compaction and were tested to failure at a cooling rate of 10°C/hr. Fracture temperature and stress were determined and used as indicators of mix performance.

4. *Aging.* A resilient modulus test was used to follow the course of aging on the asphalt-aggregate mixes. All mixes, before compaction, were subjected to short-term oven aging (STOA) in a forced-draft oven at 135°C for 4 hr to simulate the construction process. For binders, the RTFOT also represents the same condition. After STOA, the resilient moduli of the mix were determined.

   These specimens were then subjected to long-term oven aging in a forced-draft oven at 85°C for 5 days or low-pressure oxidation aging at 60°C or 85°C for 5 days to simulate aging in the pavement after 5 to 10 years. The pressure-aging vessel represents the same level of aging on binders alone. Changes in mix properties as a function of aging method were measured.

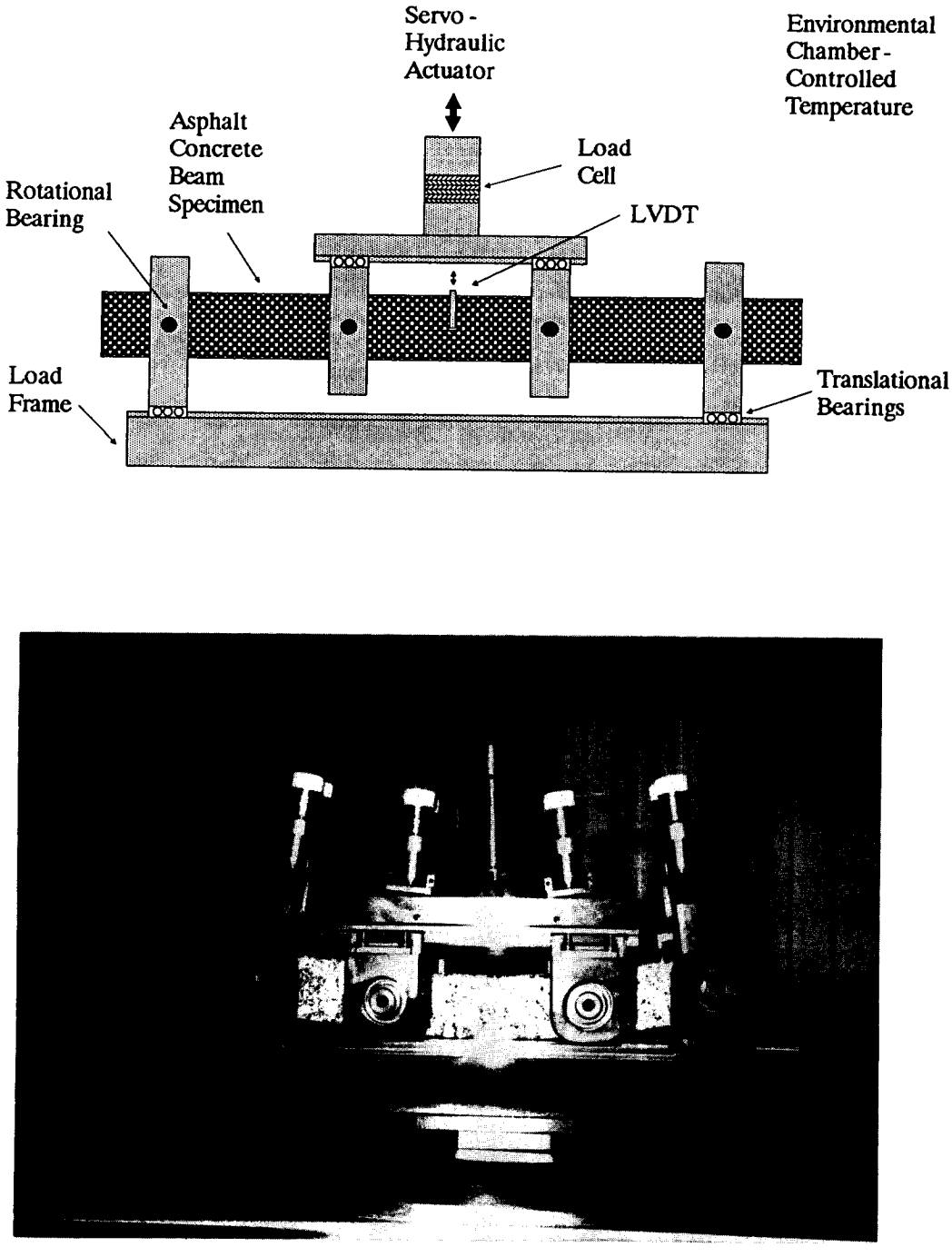

Figure 2.2. Flexural beam test device at UCB—used for fatigue cracking

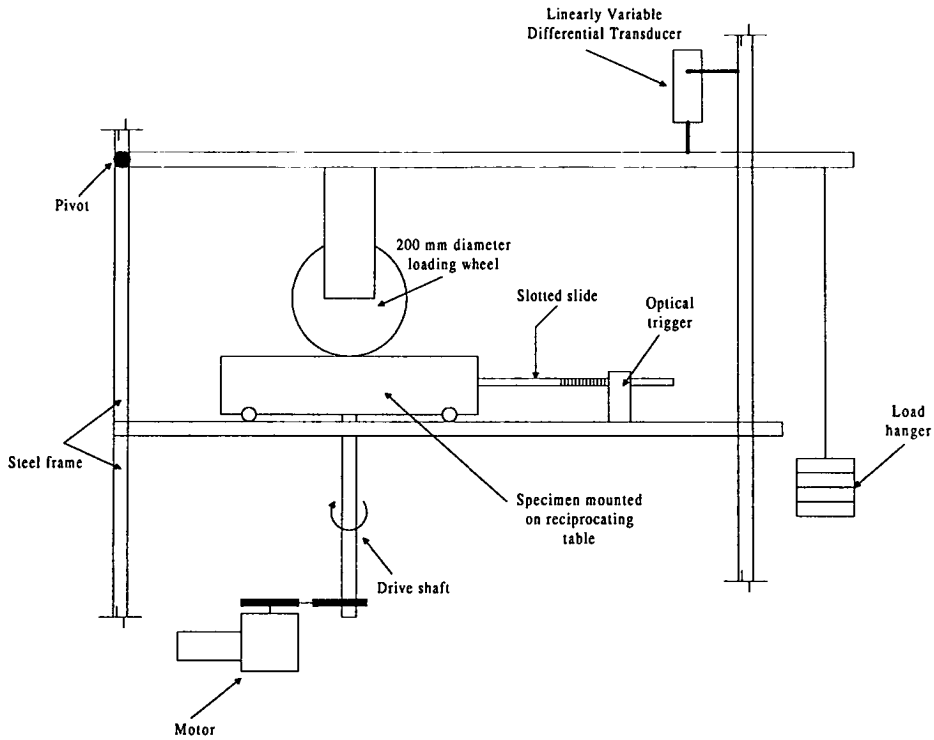

Figure 2.3. Wheel-tracking device at University of Nottingham—used for permanent deformation

5. *Water sensitivity.* Several tests were employed to evaluate the resistance of asphalt-aggregate mixes to the damaging effects of water. These included the Environmental Conditioning System (ECS) developed at OSU as well as the wheel-tracking tests (LCPC) at OSU and the immersion wet wheel-track (IWWT) device at the University of Nottingham. In addition, net adsorption tests were performed at the University of Nevada at Reno. In the ECS, the resilient modulus ratio was used to rank mix performance, while in the wheel-tracking tests the resistance to either surface deformation or disintegration was used. Figure 2.7 presents photos of the ECS equipment, while Figure 2.8 presents a photo and a schematic of the wheel-tracking devices.

Materials

The materials used in the validation effort were all obtained from the Material Reference Library (MRL) in Austin, Texas. Eight to 16 asphalt binders were employed for the various studies. These asphalts are identified in Table 2.1. Properties of the asphalts are available from SHRP and are described in the appropriate chapters that follow. The asphalts were selected by the A-001 contractor to represent a wide cross section of materials available in the United States as well as elsewhere (SHRP 1991).

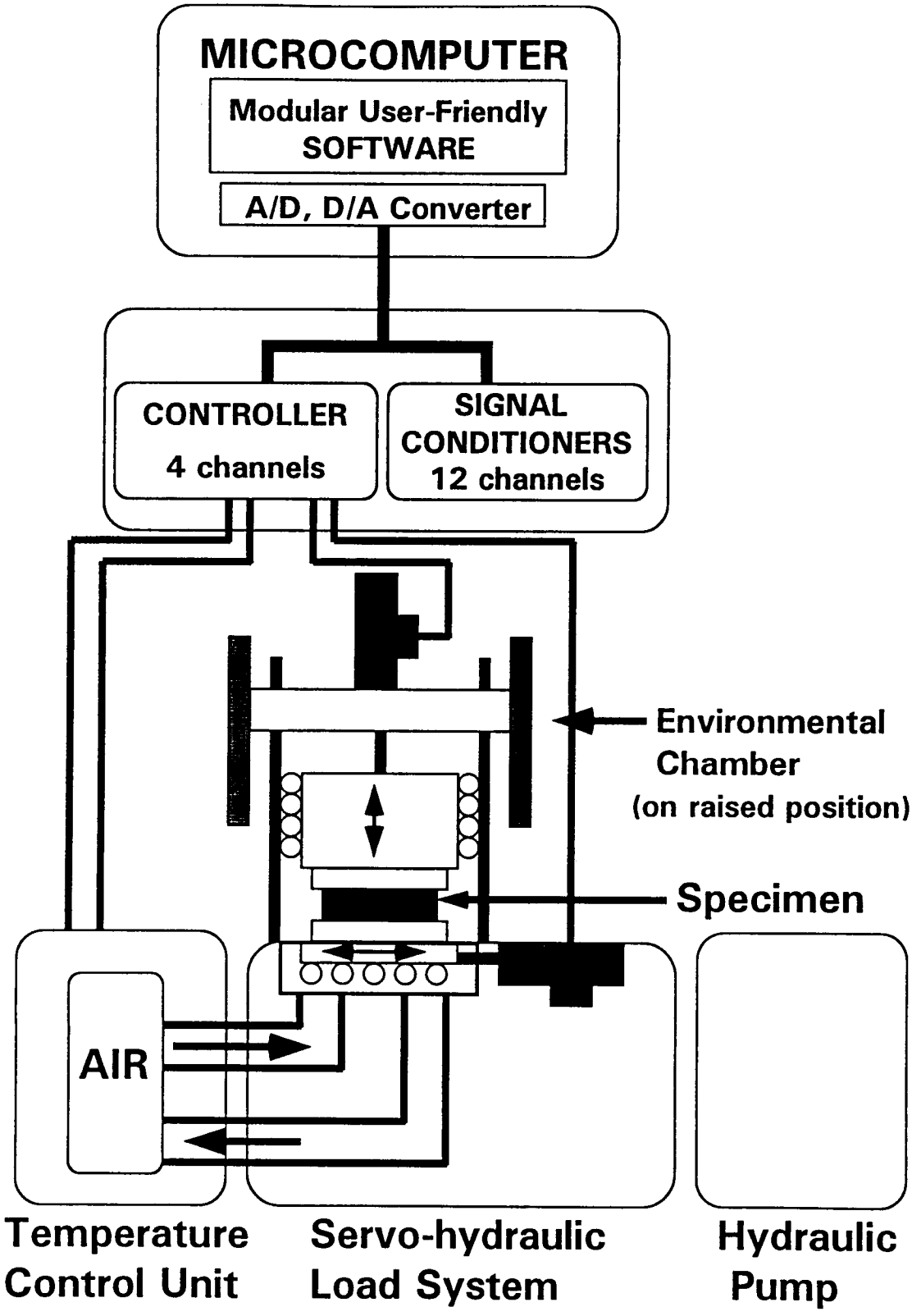

Figure 2.4. Repetitive shear test device at UCB—used for permanent deformation

Two to four aggregates were used in the various studies and are also identified in Table 2.1. For the fatigue, permanent deformation, and thermal cracking studies, two aggregates were used while four materials were used, for the aging and water-sensitivity studies because of the dominant effect of aggregate on these modes of distress. Aggregate gradations and asphalt contents used in the studies are presented in Table 2.2 by aggregate type. All asphalt contents were determined using the Hveem stabilimeter (California Department of Transportation 1984). Generally, the mixes have stabilimeter S values of 35 at the asphalt content that has been used.

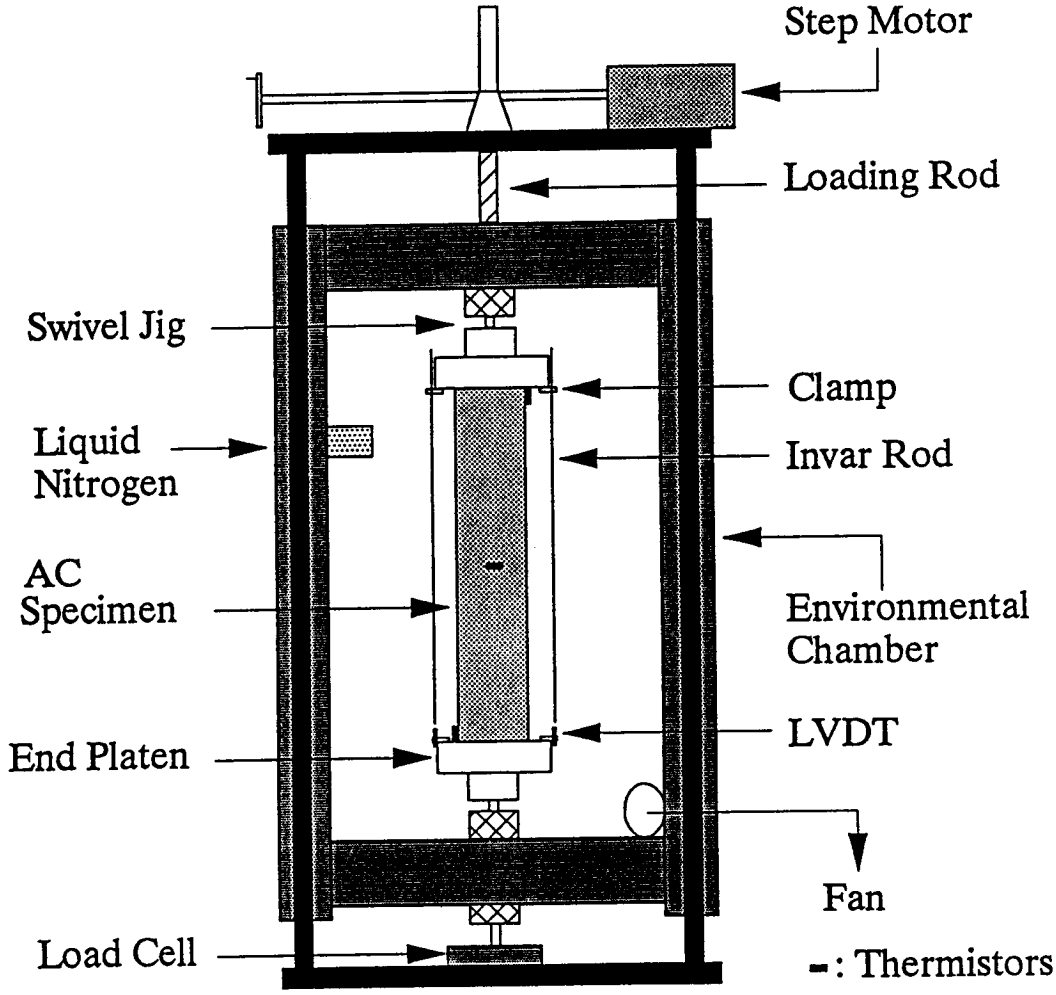

Figure 2.5. Schematic of TSRST apparatus—used for thermal cracking

Figure 2.6. Photo of TSRST apparatus

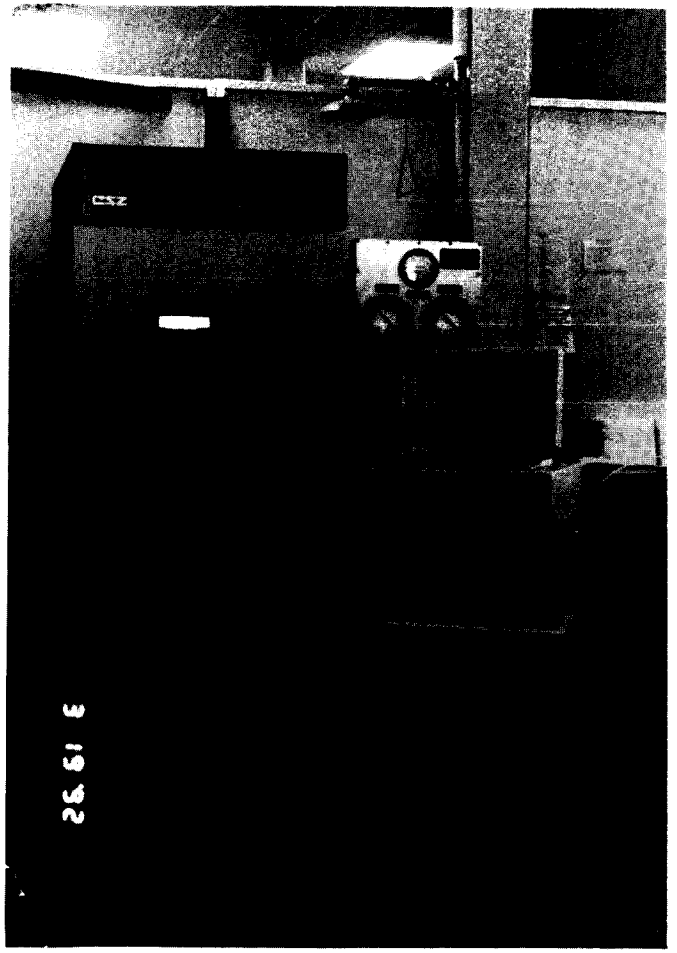

(a) ECS system

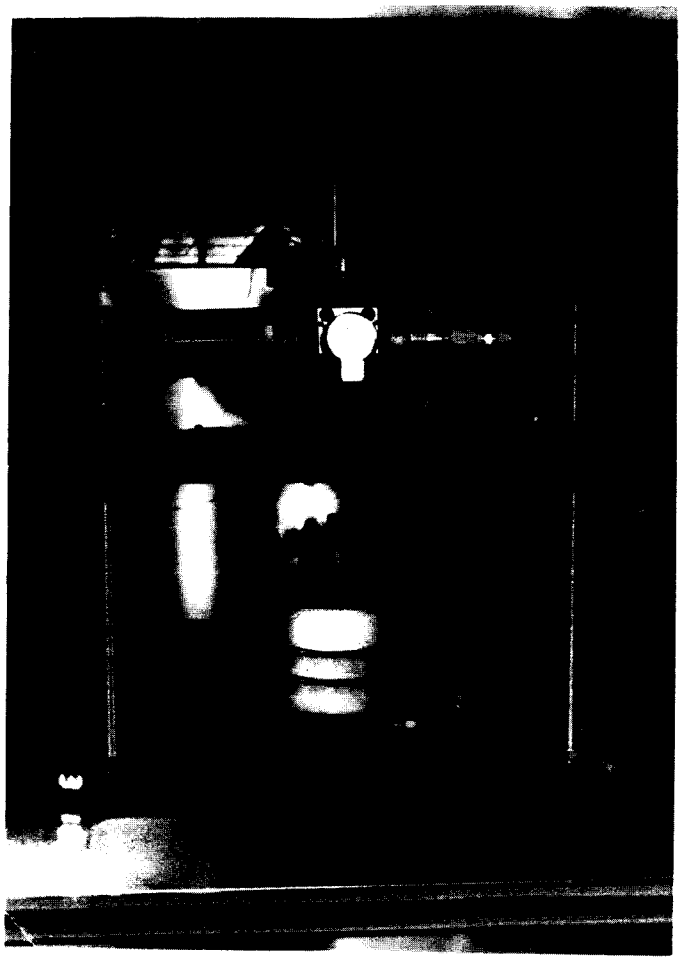

(b) Closeup of test specimen in ECS

Figure 2.7. Photos of ECS

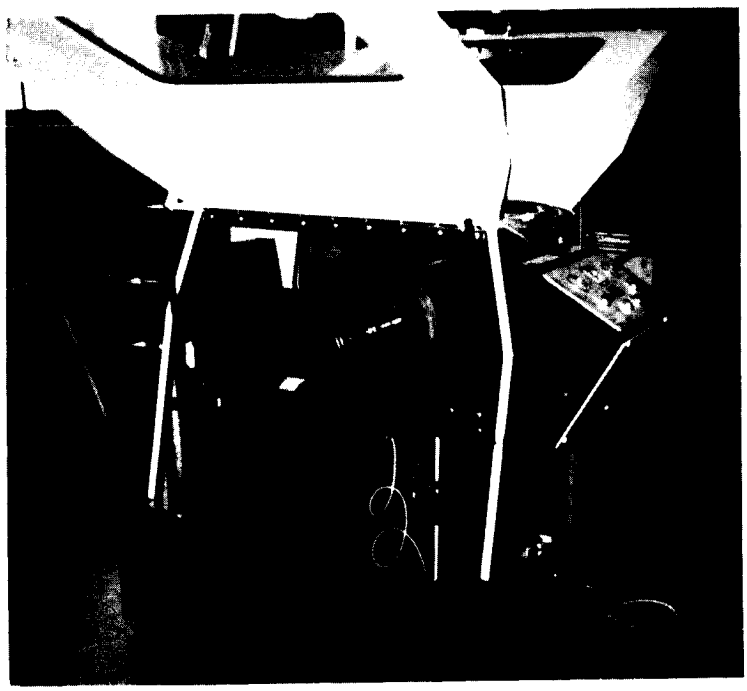

(a) LCPC at OSU

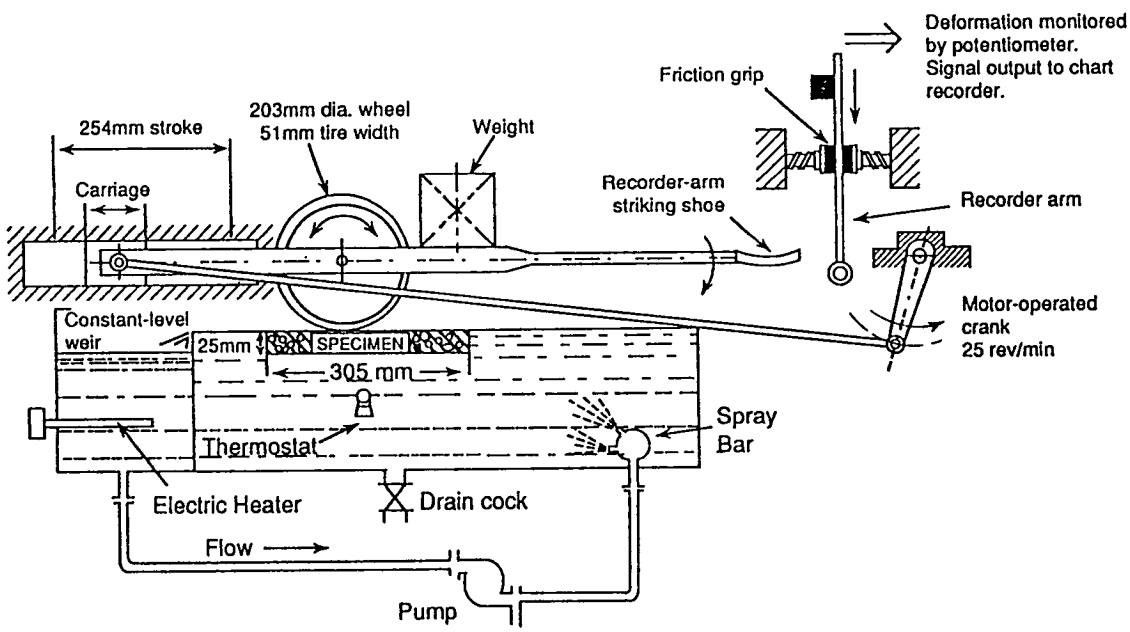

(b) Schematic of device used at University of Nottingham

Figure 2.8. Wheel-tracking devices used in the water-sensitivity study

Table 2.1. Asphalt binders and aggregates used in validation effort

Asphalts:	
MRL Code	**Grade**
AAA	150/200 (pen grade)
AAB	AC-10
AAC	AC-8
AAD	AR-4000
AAF	AC-20
AAG	AR-4000
AAK	AC-30
AAL	150/200 (Pen Grade)
AAM	AC-20
AAV	AC-5
AAW	AC-20
AAX	AC-20
AAZ	AC-20
ABA	AC-20
ABC	AC-20
ABD	AR-4000
Aggregates:	
MRL Code	**Characteristics**
RC	Limestone, high absorption
RD	Limestone, low absorption, fully crushed quarry rock
RH	Greywacke, partially crushed river gravel
RJ	Conglomerate, gravel

Table 2.2. Job-mix formula for the validation studies

	Percent Passing			
Sieve Size	**RC**	**RD**	**RH**	**RJ**
25 mm	100	100	100	100
19 mm	95	95	95	95
12.5 mm	80	80	80	80
9.5 mm	68	68	68	68
6 mm (#4)	48	48	48	48
2.36 mm (#8)	35	35	35	35
1.18 mm (#16)	25	25	25	25
0.6 mm (#30)	17	17	17	17
0.3 mm (#50)	12	12	12	12
0.15 mm (#100)	8	8	8	8
0.074 mm (#200)	5.5	5.5	5.5	5.5
Asphalt content by mass of aggregate, %	6.25	4.5	5.2	5.0
Asphalt content by total mass of mix, %	5.9	4.3	4.9	4.8

3

Validation of Binder Properties Related to Fatigue

This chapter summarizes studies performed to validate the relationships between asphalt binder properties and the fatigue response of asphalt-aggregate mixes. Asphalt binder properties considered critical to fatigue performance were provided by the A-002A contractor and were compared with

1. Fatigue response of asphalt-aggregate mixes tested with the newly developed laboratory flexural beam fatigue equipment

2. Fatigue response of asphalt-aggregate mixes predicted using a strain-based model in which strains were calculated in simulated pavements using layered elastic analysis

This chapter is divided into two main sections, that present the findings related to the items listed above. Detailed results and comparisons are contained in Tayebali et al. (1993).

Validation by Laboratory Flexural Beam Fatigue Testing

Asphalt binder properties were compared with the fatigue response of asphalt-aggregate mix specimens subjected to controlled-strain flexural beam fatigue testing. The basis for the selection of flexural beam test is described in Tayebali et al. (1993, Part I).

Materials

Eight asphalts and two aggregates from the Material Reference Library (MRL) were used in this study: asphalts AAA, AAB, AAC, AAD, AAF, AAG, AAK, and AAM and aggregates RD, and RH.

Table 2.1 lists the grade (current American Association of State Highway and Transportation Officials specifications) for each asphalt. Asphalt binder properties to be validated are discussed in a later section of this chapter. Table 2.1 also provides information on the characteristics of each aggregate.

Aggregate gradations are shown in Table 2.2. All mixes were prepared at the asphalt contents shown in Table 2.2 for the RD and RH aggregates.

Mixes were compacted by rolling-wheel compaction to produce specimens with target air-void contents of 4 and 7 percent. Since it was not possible to precisely control the air-void content during the compaction of the mixes, the actual air-void contents were measured for each specimen, and adjustments were made to test data (discussed later in this chapter) before analyzing the specimen. Details of the compaction procedure and methods for measuring air-void content are included in Harvey (1991).

Experiment

A full-factorial experiment was designed to allow all main effects and two-factor interactions to be evaluated. The factorial matrix consisted of 8 asphalts, 2 aggregates, 2 air-void content levels, and 2 flexural strain levels, resulting in a total of 64 cells. Each cell had 2 replicates to allow for estimation of experimental error, for a total of 128 flexural fatigue tests. Replication permitted higher-order interactions to be tested; however, only two-factor interactions were included in statistical models, since the effects of higher-order interactions tend to be minor, and meaningful engineering interpretation is generally difficult. The factorial experiment is summarized below.

Experimental Design Factors and Levels (independent variables):

Factor	Levels
Asphalt source	8 (Table 2.1)
Aggregate source	2 (RD, RH)
Air-void content, %	2 (4, 7)
Strain, level, μmm/mm	2 (400, 700)
Replicates:	2 per cell
Total number of tests:	128

Fatigue Response Variables (dependent variables, to be explained later):

Initial flexural stiffness (MPa)—measured at the 50th load cycle

Fatigue life (cycles)—number of load cycles corresponding to 50 percent reduction in flexural stiffness

Total dissipated energy (MPa)—summation of dissipated energy per cycle to 50 percent reduction in flexural stiffness

Asphalt Binder Tests and Properties

Asphalt binder properties were provided by the A-002A contractor for this study. The properties were measured using dynamic mechanical analysis on asphalt cement binders. Binder properties included complex shear modulus (G*), phase angle (δ), storage modulus (G′, which is equal to G* cos δ), loss modulus (G″, equal to G* sin δ), and loss tangent (tan δ, equal to G″/G′). More detailed information on asphalt binder tests and properties is presented in Peterson et al. (1992).

The Strategic Highway Research Program (SHRP) binder specification suggests that the loss modulus, G* sin δ, is inversely related to fatigue cracking in asphalt-aggregate mixes. Specifically, the fatigue life of the asphalt binder, in an asphalt-aggregate mix, decreases with increasing values of G* sin δ (Table 1.1). The specification limits the value of G* sin δ to 3000 kPa when a binder is tested at 10 rad/sec at the specified temperature after having been aged in the pressure-aging vessel (PAV). Thus, the implication is that aged asphalt binders with G* sin δ values exceeding this limit may be susceptible to premature fatigue cracking, whereas aged asphalt binders with lower G* sin δ values should provide acceptable fatigue resistance in asphalt-aggregate mixes.

Both A-002A and A-003A researchers have concluded that fatigue properties of the binder and the mix are related to dissipated energy. For the binder, G* sin δ should be related to dissipated energy because G* and δ both capture the viscous response of the binder.

Similarly for the mix, dissipated energy is dependent on the flexural stiffness modulus (S) and phase angle (ϕ) determined from the flexural beam test. Thus, it is logical to conclude that the energy-dependent properties of the binder would influence the fatigue properties of the mix.

Asphalt binder properties provided by the A-002A contractor and used in this study are presented in Table 3.1. The binders were aged according to ASTM D-1754, the thin-film oven test (TFOT), before testing in order to simulate short-term aging during the construction process. The A-002A contractor tested asphalt binders over a wide range of temperatures and load frequencies to develop a rheological model that explains asphalt binder response. From such a model, binder properties can be calculated for any combination of test temperature and load frequency. Although Table 3.1 reports asphalt binder properties for a test temperature of 20°C and a load frequency of 10 Hz (63 rad/sec), binders were not tested under these conditions. Rather, the properties shown in Table 3.1 were calculated using the rheological model developed by the A-002A contractor.

It will be noted that the binder properties presented in Table 3.1 represent aging and load frequency conditions different from those required in the SHRP binder specification for fatigue cracking evaluation. The specification requires binders to be long-term aged in the pressure-aging vessel (PAV) and tested at a load frequency of 10 rad/sec (see Table 3.2). The properties reported in Table 3.1 were used in this study because they more closely represent the conditions under which asphalt-aggregate mixes were aged and tested in the flexural beam test. Mixes were subjected to short-term aging (4 hr at 135°C), but not long-term aging because of time constraints, and were tested at a load frequency of 10 Hz to better simulate traffic speeds.

Table 3.1. Asphalt binder properties provided by the A-002A contractor (after TFOT, at 20°C and 10 Hz)

Asphalt Source	G* (kPa)	G* sin δ (kPa)	G′ (kPa)	tan δ
AAA	3,197	2,732	1,661	1.645
AAB	6,098	4,600	4,001	1.150
AAC	9,769	7,295	6,499	1.122
AAD	3,845	3,149	2,205	1.428
AAF	18,321	12,326	13,551	0.910
AAG	23,517	17,975	15,179	1.183
AAK	10,833	8,134	7,150	1.138
AAM	8,230	5,609	6,019	0.933

Table 3.2. Asphalt binder properties provided by the A-002A contractor (after PAV, at 20°C and 10 rad/sec)

Asphalt Source	G* (kPa)	G* sin δ (kPa)	G′ (kPa)	tan δ
AAA	3,347	2,542	2,177	1.168
AAB	6,677	4,444	4,983	0.892
AAC	7,809	5,200	5,825	0.893
AAD	4,292	3,144	2,923	1.076
AAF	20,902	12,114	17,035	0.711
AAG	22,165	16,336	14,984	1.090
AAK	7,558	5,306	5,382	0.986
AAM	7,757	4,614	6,235	0.740

G* sin δ values in Tables 3.1 and 3.2 were compared to examine the relationship between the two data sets and to determine how that relationship might affect the conclusions of this study. Figure 3.1 illustrates the comparison. There appears to be a strong linear relationship between G* sin δ values from the two data sets. Also note that the slope of the regression line is almost 1, indicating that the G* sin δ value for a given asphalt is nearly the same regardless of which aging and loading conditions it represents. Thus, it is expected that the conclusions drawn from this study would not change significantly if asphalt-aggregate mix fatigue response had been compared with asphalt binder properties representing the aging and loading conditions of the SHRP binder specification.

According to the A-002A contractor, the precision of the values in Tables 3.1 and 3.2 is a function of the magnitude of each value, and the coefficient of variation for each of the properties is approximately 10 percent within the ranges of the data tested. In later tables and figures, a log (base 10) transformation was applied to the binder data (Tayebali et al. 1993).

Asphalt-Aggregate Mix Tests and Properties

Flexural fatigue tests were conducted on 51 × 64 × 381 mm beam specimens in the controlled-strain mode at 20°C in sinusoidal loading at a frequency of 10 Hz. The loading was controlled so that the peak tensile strain at the bottom of the specimen was constant throughout the test at either 400 or 700 μmm/mm. Although these strain levels are relatively large in comparison with strains experienced by mixes in typical pavements, they were applied to ensure that failure would occur within a reasonable time.

Flexural stiffness, fatigue life, and total dissipated energy were the response variables measured in the fatigue tests and used in the analyses reported here. Flexural stiffness is an important parameter in that it affects the strain experienced by an asphalt-concrete layer when subjected to load. Although flexural stiffness was measured throughout the test, only the "initial" value is reported (the value measured at the 50th load cycle). This value for N was selected to allow the specimen to become seated in the test equipment, while minimizing the accumulated fatigue damage in the specimen, before the measurement.

The importance of beam fatigue life is obvious in that it can provide an indication of the relative fatigue life of different asphalt-aggregate mixes. For this study, fatigue life was defined as the number of load cycles corresponding to a reduction in flexural stiffness of 50 percent of the initial value. This level of reduction in stiffness was chosen because 80 percent of the total fatigue life (i.e., up to fracture) has typically been consumed by this point.

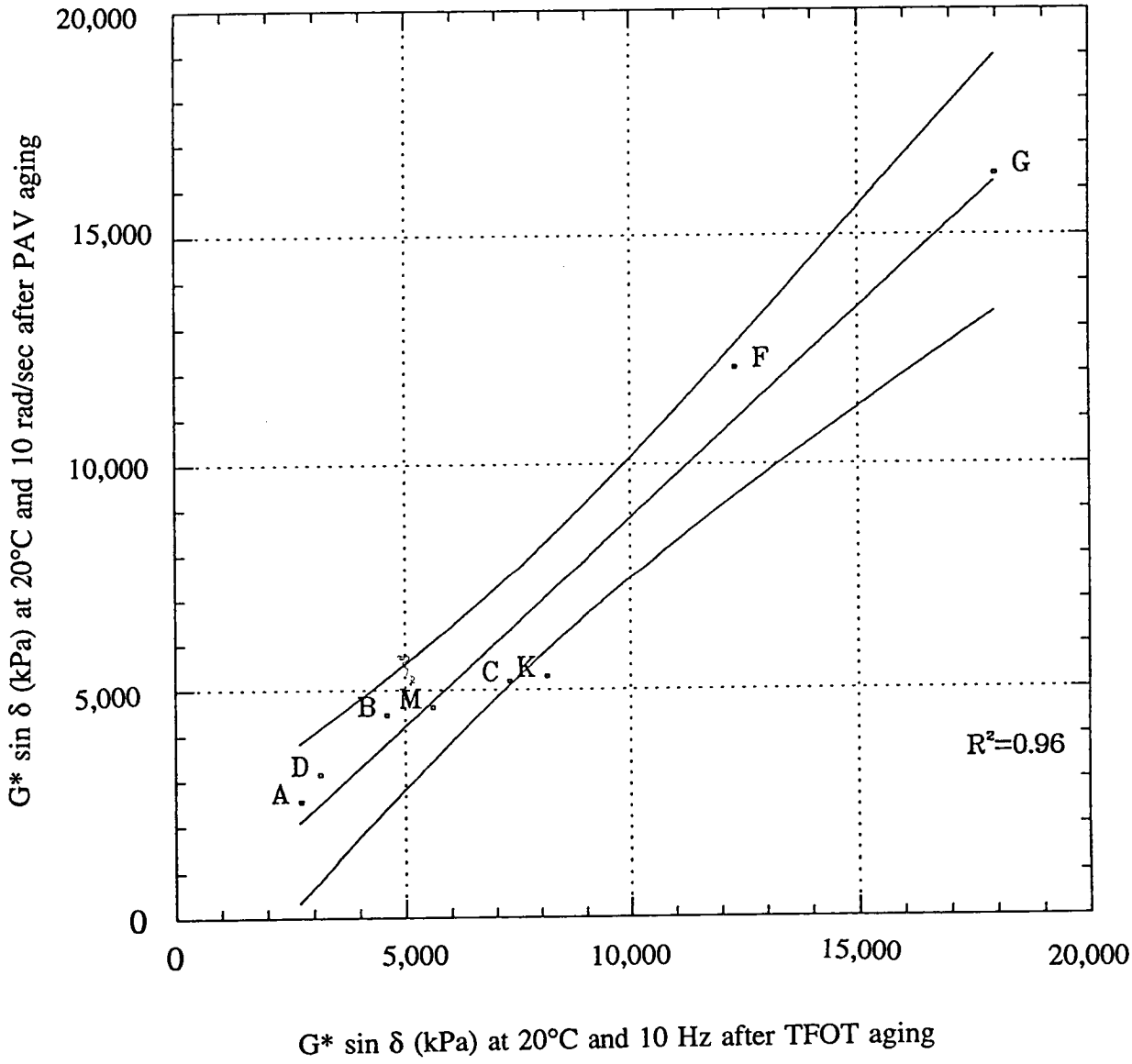

Figure 3.1. G* sin δ after PAV at 10 rad/sec versus G* sin δ after TFOT at 10 Hz

Total dissipated energy[1] was also measured, since research reported by European investigators suggests that this parameter is related to the fatigue response of asphalt-aggregate mixes and that this parameter is independent of the mode of testing (controlled-strain versus controlled-stress) and frequency of loading (thus allowing fatigue testing to be completed more quickly). These observations have not been substantiated by this study. Detailed information on the flexural fatigue test method and the fatigue properties of asphalt-aggregate mixes is presented in Tayebali et al. (1993).

Although asphalt-aggregate specimens were prepared at low and high air-void contents, it was impossible to achieve the target air-void content of 4 or 7 percent in each specimen. Since it was known from previous studies that air-void content affects the fatigue response of asphalt-aggregate mixes, it was important that comparisons be made at a specific air-void content. Therefore, the fatigue response variables for each specimen were adjusted to account for the difference between the specimen's actual air-void content and the target value. This adjustment was performed statistically by using an analysis of variance (ANOVA) model to determine the effect of air-void content, and any interaction it had with asphalt source or aggregate source, and then adjusting the response variable according to the coefficient(s) resulting from the ANOVA (Tayebali et al. 1993).

Asphalt-aggregate mix fatigue test results are presented in Table 3.3. Each specimen is identified by a unique combination of asphalt source, aggregate source, air-void content, and strain level. The data in Table 3.3 have been adjusted to account for variations in air-void content from the experiment target values. The statistical analyses presented herein were performed on this data. Raw test data (i.e., before adjustment) are presented in Tayebali et al. (1993). In later tables and figures, log (base 10) transformations were also applied to mix fatigue results.

Relationships between Binder and Mix Properties

Analysis of Variance

As stated earlier, ANOVA was performed to determine the influence of experiment factors and interactions on fatigue response variables. The analysis indicated that asphalt source, aggregate source, and air-void content each had a significant effect on measured fatigue response. In addition, the interactions of asphalt source and aggregate source, asphalt source and air-void content, and aggregate source and air-void content were shown to significantly affect fatigue behavior. A minimum confidence level of 95 percent was used to determine significance; however, many of the factors and interactions were significant at confidence levels greater than 99 percent.

[1]Total dissipated energy is the cumulative sum of the dissipated energy per load cycle up to the number of cycles corresponding to a 50 percent reduction in mix stiffness.

Table 3.3. Flexural beam fatigue test results, adjusted for air-void contents (after short-term oven aging, at 20°C and 10 Hz)

Asphalt Source	Aggregate Source	Air Voids (%)	Strain (μmm/mm)	Stiffness (MPa)	Fatigue Life (Cycles)	Total Dissipated Energy (MPa)
AAA	RD	4.0	400	2,891	457,627	75
		4.0	400	3,234	90,183	16
		4.0	700	2,696	8,030	4
		4.0	400	2,989	25,924	14
		7.0	400	2,151	234,738	29
		7.0	400	2,312	178,819	25
		7.0	700	1,804	33,517	12
		7.0	700	1,741	32,808	11
AAB	RD	4.0	400	3,917	123,873	27
		4.0	400	4,116	277,245	59
		4.0	700	3,814	14,964	9
		4.0	400	3,652	32,675	19
		7.0	400	3,106	168,247	27
		7.0	400	3,106	168,247	27
		7.0	700	2,271	18,443	7
		7.0	700	2,205	8,406	3
AAC	RD	4.0	400	6,030	91,812	25
		4.0	400	5,206	117,199	30
		4.0	700	6,242	12,109	12
		4.0	400	5,885	10,567	10
		7.0	400	3,155	72,540	13
		7.0	400	3,586	63,051	11
		7.0	700	4,160	10,148	7
		7.0	700	3,724	10,478	6
AAD	RD	4.0	400	4,974	94,025	23
		4.0	400	4,146	142,751	31
		4.0	700	4,964	7,833	7
		4.0	400	4,572	9,188	7
		7.0	400	3,353	74,123	12
		7.0	400	2,810	258,846	40
		7.0	700	2,831	22,412	11
		7.0	700	2,722	25,889	12
AAF	RD	4.0	400	8,969	90,061	32
		4.0	400	8,969	90,061	32
		4.0	700	9,197	10,744	12
		4.0	400	7,550	7,460	7
		7.0	400	8,137	51,732	16
		7.0	400	8,903	55,666	19
		7.0	700	8,220	5,946	6
		7.0	700	8,196	8,221	8

Table 3.3 (continued). Flexural beam fatigue test results, adjusted for air-void contents (after short-term oven aging, at 20°C and 10 Hz)

Asphalt Source	Aggregate Source	Air Voids (%)	Strain (μmm/mm)	Stiffness (MPa)	Fatigue Life (Cycles)	Total Dissipated Energy (MPa)
AAG	RD	4.0	400	11,454	25,451	11
		4.0	400	7,447	14,961	6
		4.0	700	8,135	1,957	2
		4.0	400	8,011	2,084	3
		7.0	400	9,788	20,393	6
		7.0	400	9,797	19,689	7
		7.0	700	7,796	3,951	5
		7.0	700	8,484	1,522	2
AAK	RD	4.0	400	4,710	112,100	27
		4.0	400	5,446	177,219	45
		4.0	700	4,816	15,688	12
		4.0	400	4,320	26,435	18
		7.0	400	4,304	131,698	28
		7.0	400	4,794	119,236	28
		7.0	700	3,976	13,614	9
		7.0	700	3,905	10,055	6
AAM	RD	4.0	400	5,075	313,987	68
		4.0	400	4,993	457,713	99
		4.0	700	5,003	17,100	13
		4.0	400	4,640	22,547	15
		7.0	400	6,182	178,769	41
		7.0	400	6,025	168,878	42
		7.0	700	4,456	26,309	17
		7.0	700	4,637	13,644	9
AAA	RH	4.0	400	1,852	394,512	47
		4.0	400	1,804	424,190	44
		4.0	700	1,846	80,984	29
		4.0	400	1,942	68,137	26
		7.0	400	1,634	605,553	57
		7.0	400	1,727	209,243	23
		7.0	700	1,394	73,502	20
		7.0	700	1,578	26,110	8
AAB	RH	4.0	400	3,358	592,968	99
		4.0	400	3,080	245,285	40
		4.0	700	3,100	39,866	20
		4.0	400	3,720	20,058	11
		7.0	400	1,798	364,241	38
		7.0	400	2,014	473,386	46
		7.0	700	1,746	15,564	5
		7.0	700	2,025	15,554	6

Table 3.3 (continued). Flexural beam fatigue test results, adjusted for air-void contents (after short-term oven aging, at 20°C and 10 Hz)

Asphalt Source	Aggregate Source	Air Voids (%)	Strain (μmm/mm)	Stiffness (MPa)	Fatigue Life (Cycles)	Total Dissipated Energy (MPa)
AAC	RH	4.0	400	3,411	175,365	36
		4.0	400	3,721	238,982	52
		4.0	700	3,008	25,077	13
		4.0	400	3,574	24,746	16
		7.0	400	3,010	93,134	15
		7.0	400	2,793	135,591	21
		7.0	700	3,362	25,227	15
		7.0	700	2,538	12,319	6
AAD	RH	4.0	400	2,070	251,189	33
		4.0	400	1,890	225,666	26
		4.0	700	2,110	44,154	17
		4.0	400	1,936	58,121	21
		7.0	400	1,733	394,981	39
		7.0	400	1,756	562,597	56
		7.0	700	2,108	50,872	19
		7.0	700	1,830	49,668	16
AAF	RH	4.0	400	7,031	179,682	48
		4.0	400	6,972	171,404	34
		4.0	700	6,927	13,087	12
		4.0	400	6,533	12,151	10
		7.0	400	5,072	41,867	8
		7.0	400	4,744	30,803	6
		7.0	700	6,252	10,624	9
		7.0	700	4,823	5,689	4
AAG	RH	4.0	400	8,432	24,960	10
		4.0	400	8,828	21,921	9
		4.0	700	7,310	4,200	5
		4.0	400	7,938	3,491	4
		7.0	400	7,258	12,526	4
		7.0	400	6,395	25,808	7
		7.0	700	6,800	2,148	2
		7.0	700	6,946	2,270	2
AAK	RH	4.0	400	3,968	181,982	34
		4.0	400	3,249	205,814	36
		4.0	700	4,632	32,570	22
		4.0	400	4,254	17,862	11
		7.0	400	3,263	162,641	28
		7.0	400	3,942	82,143	16
		7.0	700	2,854	9,196	4
		7.0	700	3,801	8,949	5

Table 3.3 (continued). Flexural beam fatigue test results, adjusted for air-void contents (after short-term oven aging, at 20°C and 10 Hz)

Asphalt Source	Aggregate Source	Air Voids (%)	Strain (μmm/mm)	Stiffness (MPa)	Fatigue Life (Cycles)	Total Dissipated Energy (MPa)
AAM	RH	4.0	400	3,917	210,320	38
		4.0	400	4,176	270,178	49
		4.0	700	3,870	50,644	28
		4.0	400	3,776	42,280	22
		7.0	400	2,911	262,740	36
		7.0	400	3,510	256,214	40
		7.0	700	2,721	13,374	6
		7.0	700	2,777	6,619	3

The ANOVA model indicated that the factors and interactions accounted for the variation of fatigue response in the following approximate proportions:

Fatigue Response Variable	Factor or Interaction	Proportional Effect (%)
Flexural stiffness	Asphalt	76
	Aggregate	12
	Air-void content	4
	Asphalt-aggregate	2
	Asphalt air-void content	2
	ANOVA model error	4
Fatigue life	Asphalt	71
	Aggregate	5
	Air-void content	2
	Asphalt-aggregate	4
	Asphalt air-void content	3
	Aggregate air-void content	1
	ANOVA Model Error	13
Dissipated energy	Asphalt	49
	Aggregate	1
	Air-void content	11
	Asphalt-aggregate	5
	Asphalt air-void content	5
	Aggregate air-void content	2
	ANOVA model error	23

The data above illustrate the dominant effect of asphalt on mix fatigue response. Note that the effect of asphalt is reduced for the dissipated energy response and that the ANOVA model error increased. The ANOVA model error represents the variation in fatigue response that cannot be attributed to any of the factors or interactions.)

Since asphalt source significantly affected fatigue response, it was expected that further analysis would show strong relationships between asphalt binder properties and asphalt-aggregate mix fatigue response. However, since aggregate characteristics and air-void content also significantly influenced the fatigue response of asphalt-aggregate mixes, it was expected that the effect of asphalt properties might be masked somewhat by these other influences. Therefore, separate analyses were made on the following data sets:

Aggregate Source	Air-Void Content (%)
RD	4
RD	7
RH	4
RH	7

Flexural strain level did not interact with any of the other experiment factors in its effect on mix fatigue response. Therefore, flexural stiffness, fatigue life, and dissipated energy results were averaged across strain level to simplify later analyses; data presented in the following tables and graphs reflect this averaging.

Scatterplots

Scatterplot matrices (SPLOMs) were prepared to graphically illustrate the relationships between the fatigue response variables and each of the asphalt binder properties. The SPLOMs provide a quick graphical view of relationships between several variables at the same time. The results are presented in Figures 3.2 through 3.4. Each matrix is a compilation of 16 individual scatterplots. For any given scatterplot, the independent variable (binder property) is listed at the top of each column and is plotted along the x axis, while the dependent variable (fatigue response) is plotted along the y axis. Each row of plots presents the results for each mix data set, as indicated in the leftmost column. The data points are depicted by the last letter of the asphalt source (MRL code) for each asphalt. The lines show the best linear fit by least squares regression.

Figure 3.2 indicates that the flexural stiffness of mixes is strongly related to $G^* \sin \delta$, G^*, and G'. As the binder stiffness increases—whether because of an increase in the storage modulus ($G^* \cos \delta$ or G'), the loss modulus ($G^* \sin \delta$, or G''), or the complex modulus (G^*)—so does the mix flexural stiffness; this relationship was expected. The relationship of flexural stiffness to $\tan \delta$ is not as strong, but there is a definite trend of decreasing flexural stiffness with increasing values of $\tan \delta$.

Figure 3.3 indicates an inverse relationship between binder stiffness and mix fatigue life—as binder stiffness increases, fatigue life decreases. The relationship of fatigue life to tan δ is opposite to that for flexural stiffness (Figure 3.2). G* sin δ, G*, and G′ again provide strong relationships, except for mixes containing aggregate RD and 4 percent air voids.

Figure 3.4 presents the relationships between total dissipated energy and binder properties. The trends of the relationships are the same as those for fatigue life (Figure 3.3), but the relationships, overall, are not as strong. Again, the weakest relationships correspond to mixes containing aggregate RD and 4 percent air voids.

Whether the comparison is with flexural stiffness, fatigue life, or dissipated energy, all binder modulus properties (G* sin δ, G*, and G′) appear to provide equally strong relationships.

Pearson Correlation

The strength of the relationships depicted in Figures 3.2 through 3.4 was quantified through the use of Pearson correlations. The Pearson correlation coefficient measures the strength of a linear relationship between two variables. The coefficient, R, can range between -1 and +1, with negative coefficients indicating a negative slope or inverse relationship between the two variables. Coefficients close to -1 or +1 indicate strong relationships.

Pearson correlation coefficients are presented in Table 3.4. Values corroborate the conclusions drawn from visual examination of the SPLOMs. Flexural stiffness (log) has a strong linear relationship to the log of G* sin δ, G*, and G′ across all mixes tested. Fatigue life (log) also has a strong linear relationship to these binder properties, except for mixes containing aggregate RD and 4 percent air void. Relationships involving dissipated energy are generally weaker, except for the mix containing aggregate RH and 7 percent air voids. In cases where the relationships are weaker, G* sin δ provides a slightly stronger relationship than G* or G′. Log (tan δ) does not exhibit a strong linear relationship to any mix fatigue response variable.

Spearman Rank Correlation

Spearman rank correlations were performed to see whether weak relationships indicated by the Pearson correlations were perhaps stronger when based on relative ranking of asphalt performance represented by binder properties and mix fatigue response. The Spearman rank correlation is simply a Pearson correlation computed on the same data after converting the data to ranks. Table 3.5 presents Spearman rank correlation coefficients. A review of the results indicates that previously weak relationships were not significantly improved.

Linear Regression Analysis

Linear least-squares regressions between the fatigue response variables and G* sin δ were performed to further evaluate the relationships between these variables. Other binder properties were not included because they did not produce significantly stronger relationships to the fatigue response variables. Furthermore, G* sin δ is the binder parameter that has been included in the SHRP binder specification to control fatigue cracking.

The regression relationships and coefficients of determination (R^2) are presented graphically in Figures 3.5 through 3.7. Each plot represents a separate mix data set. In these graphs, the least-squares regression line is plotted through the data, and it is surrounded by curved lines that represent a 95 percent confidence interval bounding the regression line. The coefficient of determination (R^2) is reported in the bottom right-hand corner of each graph. The value of R^2 represents the percentage of the variation in the fatigue response variable that is explained by changes in the value of G* sin δ. The confidence interval represents our confidence that the average fatigue response of a mix containing an asphalt included in this study will fall within the confidence band at the G* sin δ value for that asphalt. For instance, considering asphalt AAB (Figure 3.5), the average flexural stiffness of a mix containing this asphalt and aggregate RH with a 4 percent air-void content will fall within the confidence band directly above the G* sin δ value of 4600 kPa (refer to Table 3.1) 95 out of 100 times (i.e., 95 percent confidence).

Figure 3.5 demonstrates the strong relationship between G* sin δ and flexural stiffness. The narrow confidence bands indicate that a reasonably accurate estimate of flexural stiffness can be made by knowing the G* sin δ value of the asphalt binder. Note that the regression line in each graph crosses the vertical line associated with a G* sin δ value of 10,000 kPa at a different point along the y axis, or flexural stiffness scale. This shifting of regression lines demonstrates the effects of aggregate source and air-void content on flexural stiffness. Also note that the slopes of the regression lines are similar, except that the slope associated with the mix containing aggregate RD and 4 percent air voids is flatter. All the regressions shown in Figure 3.5 are statistically significant at a confidence level of 99 percent or higher.

Figure 3.6 demonstrates the strong relationship between G* sin δ and fatigue life, except for mixes containing aggregate RD with 4 percent air voids. As expected from the low R^2 value and the wide confidence band, the regression for the mix containing aggregate RD with 4 percent air voids was not statistically significant (i.e., confidence level is less than 95 percent). Relatively accurate estimates of fatigue life could be made from G* sin δ for all other mixes. These data also demonstrate the influence of the aggregate and air-void content on fatigue life as shown by the shift in regression lines along the fatigue life scale for different mixes at a given value of G* sin δ.

The slopes of the lines in Figure 3.7 indicate that total dissipated energy definitely decreases with increasing G* sin δ. However, the scatter in the data does not permit reliable estimates of dissipated energy based on G* sin δ (as indicated by the wide confidence bands in three of

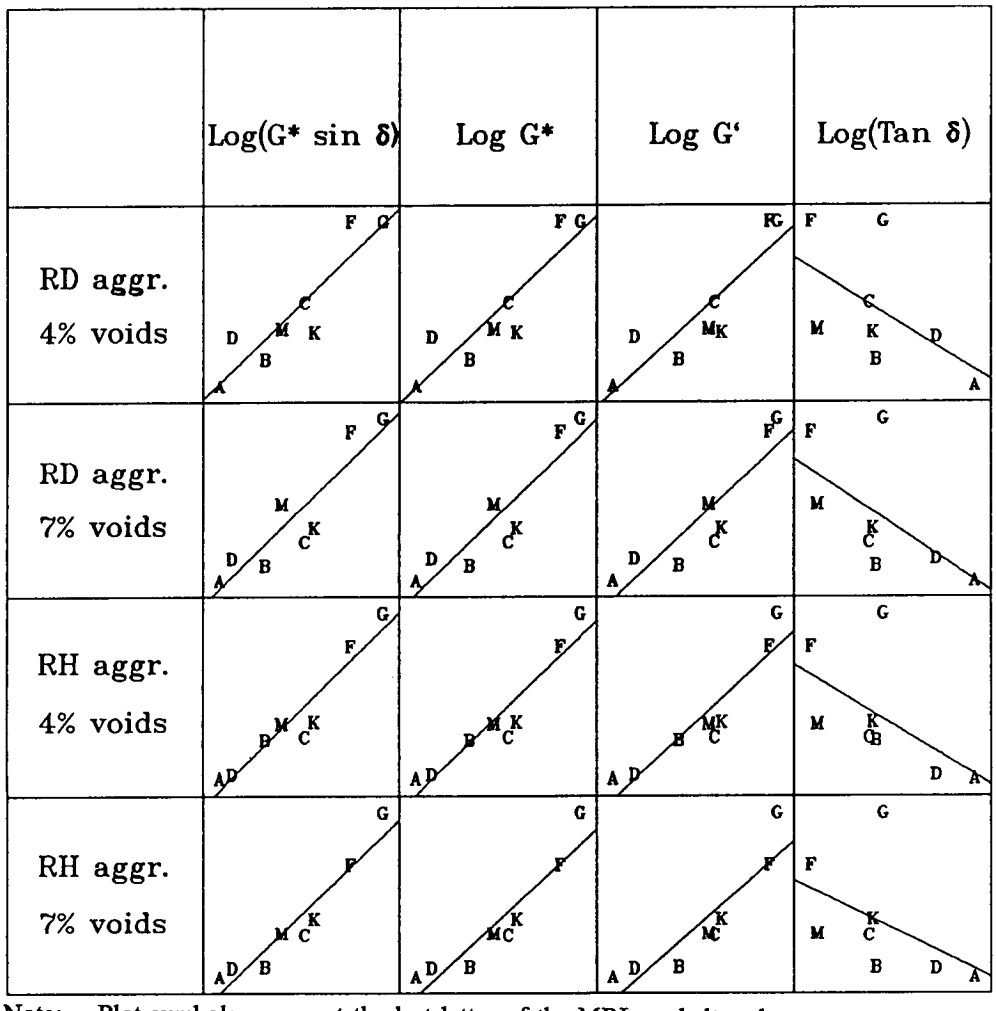

Note: Plot symbols represent the last letter of the MRL asphalt code.

Figure 3.2. SPLOM of flexural stiffness versus asphalt binder properties

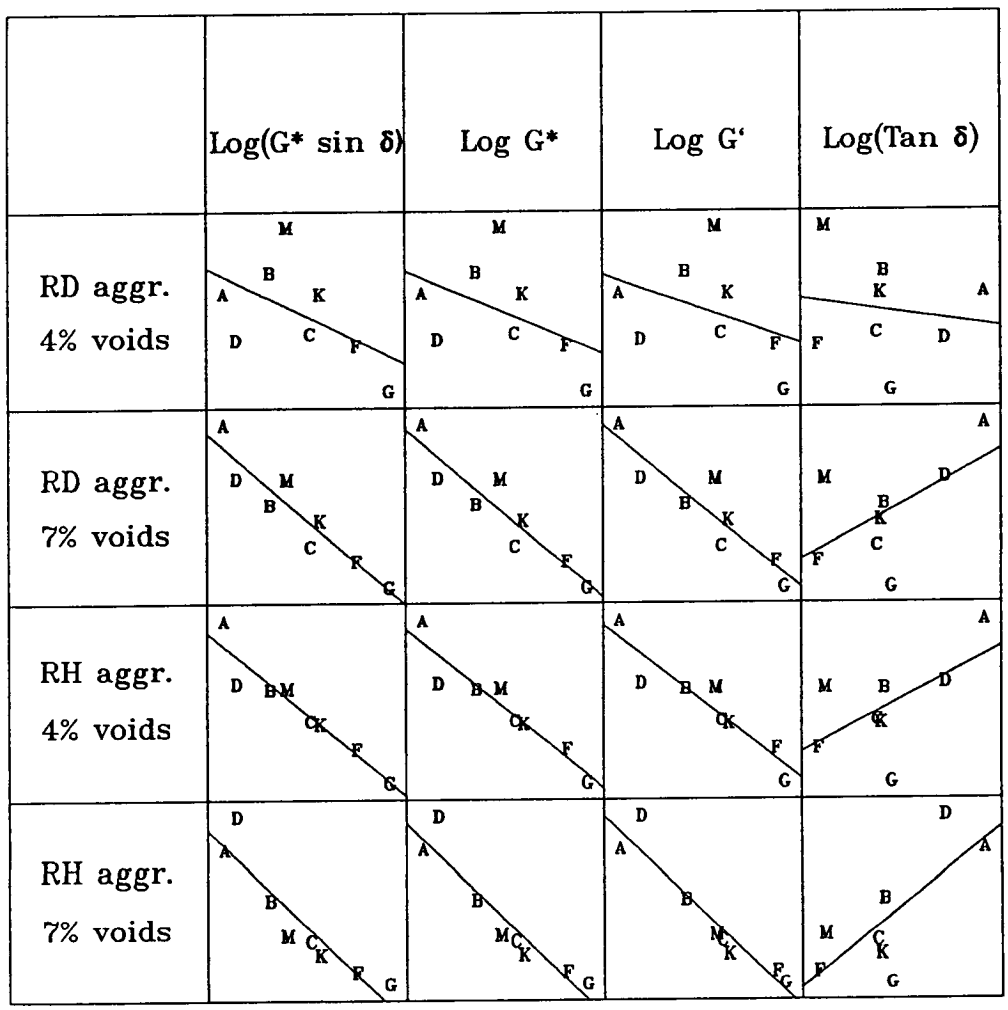

Note: Plot symbols represent the last letter of the MRL asphalt code.

Figure 3.3. SPLOM of fatigue life versus asphalt binder properties

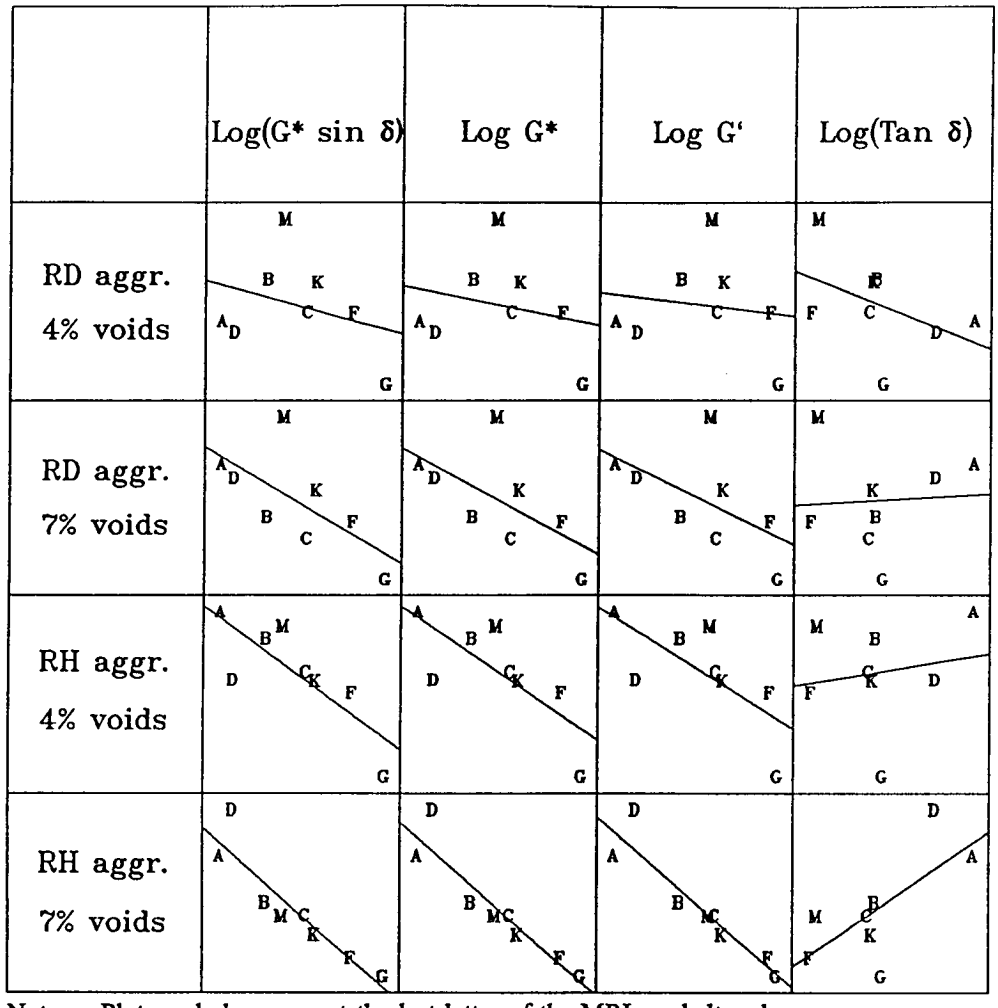

Note: Plot symbols represent the last letter of the MRL asphalt code.

Figure 3.4. SPLOM of total dissipated energy versus asphalt binder properties

Table 3.4. Pearson correlation coefficients

Mix Property	Flexural Stiffness	Fatigue Life	Dissipated Energy
Aggregate RD, 4% air voids			
Log(G* sin δ)	0.906	-0.535	-0.320
Log G*	0.904	-0.474	-0.241
Log G′	0.888	-0.401	-0.149
Log(tan δ)	-0.564	-0.156	-0.456
Aggregate RD, 7% air voids			
Log(G* sin δ)	0.905	-0.935	-0.672
Log G*	0.909	-0.927	-0.622
Log G′	0.897	-0.915	-0.568
Log(tan δ)	-0.606	0.578	0.062
Aggregate RH, 4% air voids			
Log(G* sin δ)	0.951	-0.951	-0.806
Log G*	0.946	-0.945	-0.760
Log G′	0.926	-0.933	-0.707
Log(tan δ)	-0.571	0.600	0.175
Aggregate RH, 7% air voids			
Log(G* sin δ)	0.952	-0.927	-0.925
Log G*	0.935	-0.944	-0.935
Log G′	0.902	-0.952	-0.935
Log(tan δ)	-0.473	0.753	0.692

Table 3.5. Spearman rank correlation coefficients

Mix Property	Flexural Stiffness	Fatigue Life	Dissipated Energy
Aggregate RD, 4% air voids			
Log(G* sin δ)	0.881	-0.595	-0.119
Log G*	0.881	-0.595	-0.119
Log G′	0.881	-0.595	-0.119
Log(tan δ)	-0.690	-0.048	-0.571
Aggregate RD, 7% air voids			
Log(G* sin δ)	0.905	-0.952	-0.714
Log G*	0.905	-0.952	-0.714
Log G′	0.905	-0.952	-0.714
Log(tan δ)	-0.571	0.500	0.167
Aggregate RH, 4% air voids			
Log(G* sin δ)	0.976	-0.976	-0.833
Log G*	0.976	-0.976	-0.833
Log G′	0.976	-0.976	-0.833
Log(tan δ)	-0.571	0.476	0.214
Aggregate RH, 7% air voids			
Log(G* sin δ)	0.976	-0.976	-0.952
Log G*	0.976	-0.976	-0.952
Log G′	0.976	-0.976	-0.952
Log(tan δ)	-0.571	0.524	0.548

the four plots). Only the regression on the mix containing aggregate RH and 7 percent air voids produces a high coefficient of determination and narrow confidence band. Regressions were statistically significant only for the mixes containing the aggregate RH. As with the other binder properties, different slopes of the regression lines and the different locations on the total dissipated energy axis are obtained for different mixes.

Binder Specification Compliance versus Mix Fatigue Response

A comparison was made between the SHRP binder specification for G* sin δ at 20°C related to fatigue cracking (Tables 1.1 and 3.2) and the fatigue life observed from flexural beam fatigue testing (Figure 3.6). In Table 3.2, asphalt AAA is the only asphalt that meets the specification requirement (G* sin $\delta \leq 3000$ kPa). Asphalt AAD almost meets the specification and, considering the precision of the binder property values reported by A-002A (10 percent coefficient of variation), might also be accepted. All other asphalts would be rejected for a project requiring a PG2-3 asphalt where the critical pavement distress was expected to be fatigue cracking.

According to Figure 3.6, mixes containing asphalts AAA and AAD generally provide the greatest fatigue lives. Thus, in most cases, the decision to allow only asphalt AAA or asphalt AAD on the project would have resulted in superior fatigue performance of the asphalt-aggregate mix. However, if the project was restricted to aggregate RD, and it was expected that good compaction would be achieved in the field (i.e., low air-void content), then some of the rejected asphalts might provide equal or greater fatigue lives. This observation underscores the importance of considering mix effects when evaluating asphalts and designing mixes for fatigue cracking resistance. It is recognized that the mixes used in this study were not subjected to long-term aging, which the binder properties in Table 3.2 reflect; however, the comparison has been made to illustrate the importance of mix effects.

Summary and Discussion of Results

The findings of the laboratory flexural beam fatigue validation effort are summarized and discussed below.

1. ANOVA indicates that the effect of asphalt on mix fatigue response is significant, but so are the effects of aggregate, air-void content, and the interactions of asphalt with aggregate, asphalt with air-void content, and aggregate with air-void content. However, the influence of asphalt on mix fatigue response was much greater than that of aggregate or air-void content; influences of interactions were relatively small.

2. The relationships between asphalt binder properties and asphalt-aggregate mix flexural stiffness and fatigue life were very strong. Relationships with dissipated energy were weaker but still strong for most cases. ANOVA

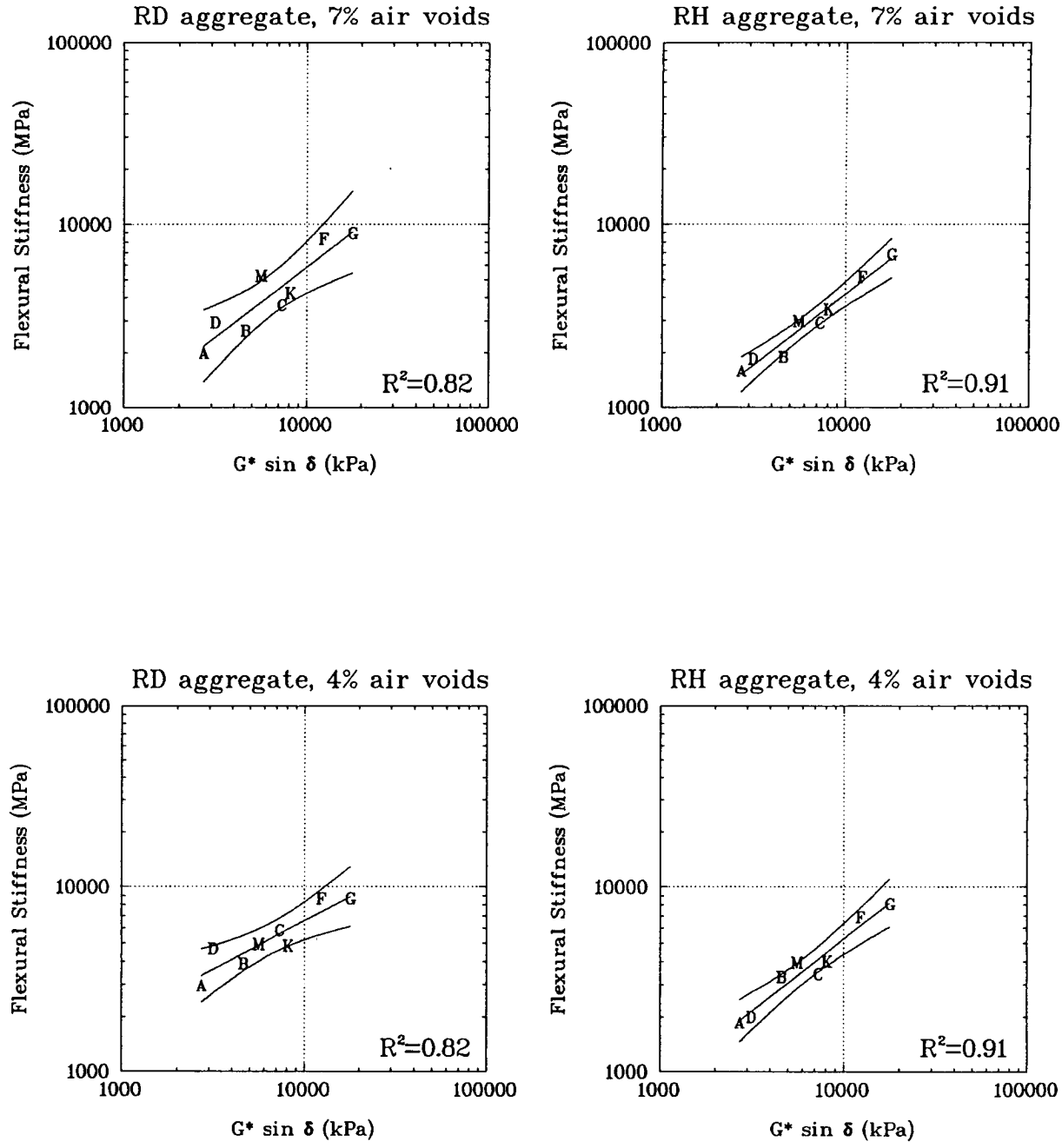

NOTE: Plot symbols represent the last letter of the MRL asphalt code.

Figure 3.5. Linear regression plots of flexural stiffness versus G* sin δ

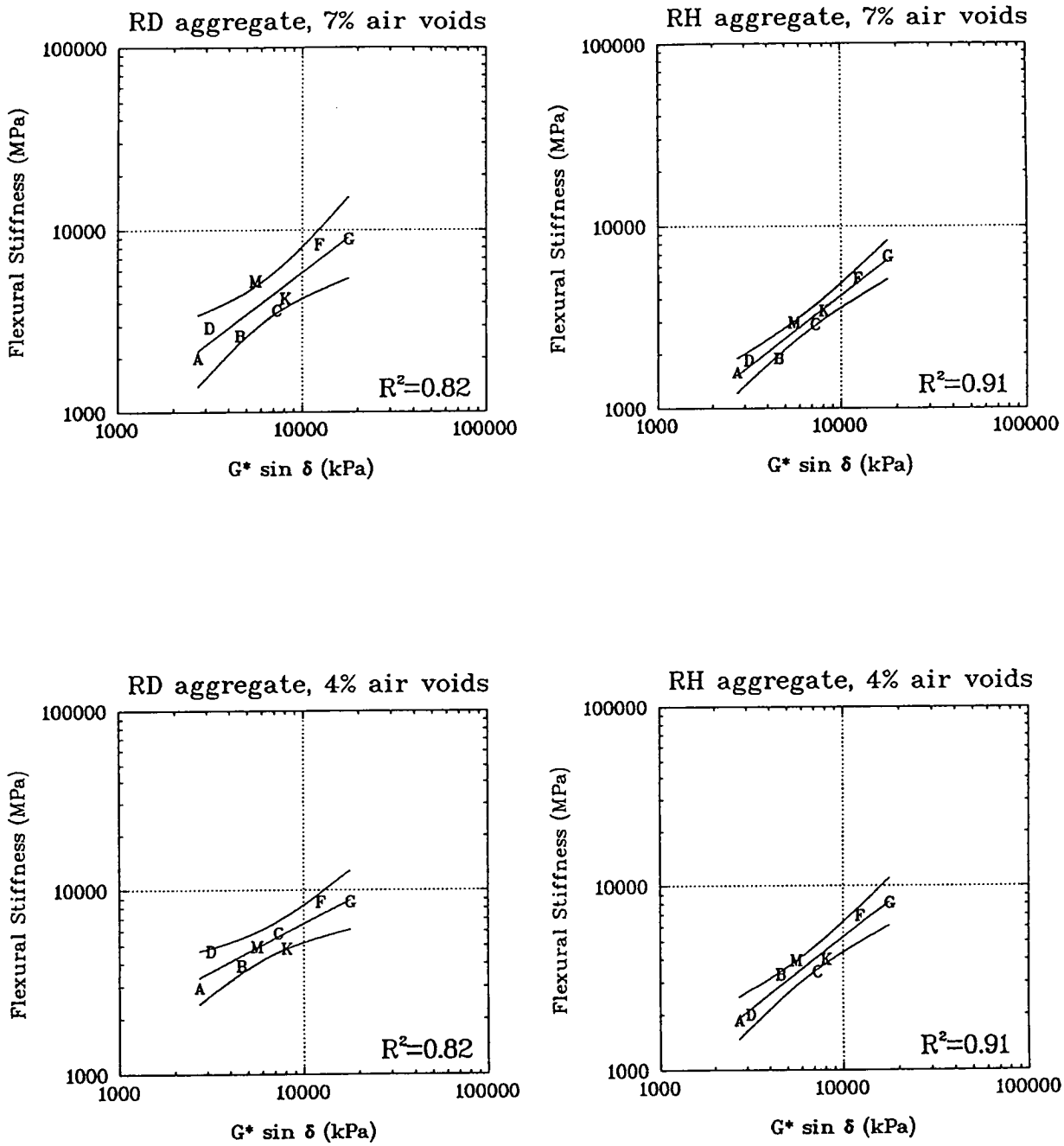

NOTE: Plot symbols represent the last letter of the MRL asphalt code.

Figure 3.6. Linear regression plots of fatigue life versus G* sin δ

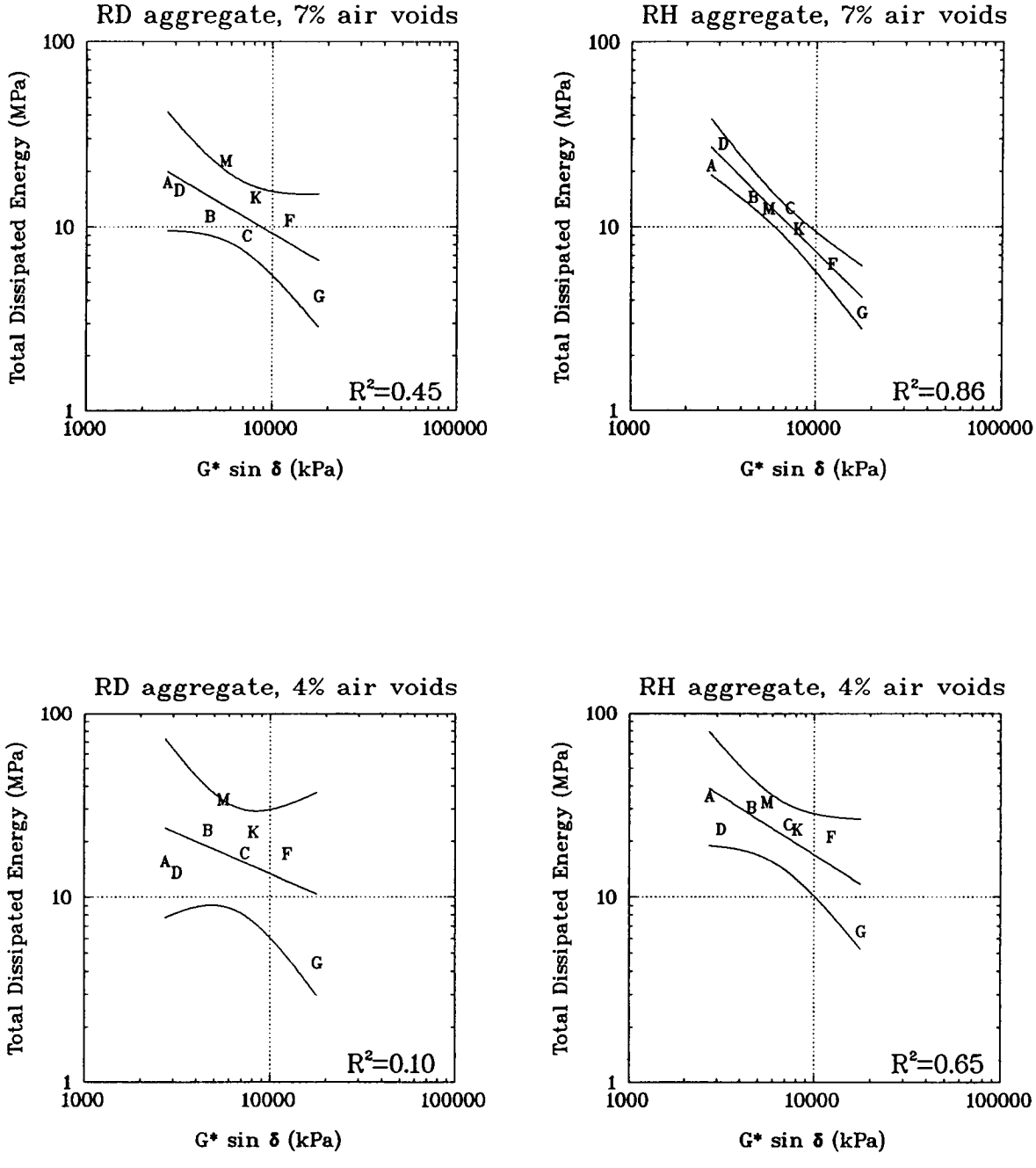

NOTE: Plot symbols represent the last letter of the MRL asphalt code.

Figure 3.7. Linear regression plots of total dissipated energy versus G* sin δ

indicated less influence of asphalt on dissipated energy and more unexplained error in the data. This suggests that the weaker relationships shown for dissipated energy are probably due to experimental error in the measurement or determination of dissipated energy.

Relationships between binder properties and fatigue life or dissipated energy were also weaker for mixes containing RD aggregate and low air-void contents. This probably reflects the effect of interparticle friction within the mix; RD aggregate is a 100 percent crushed quarry product, whereas RH aggregate is a partially crushed river gravel (Table 2.1).

3. Mix fatigue response is strongly related to G* sin δ, G*, and G′. Hence, it appears, the effect of the sin δ term of G* sin δ is negligible, and any of these terms could be used in the SHRP binder specification. However, the effect of sin δ may still be important for modified asphalts.

4. Results of regression analyses indicate that mix fatigue life can vary by as much as 100 percent for the same value of G*sinδ, depending on mix characteristics such as aggregate type and air-void content.

5. Overall, asphalt binder properties play an important role in the fatigue response of asphalt-aggregate mixes as measured in the laboratory. On the basis of the test results presented herein, the laboratory fatigue response of asphalt-aggregate mixes can be estimated from G* sin δ. However, depending on other mix characteristics (aggregate and air-void content), the reliability of such estimates may not be acceptable.

6. Based on the data presented herein, using the SHRP binder specification and the value of G* sin δ to accept or reject asphalts for a particular project in which fatigue cracking is of critical concern will, in many cases, result in a superior asphalt-aggregate mix. It is possible, however, that certain asphalts might be rejected based on the binder specification even though the mixes in which they have been incorporated would have provided equal or better fatigue performance.

7. On critical projects, asphalt-aggregate mix fatigue testing should be performed, since it will increase the reliability of estimates of mix fatigue response and prevent acceptable asphalts from being rejected.

Validation by Layered Elastic Analyses

Asphalt binder properties were compared with fatigue life estimates for hypothetical pavements constructed with various asphalts. Fatigue life estimates were made for two representative structural sections by (1) determining the maximum principal tensile strain at the bottom of the asphalt-concrete layer using a layered elastic analysis and (2) estimating

fatigue life from the relationship between fatigue life and tensile strain for a specific asphalt-aggregate mix using the calculated tensile strain.

Materials

The same materials used in the laboratory flexural fatigue analysis were used in this analysis.

Experiment

The same parameters that have been incorporated in the factorial experiment for the laboratory flexural fatigue study were used for this analysis, with the following exceptions:

1. Two different pavement structures were analyzed in place of two different strain levels (Figure 3.8), since strain level varies with the flexural stiffness of each mix.

2. Fatigue life was the only response variable analyzed.

Asphalt Binder Tests and Properties

Refer to the *Asphalt Binder Tests and Properties* section earlier in this chapter, under *Validation by Laboratory Flexural Beam Testing.*

Pavement Fatigue Life Analysis

Fatigue life calculations were made for a total of 64 pavement sections: 32 asphalt-aggregate mixes representing the asphalt-concrete layer in the 2 structural cases of Figure 3.8. Fatigue lives for each structure were estimated from the maximum principal tensile strain on the underside of the asphalt-concrete layer. Calculations of tensile strain were made using layered elastic theory with the ELSYM5 program (Federal Highway Administration 1985). Corresponding fatigue lives were then estimated from relationships obtained from laboratory testing. Figure 3.8 illustrates the assumed loading conditions and the locations for the strain calculations.

The following pavement structural sections were analyzed:

Case 1	Case 2
150 mm asphalt concrete	254 mm asphalt concrete
300 mm aggregate base	Weak subgrade
Moderate strength subgrade	

The loading condition corresponds to a 44 kN dual tire (one side of a 88 kN single axle) with a 300 mm center-to-center spacing between the tires and a tire pressure to 690 kPa. The initial flexural stiffnesses of the asphalt-concrete mixes as measured at the beginning of the laboratory fatigue test were used for the asphalt-concrete layer moduli. Stiffness was measured at 20°C and 10 Hz frequency and is considered to be representative of typical field conditions. A Poisson's ratio of 0.35 was used for all mixes. A stiffness modulus of 138 MPa and a Poisson's ratio of 0.3 were used for aggregate base, while stiffness moduli of 69 MPa and 34 MPa were used for the moderate and weak subgrades, respectively. Poisson's ratio was assumed to be 0.3 for both subgrades.

Locations of strain calculation were chosen at the bottom of the asphalt-concrete layer directly beneath the inside edge of the dual tire. ELSYM5 permits determination of the tensile strains for each component—that is, x, y, and z, as well as the principal strains. The maximum principal strain was input into the fatigue life relationship developed for each mix from the laboratory flexural fatigue testing program.

In the laboratory flexural fatigue testing validation effort, 32 asphalt-aggregate mixes were tested at two strain levels with a replicate at each level; refer to the *Experiment* section earlier in this chapter, under *Validation by Laboratory Flexural Beam Testing*. Using the laboratory test results, a linear regression model of log(fatigue life) versus log(flexural strain) was determined for each mix. The model is of the following general form:

$$n_f = K_1(1/\varepsilon)^{K_2}$$

where: n_f = fatigue life
ε = strain, μmm/mm
K_1, K_2 = regression coefficients

The strain calculated by ELSYM5 for the hypothetical pavement was entered into the above equation, and the corresponding fatigue life was predicted. Tables 3.6 and 3.7 present the strains calculated by ELSYM5, the regression equation coefficients and coefficients of Zdetermination (R^2), and the predicted fatigue lives for each pavement case.

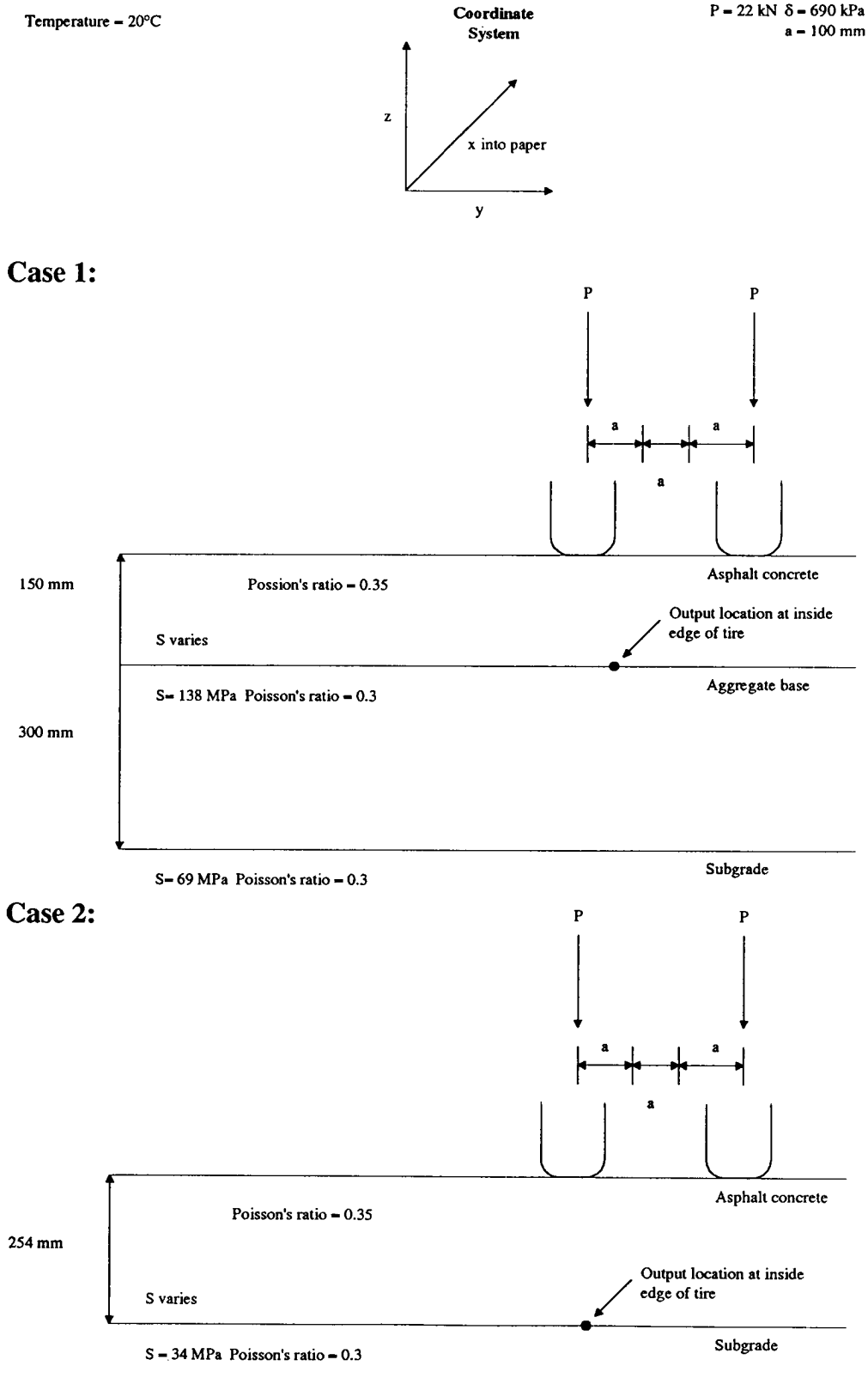

Figure 3.8. Hypothetical pavement structures and loading condition for layered elastic theory analysis

Relationships between Binder Properties and Fatigue Life Predictions

Figures 3.9 and 3.10 present SPLOMs for the two pavement cases. In general, there appear to be relationships between asphalt binder properties and predicted pavement fatigue life, except for mixes containing aggregate RH and 7 percent air voids. However, the relationships are not very strong, and there is significant scatter in the data. In this study, tan δ provides the strongest relationships. Note that the directions of the trends are opposite to those obtained in the laboratory flexural fatigue analysis; that is, in this study, predicted fatigue life generally increases as binder stiffness increases.

Table 3.8 presents Pearson and Spearman correlation results. Once again, these correlations corroborate the conclusions drawn from visual examination of the SPLOMs. The correlation coefficients confirm that tan δ provides the strongest relationship to predicted pavement fatigue life. Also note that the signs of the coefficients are opposite to those presented in Tables 3.4 and 3.5 for the laboratory flexural fatigue data.

Linear regressions between G* sin δ and predicted pavement fatigue life were also performed. As expected, the coefficients of determination (R^2) were low, ranging from 0.0 to 0.4; accordingly, the regressions were not statistically significant. Since the correlations were poor, regression plots are not shown; however, the lines in the SPLOMs are the regression lines.

Binder Specification Compliance versus Pavement Fatigue Life Predicted from Layered Elastic Theory

A comparison between the SHRP binder specification for G* sin δ related to fatigue cracking and the pavement fatigue life predicted from layered elastic theory is difficult because of the reversed relationship between G* sin δ and predicted pavement fatigue life. If it is confirmed in future studies that the direction of this relationship holds for certain pavement structures, the binder specification limit should be modified.

Summary and Discussion of Results

The findings of the layered elastic theory fatigue validation effort are summarized and discussed below.

1. The relationships between asphalt binder properties and predicted pavement fatigue life are the reverse of those observed in the laboratory flexural fatigue validation effort. For example, as the value of G* sin δ increases, laboratory flexural fatigue life decreases but predicted pavement fatigue life (for the pavement cases in this study) generally increases. This reversal in trends is believed to be caused by the different effect that asphalt binder stiffness, and

Table 3.6. Strains calculated from ELSYM5, mix fatigue life model constants, and fatigue lives predicted from the model (pavement case 1)

Asphalt-Aggregate Mix	x Strain (μmm/mm)	y Strain (μmm/mm)	K_1	K_2	R_2	Fatigue Life (Cycles)
AAA-RH-4	307	108	2.287E-05	-3.02	0.99	929,198
AAA-RH-7	342	110	5.589E-08	-3.77	0.81	651,712
AAB-RH-4	222	95.7	7.450E-10	-4.33	0.86	4,925,472
AAB-RH-7	309	109	8.678E-16	-6.10	0.99	2,237,036
AAC-RH-4	227	96.8	4.829E-08	-3.70	0.99	1,467,444
AAC-RH-7	247	101	5.279E-07	-3.33	0.95	543,089
AAD-RH-4	304	108	2.909E-05	-2.93	0.97	587,387
AAD-RH-7	311	109	9.859E-09	-4.02	0.99	1,238,614
AAF-RH-4	144	73	1.083E-09	-4.14	0.99	8,689,759
AAF-RH-7	170	82	5.073E-06	-2.90	0.95	433,474
AAG-RH-4	126	66.4	5.489E-08	-3.43	0.99	1,303,834
AAG-RH-7	145	73.4	3.830E-09	-3.72	0.95	729,306
AAK-RH-4	208	92.5	1.643E-10	-4.45	0.96	3,983,417
AAK-RH-7	215	94.2	6.821E-11	-4.50	0.95	2,177,083
AAM-RH-4	208	92.4	2.746E-05	-2.91	0.98	1,422,775
AAM-RH-7	238	99.1	7.660E-16	-6.05	0.99	6,396,438
AAA-RD-4	243	100	9.340E-11	-4.51	0.74	1,867,508
AAA-RD-7	298	108	3.609E-06	-3.16	0.99	499,877
AAB-RD-4	210	92.9	4.101E-08	-3.72	0.89	1,968,947
AAB-RD-7	263	103	7.721E-11	-4.51	0.94	1,080,620
AAC-RD-4	154	76.5	2.178E-09	-4.03	0.99	5,039,058
AAC-RD-7	212	93.5	2.184E-07	-3.38	1.00	570,476
AAD-RD-4	186	86.5	1.141E-10	-4.42	0.99	3,515,916
AAD-RD-7	239	99.3	1.024E-05	-2.97	0.72	584,061
AAF-RD-4	120	63.9	1.198E-10	-4.39	0.99	19,536,697
AAF-RD-7	122	64.9	1.584E-07	-3.39	0.97	2,930,862
AAG-RD-4	118	63.3	3.132E-10	-4.06	0.97	2,779,590
AAG-RD-7	116	62.3	3.948E-08	-3.42	0.88	1,137,446
AAK-RD-4	178	84.4	1.527E-06	-3.22	0.90	1,809,200
AAK-RD-7	191	88	3.331E-10	-4.30	0.98	3,266,865
AAM-RD-4	176	83.7	5.285E-13	-5.25	0.99	27,170,866
AAM-RD-7	165	80.1	3.360E-09	-4.04	0.98	6,422,500

Note: Fatigue life = K_1(strain K_2). Maximum strain (x or y) is used in fatigue life calculation.

Table 3.7. Strains calculated from ELSYM5, mix fatigue life model constants, and fatigue lives predicted from the model (pavement case 2)

Asphalt-Aggregate Mix	x Strain (μmm/mm)	y Strain (μmm/mm)	K_1	K_2	R_2	Fatigue Life (Cycles)
AAA-RH-4	237	157	2.287E-05	-3.02	0.99	2,030,141
AAA-RH-7	280	181	5.589E-08	-3.77	0.81	1,385,314
AAB-RH-4	151	104	7.450E-10	-4.33	0.86	26,132,809
AAB-RH-7	240	158	8.678E-16	-6.10	0.99	10,450,356
AAC-RH-4	156	107	4.829E-08	-3.70	0.99	5,878,902
AAC-RH-7	175	119	5.279E-07	-3.33	0.95	1,710,941
AAD-RH-4	235	155	2.909E-05	-2.93	0.97	1,248,863
AAD-RH-7	242	160	9.859E-09	-4.02	0.99	3,395,432
AAF-RH-4	87.3	62.8	1.083E-09	-4.14	0.99	68,996,886
AAF-RH-7	108	76.2	5.073E-06	-2.90	0.95	1,615,608
AAG-RH-4	74.7	54.3	5.489E-08	-3.43	0.99	7,834,361
AAG-RH-7	88.1	63.3	3.830E-09	-3.72	0.95	4,654,665
AAK-RH-4	139	96.4	1.643E-10	-4.45	0.96	23,945,378
AAK-RH-7	145	100	6.821E-11	-4.50	0.95	12,814,216
AAM-RH-4	139	96.2	2.746E-05	-2.91	0.98	4,597,561
AAM-RH-7	166	114	7.660E-16	-6.05	0.99	56,568,523
AAA-RD-4	171	117	9.340E-11	-4.51	0.74	9,110,336
AAA-RD-7	228	151	3.609E-06	-3.16	0.99	1,164,965
AAB-RD-4	140	97.4	4.101E-08	-3.72	0.89	8,898,022
AAB-RD-7	191	129	7.721E-11	-4.51	0.94	4,573,125
AAC-RD-4	94.8	67.8	2.178E-07	-4.03	0.99	35,605,761
AAC-RD-7	143	98.9	2.184E-07	-3.38	1.00	2,158,822
AAD-RD-4	120	84.3	1.141E-10	-4.42	0.99	24,395,209
AAD-RD-7	167	114	1.024E-05	-2.97	0.72	1,693,683
AAF-RD-4	70.4	51.4	1.198E-10	-4.39	0.99	203,054,606
AAF-RD-7	72.2	52.6	1.584E-07	-3.39	0.97	17,350,583
AAG-RD-4	69.3	50.6	3.132E-10	-4.06	0.97	24,123,750
AAG-RD-7	67.7	49.6	3.948E-08	-3.42	0.88	7,174,042
AAK-RD-4	114	80.5	1.527E-06	-3.22	0.90	7,596,358
AAK-RD-7	124	87.1	3.331E-10	-4.30	0.98	20,934,442
AAM-RD-4	112	79.2	5.285E-13	-5.25	0.99	291,507,929
AAM-RD-7	103	73.2	3.360E-09	-4.04	0.98	43,099,962

Notes Fatigue life = K_1(strain K_2). Maximum strain (x or y) is used in fatigue life calculation.

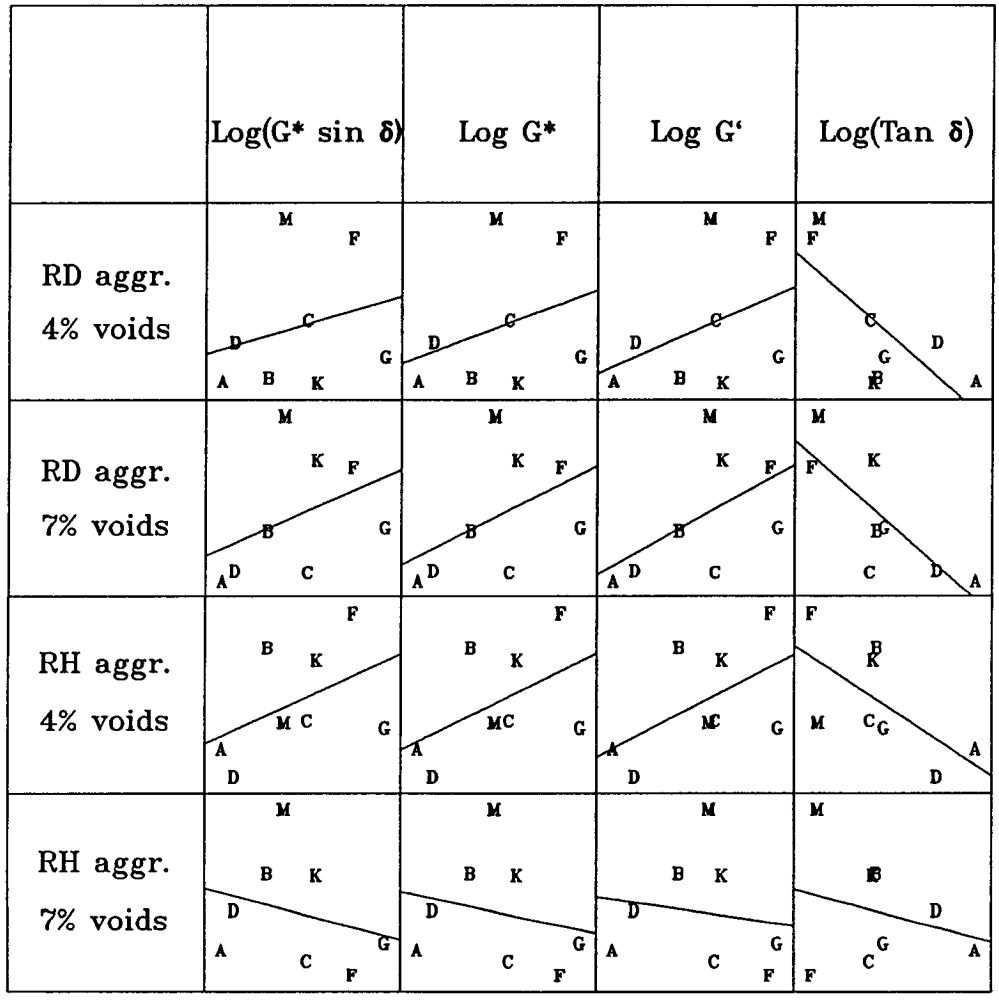

Note: Plot symbols represent the last letter of the MRL asphalt code.

Figure 3.9. SPLOM of fatigue life versus asphalt binder properties for pavement case 1

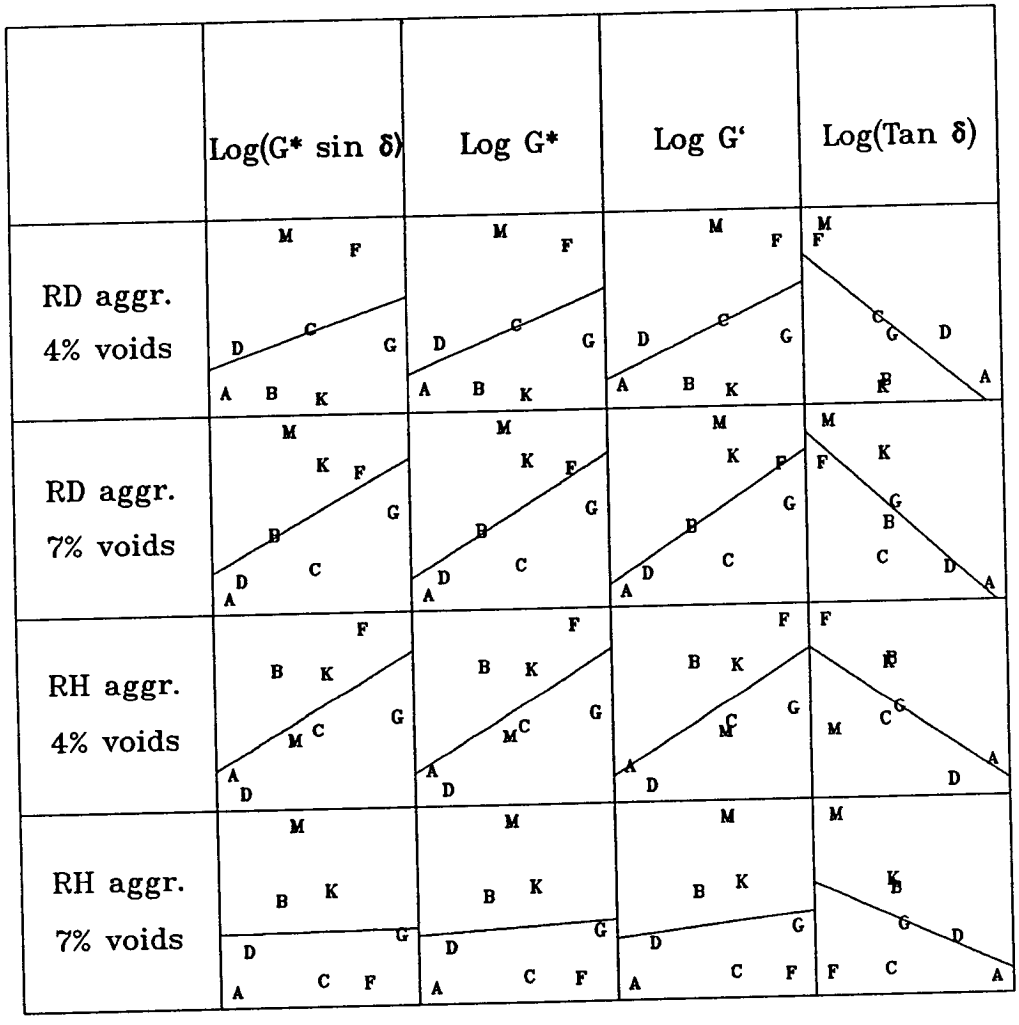

Note: Plot symbols represent the last letter of the MRL asphalt code.

Figure 3.10. SPLOM of fatigue life versus asphalt binder properties for pavement case 2

hence mix flexural stiffness, has on laboratory flexural fatigue specimens as compared with the same mix in an asphalt-concrete pavement layer. Recall that laboratory fatigue testing was performed in the controlled-strain mode of loading; thus all specimens, regardless of their flexural stiffness, were subjected to the same strain level. At the strain levels used in the laboratory validation effort, fatigue damage accumulates more rapidly in mixes with higher flexural stiffness, causing the specimens to fail more quickly. In the case of asphalt-concrete pavement layers, under a constant level of load, the strain varies as a function of flexural stiffness. These conditions are analogous to laboratory flexural fatigue tests performed under controlled-stress conditions. Apparently, the fatigue damage experienced in fatigue damage experienced by the asphalt-concrete layer when it deflects less because of the increase in flexural stiffness. Thus, the net effect is that pavement fatigue life increases as flexural stiffness increases.

2. The reversal in relationships between asphalt binder stiffness and fatigue life may not occur for pavements with asphalt-concrete layer thicknesses less than those in the examples used in this study. The fatigue response of pavements with thin asphalt-concrete layers (e.g., less than 102 mm) is generally assumed to represent a controlled-strain condition. Had a hypothetical pavement structure with a thin asphalt-concrete layer been included in this study, it might have been observed that the relationship between asphalt binder stiffness and fatigue life was the same as that observed in the laboratory fatigue validation investigation. Additional study will be necessary to confirm this.[4]

---

[4]A later study (Tayebali et al. 1993) completed after this report does suggest for a range in asphalt-concrete layers thicknesses from 50 mm to 300 mm the following:

> Once again, results of the simulation generally seem to be independent of mode of loading. For the same mix stiffness, low air-void mixes were always superior to high air-void mixes. As anticipated, for thin pavements stiffer mixes demonstrated inferior fatigue resistance while, for thick pavements, stiffer mixes were preferred. The only difference between mode of loading is in identifying the borderline between "thin" and "thick" pavements. Based on this analysis, this difference becomes important for surface thicknesses in the range of three to five inches. The borderline thickness, however, is expected to vary depending on such factors as temperature, mix properties, and the stiffness of the pavement surface layer relative to that of its support.
>
> In summary, this analysis has demonstrated the importance of mode of loading in the proper interpretation of laboratory fatigue data. It has confirmed that fatigue lives under controlled-strain loading generally exceed those under controlled-stress loading and that, upon casual inspection, effects of mix stiffness on fatigue life are generally reversed for the two modes of loading. However, when test results are interpreted in terms of the performance expected of the pavements in which they are placed, it appears that controlled-stress and controlled-strain testing may yield similar mix rankings especially for the substantial pavement structures characteristic of the nation's primary trucking highways.

Table 3.8. Pearson and Spearman correlation coefficients of predicted pavement fatigue life versus asphalt binder properties

Mix	Log(G* sin δ)	Log G*	Log G′	Log(tan δ)
Pearson Correlations				
Pavement case 1				
Aggregate RD, 4% air voids	0.253	0.327	0.395	-0.743
Aggregate RD, 7% air voids	0.404	0.469	0.532	-0.792
Aggregate RH, 4% air voids	0.460	0.501	0.541	-0.647
Aggregate RH, 7% air voids	-0.260	-0.212	-0.148	-0.257
Pavement case 2				
Aggregate RD, 4% air voids	0.313	0.380	0.439	-0.720
Aggregate RD, 7% air voids	0.534	0.593	0.650	-0.833
Aggregate RH, 4% air voids	0.614	0.647	0.678	-0.686
Aggregate RH, 7% air voids	0.013	0.060	0.121	-0.436
Spearman Correlations				
	Log(G* sin δ)	**Log G***	**Log G′**	**Log(tan δ)**
Pavement case 1				
Aggregate RD, 4% air voids	0.190	0.190	0.190	-0.643
Aggregate RD, 7% air voids	0.548	0.548	0.548	-0.643
Aggregate RH, 4% air voids	0.476	0.476	0.476	-0.738
Aggregate RH, 7% air voids	-0.262	-0.262	-0.262	0.071
Pavement case 2				
Aggregate RD, 4% air voids	0.413	0.413	0.413	-0.571
Aggregate RD, 7% air voids	0.619	0.619	0.619	-0.738
Aggregate RH, 4% air voids	0.643	0.643	0.643	-0.571
Aggregate RH, 7% air voids	0.190	0.190	0.190	-0.262

3. In addition to the reversal of relationships, the relationships between asphalt binder properties and predicted pavement fatigue life were not nearly as strong as those observed in the laboratory fatigue validation effort. Further analysis also showed that the relationship between flexural stiffness of the mix and fatigue life was weaker for predicted pavement fatigue life than for laboratory fatigue life. The weaker relationship may be a result of using the mix regression equations to calculate fatigue life. Refer to Tables 3.6 and 3.7. These equations introduce some additional error (because $R^2 < 1$) into the prediction of pavement fatigue life from $G^* \sin \delta$.

4. The results of this study still indicate that asphalt binder properties are important in evaluating fatigue cracking. In this study, $\tan \delta$ appears to have the most influence on predicted pavement fatigue life, as opposed to $G^* \sin \delta$. However, the importance of considering the influence of pavement structure effects is also demonstrated.

Conclusions

Results of the investigation to validate the effect of asphalt binder properties on the fatigue response of asphalt-aggregate mixes indicate that the asphalt has a significant influence on fatigue response. However, the results also indicate that other mix characteristics, such as the type of aggregate and the air-void content, also influence this response, although to a lesser degree. Therefore, estimates of asphalt-aggregate mix fatigue response may be improved by performing laboratory flexural fatigue testing on mixes, in addition to or in lieu of asphalt binder testing.

In the prediction of fatigue cracking in pavement structures, it appears that asphalt binder properties are also important, but pavement structure effects may be equally or more important. In fact, pavement structure effects may influence fatigue cracking so much that the relationship between $G^* \sin \delta$ and pavement fatigue life may completely reverse as the thickness of the asphalt-concrete layer changes. Although this study has some limitations, it identifies an issue worthy of further evaluation. That is, if further investigation confirms that the direction of the relationship between $G^* \sin \delta$ and pavement fatigue life depends on the pavement structure, the binder specification will need to include provisions for pavement structure effects.

4

Validation of Binder Properties Related to Permanent Deformation

This chapter summarizes studies performed by the A-003A investigators to validate the relationships between asphalt binder properties and the permanent deformation response of asphalt-aggregate mixes. The asphalt binder properties were those recommended by the A-002A contractor and shown in Strategic Highway Research Program (SHRP) binder specifications (Table 1.1). Validation then consisted of evaluation of the relationship of these binder properties to the following:

1. Rutting response of mixes tested in a wheel-tracking device.

2. Permanent deformation response of the same mixes tested in the shear test equipment developed as part of the A-003A endeavor.

This chapter is divided into two main sections, presenting the findings related to the items listed above. For more details see Sousa et al., (1993).

Validation by Wheel-Tracking Testing

Asphalt binder properties were compared with the permanent deformation response of asphalt-aggregate mix specimens subjected to wheel-tracking loading. In this study, the wheel-tracking test was used as a surrogate for real pavement performance. It attempts to simulate the stress conditions caused by a wheel rolling across an asphalt-aggregate mix surface.

Materials

Sixteen asphalt binders and two aggregates from the Materials Reference Library (MRL) were used in this study: asphalts AAA, AAB, AAC, AAD, AAF, AAG, AAK, AAL, AAM, AAV, AAW, AAX, AAZ, ABA, ABC, and ABD and aggregates RD and RH.

Table 2.1 lists the grade (current America Association of State Highway and Transportation Officials specifications) for each asphalt. Asphalt binder properties to be validated are discussed in a later section of this chapter. Table 2.1 also provides information on the characteristics of each aggregate.

The aggregate gradations shown in Table 2.2 were used to prepare mixes by rolling-wheel compaction at the asphalt contents shown in Table 2.2 for the two aggregates. Specimens were compacted to target air-void contents of 4 and 7 percent. Since it was not possible to precisely control the air-void content during the compaction of the mixes, actual air-void contents were measured for each specimen and adjustments were made to test data (discussed later in this chapter) before analyzing it. Details of the compaction procedure and methods for air-void measurement are included in Harvey (1991).

Experiment Design

A full-factorial experiment was designed to allow all main factors and two-factor interactions to be evaluated. The factorial matrix consisted of 16 asphalts, 2 aggregates, and 2 air-void content levels, resulting in a total of 64 cells. Each cell had only 1 replicate, for a total of 64 tests. Therefore, the three-factor interaction of asphalt source, aggregate source, and air-void content was used as an estimate of experimental error. The factorial experiment is summarized below

Experimental Design Factors and Levels (Independent Variables):

Factor	Levels
Asphalt source	16 (see list above)
Aggregate source	2 (see list above)
Air-void content, %	2 (4, 7)
Replicates:	1 per cell
Total number of tests:	64

Rutting Response Variables (dependent variables, to be explained later):

Normalized rutting rate (mm/MPa/hr)—linear regressed rut rate between 2000 and 4000 passes divided by contact stress

Total rut depth (mm)—rut depth after 5000 passes

Asphalt Binder Tests and Properties

Asphalt binder properties were provided by the A-002A contractor for this study. The properties were measured using dynamic mechanical analysis of asphalt cement binders. Binder properties included complex shear modulus (G*), phase angle (δ), storage modulus (G′, which is equal to G* cos δ), loss modulus (G″, which is equal to G* sin δ), and loss tangent (tan δ, which is equal to G″/G′). G′ includes the elastic response of the binder, and G″ includes its viscous response; both parameters include "delayed elastic" response of the binder. The complex shear modulus incorporates both elastic and viscous responses of the binder in that $(G^*)^2 = (G')^2 + (G'')^2$. More detailed information on the asphalt binder properties and their interrelationships is presented in the SHRP Project A-002A report (Petersen et al. 1992).

The SHRP binder specification is based on the premise that G*/sin δ is inversely related to permanent deformation of asphalt-aggregate mixes. Specifically, as the value of G*/sin δ increases, the propensity of a mix to rut decreases (Table 1.1). The specification requires the value of G*/sin δ to exceed 2.0 kPa when tested at 10 rad/sec at the specified temperature after having been aged in the rolling thin-film oven test (RTFOT).

The A-002A contractor has hypothesized that the parameter used to assess the permanent deformation characteristics of asphalt binders should consider both elastic and viscous binder response. G* has both elastic and viscous components. The sin δ component of the G*/sin δ parameter varies depending on whether the response of the binder is elastic or viscous. Elastic binder response is represented by a low phase angle (δ) value, and viscous binder response is represented by a high δ value. The phase angle δ varies between 0 and 90 degrees, so sin δ varies between 0 and 1. The value of sin δ is always less than 1, so the value of G*/sin δ will always be greater than the value of G*. Also, sin δ approaches 1 asymptotically as δ approaches 90 degrees. Thus, G*/sin δ is much greater than G* for elastic binders because the value of sin δ is relatively low. The values of G*/sin δ and G* are nearly equal for viscous binders because the value of sin δ is close to 1. In conclusion, G*/sin δ reflects both the elastic and viscous behavior of asphalt binders, and its selection for use in the binder specification appears to be justified.

Asphalt binder properties provided by the A-002A contractor for this study are presented in Table 4.1. The binders were aged according to ASTM D-1754, the thin-film oven test (TFOT), before testing in order to simulate short-term aging during the construction process. For short-term aging, the SHRP binder specification prefers ASTM D-2872 (the RTFOT) but permits the TFOT.

The A-002A contractor tested asphalt binders over a wide range of temperatures and load frequencies to develop a rheological model that explains asphalt binder response. From such a model, binder properties can be calculated for any combination of test temperature and load frequency. Although Table 4.1 reports asphalt binder properties for a test temperature of 40°C and a load frequency of 10 rad/sec (1.59 Hz), binders were not tested under this combination of conditions. Rather, the properties shown in Table 4.1 were calculated using the rheological model developed by the A-002A researchers.

It should be noted that the 40°C test temperature is less than the test temperature of any performance grade (PG) of asphalt listed in the binder specification (see Table 1.1). The lowest test temperature in the specification is 45°C, for PG1 asphalts. Asphalt binder properties were calculated for a temperature of 40°C, since the wheel-tracking specimens were tested at this temperature. (Note that 40°C may not be appropriate for the evaluation of permanent deformation under all circumstances.)

According to the A-002A contractor, the precision of the values in Table 4.1 is a function of the magnitude of each value, and the coefficient of variation for each of the properties is approximately 10 percent within the ranges of the data tested. In later tables and figures, a log (base 10) transformation was applied to G′ and tan δ values for statistical purposes (Coplantz and Tayebali 1992).

Asphalt-Aggregate Mix Tests and Properties

In the wheel-tracking tests performed by SWK Pavement Engineering Ltd. at the University of Nottingham, a wheel, fitted with a solid rubber tire, passes over the top of a 203 mm diameter cylindrical core specimen at a frequency of approximately 3 Hz (20 rad/sec). Each specimen was subjected to 5000 load repetitions (approximately 2 hr). Tests were performed with an applied load of approximately 620 N; the contact area of the tire is 850 mm^2, which gives a corresponding contact stress of approximately 730 kPa.

During the test, the average rut depth was calculated at every 20th pass from 11 individual readings taken over a 100 mm length. The area of the rut section was calculated, using Simpson's rule, and the average depth computed, given the base length of 100 mm and assuming that the section was rectangular.

Two rutting parameters were measured from the wheel-tracking test data: normalized rut rate and total rut depth. The normalized rut rate is the rate of increase in rut depth (in millimeters per hour) between 2000 and 4000 load passes divided by the contact stress of the wheel. The total rut depth is the average rut depth (in millimeters) at the end of the test (i.e., after 5000 passes). SWK staff consider rut rate a more reliable indicator of permanent deformation performance because it is less likely to be affected by "initial start-up errors" and, perhaps, additional compaction of the specimen during the initial stages of the test.

Detailed information on the wheel-tracking equipment and procedure is presented in a report by Gibb et al. (1991).

Although asphalt-aggregate specimens were prepared at low and high air-void content it was impossible to achieve the target air-void content of 4 or 7 percent in each specimen. Since it was known from previous studies that air-void content affects the permanent deformation response of asphalt-aggregate mixes, it was important that mixes represent the same air-void content so that meaningful comparisons could be made. Therefore, the rutting response variables for each specimen were adjusted to account for the difference between the specimen's actual air-void content and the desired target content. This

Table 4.1. Asphalt binder properties provided by A-002A (after TFOT, at 40°C and 10 rad/sec)

Asphalt Source	G* (kPa)	G′ (kPa)	G″ (kPa)	tan δ	G*/sin δ (kPa)
AAA	51	14	49	3.50	53
AAB	76	24	72	3.05	80
AAC	88	22	85	3.88	90
AAD	71	26	66	2.57	76
AAF	172	43	166	3.83	178
AAG	146	17	145	8.66	147
AAK	137	54	126	2.33	149
AAL	51	15	49	3.17	54
AAM	113	43	105	2.44	123
AAV	32	18	27	1.48	39
AAW	138	49	129	2.62	148
AAX	163	44	157	3.57	169
AAZ	93	13	92	6.82	94
ABA	110	51	97	1.90	124
ABC	88	34	81	2.36	95
ABD	155	95	123	1.30	196

adjustment was performed statistically by using an analysis of variance (ANOVA) model to determine the effect of air-void content and any interaction it had with asphalt source or aggregate source and then using the resulting coefficients to adjust the response variable (Coplantz and Tayebali 1992).

The wheel-tracking test results are presented in Table 4.2. Each specimen is identified by a unique combination of asphalt source, aggregate source, and air-void content. The data in Table 4.2 have been adjusted to account for variations in air-void content from the experiment target values. The statistical analyses presented herein were performed on this data. Raw test data (i.e., before adjustment) are contained in the report from SWK Pavement Engineering (Gibb et al. 1991).

Relationships between Binder and Mix Properties

Both the asphalt binders and asphalt-aggregate mixes were subjected to similar aging and testing conditions. The asphalts were aged according to the TFOT to simulate the short-term aging effects of the construction process. Asphalt-aggregate mixes were also subjected to short-term aging; after mixing, they were placed in an oven at 135°C for 4 hr.

The asphalt properties were calculated for the same temperature at which the mixes were tested, 40°C. Although asphalt binder properties were calculated for a load frequency of 10 rad/sec (1.6 Hz)—that called for in the binder specifications—and asphalt-aggregate mixes were tested at a load frequency of 20 rad/sec (3.2 Hz), the difference in loading rates is not considered significant, since the binder properties are logarithmic functions of loading time.

Analysis of Variance

As mentioned above, ANOVA was performed to determine the influence of experiment factors on rutting response variables (Coplantz and Tayebali 1992). ANOVA indicated that the asphalt source, aggregate source, and air-void content each significantly affect the rutting response of asphalt-aggregate mixes. In addition, the interaction of asphalt source with aggregate source was shown to significantly affect rutting response. A minimum confidence level of 95 percent was used to determine significance; however, all the factors and the interaction were significant at confidence levels equal to or greater than 99 percent.

The ANOVA model indicated that the factors and the interaction accounted for the variation of rutting response in the following approximate proportions:

Rutting Response Variable	Factor or Interaction	Proportional Effect, %
Rut rate	Asphalt	26
	Aggregate	29
	Air-void content	8
	Asphalt-aggregate	27
	ANOVA model error	15
Rut depth	Asphalt	31
	Aggregate	19
	Air-void content	8
	Asphalt-aggregate	28
	ANOVA model error	14

The above results illustrate the dominant effects of asphalt and aggregate on mix rutting response. Since asphalt source significantly affects rutting response, it was expected that additional analyses would show some level of relationship between asphalt binder properties and asphalt-aggregate mix rutting response. However, since the aggregate factor and the interaction of asphalt with aggregate were so significant, it was expected that the effect of

Table 4.2. Wheel-tracking rutting results, adjusted for air-void content (after short-term oven aging, at 40°C and 20 rad/sec)

Asphalt Source	Aggregate Source	Air Voids (%)	Total Rut Depth at 5000 Passes (mm)	Normalized Rut Rate between 2000 and 4000 Passes (mm/MPa/hr)
AAA	RD	4.0	2.07	0.37
AAA	RD	7.0	1.90	0.47
AAA	RH	4.0	2.75	0.71
AAA	RH	7.0	3.07	0.84
AAB	RD	4.0	1.38	0.34
AAB	RD	7.0	2.45	0.37
AAB	RH	4.0	1.50	0.36
AAB	RH	7.0	2.80	0.57
AAC	RD	4.0	1.23	0.23
AAC	RD	7.0	1.01	0.21
AAC	RH	4.0	4.64	1.49
AAC	RH	7.0	5.57	1.52
AAD	RD	4.0	0.96	0.26
AAD	RD	7.0	2.43	0.47
AAD	RH	4.0	306	1.02
AAD	RH	7.0	3.70	1.18
AAF	RD	4.0	1.21	0.36
AAF	RD	7.0	0.89	0.22
AAF	RH	4.0	1.01	0.31
AAF	RH	7.0	2.04	0.66
AAG	RD	4.0	1.03	0.21
AAG	RD	7.0	2.53	0.84
AAG	RH	4.0	1.57	0.40
AAG	RH	7.0	3.72	0.95
AAK	RD	4.0	1.51	0.31
AAK	RD	7.0	1.92	0.64
AAK	RH	4.0	2.05	0.46
AAK	RH	7.0	1.31	0.34
AAL	RD	4.0	1.70	0.34
AAL	RD	7.0	2.36	0.43
AAL	RH	4.0	3.27	0.79
AAL	RH	7.0	3.11	0.95

Table 4.2 (continued). Wheel-tracking rutting results, adjusted for air-void content (after short-term oven aging at 40°C and 20 rad/sec)

Asphalt Source	Aggregate Source	Air Voids (%)	Total Rut Depth at 5000 Passes (mm)	Normalized Rut Rate between 2000 and 4000 Passes (mm/MPa/hr)
AAM	RD	4.0	1.31	0.17
AAM	RD	7.0	1.04	0.27
AAM	RH	4.0	1.08	0.22
AAM	RH	7.0	0.85	0.43
AAV	RD	4.0	1.46	0.36
AAV	RD	7.0	2.04	0.44
AAV	RH	4.0	2.20	0.66
AAV	RH	7.0	2.56	0.78
AAW	RD	4.0	1.36	0.21
AAW	RD	7.0	1.52	0.27
AAW	RH	4.0	0.83	0.23
AAW	RH	7.0	3.13	1.04
AAX	RD	4.0	1.35	0.15
AAX	RD	7.0	1.80	0.35
AAX	RH	4.0	1.05	0.31
AAX	RH	7.0	1.93	0.32
AAZ	RD	4.0	1.13	0.22
AAZ	RD	7.0	1.96	0.59
AAZ	RH	4.0	2.18	0.49
AAZ	RH	7.0	2.69	0.77
ABA	RD	4.0	1.04	0.28
ABA	RD	7.0	1.77	0.31
ABA	RH	4.0	1.48	0.41
ABA	RH	7.0	2.82	0.54
ABC	RD	4.0	0.81	0.16
ABC	RD	7.0	1.19	0.29
ABC	RH	4.0	1.13	0.38
ABC	RH	7.0	1.63	0.63
ABD	RD	4.0	1.68	0.31
ABD	RD	7.0	1.67	0.58
ABD	RH	4.0	1.83	0.70
ABD	RH	7.0	1.89	0.74

asphalt properties alone would be masked somewhat by these other influences. Therefore, separate analyses were made on the following data sets:

Aggregate Source	Air Void Content, %
RD	4
RD	7
RH	4
RH	7

Scatterplots

Scatterplot matrices (SPLOMs) were prepared to graphically illustrate the relationships between the rutting response variables and each of the asphalt binder properties. The SPLOMs provide a quick graphical look at relationships between several variables at the same time. The results are presented in Figures 4.1 and 4.2. Each matrix is a compilation of 20 individual scatterplots. For any given scatterplot, the independent variable (binder property) is listed at the top of each column and is plotted along the x axis of each plot. The dependent variable (mix rutting response) is plotted along the y axis. Each row of plots presents the results for the indicated rutting response variable measured from mixes with the indicated air-void contents. Figure 4.1 presents results for mixes containing aggregate RD, and Figure 4.2 presents results for mixes containing aggregate RH. The data points in each plot are depicted by the last letter of the MRL source code for each asphalt. The lines show the best linear fit by least-squares regression.

These results indicate a rather weak relationship between binder properties and mix rutting response. In general, as $G^*/\sin\delta$, G^*, G', or G'' increases, rut rate and rut depth decrease. This trend satisfies engineering logic and conforms to the rationale presented in the binder specification (i.e., less rutting potential with stiffer asphalts). As for $\tan\delta$, the opposite trend is shown for most mix cases. No one binder property stands out as providing the strongest relationship with rutting response. Overall, $\tan\delta$ appears to provide the weakest relationship. Neither rut rate nor rut depth is more strongly related to binder properties. Finally, there is substantial data scatter that suggests it will be difficult to reliably predict rutting from binder properties. There appears to be less data scatter associated with mixes containing aggregate RH (with the exception of those containing asphalt AAC).

Pearson Correlations

The strength of the relationships depicted in Figures 4.1 and 4.2 was quantified through the use of Pearson correlations. The Pearson correlation coefficient measures the strength of a linear relationship between two variables. The coefficient, R, can range between -1 and +1, with negative coefficients indicating a negative slope or inverse relationship between the

two variables. Coefficients close to -1 or +1, indicate strong relationships between the two variables.

Pearson correlation coefficients are presented in the first and second columns of Table 4.3. The coefficient values generally corroborate the conclusions drawn from visual examination of the SPLOMs. However, the values in Table 4.3 indicate that binder properties have a slightly better relationship to total rut depth than to rut rate, except for mixes containing aggregate RD and 4 percent air voids. None of the coefficients are very high (i.e., close to -1.0 or +1.0) because of the data scatter exhibited in Figures 4.1 and 4.2. The strongest relationship is between G*/sin δ, G*, or G″ and total rut depth for mixes containing aggregate RH and 4 percent air voids.

Ranking Analysis

Spearman rank correlations were performed to see whether weak relationships indicated by Pearson correlations were perhaps stronger when based on relative ranking of asphalt performance represented by binder properties and mix rutting response. The Spearman rank correlation is simply a Pearson correlation computed on the same data after converting the data to ranks. Table 4.3 presents Spearman rank correlation coefficients in the third and fourth columns. A review of the results indicates that relationships are strengthened slightly by using ranks instead of actual data, except for mixes containing aggregate RD and 4 percent air voids. Again, the strongest relationship exists between G*/sin δ, G*, or G″ and total rut depth for mixes containing RH aggregate and 4 percent air voids.

Linear Regression Analysis

Linear least-squares regressions between the rutting response variables and G*/sin δ were performed to further evaluate the relationships between these variables. Other binder properties were not included in this analysis because they did not produce significantly stronger relationships to the rutting response variables. Furthermore, G*/sing δ is the binder parameter specified in the SHRP binder specification associated with permanent deformation.

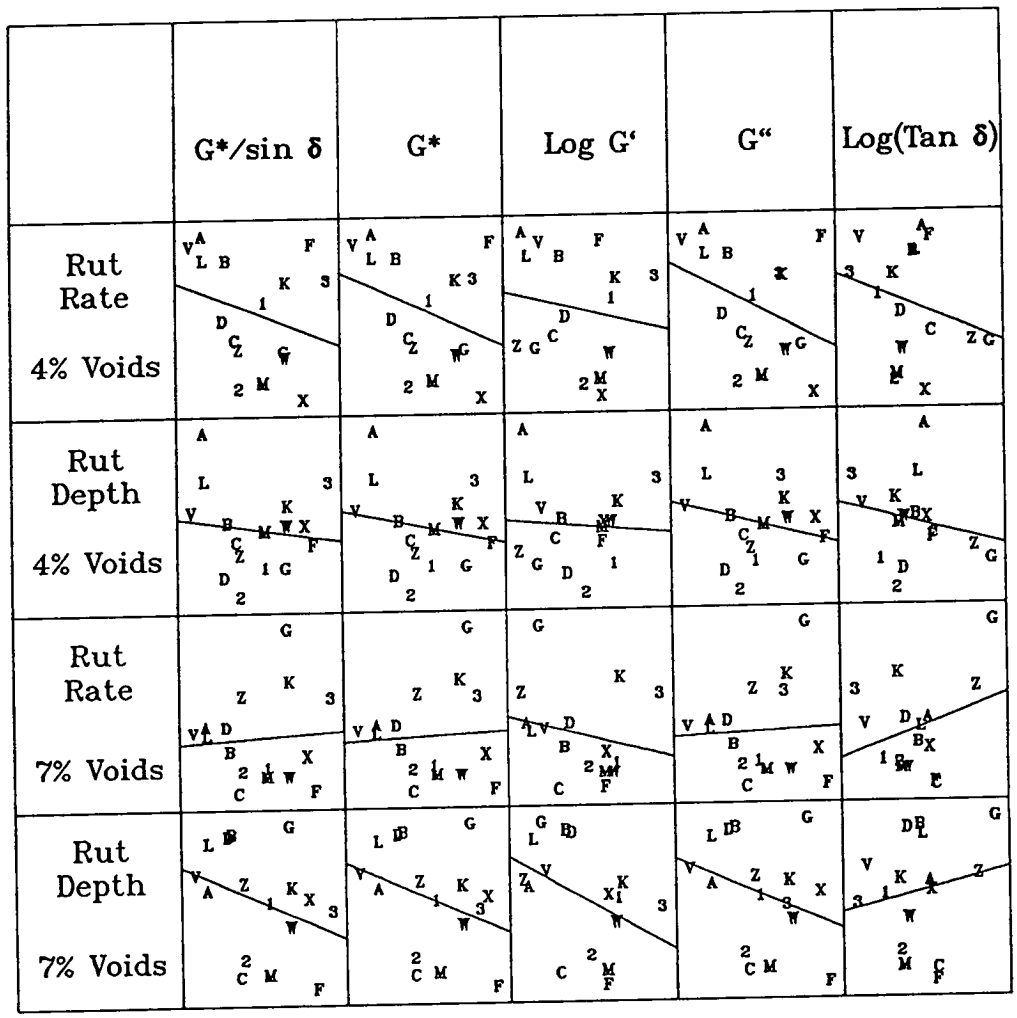

NOTE: Plot symbols represent the last letter of the MRL asphalt, except that the symbols for ABA, ABC and ABD are 1, 2, and 3, respectively.

Figure 4.1. SPLOM of mix rutting response versus asphalt binder properties for mixes containing aggregate RD

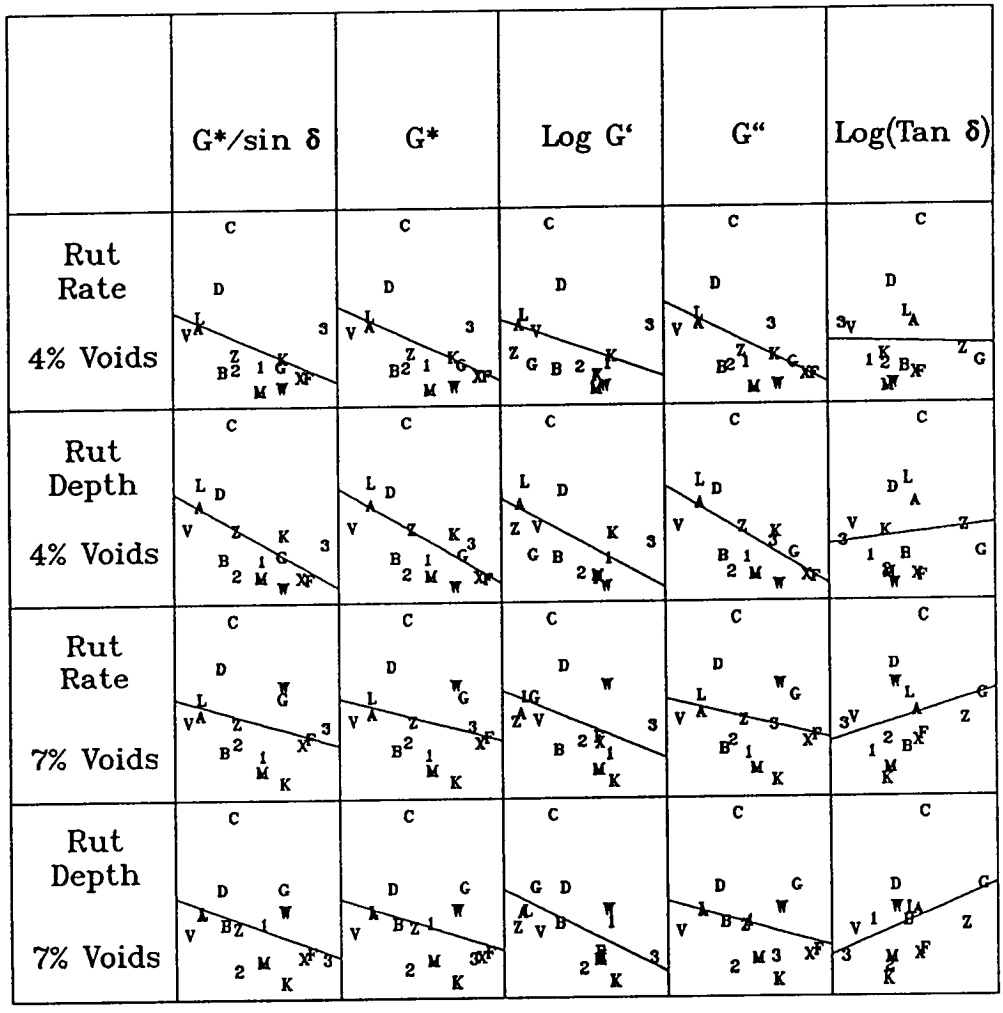

NOTE: Plot symbols represent the last letter of the MRL asphalt, except that the symbols for ABA, ABC and ABD are 1, 2, and 3, respectively.

Figure 4.2. SPLOM of mix rutting response versus asphalt binder properties for mixes containing aggregate RH

The regression relationships and coefficients of determination (R^2) are presented graphically in Figures 4.3 and 4.4. Each graph represents a separate mix data set. In these graphs, the least-squares regression line is plotted through the data and is surrounded by curved lines that represent a 95 percent confidence interval around the regression line. The coefficient of determination (R^2) is reported in the bottom of the left-hand corner of each graph. The value of R^2 is represents the percentage of the variation in the rutting response variable that is explained by changes in the value of G*/sin δ. The confidence interval represents our confidence that the average rutting response of a mix containing an asphalt included in this study will fall within the confidence band at the G* sin δ value for the asphalt. For instance, considering AAK asphalt in the bottom right-hand plot of Figure 4.3, the average rutting rate of a mix containing AAK asphalt, aggregate RH, and 4 percent air voids will fall within the confidence band directly above the G* sin δ value of 150 kPa (from Table 4.1) 95 out of 100 times (i.e., 95 percent confidence).

The regression results are similar to those presented earlier in this chapter except that the strength of the relationships and mix effects are more clearly demonstrated in the regression plots. The flat slopes of the regression lines for mixes containing aggregate RD indicate that the effect of G*/sin δ is minimal. Data for mixes containing aggregate RH exhibit a steeper slope in the regression line, indicating that asphalt has a greater effect in these mixes. It is interesting to compare the vertical shift in the regression lines between mixes with low air-void contents and those with higher contents. Mixes with high air-void contents exhibited slightly greater rut rates and larger total rut depths.

R^2 values ranged from 0.0 to 0.3. In most cases, less than 15 percent of the observed variation in rutting response is caused by the variation in G*/sin δ. Most of the variation in rutting response is probably due to other factors, such as aggregate characteristics or the testing process. Also note that many test results lie outside the 95 percent confidence band, demonstrating the wide variation in rutting response for a given value of G*/sin δ. These findings suggest that estimates of rutting response predicted using the asphalt property G*/sin δ will not be very reliable.

Table 4.3. Pearson and Spearman correlation coefficients

Mix Property	Pearson Correlation		Spearman Correlation	
	Normalized Rut Rate	Total Rut Depth	Normalized Rut Rate	Total Rut Depth
Aggregate RD, 4% air voids				
G*/sin δ	-0.293	-0.143	-0.082	-0.132
G*	-0.347	-0.206	-0.108	-0.196
Log G′	-0.175	-0.080	-0.233	0.006
G″	-0.383	-0.250	-0.128	-0.234
Log(tan δ)	-0.263	-0.220	-0.032	-0.221
Aggregate RD, 7% air voids				
G*/sin δ	0.068	-0.350	-0.335	-0.438
G*	0.055	-0.349	-0.377	-0.412
Log G′	-0.237	-0.436	-0.224	-0.447
G″	0.050	-0.333	-0.411	-0.377
Log(tan δ)	0.312	0.178	-0.132	0.097
Aggregate RH, 4% air voids				
G*/sin δ	-0.423	-0.549	-0.524	-0.668
G*	-0.450	-0.556	-0.582	-0.694
Log G′	-0.328	-0.497	-0.397	-0.559
G″	-0.464	-0.547	-0.620	-0.701
Log(tan δ)	-0.022	0.099	-0.012	0.074
Aggregate RH, 7% air voids				
G*/sin δ	-0.296	-0.379	-0.394	-0.403
G*	-0.269	-0.330	-0.324	-0.296
Log G′	-0.404	-0.500	-0.496	-0.481
G″	-0.236	-0.277	-0.300	-0.225
Log(tan δ)	0.272	0.379	0.391	0.500

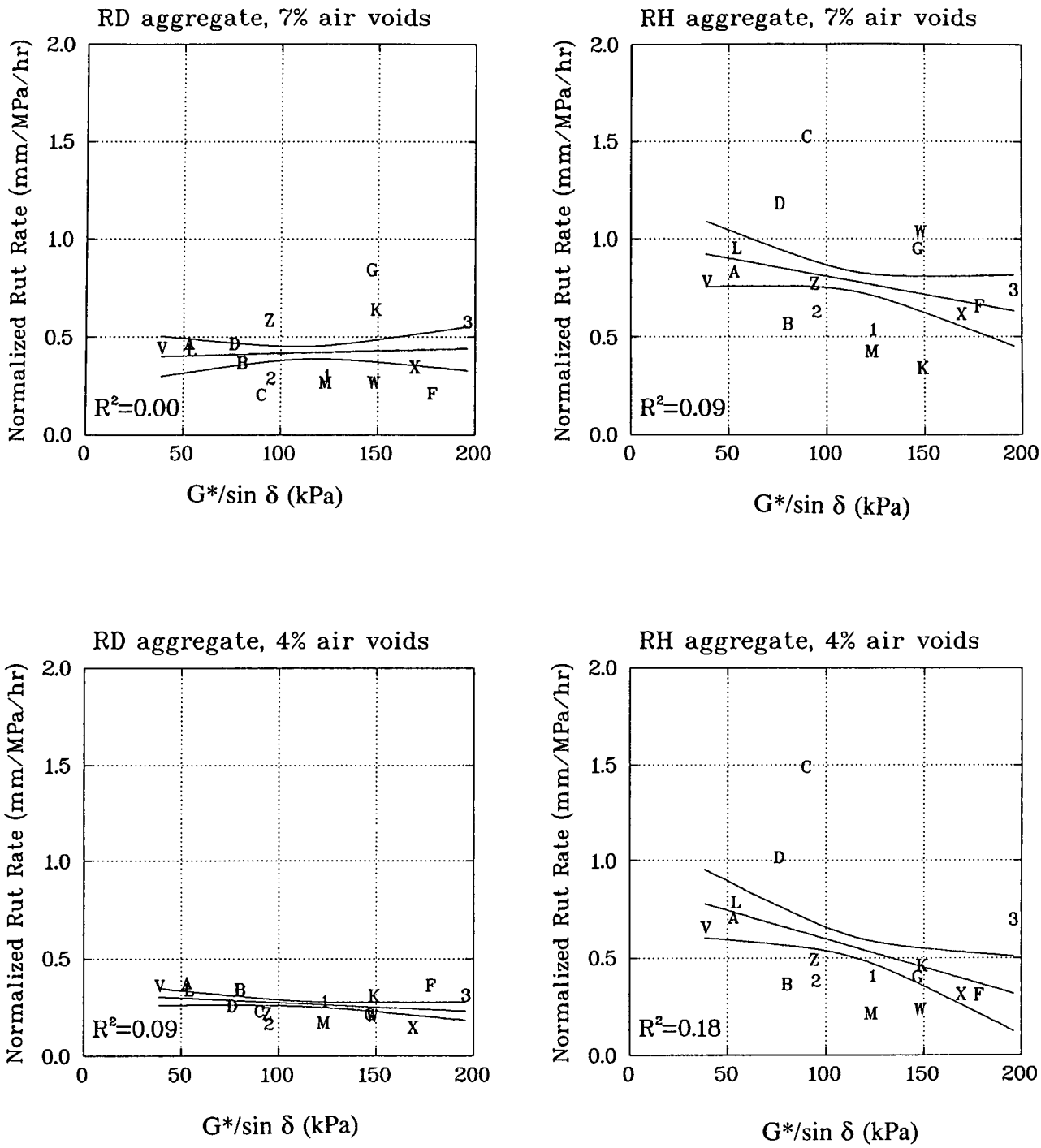

NOTE: Plot symbols represent last letter of MRL asphalt code, except symbols 1, 2, and 3, which are for ABA, ABC, and ABD, respectively.

Figure 4.3. Linear regression plots of rut rate versus G*/sin δ

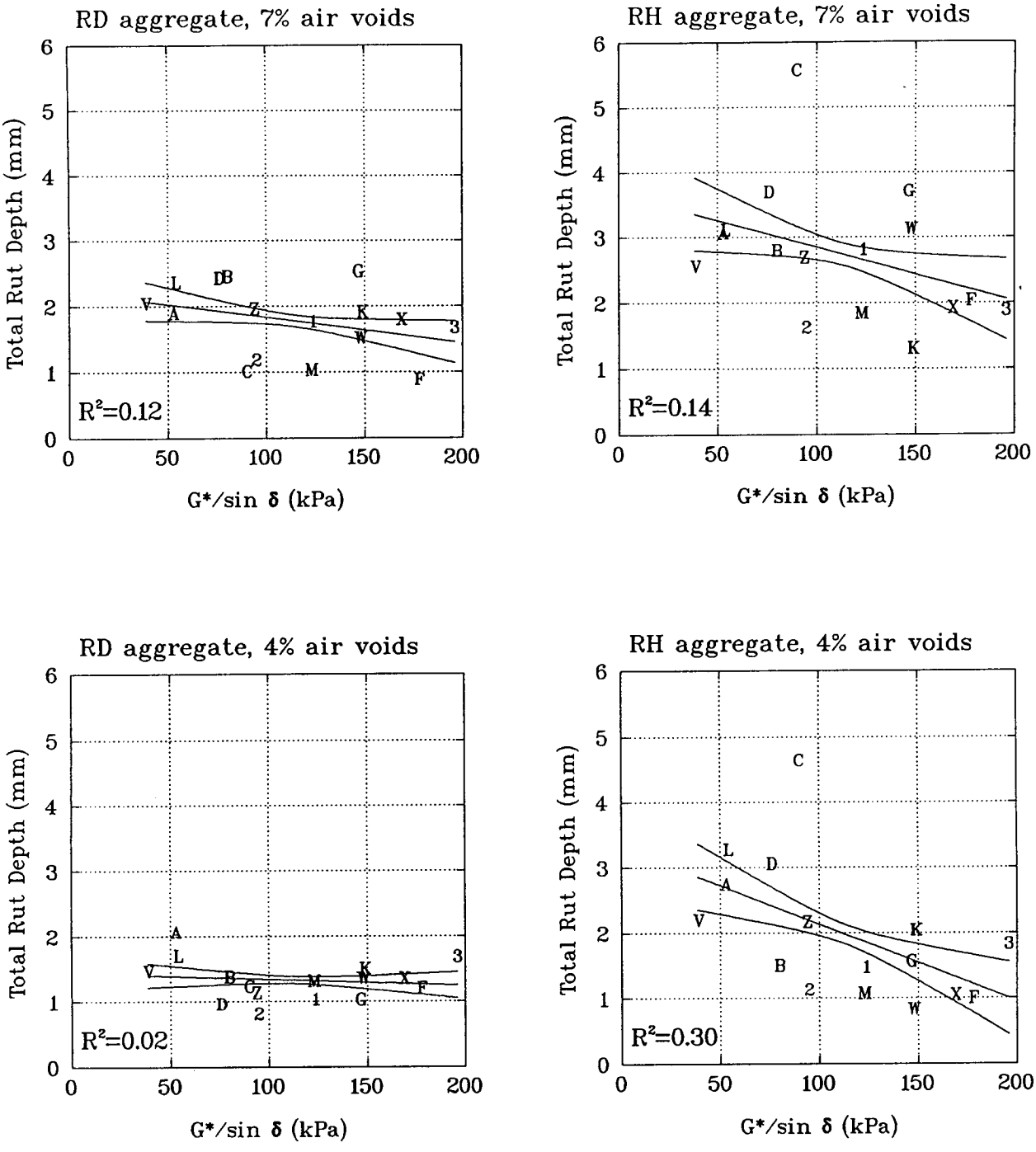

NOTE: Plot symbols represent last letter of MRL asphalt code, except symbols 1, 2, and 3, which are for ABA, ABC, and ABD, respectively.

Figure 4.4. Linear regression plots of rut depth versus G*/sin δ

Grouping Analysis

Since analyses up to this point indicated weak or nonexistent relationships between asphalt binder properties and mix rutting response, asphalts were separated into groups of similar performance (ranging from "good" to "poor") determined from G*/sin δ values and rutting response. The groups were then compared to see whether there was a consistent grouping of asphalts for both the magnitude of G*/sin δ and rutting response.

Line graphs were constructed first to illustrate the relative performance of asphalts by G*/sin δ, rut rate, and rut depth (Figure 4.5). The rut rate and rut depth data points represent the average response from all four mix data sets. Moreover, G*/sin δ values have been plotted in the reverse direction because of the inverse relationship between the two rutting response variables. Tukey pairwise mean comparisons were then used to assist in forming groups of asphalts exhibiting similar performance as measured by rut rate or rut depth, while groups of similar performance based on G*/sin δ were determined visually from Figure 4.5.

The resulting groups of similar performance are presented in Table 4.4. The performance placements are generally inconsistent; it will be noted that only AAF asphalt consistently places in the same group level—good. If asphalt performance is combined further, into two groups, most asphalts consistently fall into the same group (see Table 4.5). Thus at best, G*/sin δ appears to be able to estimate rutting response within only two broad levels.

Binder Specification Compliance versus Mix Rutting Response

The SHRP binder specification limit for G*/sin δ related to permanent deformation was compared with the rut depths observed from wheel-tracking testing. The binder specification limit for G*/sin δ is a minimum of 2 kPa (Table 1.1). In Table 4.1, all the asphalts meet this requirement. This is not surprising, since the properties in Table 4.1 are for a test temperature of 40°C, which is less than any of the test temperatures called for in the binder specification. It is interesting to note the relatively high rut depths associated with mixes containing AAC asphalt and aggregate RH (Figure 4.4). One cannot be certain, however, that this level of rut depth measured in the wheel-tracking test indicates that rutting would occur in a pavement built with asphalt AAC. Furthermore, this observation does not necessarily indicate that the binder specification limit is faulty. It does, however, point out that if a better estimate of potential rutting is desired, mix testing in addition to binder testing is mandatory.

Summary and Discussion of Results

The results of this study indicate that the binder property G*/sin δ is not a reliable predictor of potential rutting in asphalt-aggregate mixes. Aggregate characteristics and degree of compaction have a significant influence on rutting propensity and more than likely override

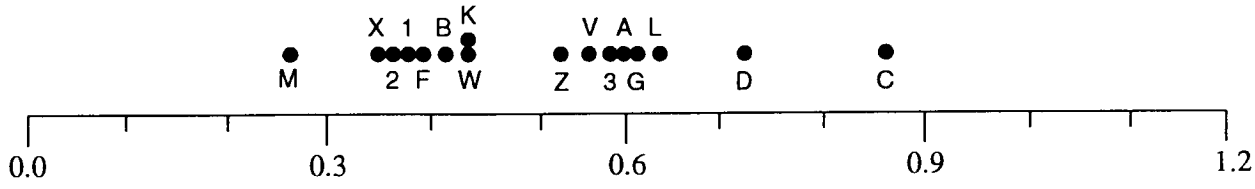

Average normalized rut rate (mm/MPa/hr)

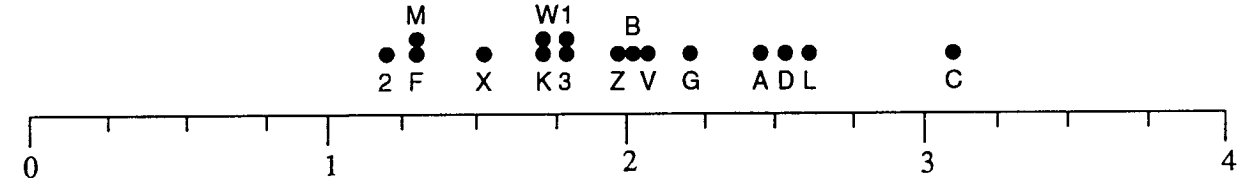

Average total rut depth (mm)

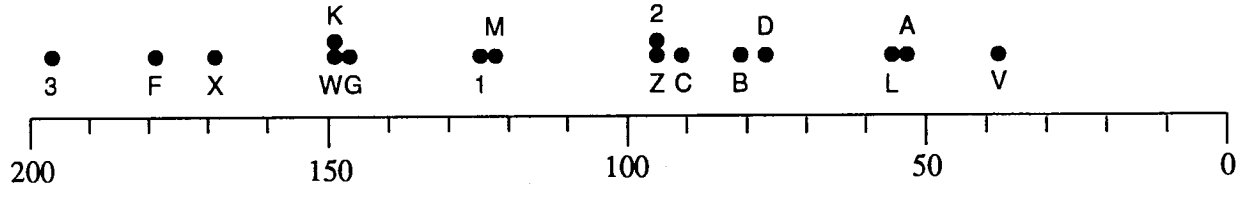

G*/sinδ (KPa)

NOTE: Plot symbols represent last letter of MRL asphalt code, except symbols 1, 2, and 3, which are for ABA, ABC, and ABD, respectively.

Figure 4.5. Relative asphalt performance by rut rate, rut depth, and G*/sin δ

Table 4.4. Asphalt performance groups (first grouping)

Rut Rate:	Group 1 (good)	Group 2	Group 3 (poor)		
	AAB	AAA	AAC		
	AAF	AAG	AAD		
	AAK	AAL			
	AAM	AAV			
	AAW	AAZ			
	AAX	ABD			
	ABA				
	ABC				
Rut Depth:	**Group 1 (good)**	**Group 2**	**Group 3**	**Group 4**	**Group 5 (poor)**
	AAF	AAK	AAB	AAA	AAC
	AAM	AAW	AAG	AAD	
	ABC	AAX	AAV	AAL	
		ABA	AAZ		
		ABD			
G*/sin δ:	**Group 1 (good)**	**Group 2**	**Group 3**	**Group 4**	**Group 5 (poor)**
	AAF	AAG	AAM	AAB	AAA
	AAX	AAK	ABA	AAC	AAL
	ABD	AAW		AAD	AAV
				AAZ	
				ABC	

Table 4.5. Asphalt performance groups (second grouping)

Rut Rate:	Group 1 (good)	Group 2 (poor)
	AAB	AAA
	AAF	AAC
	AAK	AAD
	AAM	AAG
	AAW	AAL
	AAX	AAV
	ABA	AAZ
	ABC	ABD
Rut Depth:	**Group 1 (good)**	**Group 2 (poor)**
	AAF	AAA
	AAK	AAB
	AAM	AAC
	AAW	AAD
	AAX	AAG
	ABA	AAL
	ABC	AAV
	ABD	AAZ
G*/sin δ:	**Group 1 (good)**	**Group 2 (poor)**
	AAF	AAA
	AAG	AAB
	AAK	AAC
	AAM	AAD
	AAW	AAL
	AAX	AAV
	ABA	AAZ
	ABD	ABC

the influence of the binder. However, there are several considerations that temper this conclusion:

1. As noted in the SWK report, the repeatability of wheel-tracking tests can be poor (Gibb et al. 1991). It was concluded that to obtain a reliable determination of rutting rate, a significant number of replicate tests should be performed. A similar wheel-tracking rutting study was performed on earlier mixes made from two asphalts (AAG, AAK) and two aggregates (RB, RL) (Gibb et al. 1991). Each cell of the experiment in that study included two replicates, from which test precision was calculated. The testing error in that study was nearly as significant as the asphalt effect was in this study. It is thus probable that the relatively low test precision contributed to the low coefficients of determination (R^2) when trying to predict rutting response from $G^*/\sin \delta$.

2. Binder and wheel-tracking tests were conducted at 40°C. This temperature may not be high enough to allow the viscous characteristics of binders to affect the mix rutting response. Note that the SHRP binder specification does not provide for a climatic region for which binders would be tested at 40°C for permanent deformation evaluation; the lowest test temperature is 45°C. At high test temperatures, the binder effect might be more pronounced.

3. The magnitude of total rut depths for the better-performing mixes was small relative to the testing error. SWK noted this fact, and also suggested that an increase in the contact pressure and load applications may reduce the testing error.

4. While the wheel-tracking test equipment at the University of Nottingham is considered useful, it is relatively small. The surface area of the mix specimen is 32,000 mm^2, and the contact area of the rubber wheel is 850 mm^2, yet the aggregate size was typical of that used in conventional pavement mixes. Thus, the dimensional ratios in the wheel-tracking test were not the same as those that occur in real pavements.

Based on the preceding, the value of $G^*/\sin \delta$ may have a greater effect on mix rutting response than that observed in this study. It is recommended that future permanent deformation studies that employ wheel-tracking devices use higher contact stresses or more load repetitions (or both). The precision of wheel-tracking equipment should be improved to minimize the testing error. Fortunately, larger-scale wheel-tracking test equipment is beginning to appear in the United States. These devices will permit testing of larger slabs of asphalt-concrete with boundary conditions representative of actual pavement structures.

Validation by Laboratory Shear Testing

Asphalt binder properties were compared with the permanent deformation response of asphalt-aggregate mix specimens subjected to repetitive simple shear loading under controlled conditions in the laboratory. The following hypothesis was proposed by the A-003A researchers for permanent deformation in asphalt-aggregate mixes:

1. Permanent deformation (rutting) in an asphalt-concrete layer is caused by a combination of densification (volume change) and shear deformation, each resulting from the repetitive applications of traffic loads.

2. Permanent deformation is caused primarily by large shear stresses in the upper portions of the asphalt-concrete layer.

3. Properties of asphalt (elastic and viscous) and aggregate that contribute to permanent deformation in asphalt-aggregate mixes can be quantified by using a simple shear test.

Therefore, the selection of the simple shear test is consistent with both A-002A and A-003A hypotheses regarding permanent deformation. This test can measure the elastic (linear and nonlinear) and viscous influences of the binder in the asphalt-aggregate mix. It can also simulate shear stress conditions believed to be responsible for causing most of the permanent deformation in asphalt-concrete pavements.

Materials

Nine asphalt binders and two aggregates from the MRL were used in this study: asphalts AAB, AAC, AAD, AAG, AAK, AAM, AAV, AAZ, and ABC and aggregates RD, and RH.

Table 2.1 lists asphalt grades and aggregate characteristics, while Table 2.2 contains aggregate gradations and asphalt contents, with each of the aggregates. All mixes were prepared by rolling-wheel compaction as described in the Materials section earlier in this chapter, under Validation by Wheel-Tracking Testing.

Experiment Design

A full-factorial experiment was designed to allow all main effects and two-factor interactions to be evaluated. The factorial matrix consisted of 9 asphalts, 2 aggregates, and 2 levels of air-void contents, resulting in a total of 36 cells. Each cell had only 1 replicate, for a total of 36 tests for each of two shear test conditions (described later). Thus, 72 shear test results were analyzed. Since no replicates were provided, the three-factor interaction of asphalt source, aggregate source, and air-void content was used as an estimate of experimental error. The factorial experiment is summarized below.

Experimental Design Factors and Levels (independent variables):

Factor	Levels
Asphalt source	9 (see list above)
Aggregate source	2 (see list above)
Air-void content, %	2 (4, 7)
Replicates:	1 per cell
Test condition:	Constant height or field state of stress
Total number of tests:	72

Shear Response Variables (dependent variables, to be explained later):

Load cycles to 2 percent strain, $N_{2\%}$—number of the shear load cycles at which the asphalt-aggregate mix specimen first reaches 2 percent cumulative permanent shear strain

Cumulative permanent shear strain, $\Sigma\gamma_p$—cumulative permanent shear strain after a constant number of load cycles

Asphalt Binder Tests and Properties

See the previous section, *Validation by Wheel-Tracking Testing*, for a detailed discussion of the binder properties provided by A-002A and their relationship to permanent deformation in the SHRP binder specification.

Asphalt binder properties provided by the A-002A contractor for this study are presented in Table 4.6. The properties were calculated for a test temperature of 60°C and a load frequency of 10 rad/sec (1.59 Hz). The temperature of 60°C was selected to be compatible with the test temperature of the mix shear tests. According to the A-002A contractor, the coefficient of variation for each of the properties is approximately 10 percent. In later tables and figures, a log (base 10) transformation was applied to G′ and tan δ values for statistical purposes.

Asphalt-Aggregate Mix Tests and Properties

Half the specimens in this study were tested under a *constant height* condition (CH) and the other half under a *field state of stress* (FS) condition. The CH shear test is sensitive to elastic and viscous characteristics of the asphalt binder, and it also measures the effect of dilatancy. Dilatancy in this case is the tendency of a mix to change in volume as aggregate particles are

Table 4.6. Asphalt binder properties provided by A-002A (after TFOT, at 60°C and 10 rad/sec)

Asphalt Source	G*, (Pa)	tan δ	G′, (Pa)	G″, (Pa)	G*/sin δ, Pa
AAB	3329	8.53	376	3207	3251
AAC	2664	11.37	233	2654	2674
AAD	3784	4.89	758	3707	3862
AAG	4310	49.53	87	4309	4311
AAK	8442	4.06	2018	8197	8694
AAM	4857	7.13	675	4810	4905
AAV	1332	26.59	50	1331	1333
AAZ	4290	26.00	165	4287	4293
ABC	5802	4.98	1142	5688	5918

forced to slide past each other during shear deformation. The FS shear test incorporated loading conditions thought to represent the state of stress occurring in an asphalt-concrete layer near the edge of a truck tire.

The CH shear test, depicted in Figure 4.6, applied a cyclic (haversine) shear stress of 103 kPa ± 10 percent to the specimens. The load pulse duration was 0.1 sec, with 0.6 sec between load pulses. In addition, vertical compressive loads were applied as necessary to maintain the original specimen height throughout the test. The magnitude of the resulting vertical compressive load is a function of the specimen's propensity to dilate under shear loading. Shear strain was calculated from the difference between displacements measured by two linear variable differential transducers located 13 mm above and below the midheight of the specimen. Each test was scheduled to run for 3600 load cycles. However, tests were terminated before reaching this number of load cycles if the specimen exhibited 4 percent permanent shear strain or if failure was observed.

The FS shear test simultaneously applied a cyclic shear stress of 172 kPa ± 10 percent and a cyclic compressive axial stress of 345 kPa ± 10 percent, both with load pulse durations of 0.1 sec and 0.6 sec between load pulses. In addition, a constant confining pressure of 138 kPa was applied to the specimen (not shown in Figure 4.6). Each test was also scheduled to run for 3600 load cycles; all but three of the FS tests completed the scheduled 3600 load cycles.

Repetitive shear tests were performed on asphalt-aggregate mix specimens 152 mm in diameter by 51 mm high. All specimens were tested at 60°C. More detailed information on shear test equipment and conditions is presented in Sousa et al. (1993).

Two mix shear response variables were calculated from each of the above shear test conditions for comparison with asphalt binder properties as follows:

1. The number of the load cycle at which the specimen reached 2 percent cumulative permanent shear strain, or $N_{2\%}$.

2. Cumulative permanent shear strain after a constant number of load cycles, or $\Sigma\gamma_p$.

   Note that at the time of testing, 2 percent cumulative permanent shear strain was considered to represent a critical strain condition relating to permanent deformation performance of asphalt-aggregate mix specimens. This value was later increased to 5 percent for mix evaluations.

For CH tests, $\Sigma\gamma_p$ values at 32 load cycles were used in the following analyses. This was the highest number of load cycles that allowed all specimens to be included in the analyses. Similarly, for FS tests, $\Sigma\gamma_p$ values at 602 load cycles were used.

In later tables and figures, a log (base 10) transformation was applied to both $N_{2\%}$ and $\Sigma\gamma_p$ data for statistical purposes. In addition, the data were adjusted for actual mix air-void contents deviating from the target contents of 4 and 7 percent, as previously described. Additional information on the calculation of mix shear response parameters, log transformations, and adjustments for air-void content is presented in Paulsen and Sousa (1992).

Table 4.7 presents shear test results on asphalt-aggregate mix specimens. Each specimen is identified by a unique combination of asphalt, aggregate source, and air-void content. The data in Table 4.7 have been adjusted to account for variations in air-void contents from the experiment target values. The statistical analyses presented herein were performed on these data. Raw test data (i.e., before adjustment) are presented in Sousa et al. (1993). Note that the CH test result was not available for the mix containing asphalt AAG, aggregate RH, and 7 percent air voids.

Relationships between Binder and Mix Properties

Asphalt binder properties and asphalt-aggregate mix shear test results in this study represent similar aging and test temperature conditions. Asphalt binders were aged according to the TFOT to simulate the short-term aging effects of the construction process. Asphalt-aggregate mixes were also subjected to short-term aging; after mixing, they were placed in an oven at 135°C for 4 hr. Asphalt binder properties were calculated for a test temperature of 60°C, and asphalt-aggregate mixes were tested at this same temperature.

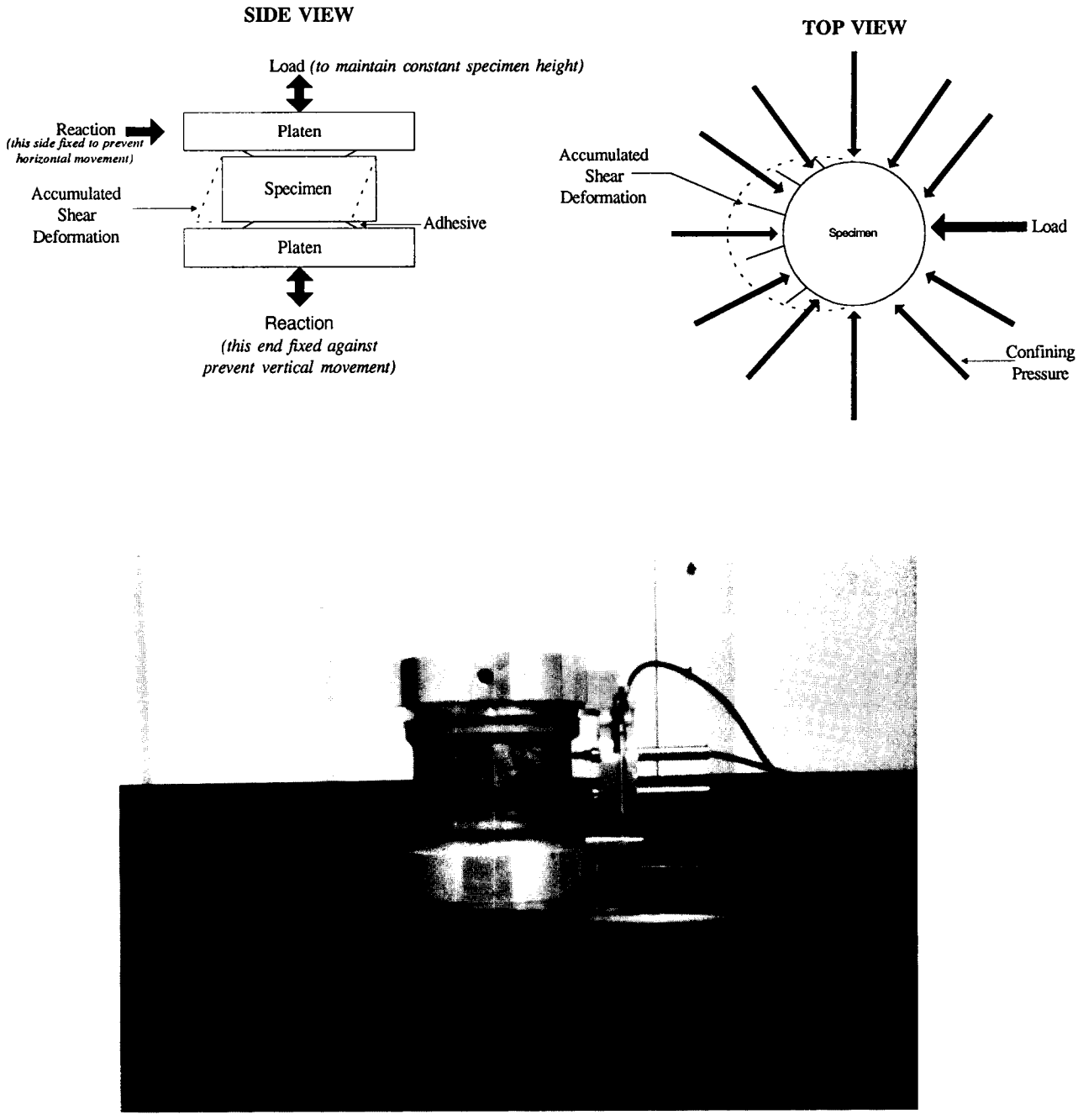

Figure 4.6. Simple shear test load conditions and specimen instrument

Table 4.7. Laboratory shear test results, adjusted for air-void content (after short-term oven aging, at 60°C and 10 Hz)

Asphalt Source	Aggregate Source	Air-Void Content (%)	Cycles to 2% Strain (CH)	Cycles to 2% Strain (FS)	Cumulative Permanent Shear Strain at 32 Cycles (CH)	Cumulative Permanent Shear Strain at 602 Cycles (FS)
AAB	RD	4.0	30	106,996	0.02082	0.00265
AAB	RD	7.0	132	134,757	0.01144	0.00585
AAB	RH	4.0	105	13,773	0.01303	0.01156
AAB	RH	7.0	14	356	0.03143	0.01993
AAC	RD	4.0	544	303,101	0.00865	0.00317
AAC	RD	7.0	166	62,175	0.01241	0.00874
AAC	RH	4.0	13	15,773	0.02894	0.00672
AAC	RH	7.0	12	693	0.03134	0.01904
AAD	RD	4.0	143	6,421	0.01117	0.01405
AAD	RD	7.0	12	100,033	0.01985	0.00777
AAD	RH	4.0	35	1,446	0.01966	0.01611
AAD	RH	7.0	9	27	0.03355	0.04459
AAG	RD	4.0	29	2,842	0.02063	0.01539
AAG	RD	7.0	67	6,010	0.01440	0.01233
AAG	RH	4.0	80	5	0.01156	0.06601
AAG	RH	7.0	NA	183	NA	0.02554
AAK	RD	4.0	97	3,409	0.01350	0.01520
AAK	RD	7.0	123	3,789	0.01125	0.01629
AAK	RH	4.0	72	66	0.01140	0.03312
AAK	RH	7.0	30	126	0.02033	0.02947
AAM	RD	4.0	205	363,300	0.01057	0.00985
AAM	RD	7.0	61	599,817	0.01553	0.00694
AAM	RH	4.0	675	29,268	0.00621	0.00825
AAM	RH	7.0	58	32	0.01604	0.03708
AAV	RD	4.0	68	2,410	0.01454	0.01600
AAV	RD	7.0	11	2,802	0.03116	0.01728
AAV	RH	4.0	13	199	0.02755	0.02646
AAV	RH	7.0	5	37	0.04219	0.03413
AAZ	RD	4.0	102	2,517,640	0.01299	0.00250
AAZ	RD	7.0	40	24,968	0.01860	0.00869
AAZ	RH	4.0	52	3,707	0.01662	0.01395
AAZ	RH	7.0	17	177	0.02706	0.02638
ABC	RD	4.0	478	1,007,580	0.00755	0.01071
ABC	RD	7.0	27	40,799	0.02128	0.01221
ABC	RH	4.0	38	841	0.01837	0.02055
ABC	RH	7.0	27	82	0.02113	0.03581

However, binder properties and mix test results represent substantially different load frequencies. Asphalt binder properties were calculated for a load frequency of 10 rad/sec (1.6 Hz). Asphalt-aggregate mixes were tested at a load frequency of 10 Hz (62.8 rad/sec), to simulate conditions associated with moving traffic. Thus, it is possible that the binders in the mixes exhibited more of their elastic nature and less of their viscous nature, because of the faster loading, than is represented by the binder properties listed in Table 4.6.

Analysis of Variance

The results of an ANOVA model on the shear test data indicated that asphalt source, aggregate source, and air-void content significantly affect the shear response ($N_{2\%}$ and $\Sigma\gamma_p$) of asphalt-aggregate mixes. A minimum confidence level of 95 percent was used to determine significance; however, many of the factors were significant at confidence levels equal to or greater than 99 percent.

The model indicated that the factors accounted for the variation of shear response in the following approximate proportions:

	Shear Response Variable	Factor	Proportional Effect, %
CH shear test:	$N_{2\%}$	Asphalt	28
		Aggregate	20
		Air-void content	18
		ANOVA model error	19
	$\Sigma\gamma_p$	Asphalt	29
		Aggregate	21
		Air-void content	18
		ANOVA model error	18
FS Shear Test:	$N_{2\%}$	Asphalt	24
		Aggregate	52
		Air-void content	5
		ANOVA model error	17
	$\Sigma\gamma_p$	Asphalt	33
		Aggregate	39
		Air-void content	6
		ANOVA model error	22

Note that the influence of asphalt is greater than that of aggregate in the CH shear tests, but the opposite is true in FS shear tests. Also, note that the influence of air-void content is greater in CH shear tests than it is in FS shear tests. The ANOVA and results are discussed more fully in the report by Paulsen and Sousa (1992). Since the effects of aggregate source and air-void content were significant, separate analyses were made on the following data sets:

Aggregate Source	Air-Void Content, %
RD	4
RD	7
RH	4
RH	7

Scatterplots

SPLOMs were prepared to obtain an initial look at the relationships between mix shear response variables and asphalt binder properties. The results are presented in Figures 4.7 through 4.10 for each combination of aggregate source and air-void content. While there is significant scatter in the data, there appear to be some relationships. The strongest relationships and least data scatter are exhibited for mixes containing aggregate RH and 7 percent air voids and tested under CH test conditions (see Figure 4.10). In Figure 4.10, the expected relationships between asphalt binder properties and mix shear response are observed. For example, as the value of any of the asphalt binder properties (with the exception of tan δ) increases, the number of load cycles before the specimen exhibits 2 percent permanent shear strain increases, and the amount of permanent shear strain, after a given number of load cycles, decreases. Tan δ has an inverse relationship to mix shear response. The relationship with G′ appears to produce more data scatter than that with G*/sin δ, G*, or G″. The relationship with tan δ exhibits the most data scatter.

Comparing scatterplots of CH shear test data in Figure 4.10 with those in Figures 4.7, 4.8, and 4.9, reveals that the strength of the relationship between asphalt binder properties and mix shear response weakens considerably as air-void content changes from 7 to 4 percent and as the aggregate source changes from RH to RD. However, the direction of the lines indicates that the expected relationships still exist.

In reviewing all the figures, it will be noted that data resulting from CH shear tests generally provide stronger relationships and less data scatter than FS shear test data. Also, in many cases the directions of the relationships exhibited by FS data are opposite to those exhibited by CH data, perhaps partly because of the extreme data scatter in the FS data. The poor relationships associated with FS shear test data are probably a result of the significant influences of aggregate characteristics, as seen, for example, from the ANOVA.

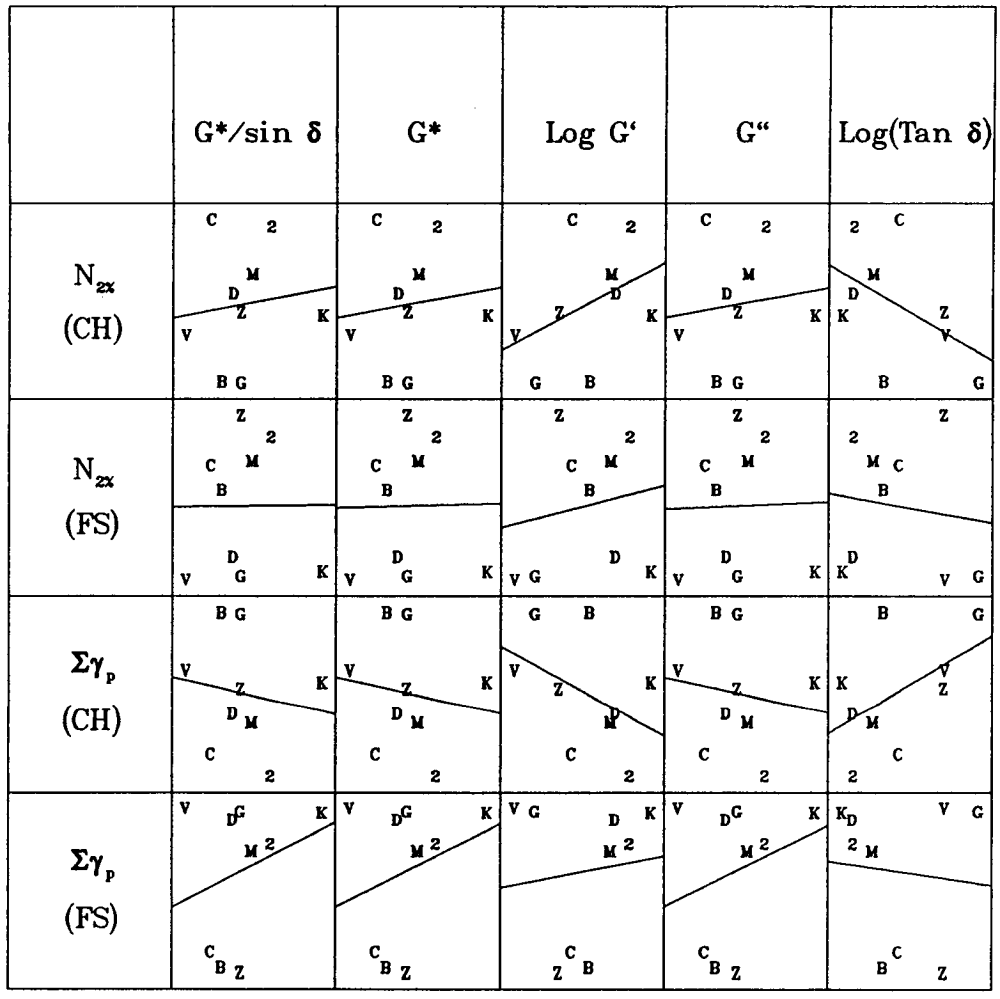

Note: Plot symbols represent the last letter of the MRL asphalt code, except the symbol for ABC is 2.

Figure 4.7. SPLOM of mix shear response versus asphalt binder properties for mixes containing aggregate RD and 4 percent air voids

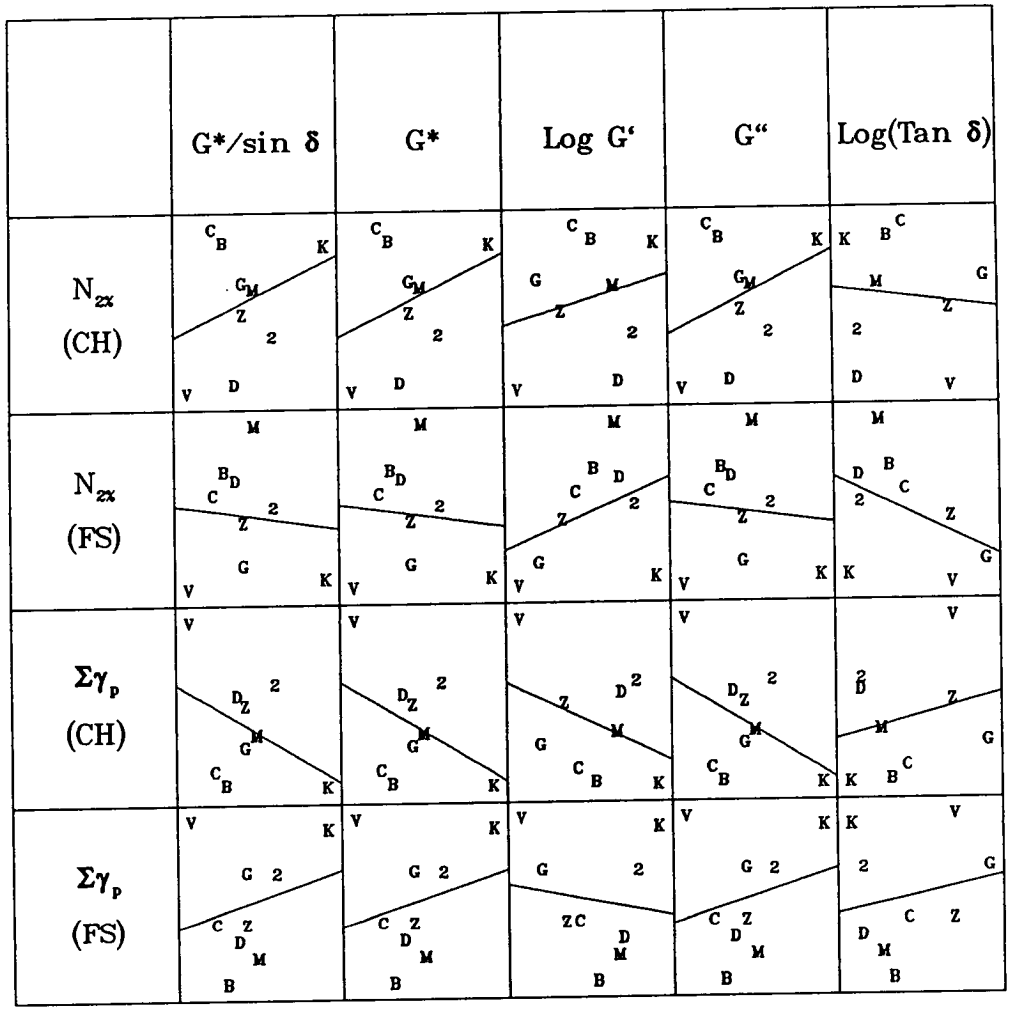

Note: Plot symbols represent the last letter of the MRL asphalt code, except the symbol for ABC is 2.

Figure 4.8. SPLOM of mix shear response versus asphalt binder properties for mixes containing aggregate RD and 7 percent air voids

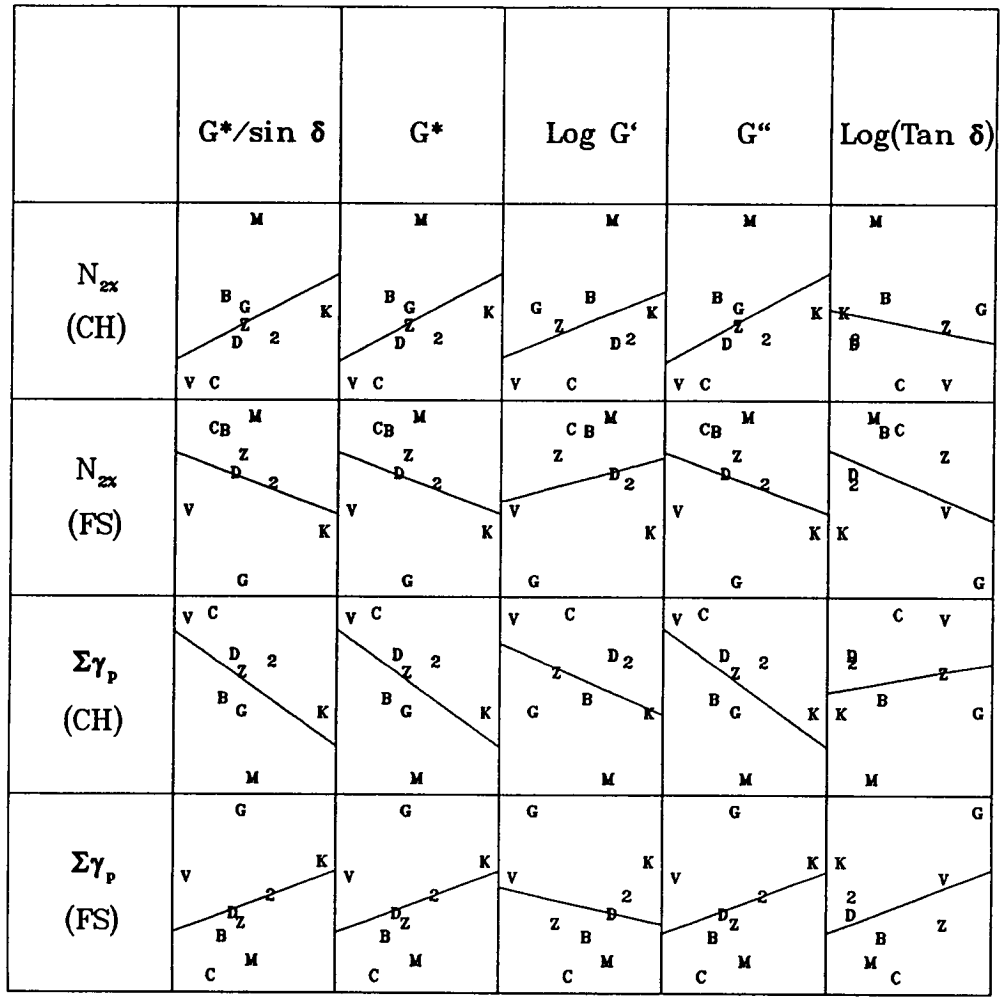

Note: Plot symbols represent the last letter of the MRL asphalt code, except the symbol for ABC is 2.

Figure 4.9. SPLOM of mix shear response versus asphalt binder properties for mixes containing aggregate RH and 4 percent air voids

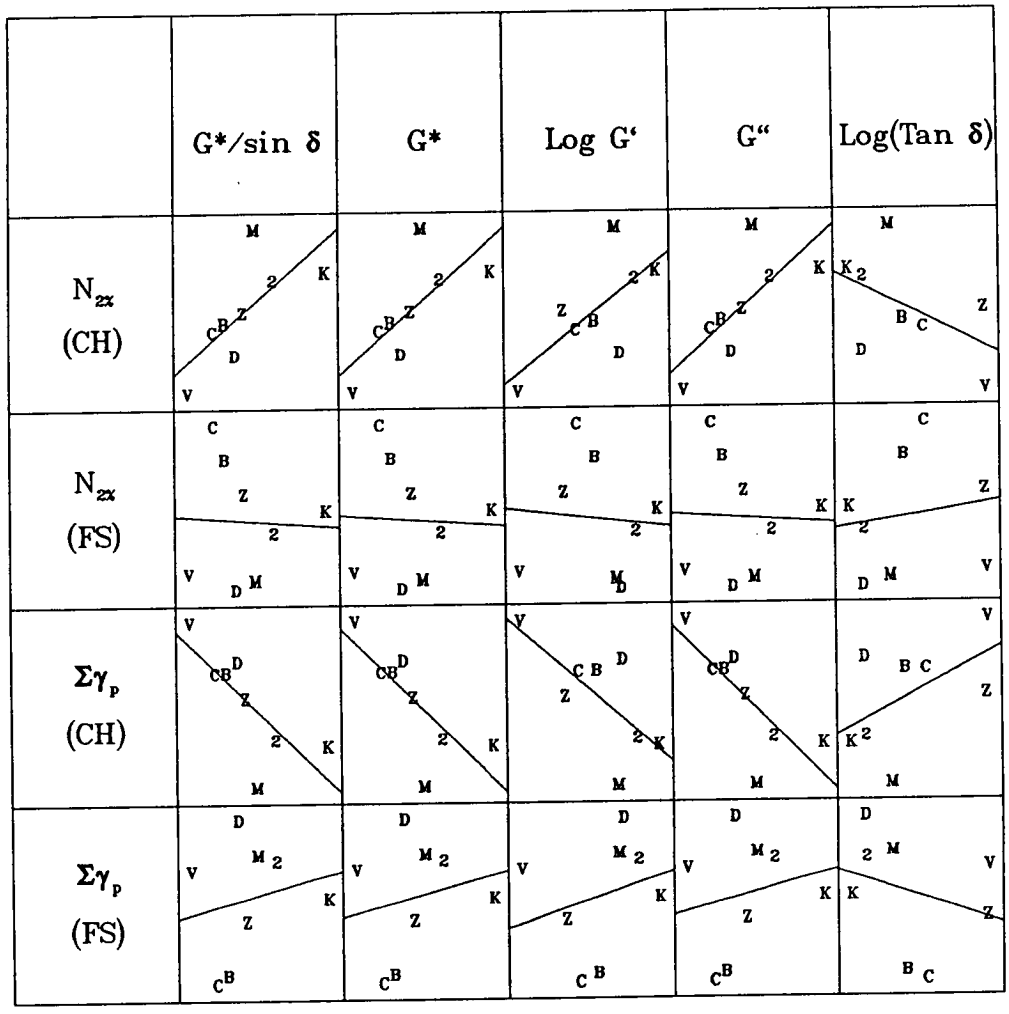

Note: Plot symbols represent the last letter of the MRL asphalt code, except the symbol for ABC is 2.

Figure 4.10. SPLOM of mix shear response versus asphalt binder properties for mixes containing aggregate RH and 7 percent air voids

Pearson Correlations

The strength of the relationships depicted in Figures 4.7 through 4.10 was quantified through the use of Pearson correlations. Pearson coefficients are presented in Table 4.8; the values generally corroborate the conclusions drawn from visual examination of the SPLOMs. Coefficients are higher for mixes containing aggregate RH than for those containing RD. Coefficients are higher for mixes having high air-void contents than for those having low air-void contents. Coefficients are higher for mixes tested under CH conditions than for those tested under FS conditions. Finally, G*/sin δ, G*, and G″ provide slightly stronger relationships to mix shear response than G′, except for mixes containing aggregate RD and 4 percent air voids.

Spearman Rank Correlations

Spearman rank correlations were performed to see whether weak relationships indicated by the Pearson correlations were perhaps stronger when based on relative ranking of asphalt performance represented by binder properties and mix shear response. Spearman rank correlation coefficients are presented in Table 4.9. Relationships become slightly stronger for mixes containing aggregate RH. However, many relationships become weaker for mixes containing aggregate RD; this is not considered significant because of the large data scatter associated with these mixes. Finally, note that for any given mix, the coefficient values are exactly the same for G*/sin δ, G*, G′, and G″. This finding indicates that the relationship of binder ranking to mix performance ranking does not change with the binder property used.

Linear Regression Analysis

Linear least-squares regressions between G*/sin δ and CH shear response were performed to further evaluate the relationships between these variables. Other binder properties were not included in this analysis because they did not produce *significantly* stronger relationships with the shear response variables. Furthermore, G*/sin δ is the binder parameter specified in the SHRP binder specification as it relates to permanent deformation. FS shear test results were not included in the regression analysis because the results of SPLOMs, Pearson correlations, and Spearman rank correlations conclusively showed that significant relationships to asphalt binder properties did not exist.

Linear regression plots are presented in Figures 4.11 and 4.12. The separate effects of aggregate type and air-void content are illustrated by the different vertical positions of the regression lines. There is a modest correlation between either $N_{2\%}$ or $\Sigma\gamma_p$ and G*/sin δ for mixes consisting of aggregate RH and 7 percent air voids and this correlation is statistically significant at a 95 percent confidence level. As the air-void content decreases to 4 percent, this correlation weakens considerably. Note that asphalt AAM appears to be an outlier for mixes containing aggregate RH. For mixes containing RD aggregate, there is practically no

Table 4.8. Pearson correlation coefficients

Mix Property	$N_{2\%}$ (CH)	$N_{2\%}$ (FS)	$\Sigma\gamma_p$ (CH)	$\Sigma\gamma_p$ (FS)
Aggregate RD, 4% air voids				
G*/sin δ	0.127	0.007	-0.158	0.282
G*	0.123	0.016	-0.153	0.275
Log G′	0.411	0.179	-0.438	0.121
G″	0.119	0.026	-0.149	0.268
Log(tan δ)	-0.485	-0.135	0.511	-0.100
Aggregate RD, 7% air voids				
G*/sin δ	0.319	-0.103	-0.432	0.240
G*	0.324	-0.098	-0.436	0.233
Log G′	0.230	0.367	-0.401	-0.156
G″	0.330	-0.093	-0.440	0.226
Log(tan δ)	-0.097	-0.430	0.251	0.196
Aggregate RH, 4% air voids				
G*/sin δ	0.412	-0.268	-0.530	0.286
G*	0.421	-0.267	-0.539	0.287
Log G′	0.365	0.220	-0.379	-0.196
G″	0.431	-0.267	-0.548	0.287
Log(tan δ)	-0.193	-0.382	0.165	0.369
Aggregate RH, 7% air voids				
G*/sin δ	0.721	-0.053	-0.761	0.202
G*	0.729	-0.049	-0.768	0.198
Log G′	0.692	-0.086	-0.712	0.256
G″	0.737	-0.045	-0.775	0.194
Log(tan δ)	-0.516	0.150	0.537	-0.298

Table 4.9. Spearman rank correlation coefficients

Mix Property	$N_{2\%}$ (CH)	$N_{2\%}$ (FS)	$\Sigma\gamma_p$ (CH)	$\Sigma\gamma_p$ (FS)
Aggregate RD, 4% air-void content				
G*/sin δ	0.100	0.267	-0.250	0.067
G*	0.100	0.267	-0.250	0.067
Log G′	0.100	0.267	-0.250	0.067
G″	0.100	0.267	-0.250	0.067
Log(tan δ)	-0.417	-0.200	0.400	0.067
Aggregate RD, 7% air-void content				
G*/sin δ	0.067	-0.017	-0.233	0.083
G*	0.067	-0.017	-0.233	0.083
Log G′	0.067	-0.017	-0.233	0.083
G″	0.067	-0.017	-0.233	0.083
Log(tan δ)	-0.017	-0.317	0.200	0.217
Aggregate RH, 4% air-void content				
G*/sin δ	0.533	-0.267	-0.717	0.350
G*	0.533	-0.267	-0.717	0.350
Log G′	0.533	-0.267	-0.717	0.350
G″	0.533	-0.267	-0.717	0.350
Log(tan δ)	-0.117	-0.117	0.217	0.083
Aggregate RH, 7% air-void content				
G*/sin δ	0.857	-0.190	-0.833	0.333
G*	0.857	-0.190	-0.833	0.333
Log G′	0.857	-0.190	-0.833	0.333
G″	0.857	-0.190	-0.833	0.333
Log(tan δ)	-0.476	0.333	0.452	-0.452

correlation. Note the flat slope of the regression line, indicating the insignificant effect of G*/sin δ, for mixes containing RD aggregate and compacted to 4 percent air voids.

Grouping Analysis

Since analyses up to this point indicated weak or nonexistent relationships between asphalt binder properties and mix shear response, asphalts were separated into groups of similar performance (ranging from "good" to "poor") determined from G*/sin δ values and mix shear response. Then the groups were compared to see whether the same asphalts generally placed in the same group level for both G*/sin δ and mix shear response.

Line graphs were constructed first to illustrate the relative performance of asphalts as a function of G*/sin δ, $N_{2\%}$, and $\Sigma\gamma_p$ (Figure 4.13). Note that $N_{2\%}$ and $\Sigma\gamma_p$ data points represent the average response from all four mix data sets; since test results were not available for one of the asphalt AAG cells, an average response is not shown for AAG. Also recall that an inverse relationship exists between G*/sin δ and $\Sigma\gamma_p$. Tukey pairwise mean comparisons were then used to assist in forming groups of asphalts exhibiting similar performance as measured by $N_{2\%}$ or $\Sigma\gamma_p$ (Paulsen and Sousa 1992). Groups of similar performance based on G*/sin δ were determined visually from Figure 4.13.

The resulting groups of similar performance are presented in Table 4.10. The performance placements are generally consistent. Asphalts AAK, AAM, and ABC consistently placed in the top two groups. Asphalt AAV always placed in the last group. However, there was substantial difference between G*/sin δ and $N_{2\%}$ or $\Sigma\gamma_p$ placements for asphalts AAC and AAM. Asphalt AAM has a G*/sin δ value near the median of asphalts, yet it provided the best mix shear resposne as measured by both $N_{2\%}$ and $\Sigma\gamma_p$. Ashalt ACC has the next-to-lowest G*/sin δ value, yet it provided $N_{2\%}$ and $\Sigma\gamma_p$ reponse near the medians for all asphalts.

Binder Specification Compliance versus Mix Shear Response

The SHRP binder specification limit for G*/sin δ related to permanent deformation was compared with $\Sigma\gamma_p$ observed in laboratory simple shear testing. As shown in Table 4.6, asphalt AAV does not meet the specification requirement of a minimum of 2.0 kPa (Table 1.1); asphalt AAC barely meets the specification. The results shown in Figure 4.12 indicate that this is a generally valid specification requirement. Mixes containing asphalt AAV exhibited the highest values of $\Sigma\gamma_p$ in most cases. However, for mixes containing aggregate RH and compacted to 4 percent air voids, the value of $\Sigma\gamma_p$ for AAC is equal to that for AAV, yet AAC meets the specification. For mixes containing aggregate RD and compacted to 4 percent air voids, AAB and AAG, which meet the specification limit, produce higher values of $\Sigma\gamma_p$ than AAV or AAC; of course, the relatively flat slope of the regression line indicates the insignificance of G*/sin δ for this mix.

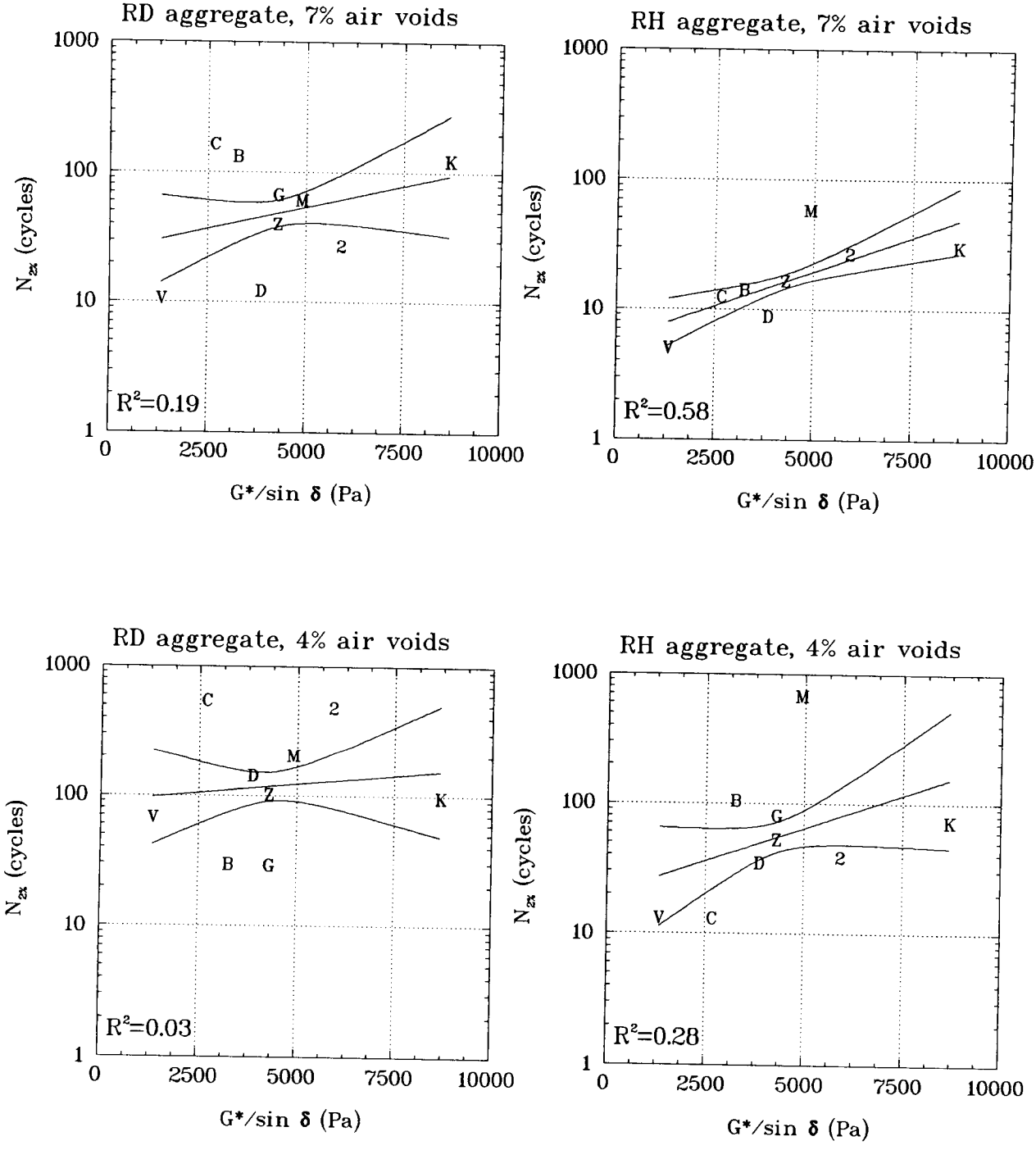

NOTE: Plot symbols represent the last letter of the MRL asphalt code, except symbol 2 which represents ABC.

Figure 4.11. Linear regression plots of $N_{2\%}$ versus G*/sin δ

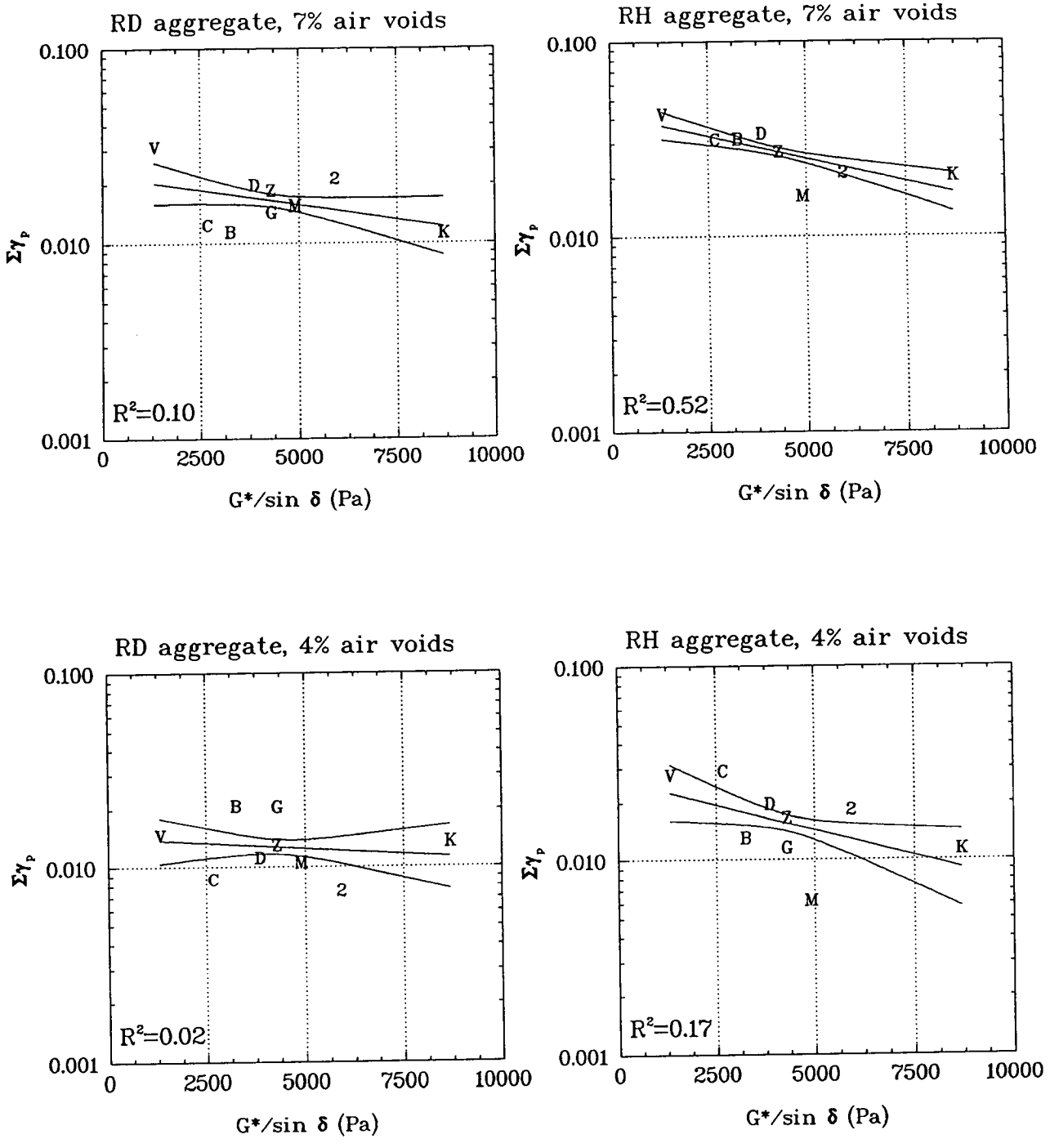

NOTE: Plot symbols represent the last letter of the MRL asphalt code, except symbol 2 which represents ABC.

Figure 4.12. Linear regression plots of $\Sigma\gamma_p$ versus G*/sin δ

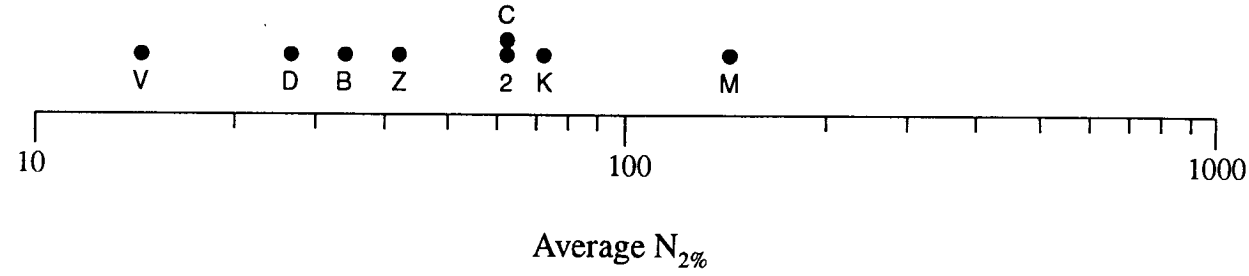

Average $N_{2\%}$

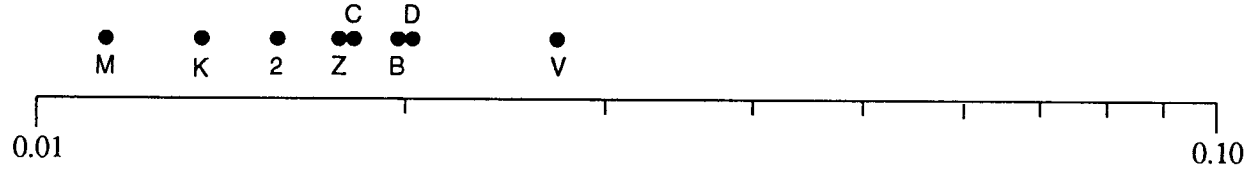

Average $\Sigma\gamma_p$

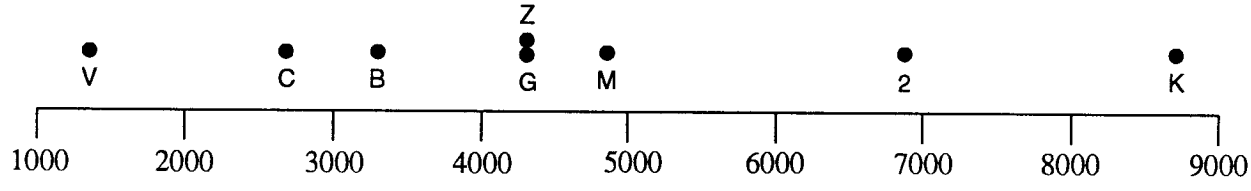

$G^*/\sin\delta$ (Pa)

NOTE: Plot symbols represent last letter of MRL asphalt code, except symbols 2 which represents ABC.

Figure 4.13. Relative asphalt performance by $N_{2\%}$, $\Sigma\gamma_p$, and $G^*/\sin\delta$

Table 4.10. Asphalt performance groups for $N_{2\%}$, $\Sigma\gamma_p$, and G*/sin δ

$N_{2\%}$	Group 1 (good)	Group 2	Group 3	Group 4 (poor)	
	AAM	AAC	AAB	AAV	
		AAK	AAD		
		ABC	AAZ		
$\Sigma\gamma_P$	**Group 1 (good)**	**Group 2**	**Group 3**	**Group 4 (poor)**	
	AAM	AAK	AAB	AAV	
		ABC	AAC		
			AAD		
			AAZ		
G*/sin δ	**Group 1 (good)**	**Group 2**	**Group 3**	**Group 4**	**Group 5 (poor)**
	AAK	AAM	AAD	AAB	AAV
		ABC	AAG	AAC	
			AAZ		

It is not known whether the magnitudes of $\Sigma\gamma_p$ shown in Figure 4.12 indicate that a rutting problem would develop in the pavement. However, this comparison does demonstrate the possibility of accepting an asphalt according to the specification limit that may result in rutting, or rejecting an asphalt that would provide acceptable performance.

Summary and Discussion of Results

Overall, the results of this study indicate that binder properties can affect the shear response of asphalt-aggregate mixes. However, aggregate characteristics can be equally or more significant. Specific findings from this study include the following:

1. Better relationships between asphalt binder properties and mix shear response ($N_{2\%}$ or $\Sigma\gamma_p$) were observed for mixes tested under CH conditions than for mixes tested under FS conditions. The researchers believe this is due to the overwhelming influence of aggregate in the FS shear test. The confining pressure in the FS shear test gives stability to the aggregate skeleton of the mix. This minimizes strains in the asphalt binder, which reduces the influence of the binder properties. The results of the ANOVA support this hypothesis; the influences of asphalt binder properties and air-void content are less pronounced in the FS shear test. The CH shear test, however, confines specimen deformation in only one direction (i.e., the height of the specimen remains constant). Aggregate particles are allowed to slide past each other during shear loading, causing larger strains in the asphalt, which highlights the influence of the binder.

2. Although relationships between asphalt binder properties and mix shear response are generally weak, it appears that any binder property ($G^*/\sin\delta$, G^*, or G'') can be used to estimate mix shear response with the same degree of reliability (poor). Thus, the significance of the $\sin\delta$ term in $G^*/\sin\delta$ is questionable, although it may have a greater effect with modified asphalt binders.

3. The strongest relationship between asphalt binder properties and mix shear response was observed for mixes containing aggregate RH and 7 percent air voids. This suggests that when mix characteristics are such that they result in low interparticle friction, the influence of asphalt binder properties becomes more significant. Aggregate RD was a quarried product that was 100 percent crushed; aggregate RH was a partially crushed river gravel that would be expected to provide less interparticle friction than aggregate RD. This observation underscores the influence of aggregate characteristics on permanent deformation.

Conclusions

The results of A-003A's efforts to validate the effect of A-002A's asphalt binder properties on the permanent deformation response of asphalt-aggregate mixes indicate that the influence of asphalt is highly dependent on the conditions to which the mix is subjected. ANOVA showed that the effect of asphalt was significant but that its influence was small compared with the influence of aggregate type and air-void content, especially when mixes were tested at lower temperatures (e.g., 40°C) or were subjected to states of stress that amplified the aggregate influence (e.g., FS shear test).

The correlations between $G^*/\sin \delta$ and the various measures of permanent deformation response were generally poor. The weak correlations are partly a result of the dominant effect of aggregate characteristics on permanent deformation response. However, in cases where mix characteristics produce low interparticle friction (e.g., aggregate RH and 7 percent air voids) and the mix is subjected to harsh environmental and loading conditions (e.g., 60°C and CH shear test), the influence of the binder becomes more important. When aggregate characteristics or compaction conditions are expected to result in a mix that is susceptible to permanent deformation, selection of a binder that can overcome these deficiencies will be important. It appears that the value of $G^*/\sin \delta$ will be used to screen binders that will provide inferior performance in such cases.

The results of these studies underscore the importance of mix testing, in addition to binder testing, for evaluation of permanent deformation in pavements. Although the mix tests used in these validation efforts are only estimates of the permanent deformation response that would actually occur in a pavement, the general conclusions presented herein are expected to hold when future studies compare asphalt binder properties with permanent deformation response of mixes measured from larger-scale wheel-tracking tests and actual pavement performance.

5

Thermal Cracking Validation of Binder Properties

A-002A Hypothesis

The Strategic Highway Research Program (SHRP) A-002A performance ranking of asphalt cements for resistance to thermal cracking is based on the following parameters (see Table 5.1):

1. Limiting stiffness temperature.

2. Ultimate strain at failure.

The limiting stiffness temperature was estimated based on a stiffness value of 200 MPa at a loading time of 2 hr in the bending beam rheometer test. The ultimate strain at failure was estimated at -26°C and a loading time of 2 hr in the direct tension test.

The asphalts were ranked from 1 (best) to 28 (worst) on the basis of the parameter values and their observed ranges.

The associated rankings for resistance to low-temperature cracking were based on the average of the two parameters and are given in Table 5.1. Individual rankings based on each parameter are given in the report by Jung and Vinson (1992).

Experiment Design

The experiment design for this task was developed to relate fundamental properties of asphalt cement suggested by the A-002A contractor to the thermal cracking characteristics of

Table 5.1. Ranking of SHRP tank asphalts for resistance to thermal cracking

Asphalt Type	Limiting Stiffness Temperature at S(t) = 200 MPa at 2 hr (°C)	Ultimate Strain Failure at -26°C, 2 hr (%)	Overall Rank (1 = best)
AAA-1	-31	3.1	1
AAB-1	-28	1.7	12
AAC-1	-25	1.5	15
AAD-1	-30	2.5	5
AAE-1	-29	2.1	8
AAF-1	-21	1.2	20
AAG-1	-18	0.8	25
AAH-1	-32	2.1	6
AAJ-1	-25	1.5	15
AAK-1	-27	1.7	12
AAL-1	-30	2.8	3
AAM-1	-24	1.5	16
AAN-1	-24	1.5	15
AAO-1	-28	2.1	9
AAP-1	-27	2.2	9
AAQ-1	-24	1.1	18
AAR-1	-26	1.7	13
AAS-1	-27	2.0	11
AAT-1	-23	1.6	16
AAU-1	-23	1.7	16
AAV-1	-25	1.2	17
AAW-1	-22	1.6	17
AAX-1	-20	1.1	21
AAY-1	-28	1.8	11
AAZ-1	-20	1.2	21
ABA-1	-29	2.4	7
ABC-1	-30	2.2	8
ABD-1	-15	0.5	28

asphalt-concrete mixes, as measured by the thermal stress restrained specimen test (TSRST). The details of experiment design are discussed in this section. Descriptions of sample and specimen preparation and TSRST as indicated by the A-002A procedure are also given.

The experiment design includes 14 asphalt cements and two aggregate types. Two degrees of aging and two levels of air-void content were also employed. A 14 x 2 x 2 x 2 x 2 replicated full-factorial design was developed as follows:

Experiment Design Variable	Levels
Asphalt type	14
Aggregate type	2
Degree of aging	2 (short, long)
Air-void content	2 (4%, 8%)
Rate of cooling	1 (10°C/hr)
Replicates	2
Total number of tests	224

The asphalts and aggregates were selected from the Materials Reference Library. The asphalts and aggregates involved in the experiment design are presented in Table 5.2. The 14 asphalt cements selected represent a variety of crude sources with a wide range of temperature susceptibility characteristics. Mineral aggregates from two sources were used in the experiment. Aggregate RC is an absorptive (3.7 percent water absorption) crushed limestone from Kansas; aggregate RH is a crushed silicious gravel—greywacke (high SiO_2 content) from California.

Table 5.2. Materials involved in experiment design

Materials	Type
Asphalt	AAA-1,[a] AAB-1,[a] AAC-1,[a] AAD-1,[a] AAF-1,[a] AAG-1,[a] AAK-1[a] AAL-1, AAM-1,[a] AAV-1, AAW-1, AAX-1, AAZ-1, ABC-1
Aggregate	RC limestone from Kansas, RH greywacke from California

[a]SHRP core asphalts

Specimen Preparation

The aggregate gradations and binder contents for the aggregates RC and RH used to prepare the asphalt-concrete mixes are given in Table 2.2. Both the aggregate and asphalt to be mixed were preheated at a specified mixing temperature depending on asphalt type. The mixing temperature for each asphalt was selected from a bitumen test data chart (BTDC) at a viscosity of 170±20 centistokes (approximately 160±20 centipoises). After mixing, the loose mix was subjected to short-term oven aging (STOA) for 4 hr at 135°C. Following STOA the mix was compacted. Some compacted specimens were also subjected to long-term oven aging (LTOA) for 5 days at 85°C.

Beam specimens were prepared by kneading compaction (Cox type). The compaction tools, compaction equipment, and mix were preheated at the compaction temperature. The compaction temperature for each asphalt type was determined from the BTDC and corresponds to a viscosity of 280±30 centistokes (approximately 265±30 centipoises). Two levels of compactive effort were employed to prepare the beam samples (15.2 × 15.2 × 40.6 cm) depending on the target air-void contents. Beams prepared at the higher air-void content were compacted in two lifts, whereas the lower air-void content beams were compacted in four lifts. Four test specimens (5.0 × 5.0 × 25.0 cm) were sawed from each large beam sample (Jung and Vinson 1992).

Test Procedures

The test used to evaluate all mixes (STOA and LTOA) was the TSRST. All test specimens were aligned with an alignment stand and bonded to end platens with an epoxy compound. After the epoxy had cured, the test specimens with end platens were cooled to 5°C for 1 hr to establish thermal equilibrium before testing. Next, the specimen with end platens was set up

in the environmental cabinet and the TSRST was performed at a monotonic cooling rate of 10°C/hr until fracture.

Typical TSRST results are shown in Figure 5.1. From the test results, four parameters may be identified to relate the fundamental properties of asphalt cement and aggregate to thermal cracking characteristics of asphalt-concrete mixes used to validate the A-002A hypothesis for thermal cracking: fracture temperature, fracture strength, slope of the thermally induced stress curve, and transition temperature. Only fracture temperature and strength are discussed here because of the direct relation to mix performances. More details on the test protocol can be found in the report by Jung and Vinson (1992).

TSRST Results for Asphalt-Aggregate Mix

Out of 224 specimens, a total of 201 TSRSTs were used to accomplish the project objectives. The remainder were discarded because the air-void content was outside the acceptable range.

Fracture Temperature

Fracture temperature is defined as the temperature at which fracture occurs and corresponds to the temperature at which the thermal stress induced in the specimen is maximum. Mean values and the coefficients of variation (CVs) of fracture temperature for a specific asphalt type, aggregate type, and degree of aging are summarized in Tables 5.3 and 5.4. Figures 5.2 and 5.3 show variations of fracture temperatures for STOA and LTOA depending on asphalt type for aggregates RC and RH, respectively.

The repeatability of TSRST for fracture temperature is considered to be good and is in the range of 1°C to 3°C. The coefficients of variation for fracture temperature are close to or below 10 percent. The fracture temperatures exhibit a wide range of values depending on the asphalt type. The fracture temperatures of specimens with aggregate RC ranged from -32.1°C to -18.6°C for STOA and from -27.8°C to -13.6°C for LTOA. For specimens with aggregate RH, fracture temperatures ranged from -32.2°C to -16.3°C for STOA and from -29.3°C to -13.6°C for LTOA. Summary statistics for fracture temperature are given in Table 5.5.

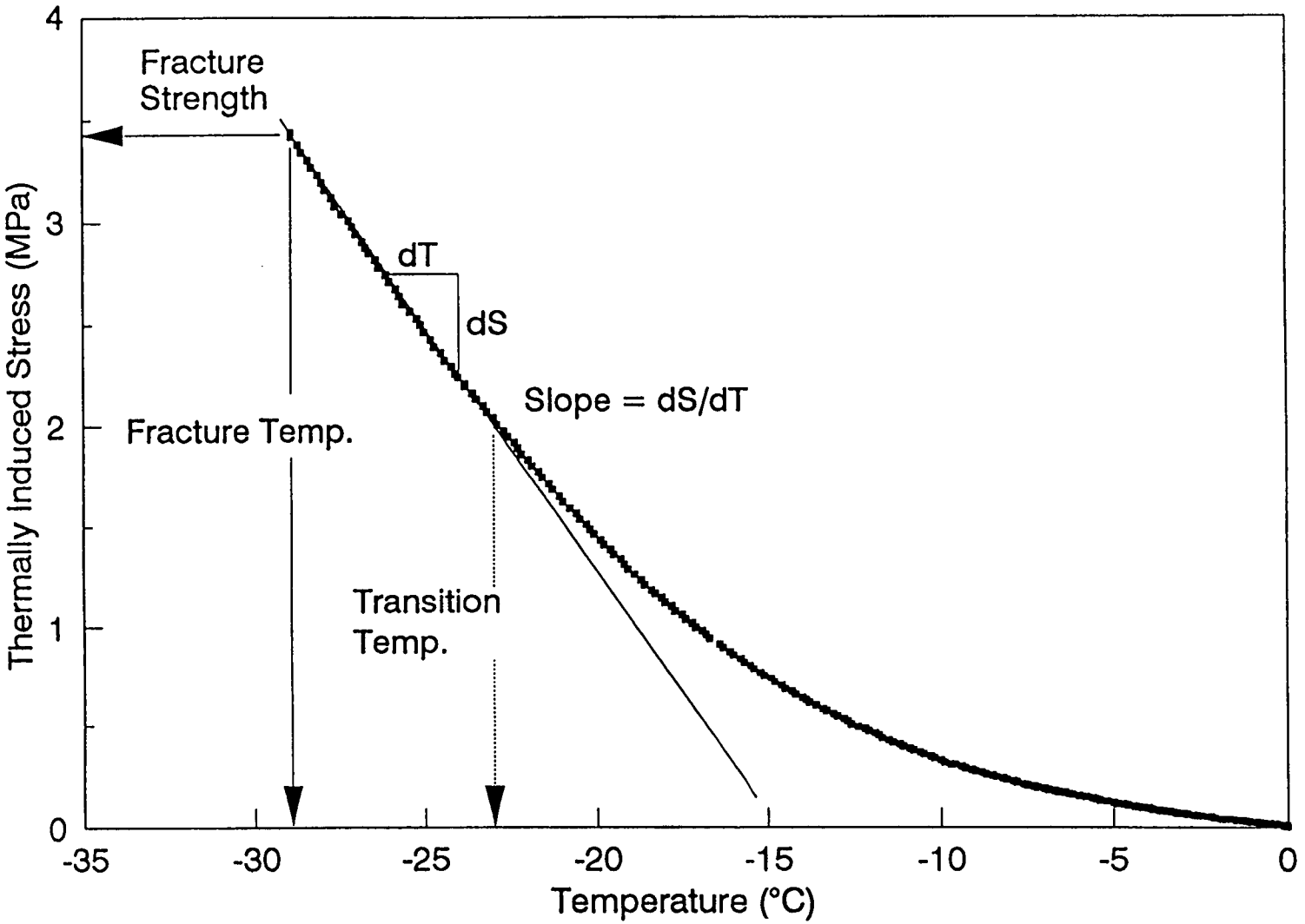

Figure 5.1. Typical results of TSRST

Table 5.3. Fracture temperature for short-term aged specimens

Asphalt	Aggregate	No. of Obs.	Minimum (°C)	Maximum (°C)	Mean (°C)	CV (%)
AAA-1	RC	3	-34.1	-30.7	-32.1	-5.60
	RH	2	-32.4	-31.9	-32.2	-1.69
AAB-1	RC	5	-28.2	-22.1	-26.2	-10.38
	RH	5	-27.9	-26.5	-27.1	-2.09
AAC-1	RC	4	-26.7	-22.3	-24.3	-7.57
	RH	5	-23.4	-20.6	-21.9	-4.67
AAD-1	RC	3	-31.6	-29.9	-30.6	-2.85
	RH	3	-28.7	-28.1	-28.4	-1.06
AAF-1	RC	4	-20.7	-17.1	-18.6	-8.31
	RH	3	-20.4	-17.1	-18.9	-7.27
AAG-1	RC	4	-21.8	-18.4	-20.1	-6.97
	RH	4	-17.9	-15.0	-16.3	-7.84
AAK-1	RC	5	-26.8	-23.0	-24.9	-6.98
	RH	4	-24.7	-23.0	-23.8	-3.34
AAL-1	RC	2	-32.2	-31.3	-31.8	-2.00
	RH	4	-31.9	-29.8	-30.8	-3.15
AAM-1	RC	4	-23.4	-19.6	-21.6	-8.51
	RH	6	-21.8	-20.2	-20.8	-2.59
AAV-1	RC	3	-28.6	-26.4	-27.5	-4.01
	RH	4	-27.0	-25.6	-26.0	-2.57
AAW-1	RC	3	-21.8	-20.9	-21.5	-2.30
	RH	5	-22.3	-20.1	-21.6	-4.04
AAX-1	RC	5	-22.3	-19.7	-21.4	-4.72
	RH	4	-20.6	19.1	-20.0	-3.49
AAZ-1	RC	4	-23.0	-21.3	-22.2	-4.06
	RH	5	-21.1	-18.2	-19.6	-5.98
ABC-1	RC	2	-30.1	-28.7	-29.4	-3.37
	RH	2	-28.8	-28.2	-28.5	-1.49

Table 5.4. Fracture temperature for long-term aged specimens

Asphalt	Aggregate	No. of Obs.	Minimum (°C)	Maximum (°C)	Mean (°C)	CV (%)
AAA-1	RC	3	-28.2	-27.3	-27.8	-1.70
	RH	2	-29.6	-28.9	-29.3	-1.69
AAB-1	RC	4	-24.4	-23.0	-23.8	-2.44
	RH	2	-22.1	-22.0	-22.1	-0.32
AAC-1	RC	3	-24.1	-22.1	-22.9	-4.62
	RH	6	-22.1	-19.6	-21.0	-4.80
AAD-1	RC	2	-25.3	-21.6	-24.2	-6.73
	RH	5	-25.5	-23.0	-23.6	-4.46
AAF-1	RC	4	-17.9	-13.5	-15.8	-14.74
	RH	3	-15.8	-14.7	-15.1	-3.87
AAG-1	RC	3	-15.8	-12.0	-13.6	-14.64
	RH	4	-14.5	-12.6	-13.06	-6.33
AAK-1	RC	4	-21.4	-18.2	-19.8	-6.82
	RH	2	-21.2	-20.8	-21.0	-1.35
AAL-1	RC	2	-26.3	-24.4	-25.4	-5.30
	RH	5	-26.9	-24.6	-25.8	-4.15
AAM-1	RC	3	-22.7	-20.1	-21.0	-6.88
	RH	5	-20.8	-19.0	-20.2	-3.65
AAV-1	RC	3	-24.3	-23.9	-24.1	-0.86
	RH	3	-23.8	-23.3	-23.6	-1.07
AAW-1	RC	5	-19.9	-18.4	-19.2	-3.60
	RH	4	-18.3	-16.0	-17.2	-5.48
AAX-1	RC	2	-18.5	-18.2	-18.4	-1.16
	RH	3	-18.8	-17.0	-17.7	-5.45
AAZ-1	RC	3	-17.5	-16.6	-17.1	-2.68
	RH	4	-18.9	-17.4	-18.2	-3.44
ABC-1	RC	3	-25.8	-24.4	-25.2	-2.86
	RH	2	-24.6	-23.1	-23.9	-4.45

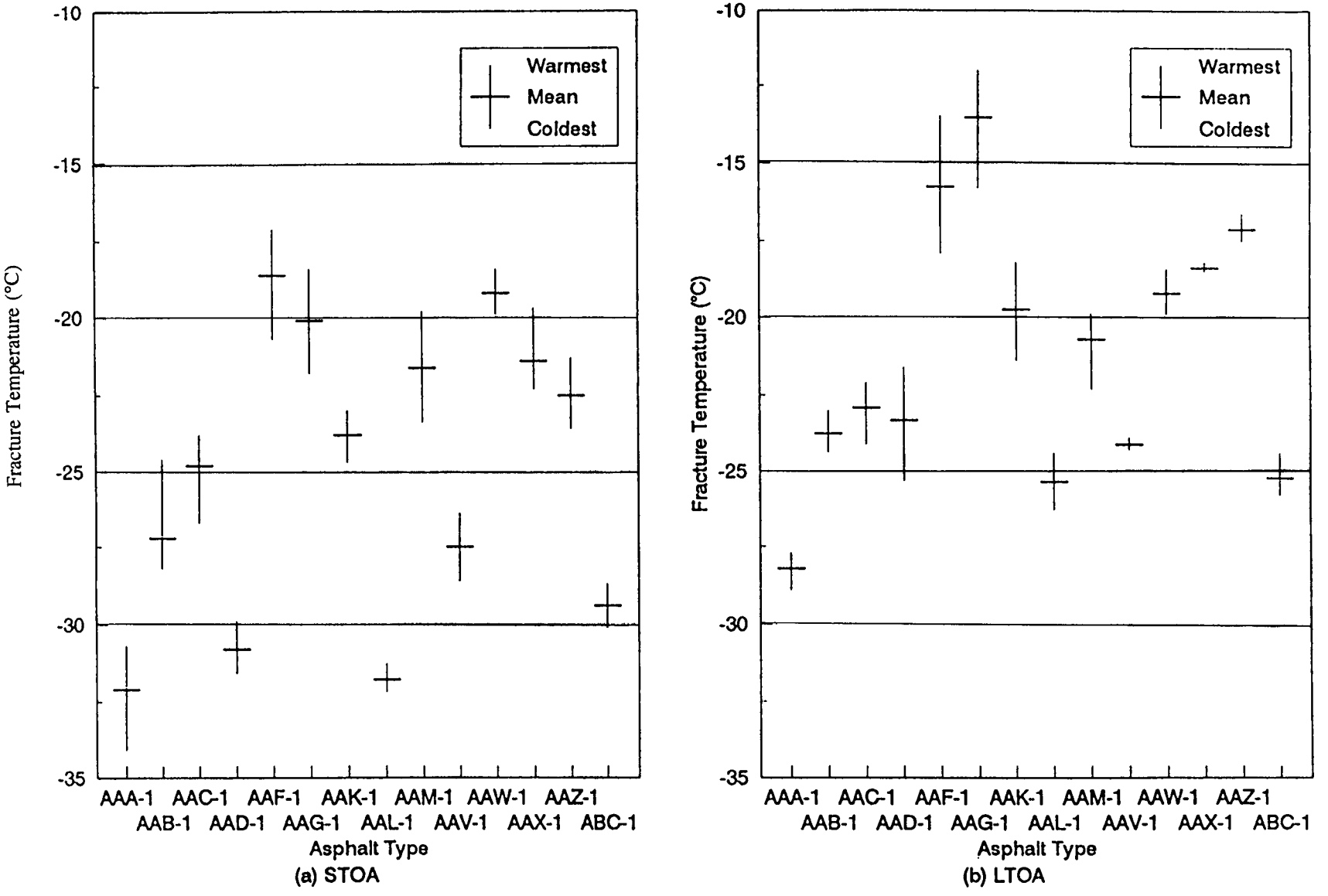

Figure 5.2. Fracture temperature (RC)

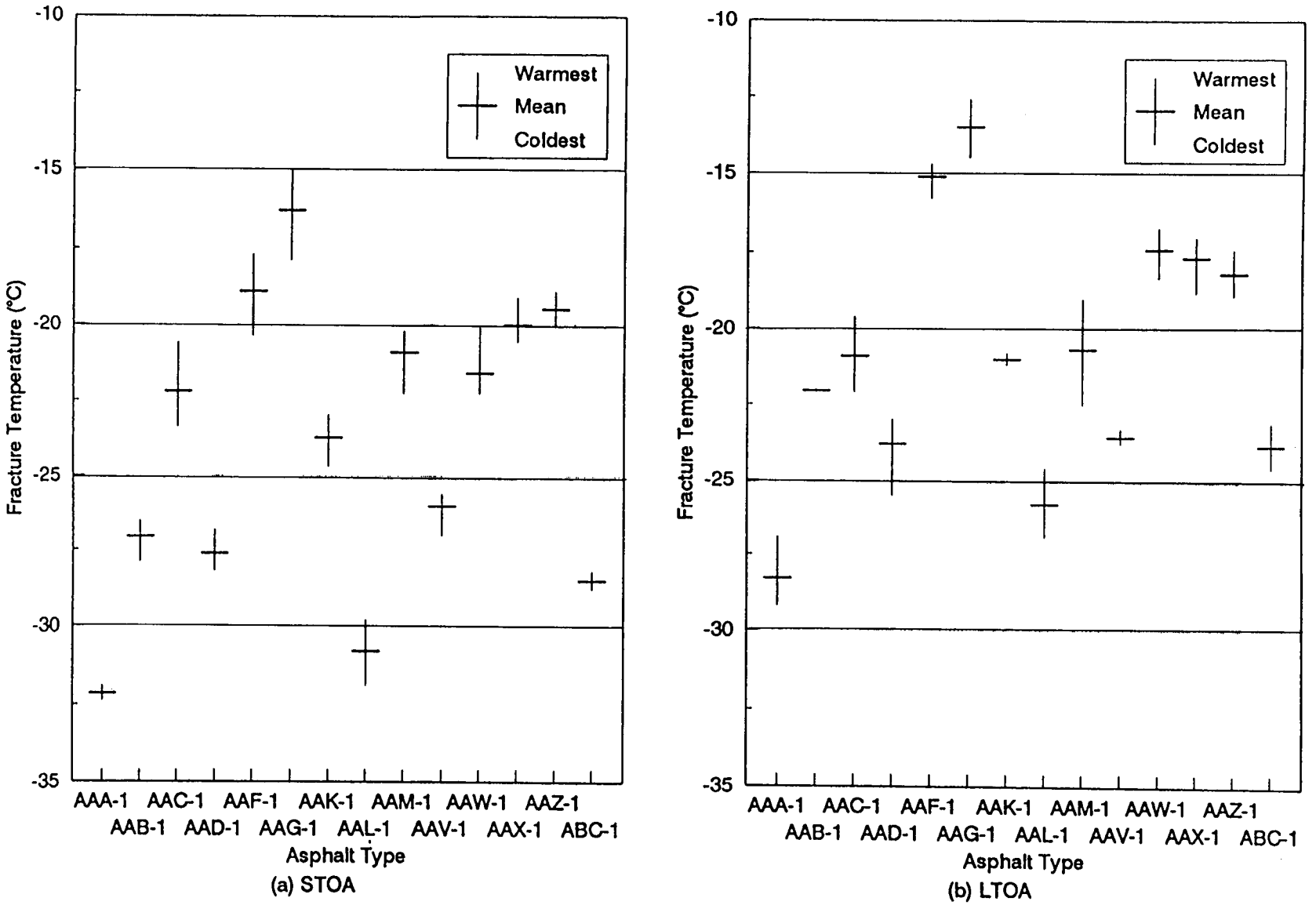

Figure 5.3. Fracture temperature (RH)

Fracture Strength

Fracture strength is defined in terms of the maximum stress developed at fracture. Mean values and the coefficients of variation of fracture strength for a specific asphalt type, aggregate type, and degree of aging are summarized in Tables 5.6 and 5.7. Figures 5.4 and 5.5 show variations of fracture strengths for STOA and LTOA depending on asphalt type for aggregates RC and RH, respectively.

The repeatability of TSRST for fracture strength is considered reasonable. Most of the coefficients of variation for fracture strength are close to or below 20 percent. The fracture strengths exhibit a wide range of values depending on the asphalt type. The fracture strengths of specimens with RC aggregate ranged from 1.9 to 2.9 MPa for STOA and from 2.1 to 2.9 MPa for LTOA. For specimens with RH aggregate, fracture strengths ranged from 2.6 to 3.5 MPa for STOA and from 2.0 to 3.4 MPa for LTOA. Summary statistics for fracture strengths are given in Table 5.8.

Statistical Analysis of TSRST Results

Statistical analyses were performed on the TSRST results using general linear model (GLM) procedures included in the SAS software package (SAS Institute Inc. 1991). The specific analyses included (1) analysis of covariance, (2) analysis of least-squares means, and (3) Waller-Duncan T-test.

Data Description

The source variables considered in the model are asphalt type (AAA-1 through ABC-1), aggregate type (RC and RH), degree of aging (short-term and long-term), and air-void content. The dependent variables in the model are fracture temperature and fracture strength. The source and dependent variables considered in the analysis are described in Table 5.9.

The experiment design included a total of $14 \times 2 \times 2 \times 2 \times 2 = 224$ experiments. In reality, it was difficult to achieve the target air-void contents of 4 and 8 percent because of difficulties in compaction with the aggregates selected. The resulting air-void contents ranged from 2 to 15 percent. In addition, for the target air-void content of 4 percent, a significant amount of aggregate breakage occurred during compaction, particularly for aggregate RC. Consequently, several specimens from the 224 identified in the original experiment design were discarded. A total of 201 test results were included in the analysis.

Table 5.5. Summary statistics for fracture temperature

Aggregate Type	Degree of Aging	Warmest Fracture Temp. (°C)	Coldest Fracture Temp. (°C)	Range (Warm minus Cold)
RC	STOA	-18.6	-32.1	15.4
	LTOA	-13.6	-27.8	12.9
	Difference (STOA minus LTOA)	Minimum -0.6	Maximum -6.5	Average -3.8
RH	STOA	-16.3	-32.2	15.7
	LTOA	-13.6	-29.3	14.8
	Difference (STOA minus LTOA)	Minimum -0.6	Maximum -5.5	Average -2.9
Difference in STOA (°C) (RC minus RH)		Maximum: -3.8 Minimum: 0.9 Average: -1.16		
Difference in LTOA (°C) (RC minus RH)		Maximum: -2.0 Minimum: 1.6 Average: -0.42		

Table 5.6. Fracture strength for short-term aged specimens

Asphalt	Aggregate	No. of Obs.	Minimum (MPa)	Maximum (MPa)	Mean (MPa)	CV (%)
AAA-1	RC	3	2.436	2.836	2.617	15.557
	RH	2	3.485	3.540	3.512	1.111
AAB-1	RC	5	2.070	2.387	2.211	6.345
	RH	5	2.512	3.319	2.919	11.645
AAC-1	RC	4	1.884	2.498	2.177	11.546
	RH	5	2.201	2.629	2.472	5.651
AAD-1	RC	3	1.904	2.636	2.244	16.408
	RH	3	2.325	3.181	2.870	16.499
AAF-1	RC	4	1.663	2.008	1.884	8.048
	RH	3	2.484	2.836	2.617	7.288
AAG-1	RC	4	1.898	2.167	2.048	5.443
	RH	4	2.443	2.808	2.589	6.371
AAK-1	RC	5	1.771	2.254	1.971	11.727
	RH	4	2.884	3.388	3.076	7.119
AAL-1	RC	2	2.332	3.209	2.770	22.367
	RH	4	2.436	3.333	2.884	14.707
AAM-1	RC	4	2.719	3.257	2.922	8.602
	RH	6	3.050	3.202	3.127	2.195
AAV-1	RC	3	1.691	1.973	1.877	8.599
	RH	4	2.036	3.443	2.705	22.194
AAW-1	RC	3	2.381	2.650	2.413	9.224
	RH	5	2.229	3.098	2.742	13.307
AAX-1	RC	5	1.870	2.939	2.378	19.966
	RH	4	2.525	2.988	2.770	8.460
AAZ-1	RC	4	2.477	3.402	2.896	13.795
	RH	5	2.123	3.098	2.600	17.233
ABC-1	RC	2	2.505	2.712	2.608	5.612
	RH	2	2.250	2.919	2.584	18.315

Table 5.7. Fracture strength for long-term aged specimens

Asphalt	Aggregate	No. of Obs.	Minimum (MPa)	Maximum (MPa)	Mean (MPa)	CV (%)
AAA-1	RC	3	2.594	3.409	2.891	15.557
	RH	2	3.436	3.457	3.447	0.425
AAB-1	RC	4	2.443	3.195	2.663	13.420
	RH	2	2.815	3.098	2.957	6.766
AAC-1	RC	3	2.236	3.098	2.903	19.923
	RH	6	2.415	3.057	2.765	8.985
AAD-1	RC	2	2.760	3.063	2.898	6.734
	RH	5	2.394	3.105	2.921	9.686
AAF-1	RC	4	1.829	2.857	2.243	19.707
	RH	3	1.642	2.754	1.983	25.919
AAG-1	RC	3	1.484	3.071	2.153	38.189
	RH	4	2.132	2.864	2.460	15.590
AAK-1	RC	4	1.753	2.933	2.377	22.385
	RH	2	2.967	3.312	3.140	7.770
AAL-1	RC	2	2.622	2.926	2.774	7.739
	RH	5	2.125	2.912	2.710	8.114
AAM-1	RC	3	2.387	3.057	2.788	12.677
	RH	5	3.298	3.540	3.413	8.970
AAV-1	RC	3	2.153	2.981	2.456	18.565
	RH	3	2.415	3.326	2.870	15.865
AAW-1	RC	5	2.353	3.181	2.654	12.576
	RH	4	2.208	2.657	2.399	9.349
AAX-1	RC	2	2.470	2.788	2.629	8.537
	RH	3	2.581	2.843	2.705	4.867
AAZ-1	RC	3	1.822	2.546	2.226	16.604
	RH	4	2.884	3.071	2.979	2.795
ABC-1	RC	3	1.208	2.629	2.109	97.165
	RH	2	2.401	2.601	2.501	18.315

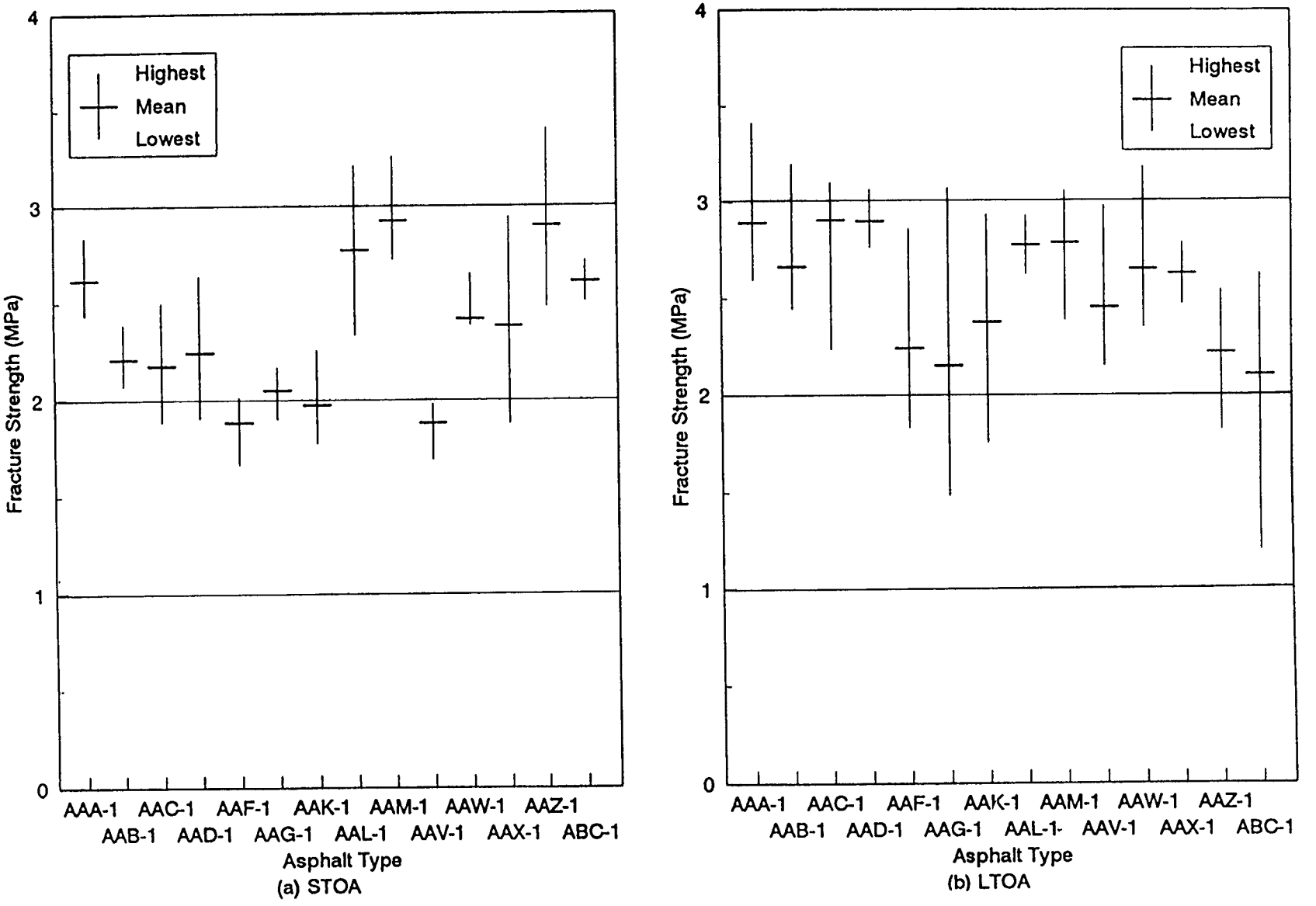

Figure 5.4. Fracture strength (RC)

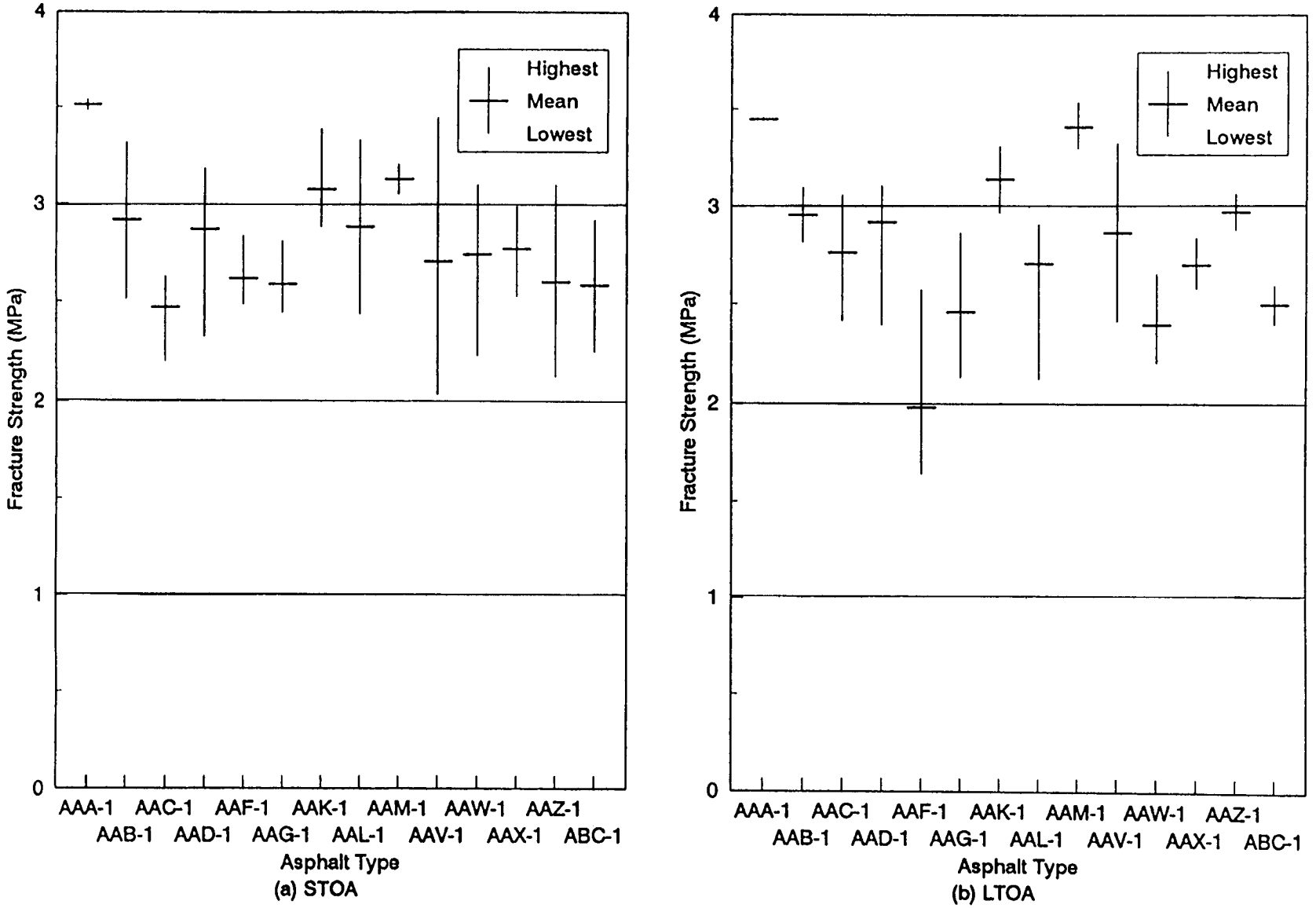

Figure 5.5. Fracture strength (RH)

Table 5.8. Summary statistics for fracture strength

Aggregate Type	Degree of Aging	Max. Fracture Strength (MPa)	Min. Fracture Strength (MPa)	Range (Max. minus Min)
RC	STOA	2.922	1.877	1.045
	LTOA	2.903	2.109	0.794
	Difference (STOA minus LTOA)	Maximum 0.726	Minimum -0.670	Average 0.20
RH	STOA	3.512	2.584	0.928
	LTOA	3.447	1.983	1.464
	Difference (STOA minus LTOA)	Maximum 0.379	Minimum -0.634	Average -0.02
Difference in STOA, MPa (RH minus RC)		Maximum: 1.105 Minimum: -0.296 Average: 0.467		
Difference in LTOA, MPa (RH minus RC)		Maximum: 0.763 Minimum: -0.260 Average: 0.249		

Table 5.9. Description of variables

Source Variables	Levels	Description
ASP	AAA-1, AAB-1, AAC-1, AAD-1, AAF-1, AAG-1, AAK-1, AAL-1, AAM-1 AAV-1, AAW-1, AAX-1, AAZ-1, ABC-1	Asphalt type
AGG	RC, RH	Aggregate type
AGE	ST (short-term aging) LT (long-term aging)	Degree of aging
VOID	Covariate	Air-void content

Dependent Variables	Description
FRTEMP	Fracture temperature
FRSTRE	Fracture strength

Analysis of Covariance

Since the air-void contents were not fully controlled, the source variable VOID was considered to be a covariate (continuous variable) in the analysis. The analysis of covariance was performed using a GLM procedure. The analysis of covariance combined some of the features of regression and analysis of variance. Typically, the covariate was introduced into the model used for analysis of variance.

The GLM procedure provides both Type I and Type III hypothesis tests. The Type I mean squares indicate the influence of a factor after the effects of the factors listed before it in the model have been removed. The Type III mean squares indicate the influence of a factor after the effects of all the other factors in the model have been removed. The procedure can also provide least-squares means (LSMEANs). LSMEANs of a variance are estimated for a given level of a given effect and adjusted for the covariate. That is, LSMEANs of fracture temperature and strength for a specific asphalt type are mean values of these variables adjusted for the average air-void content, which considered the effect of aggregate type and degree of aging.

The procedure followed in the analysis was to (1) consider the full model that includes all possible factors, (2) perform the analysis of covariance for the model, (3) select and delete insignificant factors in the model, (4) repeat the analysis for the reduced model without insignificant factors until reasonable factors can be selected, and (5) finalize the model.

Fracture Temperature Model

Following the procedures outlined above, a series of hypotheses was tested starting with the full model, including asphalt source (ASP), aggregate source (AGG), short- or long-term aging

(AGE), air-void content (VOID), and the interactions of ASP with AGG (ASP*AGG), ASP with AGE (ASP*AGE), and AGG with AGE (AGG*AGE) as independent variables and fracture temperature (FRTEMP) as the dependent variable.

According to the Type III hypothesis, all the factors indicated above were considered significant using an α value of 0.05. However, the Type III mean square for ASP*AGG was not significant compared with the other factors and was dropped according to the general procedures used for the Type III hypothesis test.

Using a reduced set of variables (without ASP*AGG), it was determined that the remaining factors were all significant at the 0.05 level but that the mean square for AGG*AGE was not significant compared with the other factors; therefore, a second reduced model was tested deleting this interaction term.

The second reduced model included AGE, ASP, AGG, VOID, and ASP*AGE. The Type III mean square for AGG was not significant, and it was dropped for the third reduced model, which includes ASP, AGE, VOID, and ASP*AGE. Testing the third reduced model indicated that all the factors were significant and should be included in the fracture temperature model.

The ranking for the factors considered in the third reduced model based on Type III mean squares is AGE >ASP > VOID > ASP*AGE. Type III mean squares for AGE and ASP are much larger than the mean squares for VOID and ASP*AGE. Thus, it can be concluded that of all the factors considered, degree of aging and asphalt source have a dominant influence on fracture temperature.

The mean square errors (MSEs) for the full model and the reduced models are given in Table 5.10. The increase in the MSE value reflects the contribution made by dropping factors in the reduced models. Since the objective is to identify the dominant factors, the relatively small increase in the MSE is to be expected. Figures 5.6 and 5.7 illustrate the relationship between fracture temperature and aging, both long- and short-term, and by aggregate type.

Fracture Strength Model

An analysis similar to that conducted for fracture temperature was also conducted for fracture strength. The full model included ASP, AGG, AGE, VOID, ASP*AGG, ASP*AGE, and AGG*AGE. The Type III mean square for ASP*AGG was not significant for this model, and this factor was dropped.

Table 5.10. Mean square errors for fracture temperature models

Model	Factors Involved	Mean Square Errors[a]
Full model	ASP, AGG, AGE, VOID, ASP*AGG, ASP*AGE, AGG*AGE	1.141
Reduced model I	ASP,AGG, AGE, VOID, ASP*AGE, AGG*AGE	1.267
Reduced model II	ASP, AGG, AGE, VOID, ASP*AGE	1.303
Reduced model III	ASP, AGE, VOID, ASP*AGE	1.385

[a]Increasing value indicates poorer correlation as a result of dropping factors.

Using a reduced set of variables (ASP, AGG, AGE, VOID, ASP*AGE, AGG*AGE), it was determined that the remaining factors were all significant at the 0.05 level, except for the factor ASP*AGE. Thus, ASP*AGE was dropped from the model.

The second reduced model included ASP, AGG, AGE, VOID, and AGG*AGE. The Type III mean square values for all the factors in this model are significant except the one for AGE.

The third reduced model included ASP, AGG, VOID, and AGG*AGE. The Type III mean squares for all the factors in this model are significant, indicating that all these factors should be included in the fracture strength model.

The ranking for the factors considered in the third reduced model based on the Type III mean squares is VOID > AGG > AGG*AGE > ASP. The Type III mean squares for VOID and AGG are much greater than those for AGG*AGE and ASP. Thus, fracture strength is highly affected by air-void content and aggregate type, and affected by the interaction between aggregate type and degree of aging and by asphalt type to a much lesser extent. Table 5.11 shows the mean square errors for all the models considered.

LSMEANs of fracture strength for STOA and LTOA specimens are compared in Figure 5.8, while LSMEANs of fracture strength for specimens with aggregates RC and RH are compared in Figure 5.9.

Since the air-void contents were not fully controlled, the test results were divided into two groups, high and low. Low air-void contents were less than 6 percent; high air-void contents were greater than 6 percent. The LSMEANs of fracture strength for high and low air-void contents were obtained for specimens with a specific asphalt type that had at least two observations for each air-void group. Figure 5.10 compares fracture strength for high and low air-void contents. As indicated, fracture strengths are greater for specimens with low air-void contents.

Waller-Duncan T-test

The Waller-Duncan T-test was performed to separate asphalt types showing similar response for a specific dependent variable. The Waller-Duncan T-test is a multiple comparison method that provides information about the differences among the means with unequal cell sizes. The test provides Waller's grouping of asphalts at a specified significance level.

The test was performed on the dependent variables FRTEMP and FRSTRE for specific asphalt types at a significance level of 0.05. Waller's groupings of asphalts for each dependent variable are presented for a specific aggregate type in Figures 5.11 through 5.14. Asphalts with the same letter are not significantly different at a significance level of 0.05. As indicated, asphalts are well divided into several groups for fracture temperature. For fracture strength, the asphalts are divided into three to six groups. Each group includes a wide range of asphalts, and the groups overlap.

Discussion of Results

Asphalt type, aggregate type, degree of aging, and air-void content have a substantial influence on the thermal cracking resistance of asphalt-concrete mixes as measured by the TSRST; interactions between these factors have a minor influence.

Fracture temperature was significantly influenced by asphalt type and degree of aging, and much less influenced by aggregate type and air-void content. LSMEAN of fracture temperature for LTOA mixes was warmer than for STOA mixes. LSMEAN of fracture temperature showed no significant difference between aggregate types.

Fracture strength was significantly influenced by air-void content and aggregate type, and less dependent on asphalt type and degree of aging. LSMEAN of fracture strength for aggregate RH was greater than that for aggregate RC. LSMEAN of fracture strength for LTOA mixes was slightly greater than for STOA mixes. However, as shown in Figure 5.8, the fracture strength was lower for a few LTOA mixes.

The thermal cracking resistance of asphalt-concrete mixes may be affected by the characteristics of aggregates in several ways. For example, the aggregate may influence thermal regime and stiffness of the mix and aging characteristics of the asphalt cement. Aggregate RC is highly porous and thus may have lower thermal conductivity, leading to lower thermal conductivity of mixes with aggregate RC. It will take longer for the mix with

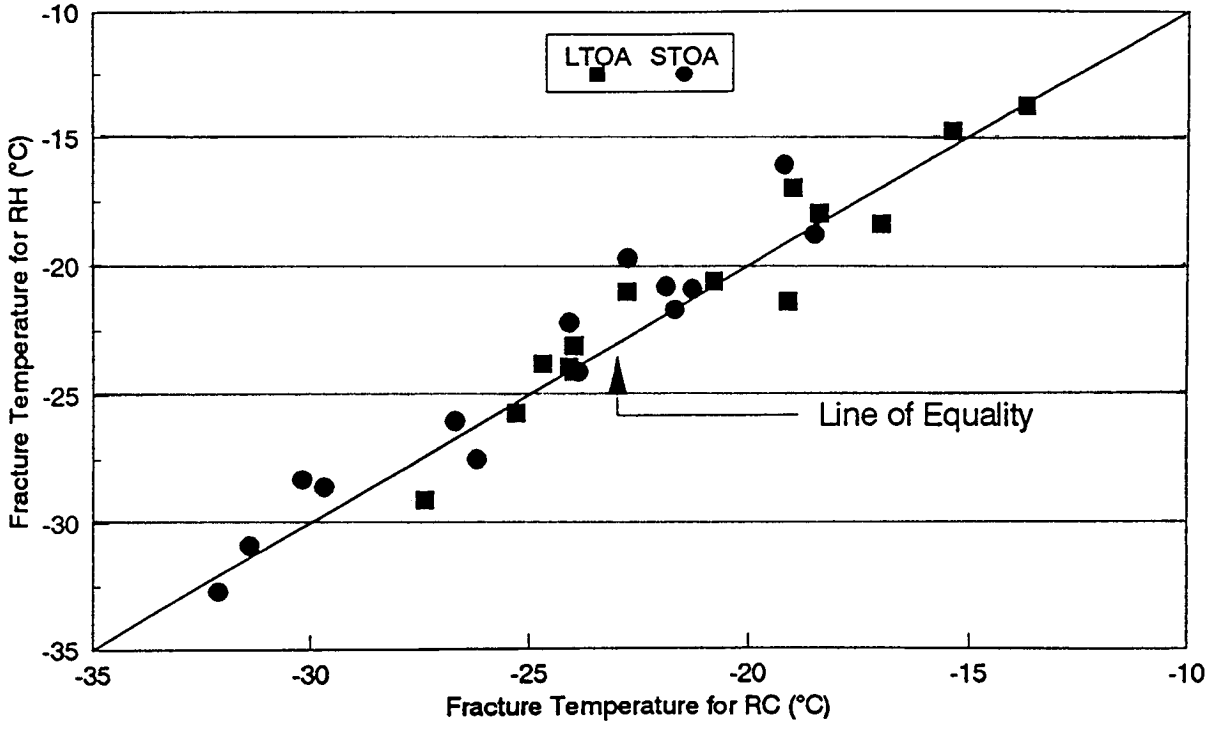

Figure 5.6. Comparison of fracture temperature for STOA and LTOA specimens

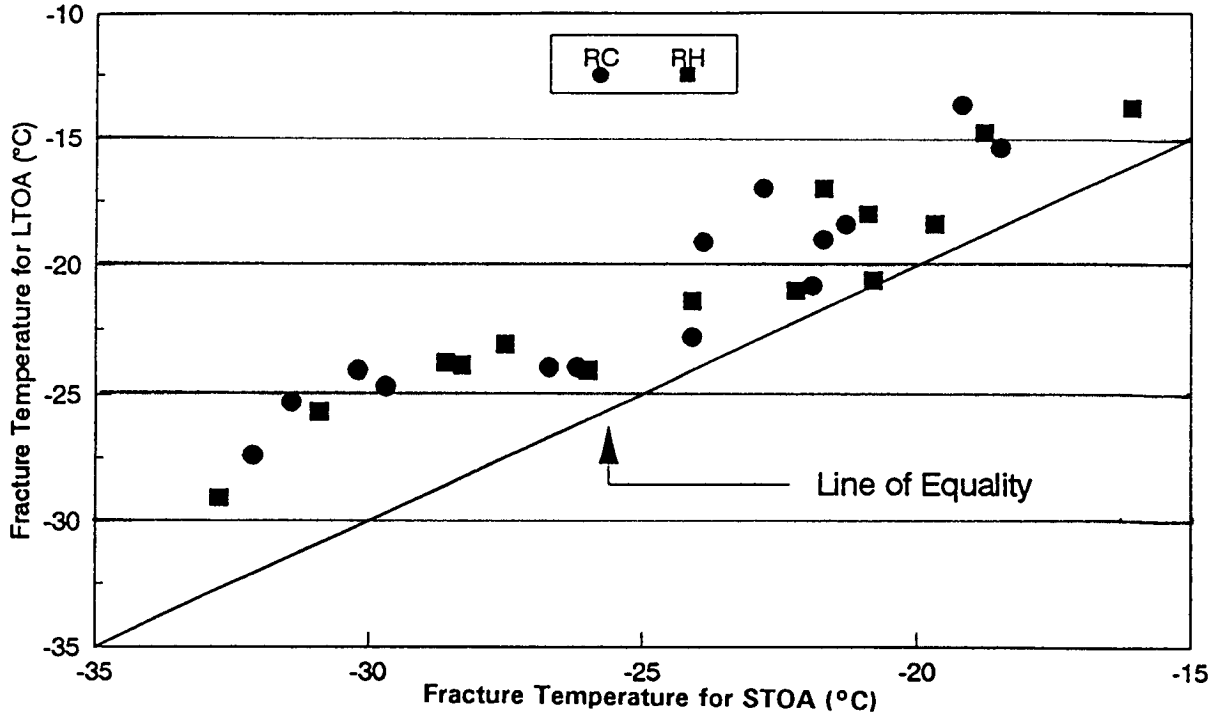

Figure 5.7. Comparison of fracture temperature for aggregates RC and RH

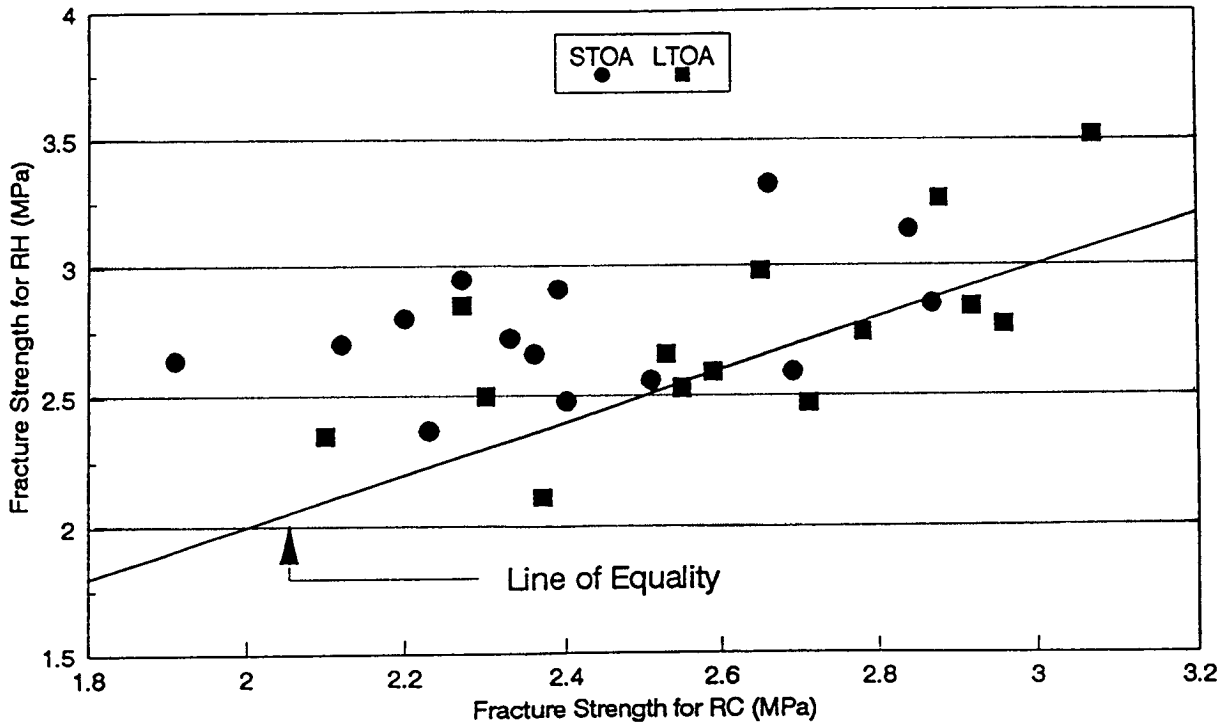

Figure 5.8. Comparison of fracture strength for STOA and LTOA specimens

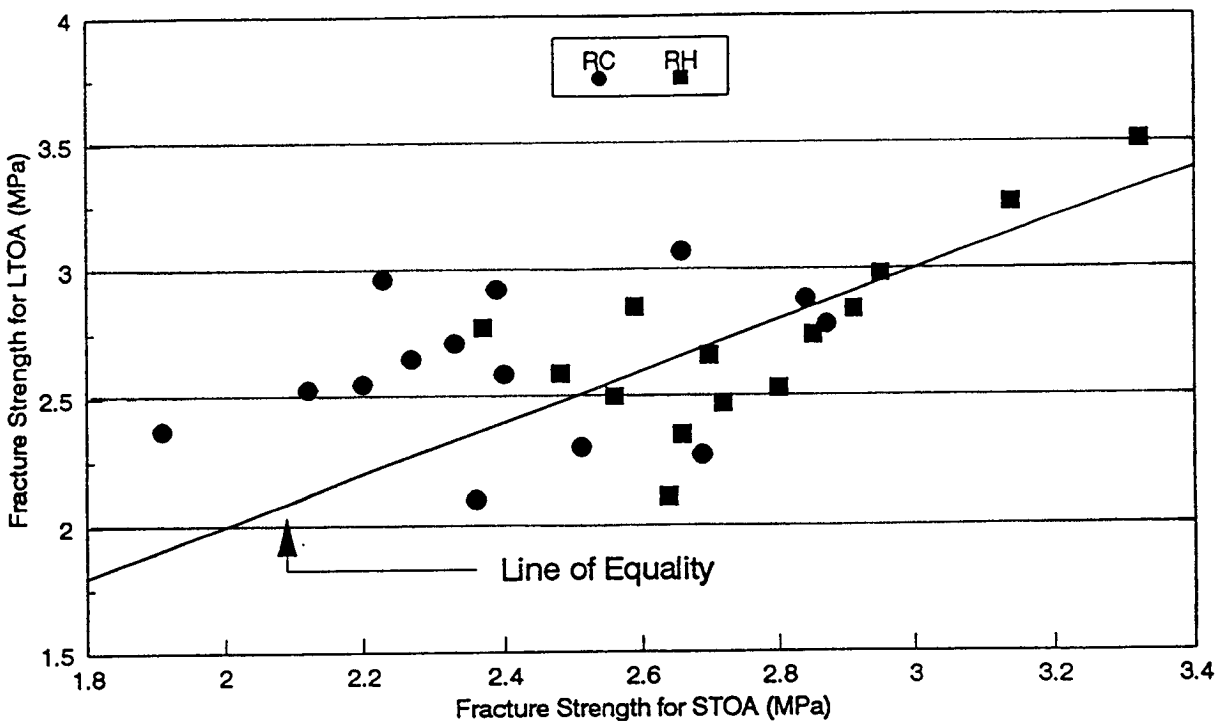

Figure 5.9. Comparison of fracture strength for aggregates RC and RH

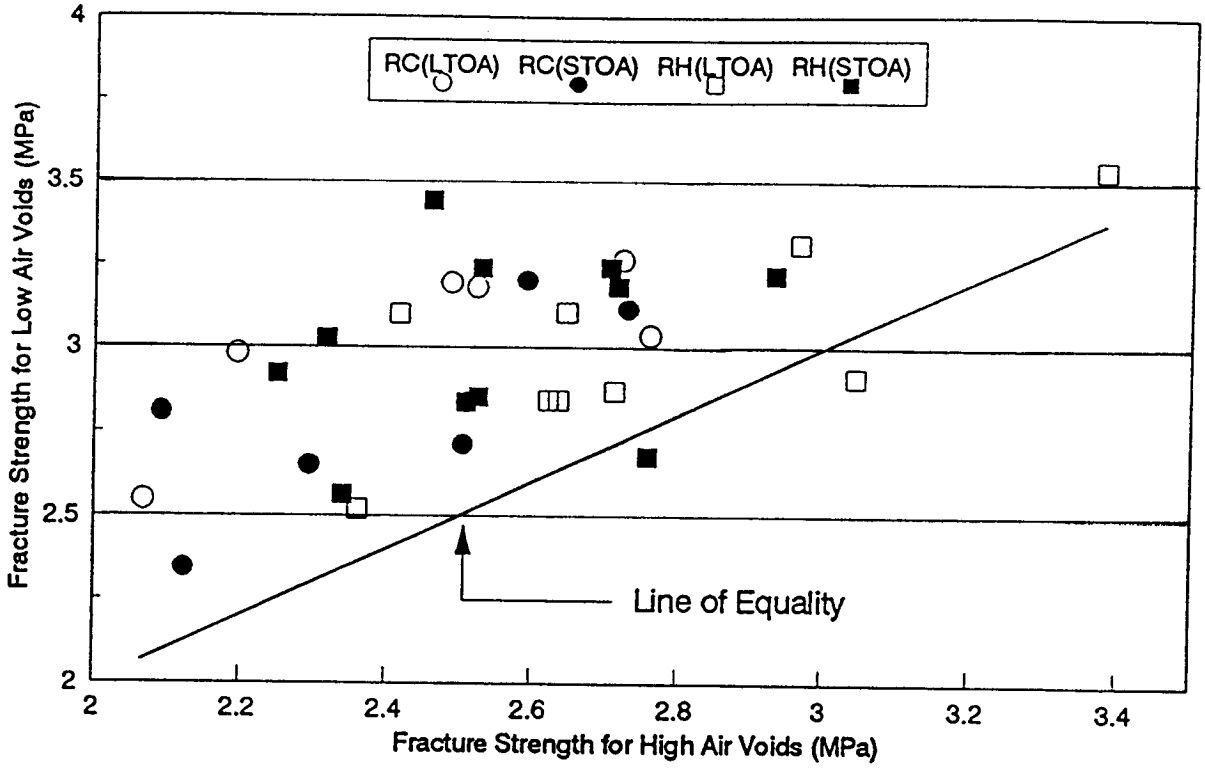

Figure 5.10. Comparison of fracture strength for high and low air-void contents

Table 5.11. Mean square errors for fracture strength models

Model	Factors	Mean Square Errors
Full model	ASP, AGG, AGE, VOID, ASP*AGG, ASP*AGE, AGG*AGE	1518.8
Reduced model I	ASP, AGG, AGE, VOID, ASP*AGE, AGG*AGE	1570.1
Reduced model II	ASP, AGG, AGE, VOID, AGG*AGE	1681.8
Reduced model III	ASP, AGG, VOID, AGG*AGE	1681.8

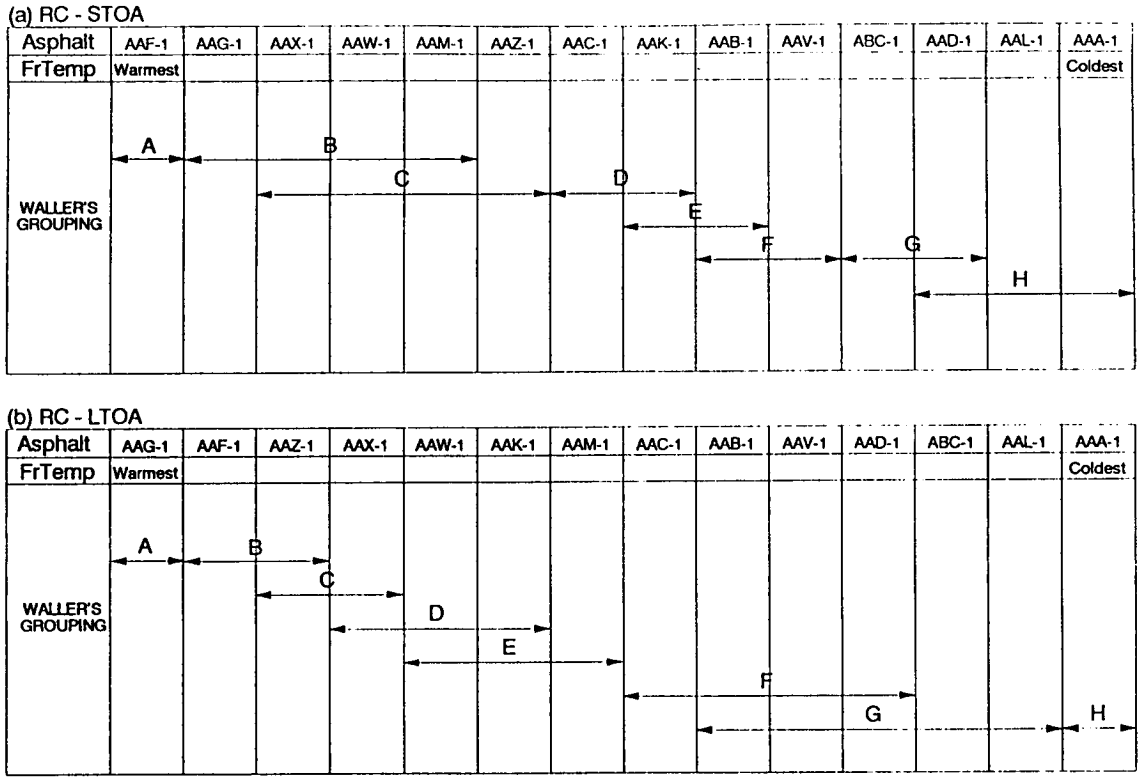

Figure 5.11. Waller's grouping of asphalts for fracture temperature (RC)

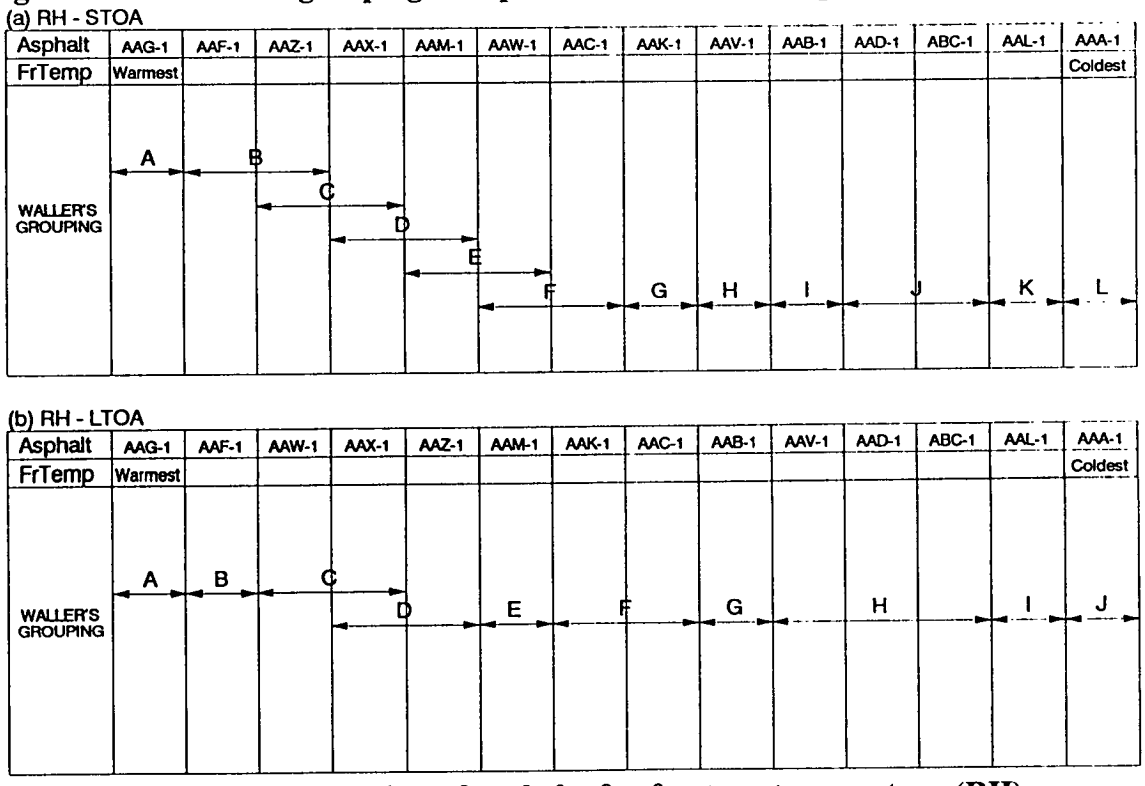

Figure 5.12. Waller's grouping of asphalts for fracture temperature (RH)

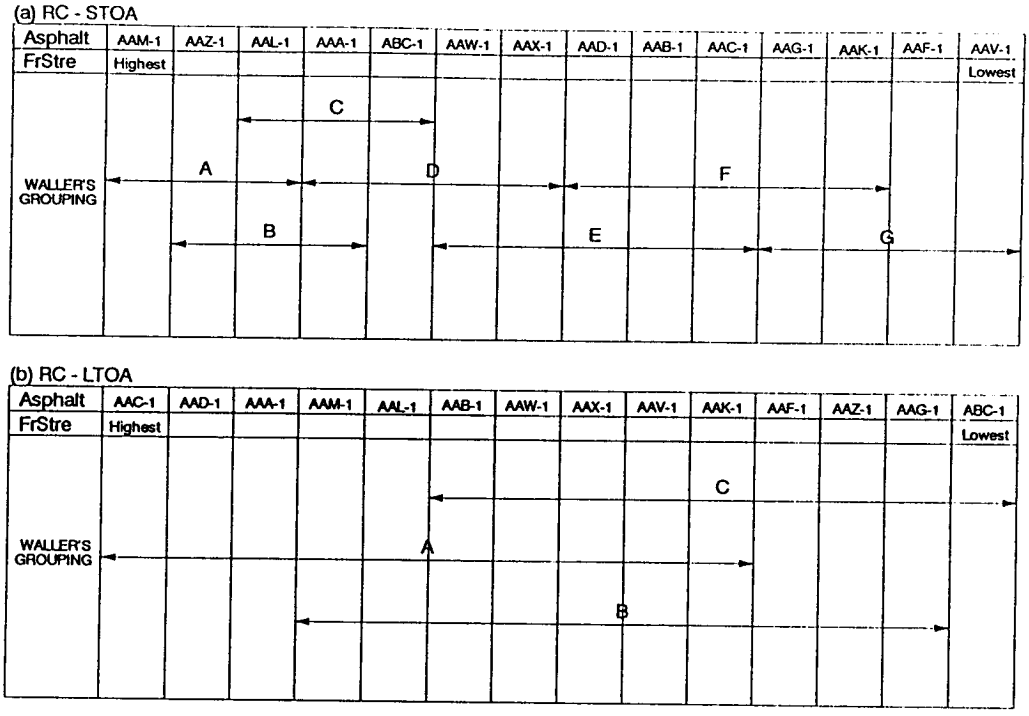

Figure 5.13. Waller's grouping of asphalts for fracture strength (RC)

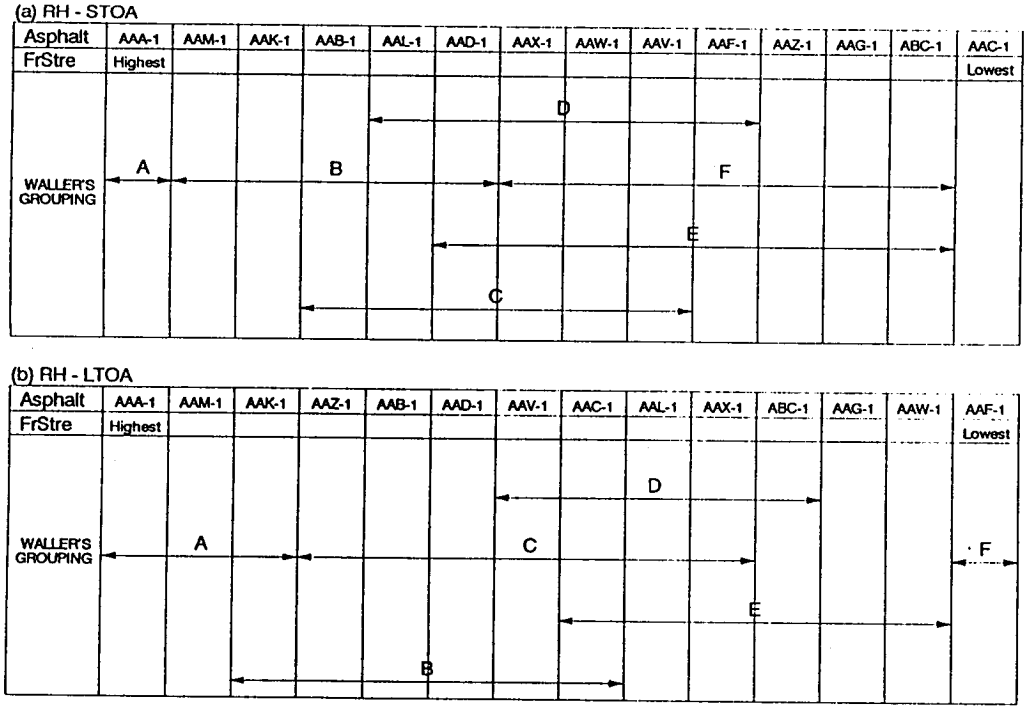

Figure 5.14. Waller's grouping of asphalts for fracture strength (RH)

aggregate RC to reach thermal equilibrium. The temperature within the mixes with aggregate RC will be warmer and the asphalt cement in the mix will be softer than the mix with aggregate RH under the same thermal conditions (cooling rate and surface temperature). Thus, in the mix with the aggregate RC, the period of stress relaxation will be extended to colder temperatures, leading to more stress relaxation. Beyond the transition temperature, in the mix with aggregate RH, the thermal stresses will accumulate faster and the slope of the thermally induced stress curve will be steeper. Also, since the stress relaxation in the mix with aggregate RH will cease at warmer temperature and less stress will be relaxed, the fracture strength of mixes with aggregate RH will be greater.

The low-temperature cracking resistance of an asphalt-concrete mix can also be significantly affected by aging of asphalt cement. As the asphalt-concrete mix is subjected to aging, the asphalt cement becomes stiffer. When subjected to cooling, the stiffer asphalt cement in the LTOA mixes (compared with the STOA mixes) will accumulate thermal stresses more quickly. The thermally induced stress in the mix will exceed the strength of the mix at warmer temperatures. Finally, fracture will occur at a warmer temperature.

To summarize, asphalt type, aggregate type, degree of aging, and air-void content are identified as significant factors relating to the thermal cracking characteristics of asphalt-concrete mixes. However, at this time, the effects of the degree of aging on fracture strength are inconclusive.

Rankings of Asphalts and Aggregates and Comparison of A-002A and A-003A Results

The A-003A performance rankings of asphalt-aggregate mixes as determined in the TSRST were compared with the A-002A rankings. Also, fracture temperature was related to the A-002A low-temperature index test results and asphalt cement properties. Linear regression analyses were performed to correlate fracture temperature with A-002A low-temperature index test results and asphalt cement properties.

Rankings of Asphalts and Aggregates

The A-003A performance rankings of asphalts and aggregates for resistance to thermal cracking were determined using the LSMEAN of fracture temperature. Asphalts were recorded from 1 to 14; lower score is associated with a colder fracture temperature. The ranking of aggregates was also based on the LSMEAN of fracture temperature.

The A-003A ranking of asphalts is presented together with the ranking given by A-002A in Table 5.12. The ranking of aggregates is presented in Table 5.13. The ranking of asphalts based on fracture temperature compares favorably with the ranking given by the A-002A contractor based on fundamental properties of the asphalt cements.

Table 5.12. Ranking of asphalts for resistance to thermal cracking indicated by A-003A and A-002A

Asphalt Type	LSMEAN of Fracture Temp. (°C)	A-003A Rank	A-002A Rank
AAA-1	-30.27	1	1
AAL-1	-28.34	2	2
AAD-1	-26.70	3	3
ABC-1	-26.70	4	4
AAB-1	-25.41	5	5
AAV-1	-25.24	6	9
AAC-1	-22.48	7	7
AAK-1	-22.07	8	5
AAM-1	-21.01	9	8
AAW-1	-19.95	10	9
AAX-1	-19.59	11	12
AAZ-1	-19.48	12	12
AAF-1	-16.86	13	11
ABC-1	-15.83	14	14

Table 5.13. Ranking of aggregates for resistance to thermal cracking indicated by fracture temperature

Aggregate Type	LSMEAN of Fracture Temp. (°C)	Rank
RC	-23.08	1
RH	-22.62	2

Relationship between Fracture Temperature and A-002A Low-Temperature Index Test Results

Fracture temperature was compared with the A-002A specification test results, specifically the temperature at limiting stiffness and m value from the bending beam rheometer test, and the ultimate strain at failure from the direct tension test. Fracture temperature shows a good correlation with the A-002A test results. Figures 5.15 and 5.16 show the relationship of fracture temperature to temperature at limiting stiffness (S (t) = 200 MPa at 2 hr) and m value, respectively. The relationship between fracture temperature and ultimate strain at failure is shown in Figure 5.17.

Relationship between Fracture Temperature and A-002A Asphalt Cement Properties

Fracture temperature has been compared with asphalt cement properties determined by A-002A researchers. Figures 5.18 and 5.19 show the relationship between fracture temperature and the penetration of asphalt cement at 15°C after tank (no treatment). It can be observed that fracture temperature has a good correlation with penetration of asphalt cement at 15°C. The fracture temperature is colder for mixes with softer asphalt cements.

The fracture temperatures for SHRP's eight core asphalts were compared with the penetration of asphalt cement at 15°C after treatments. The relationship between fracture temperature for the eight core asphalts and penetration at 15°C after TFOT (thin-film oven test) is presented in Figures 5.20 and 5.21. Fracture temperature is highly correlated with penetration at 15°C after TFOT.

The relationship between fracture temperature and penetration at 15°C after treatment in a pressure-aging vessel (PAV) is given in Figures 5.22 and 5.23. Fracture temperature has a good correlation with penetration at 15°C after PAV.

The fracture temperature for the eight core asphalts was compared with the Fraass brittle point of the asphalt cement. The relationship between fracture temperature for eight core asphalts and Fraass brittle point is shown in Figures 5.24 and 5.25. Fracture temperature has a good correlation with Fraass brittle point.

Conclusions

Based on the results presented herein, the following conclusions are appropriate:

1. The repeatability of the TSRST is estimated as good for fracture and transition temperature and reasonable for fracture strength.

2. Asphalt type, aggregate type, degree of aging, and air-void content are major factors that substantially affect the thermal cracking characteristics of asphalt-concrete mixes. Interactions between mix properties are considered to have a minor effect.

3. Asphalt type, degree of aging, air-void content, and the interaction between asphalt and degree of aging are significant factors for the fracture temperature. Fracture temperature was warmer for long-term aged mixes. Fracture temperature is most affected by asphalt type and degree of aging. It is also affected by air-void content and the interaction between asphalt type and degree of aging, though to a much lesser extent.

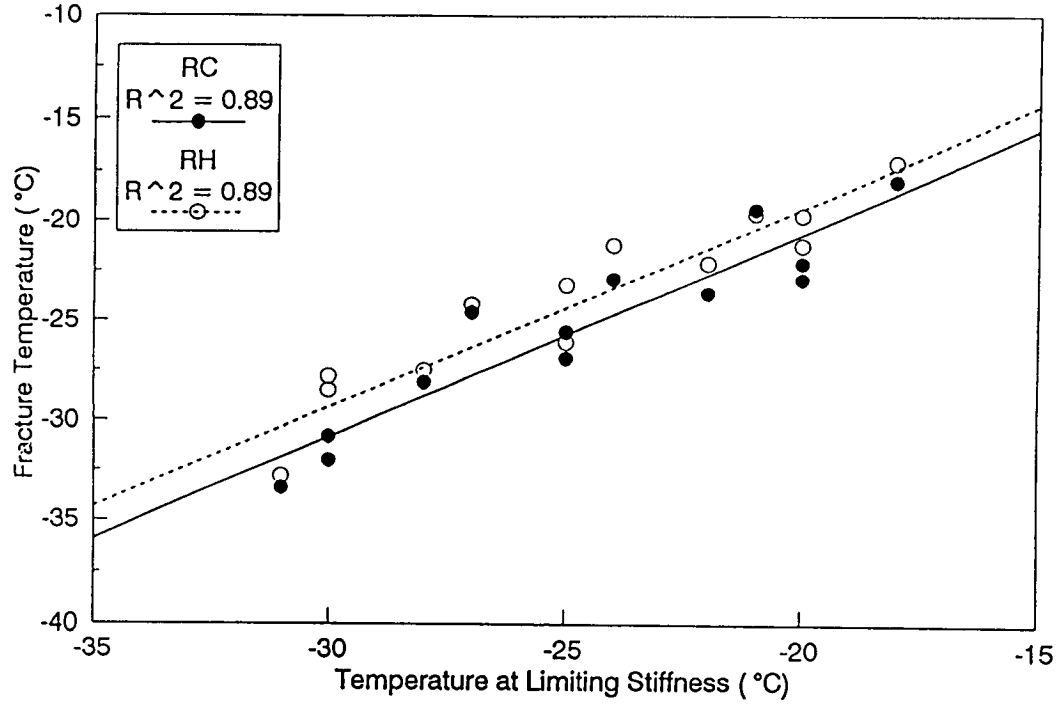

Figure 5.15. Fracture temperature (STOA) versus temperature at limiting stiffness

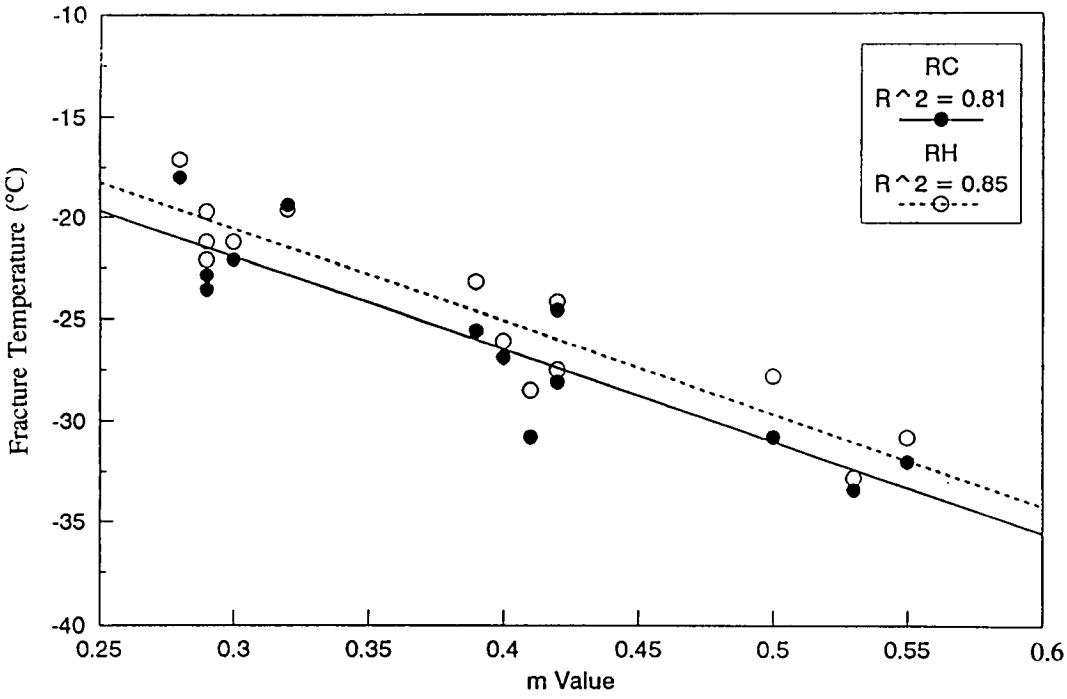

Figure 5.16. Fracture temperature (STOA) versus m value

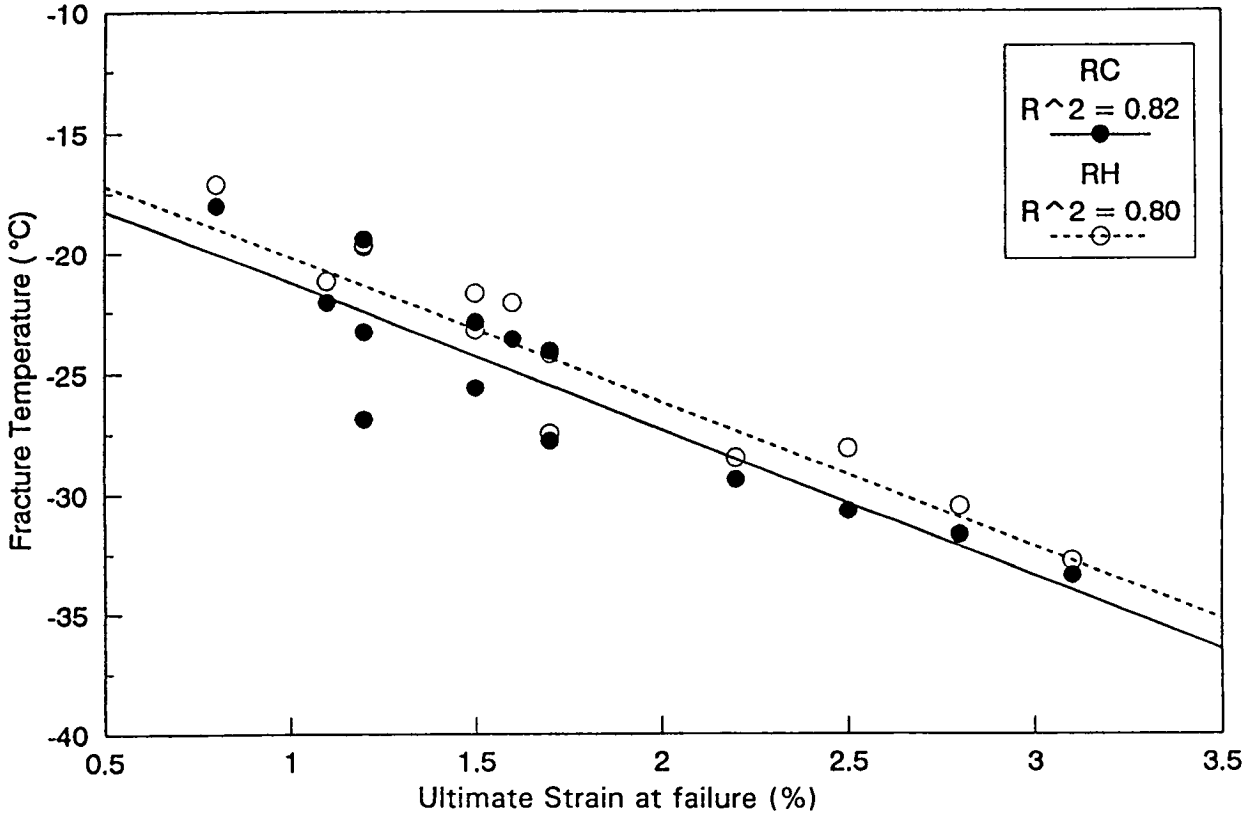

Figure 5.17. Fracture temperature (STOA) versus ultimate strain at failure

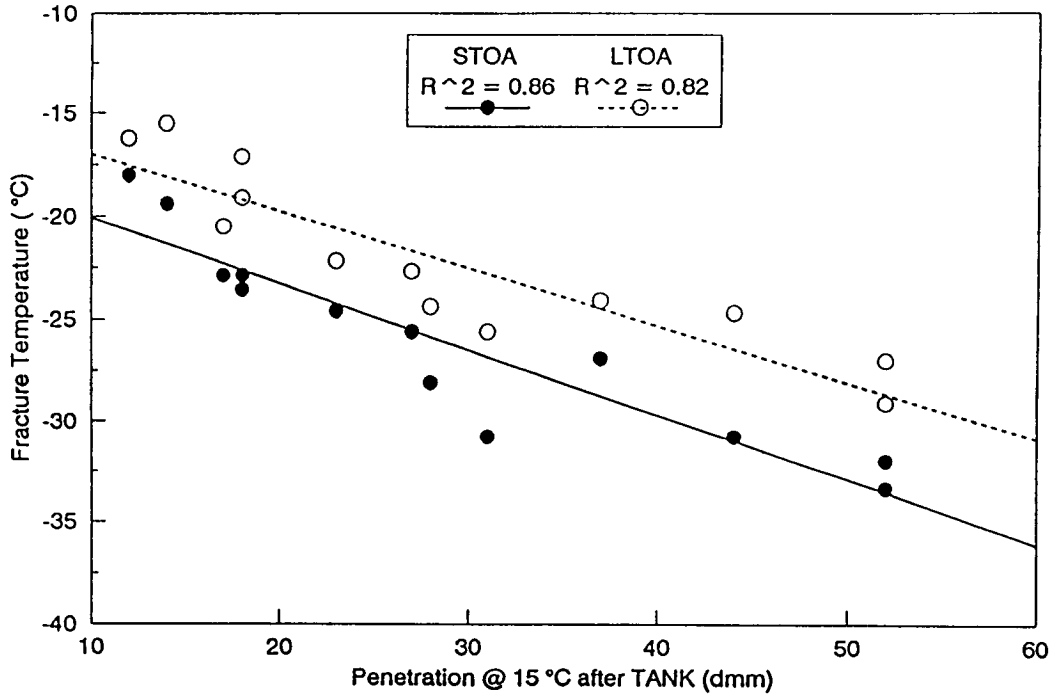

Figure 5.18. Fracture temperature (RC) versus penetration at 15°C after tank

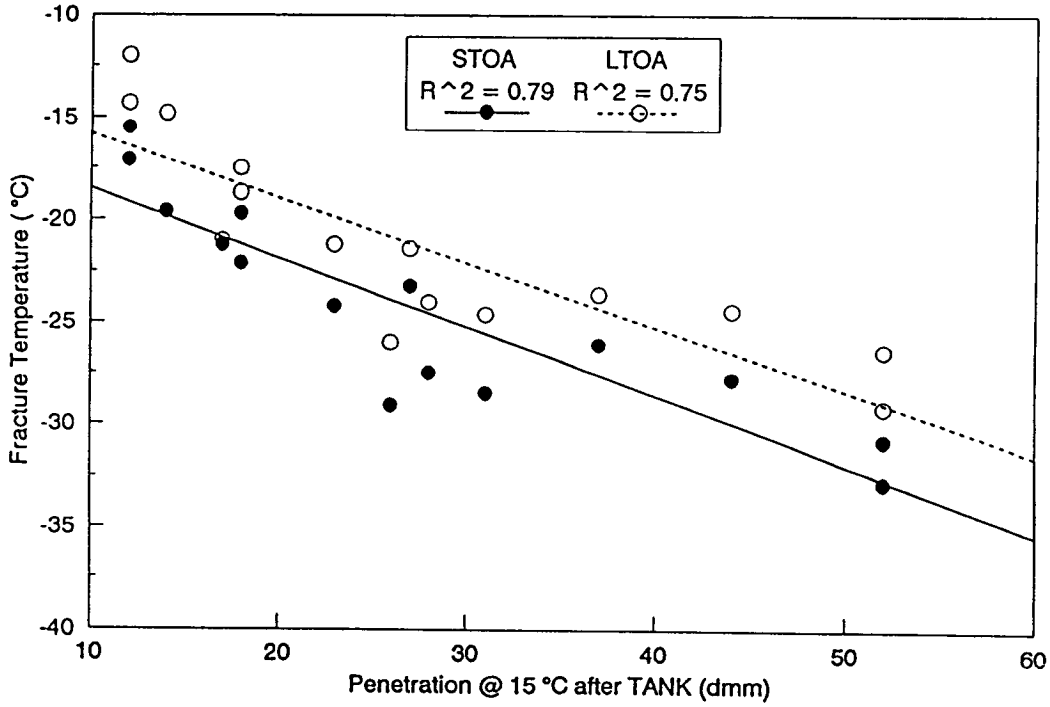

Figure 5.19. Fracture temperature (RH) versus penetration at 15°C after tank

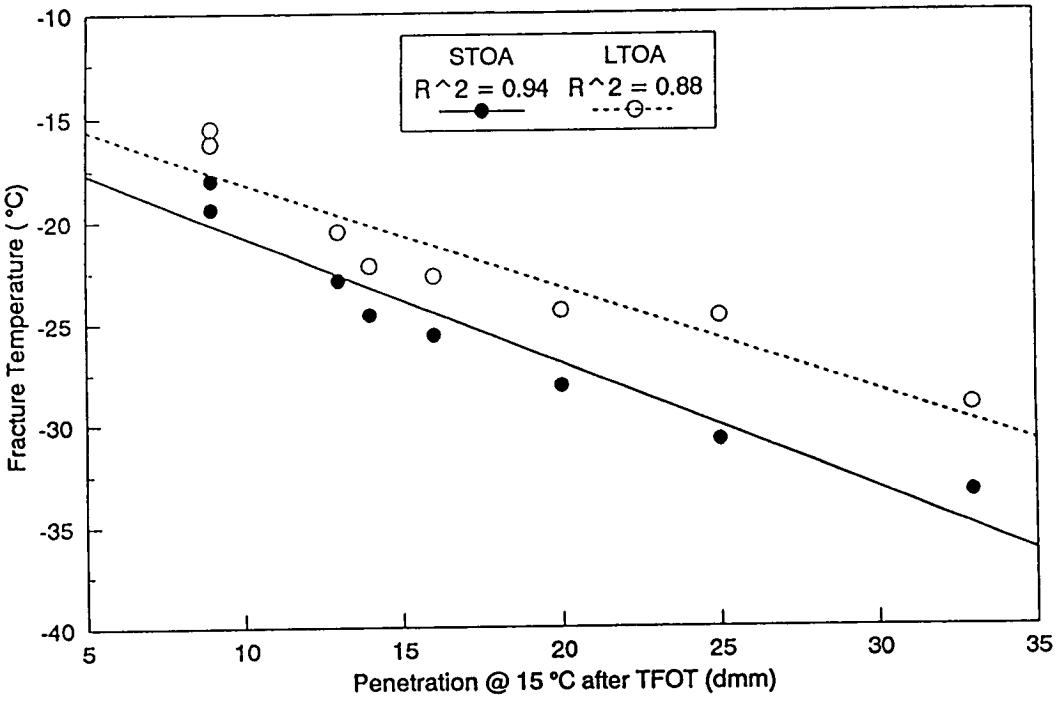

Figure 5.20. Fracture temperature (RC) versus penetration at 15°C after TFOT

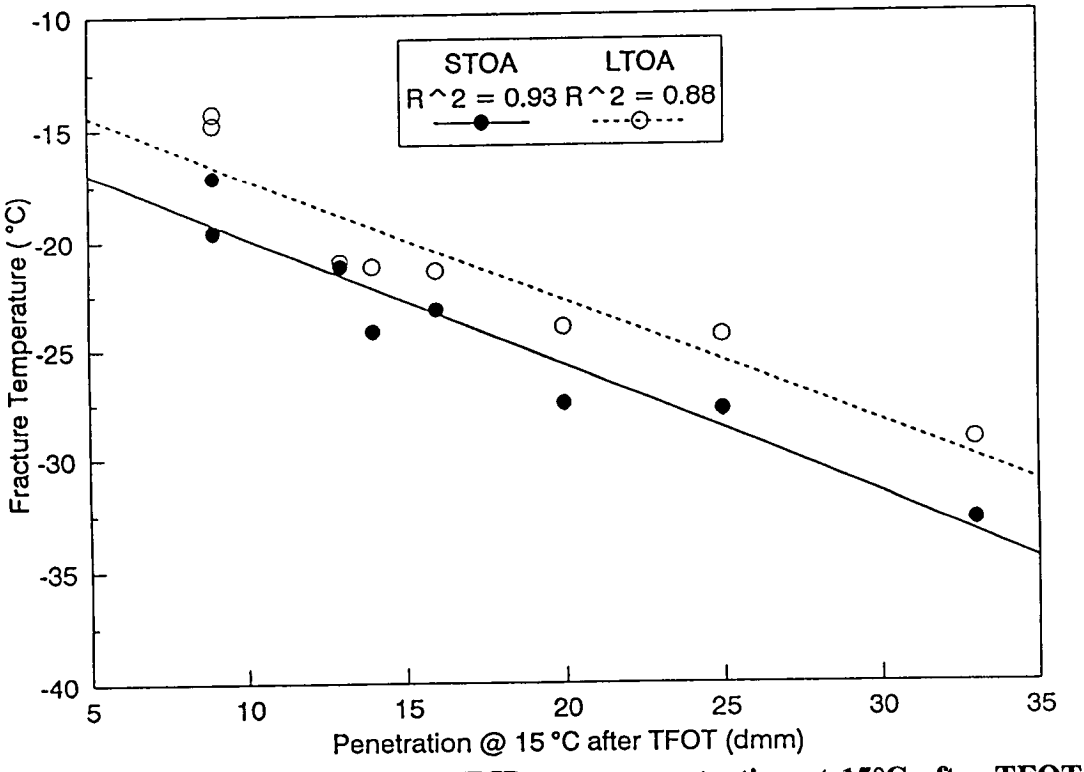

Figure 5.21. Fracture temperature (RH) versus penetration at 15°C after TFOT

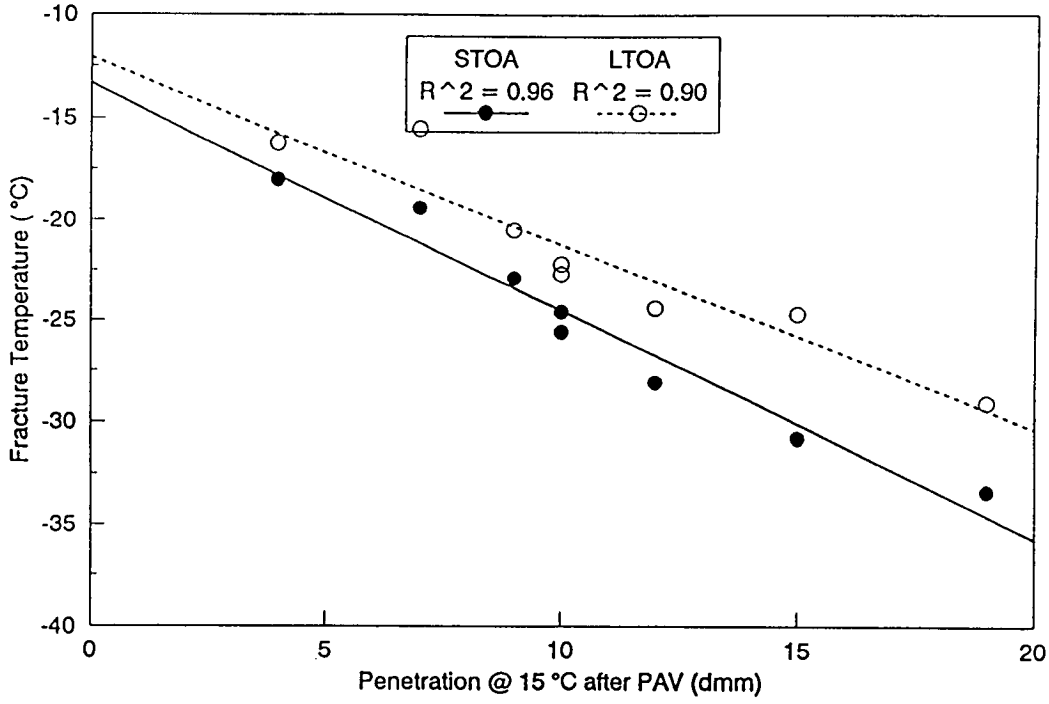

Figure 5.22. Fracture temperature (RC) versus penetration at 15°C after PAV

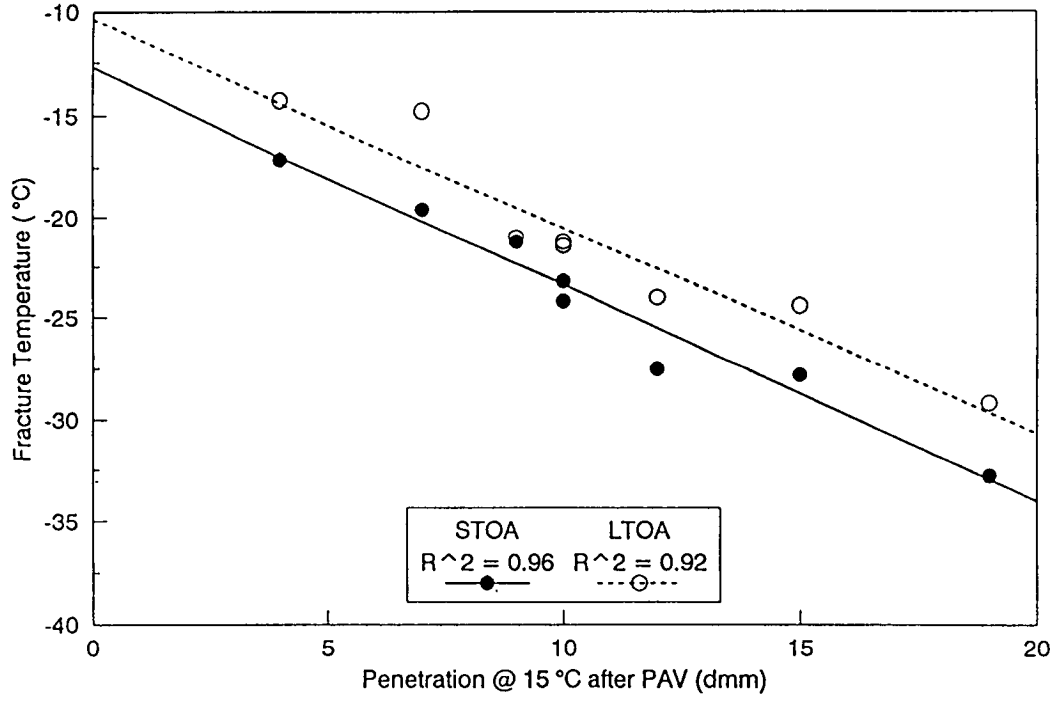

Figure 5.23. Fracture temperature (RH) versus penetration at 15°C after PAV

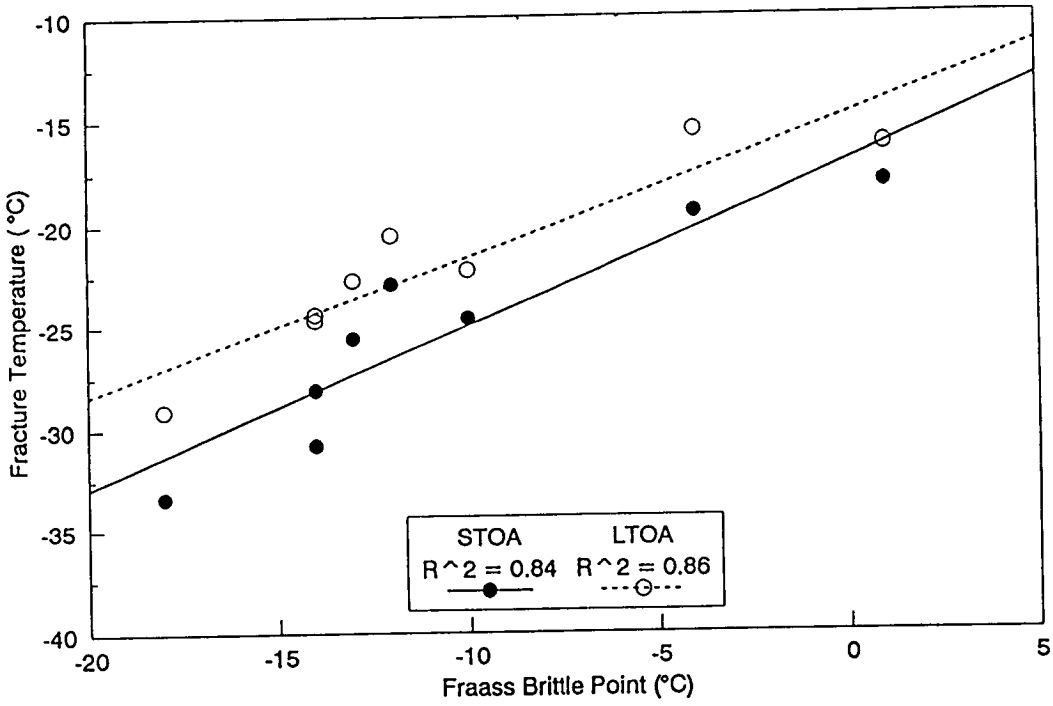

Figure 5.24. Fracture temperature (RC) versus Fraass brittle point

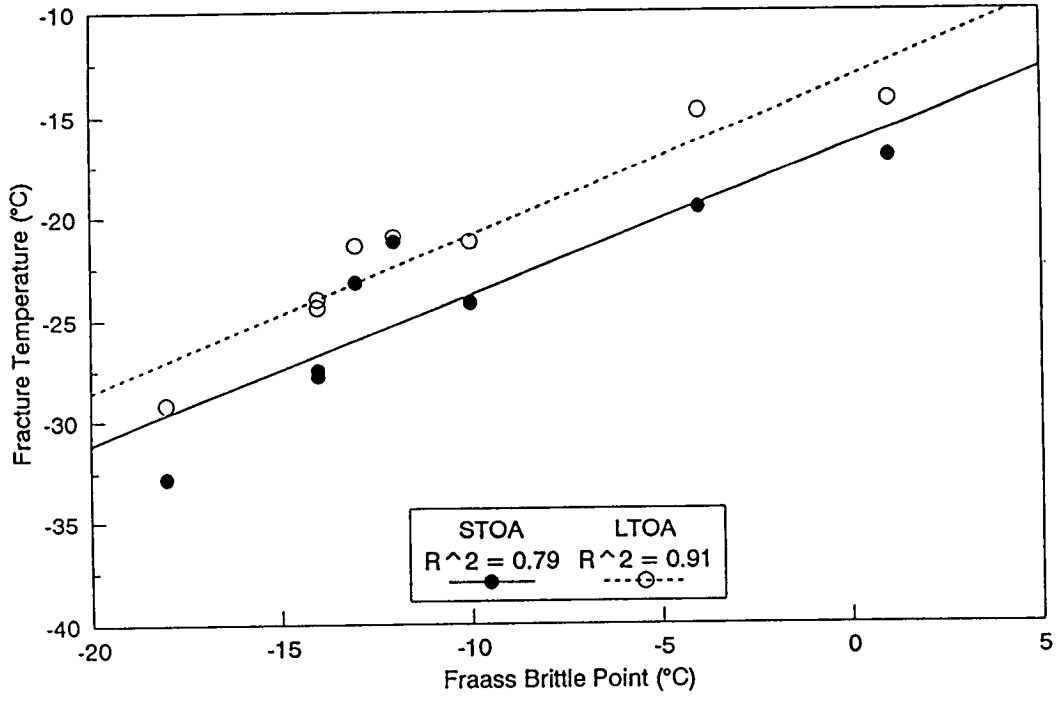

Figure 5.25. Fracture temperature (RH) versus Fraass brittle point

4. Asphalt type, aggregate type, air-void content, and the interaction between aggregate and degree of aging are significant factors for the fracture strength. Fracture strength is highly influenced by air-void content and aggregate type. Fracture strength was greater for mixes with lower air-void contents than for mixes with higher air-void contents, and also greater for mixes with aggregate RH than for those with aggregate RC. Asphalt type and the interaction between aggregate type and degree of aging have a minor influence on fracture strength. The effect of degree of aging on fracture strength is inconclusive.

5. Fracture temperature was highly correlated with A-002A low-temperature index test results, specifically the temperature at limiting stiffness, the m value, and the ultimate strain at failure.

6. The penetration of asphalt cement at 15°C is a good indicator of the thermal cracking characteristics of asphalt-concrete mixes. Fracture temperature was highly correlated with penetration at 15°C. The fracture temperature was colder for mixes with softer asphalt cements. Fraass brittle point of asphalt cement also provided a good indication of the thermal cracking characteristics of asphalt-concrete mixes.

6

Validation of Binder Properties Related to Aging

The development of laboratory aging procedures to simulate short- and long-term aging for asphalt-aggregate mixes has been undertaken as part of the work at Oregon State University (OSU). The purpose of this chapter is to report on an expanded testing program that has been conducted using these laboratory aging procedures, in an effort to validate the work of the A-002A contractor.

The procedure developed for short-term aging involves heating the loose mix in a forced-draft oven for 4 hr at 135°C. This treatment simulates the aging of the mix during the construction process while it is in the uncompacted condition. Two alternative procedures have been developed for long-term aging of the compacted mix. These are designed to simulate the aging of in-service pavements after several years. The following long-term approaches have been found to be appropriate:

1. Long-term oven aging (LTOA) of compacted specimens in a forced-draft oven.

2. Low-pressure oxidation (LPO) of compacted specimens in a triaxial cell by passing oxygen through the specimen.

With these two methods of aging, alternative combinations of temperature and time have been evaluated and are reported herein.

The effects of aging are evaluated by resilient modulus measurements at 25°C using both the diametral (indirect tension) and triaxial compression modes of testing (ASTM D-4123, D-3497).

Hypothesis of A-002A

As indicated in the proposed binder specification (Table 1.1), there is no direct provision for evaluating asphalt durability other than the effect of aging (short- or long-term) on binder properties to control fatigue, permanent deformation, and thermal cracking. Fatigue and thermal cracking are controlled on binders that are long-term aged in the pressure-aging vessel (PAV), while rutting is controlled on binders that are short-term aged using the rolling thin-film oven test (RTFOT).

This chapter presents the results of tests on mixes made from 8 binders and 4 aggregates (32 combinations). The mixes are evaluated after both short- and long-term aging, and the stiffness ratios are compared with stiffness ratios of the neat binders. The results are expected to indicate whether binder tests alone are adequate to predict the durability of asphalt-aggregate mixes.

Experiment Design

Variables

The experiment design included eight asphalt types and four aggregates types. All specimens to be long-term aged were first short-term aged at 135°C for 4 hr before compaction. Four long-term aging procedures were examined in the validation effort: LPO at 60°C and 85°C for 5 days, LTOA at 85°C for 5 days, and LTOA at 100°C for 2 days. Table 6.1 shows the variables used for the LPO series, and Table 6.2 shows the variables for the LTOA series.

Materials

The materials used for this testing program were selected from the Materials Reference Library (MRL) in Austin, Texas.

The aggregates used represent a broad range of aggregate characteristics. From a high-absorption crushed limestone (3.7 percent water absorption) to a river-run gravel. The asphalts used also cover a broad range of asphalt grades. Table 6.3 briefly describes the material properties.

Table 6.1. LPO aging experiment design

No. of asphalts		8
No. of aggregates		4
No. of asphalt contents		1
No. of air-void contents		1
Test Conditions		
Temperature:	Short-term	1 (135°C)
	Long-term	2 (60°C and 85°C)
Aging Periods		
	None (datum)	1
	Short- and long-term	1
Total Tests		
	No aging (unaged)	32
	Short- and long-term	64
Replication of unaged		32
Replication of short- and long-term		64
TOTAL		192

Table 6.2. LTOA experiment design

No. of asphalts		8
No. of aggregates		4
No. of asphalt contents		1
No. of air-void contents		1
Test Conditions		
Temperature:	Short-term	1 (135°C)
	Long-term	2 (85°C and 100°C)
Aging Periods		
	None (datum)	1
	Short- and long-term	1
Total Tests		
	No aging	32
	Short- and long-term	64
Replication of short- and long-term		64
TOTAL		160

Table 6.3. Materials used

Aggregate		Asphalt	
Code	**Description**	**Code**	**Grade**
RC	Limestone (high absorption)	AAA-1	150/200
RD	Limestone (low absorption)	AAB-1	AC-10
RH	Greywacke	AAC-1	AC-8
RJ	Conglomerate	AAD-1	AR-4000
		AAF-1	AC-20
		AAG-1	AR-4000
		AAK-1	AC-30
		AAM-1	AC-20

Aging Methods

No Aging

Three specimens were prepared at the time of mixing to represent an unaged condition. These specimens were prepared in the same manner as the others except that they were not cured for 4 hr at 135°C. As soon as mixing was complete, the specimens were placed in an oven and brought to the proper equiviscous temperature (a viscosity of 665±80 centistokes) for that mix. Once the proper temperature was achieved, the specimens were compacted using kneading compaction (Cox type).

Short-Term Aging

The short-term aging method used in this test program was developed at OSU under the Strategic Highway Research Program (SHRP) A-003A test development program (Bell et al. 1992). The method consists of curing mix samples in a forced-draft oven at 135°C for 4 hr. During the curing period, the mix is placed in a pan at a spread rate of approximately 21 kg/m^2. The mix is also stirred and turned once an hour to ensure that the aging is uniform throughout the sample. After the curing period, the samples are brought to an equiviscous temperature (a viscosity of 665±80 centistokes) and compacted by kneading compaction.

Long-Term Aging

Low-Pressure Oxidation. LPO is an aging procedure to simulate the long-term aging that a pavement experiences in service. The procedure is carried out on compacted specimens after they have been short-term aged. Figure 6.1 is a diagram of the conditioning cell. Before testing, the specimen is prepared by placing a 25 mm wide band of silicone rubber around it to ensure that the oxygen is flowing through the specimen. After allowing the silicone to dry

overnight, the specimen is placed in the triaxial pressure cell and fitted with a rubber membrane to seal the specimen from atmospheric gases. After the specimen is loaded into the cell, a confining pressure is applied to keep the membrane tight on the specimen. Once the confining pressure is reached, typically 70 to 210 kPa, oxygen flow is started though the specimen at a rate of 1.2 m^3/hr. When the oxygen rate has been adjusted, the cell is placed in a water bath preheated to the conditioning temperature (60°C or 85°C). The cell is left in the conditioning bath for 5 days after which it is extracted from the bath and left to cool to room temperature. The specimens are then removed from the cell and allowed to stand for at least 24 hours before being tested for resilient modulus. A total of 7 days is involved in this aging process.

Long-Term Oven Aging. LTOA is an alternative procedure used to simulate long-term aging. The procedure is carried out on compacted specimens after they have been short-term aged. The specimens are placed in a forced-draft oven, preheated to 85°C, and left for 5 days. Alternatively, a temperature of 100°C is used for 2 days. After the aging period, the oven is turned off and left to cool to room temperature. The specimens are then removed from the oven and prepared to be tested at least 24 hours after removal from the oven.

Evaluation Methods

Resilient Modulus

The resilient modulus is determined at 25°C using the diametral (indirect tension) (ASTM D-4123) and triaxial compression modes of testing with a 0.1 sec loading time at a frequency of 1 Hz (0.1 sec loading time and 0.9 sec with no load). A constant strain level of 100 microstrain is maintained throughout the test.

Dynamic Modulus

A selection of specimens is being subjected to a thorough dynamic modulus evaluation (ASTM D-3497) at temperatures of 0°C, 25°C, and 40°C. A selection of 11 steps of frequencies ranging from 15 to 0.01 Hz has been used in this test program. The testing system developed at OSU uses a haversine wave load pulse generated on a semi-closed-loop servohydraulic testing system. From load and deformation data collected by the testing system complex, it is possible to compute loss and storage moduli, along with the phase angle and loss tangent. Testing of this type takes approximately 8 hr per specimen because of the large temperature change. Therefore, it was not feasible to test all the specimens with this procedure. The dynamic modulus data are presented in Ab-Wahab et al. (1993).

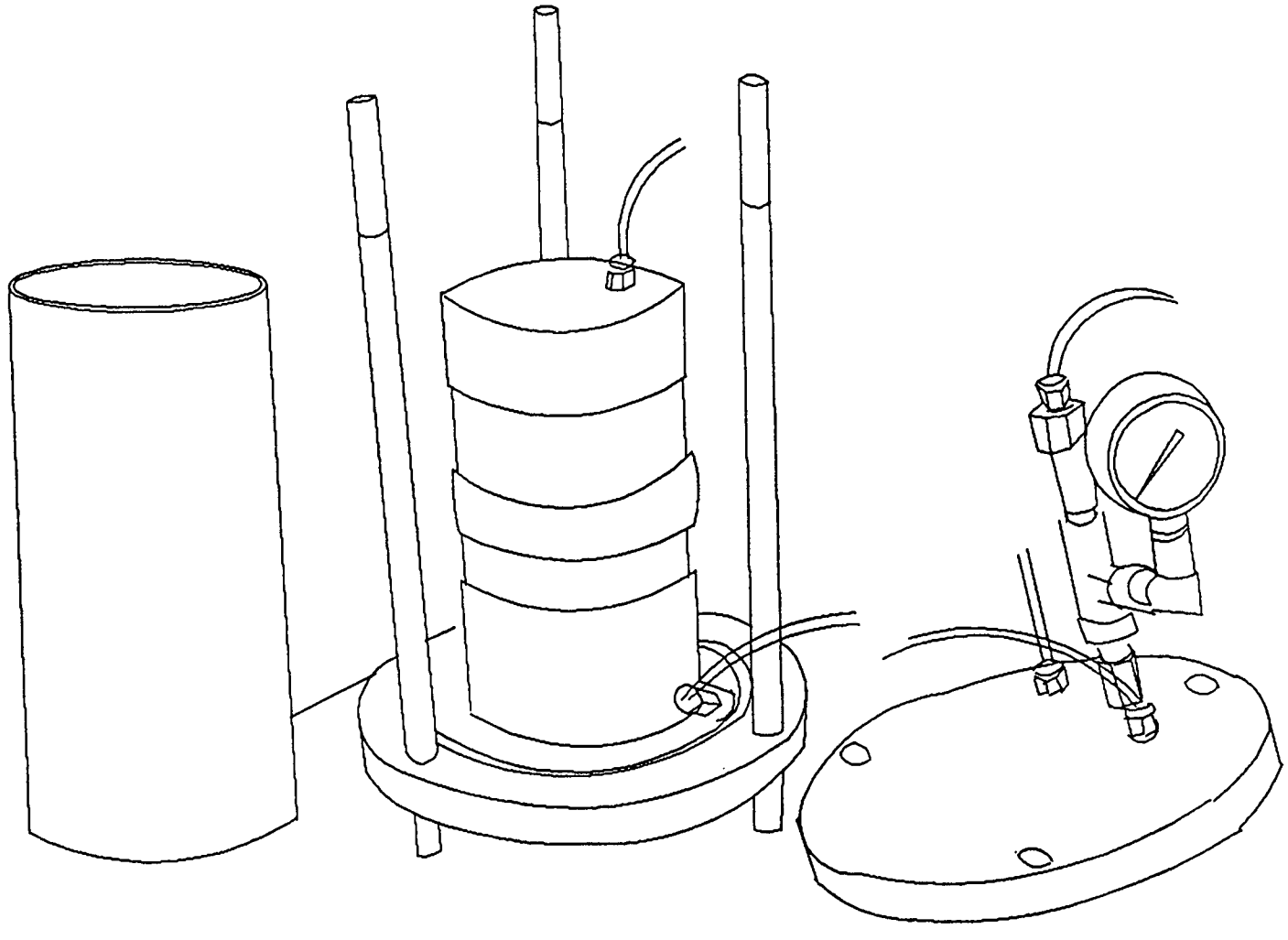

Figure 6.1. Low pressure oxidation cell

Tensile Strength Test

The indirect tensile strength test ASTM D-4123 is performed when all modulus testing is completed. A deformation rate of 50 mm/min is used, with the load and deformation of the specimen monitored continuously until failure occurs. The strains at yield and failure as well as strength are considered significant. The broken portions of the specimen may be used to obtain recovered asphalt for further testing. The results of these tests are reported in Bell et al. (1992).

Results

Resilient Modulus Data

The results of the resilient modulus data for both diametral and triaxial modes of testing are summarized in Tables 6.4 through 6.7, separated by aggregate type. These data include moduli for unaged, short-term aged, and long-term aged specimens.

Short-Term Aging Results

The modulus ratios—short-term aged modulus divided by adjusted unaged modulus—from diametral testing are shown in Figure 6.2 for each of the four aggregates, with the asphalts shown in ranking order in each case. The diametral modulus data are presented in the figures referenced in subsequent sections. Less variability was experienced with the diametral modulus data; approximately ±10 percent, versus ±15 percent with the triaxial modulus data. This difference was attributed to the relatively short (100 mm) specimen used in the triaxial mode. The asphalt showing the greatest aging (in terms of modulus change) has the highest ratio. The ratios have been developed using a procedure (described later) to adjust the modulus values to correspond to the same air-void content.

Long-Term Aging Results

The modulus ratios—long-term aged modulus divided by adjusted unaged modulus—from diametral testing of the long-term aged specimens are shown in Figures 6.3 through 6.6. These figures are similar to the short-term aging figures, with the rankings based on the ratio of long-term aged modulus to unaged modulus. As with the short-term aging results, the modulus values were adjusted as described in the next section.

Adjustment of Modulus Data

To analyze the effects of short- and long-term aging on asphalt-aggregate mixes, a method for creating an aging ratio was needed. To create this ratio, a measure of the unaged modulus was needed to compare with the aged specimens. At the time of mixing in the laboratory, three additional specimens, other than those needed for long-term aging, were prepared and compacted as soon as they could be brought to the proper compaction temperature. These specimens were said to be in an "unaged" condition and were tested for resilient modulus. In all but a few cases the unaged specimens were found to have an air-void content different from that of the short-term aged specimens, so the modulus values of the short-term aged specimens had to be adjusted to correspond to the same air-void content as the unaged specimens.

For this adjustment, an average slope was determined from the relationship between modulus and air-void content for the unaged specimens over the entire data set. With this slope and values for the average modulus and air-void content for each combination of materials, an equation for the unaged modulus at any air-void content could be determined. From this equation, an adjusted unaged modulus could be calculated for each short-term aged specimen and then used in calculating the short- and long-term aging ratios.

Analysis of Results

Short-Term Aging of Asphalt-Aggregate Mixes

The data presented in Figure 6.2 suggest that mix aging susceptibility is aggregate dependent. However, the effect of the asphalt is more significant. The rankings of the eight asphalts, based on short-term aging (Figure 6.2), vary with aggregate type. In particular, asphalt AAK-1 moves around in the rankings, showing relatively little aging with basic aggregates (RC and RD) and relatively high aging with acidic aggregates (RH and RJ).

The observed aging phenomena appear related to the adhesion of the asphalt and aggregate. A hypothesis is that the greater the adhesion, the greater the mitigation of aging. It should be noted that there is not a statistically significant difference between all asphalts; rather (for a particular aggregate) two or more asphalts show a similar degree of aging. This is illustrated in Table 6.8, which shows numerical rankings corresponding to the short-term aging rankings shown in Figure 6.2. The asphalts that have a common underscore are groups with statistically similar aging ratios as determined by Waller groupings (Waller and Kemp 1976). When groupings are examined, it can be seen that only asphalt AAM-1 is consistently in the lowest group, and asphalt AAD-1 consistently in the upper group.

Table 6.4. Modulus data for aggregate RC

Asphalt	Aging Method	% Air Voids	Modulus Values (ksi)			
			Diametral		Triaxial	
			Before	After	Before	After
AAA	LPO 85	8.2	211	572	295	805
	LPO 85	8.4	193	504	350	802
	LPO 60	8.0	233	367	434	600
	LPO 60	8.1	270	414	373	442
	LTOA 85	9.5	225	405	357	780
	LTOA 85	8.7	221	412	295	583
	LTOA 100	9.0	219	475	270	570
	LTOA 100	8.6	216	499	295	455
	NONE	8.0	152	—	230	—
	NONE	8.8	153	—	225	—
	NONE	7.9	164	—	236	—
AAB	LPO 85	8.4	299	638	517	1041
	LPO 85	9.2	317	438	419	635
	LPO 60	8.3	364	525	420	621
	LPO 60	8.3	300	644	379	1041
	LTOA 85	8.9	305	606	395	875
	LTOA 85	9.3	339	614	500	956
	LTOA 100	8.3	378	694	426	698
	LTOA 100	9.7	286	618	533	958
	NONE	8.8	216	—	385	—
	NONE	7.8	207	—	421	—
	NONE	8.2	249	—	467	—
AAC	LPO 85	8.4	329	715	574	1052
	LPO 85	9.4	398	750	440	844
	LPO 60	9.3	348	520	579	879
	LPO 60	10.2	339	460	384	667
	LTOA 85	9.1	345	561	690	889
	LTOA 85	9.3	377	600	407	787
	LTOA 100	9.4	335	557	409	697
	LTOA 100	8.9	343	623	435	643
	NONE	9.1	236	—	325	—
	NONE	9.3	235	—	277	—
	NONE	8.2	249	—	315	—
AAD	LPO 85	9.3	286	645	274	970
	LPO 85	8.8	293	694	380	950
	LPO 60	9.6	321	450	399	850
	LPO 60	9.0	257	394	432	711
	LTOA 85	8.9	324	615	391	1101
	LTOA 85	9.4	309	616	491	882
	LTOA 100	9.3	225	611	379	775
	LTOA 100	9.0	269	695	344	539
	NONE	8.2	202	—	279	—
	NONE	8.1	208	—	277	—
	NONE	8.5	182	—	275	—

NONE = No Aging
LPO 60 = Low Pressure Oxidation, 60°C, 5 days
LPO 85 = Low Pressure Oxidation, 85°C, 5 days
LTOA 85 = Long-Term Oven Aging, 85°C, 5 days
LTOA 100 = Long-Term Oven Aging, 100°C, 2 days

Table 6.4 (continued). Modulus data for aggregate RC

Asphalt	Aging Method	% Air Voids	Modulus Values (ksi)			
			Diametral		Triaxial	
			Before	After	Before	After
AAF	LPO 85	9.3	650	891	861	1384
	LPO 85	8.8	687	996	864	1275
	LPO 60	7.8	636	898	1113	1345
	LPO 60	9.4	621	896	1323	1305
	LTOA 85	9.0	612	943	890	1205
	LTOA 85	9.0	701	842	1103	1573
	LTOA 100	9.1	558	1004	823	1124
	LTOA 100	9.7	590	1016	999	1357
	NONE	9.0	507	—	779	—
	NONE	9.9	428	—	550	—
	NONE	9.1	458	—	851	—
AAG	LPO 85	10.9	652	983	853	1262
	LPO 85	10.6	606	1038	684	1141
	LPO 60	10.2	682	840	701	1000
	LPO 60	10.7	744	881	851	1134
	LTOA 85	10.9	714	1004	928	1191
	LTOA 85	11.2	656	819	1024	1520
	LTOA 100	10.2	614	1030	918	1245
	LTOA 100	10.9	587	939	921	1113
	NONE	11.0	450	—	658	—
	NONE	9.9	523	—	734	—
	NONE	9.6	476	—	804	—
AAK	LPO 85	7.9	555	974	671	1430
	LPO 85	8.5	572	1000	655	1740
	LPO 60	9.2	497	644	644	992
	LPO 60	9.3	427	577	574	866
	LTOA 85	7.9	563	827	834	1367
	LTOA 85	9.2	451	713	614	993
	LTOA 100	9.6	544	1019	607	1068
	LTOA 100	8.6	502	1049	662	1260
	NONE	9.2	345	—	413	—
	NONE	8.0	450	—	579	—
	NONE	8.1	429	—	578	—
AAM	LPO 85	8.9	470	763	436	1006
	LPO 85	8.1	445	840	641	1110
	LPO 60	8.0	421	580	577	796
	LPO 60	8.6	405	602	558	850
	LTOA 85	8.5	446	796	510	897
	LTOA 85	9.0	456	747	488	910
	LTOA 100	9.2	404	750	552	816
	LTOA 100	8.5	450	787	537	818
	NONE	8.3	332	—	453	—
	NONE	9.0	303	—	358	—
	NONE	7.9	346	—	442	—

Table 6.5. Modulus data for aggregate RD

Asphalt	Aging Method	% Air Voids	Modulus Values (ksi)			
			Diametral		Triaxial	
			Before	After	Before	After
AAA	LPO 85	8.2	211	572	295	805
	LPO 85	8.4	193	504	350	802
	LPO 60	8	233	367	434	600
	LPO 60	8.1	270	414	373	442
	LTOA 85	9.5	225	405	357	780
	LTOA 85	8.7	221	412	295	583
	LTOA 100	9	219	475	270	570
	LTOA 100	8.6	216	499	295	455
	NONE	8	152	—	230	—
	NONE	8.8	153	—	225	—
	NONE	7.9	164	—	236	—
AAB	LPO 85	8.6	356	627	320	541
	LPO 85	7.2	400	632	475	539
	LPO 60	8.9	414	456	450	535
	LPO 60	8.4	380	506	489	696
	LTOA 85	8.7	390	502	465	755
	LTOA 85	8.5	528	582	578	780
	LTOA 100	7.4	509	603	589	631
	LTOA 100	7.5	444	642	411	588
	NONE	8.4	233	—	353	—
	NONE	7.6	306	—	399	—
	NONE	7.6	302	—	314	—
AAC	LPO 85	8.3	419	657	614	950
	LPO 85	8.2	467	671	498	884
	LPO 60	6.9	486	630	762	886
	LPO 60	8.1	526	628	761	741
	LTOA 85	7.1	435	532	519	726
	LTOA 85	7.4	456	600	644	782
	LTOA 100	7.8	451	522	403	679
	LTOA 100	7.3	496	658	647	732
	NONE	7.9	304		506	
	NONE	7.1	291		464	
	NONE	7.5	319		505	
AAD	LPO 85	8.6	321	584	383	893
	LPO 85	8.2	334	633	432	966
	LPO 60	8.5	325	463	425	845
	LPO 60	8.2	362	450	352	698
	LTOA 85	7.8	356	578	472	689
	LTOA 85	8.4	393	611	410	679
	LTOA 100	9.3	341	515	398	670
	LTOA 100	9	395	544	438	441
	NONE	8.1	250	—	227	—
	NONE	6.9	253	—	298	—
	NONE	7	262	—	286	—

NONE = No Aging
LPO 60 = Low Pressure Oxidation, 60°C, 5 days
LPO 85 = Low Pressure Oxidation, 85°C, 5 days
LTOA 85 = Long-Term Oven Aging, 85°C, 5 days
LTOA 100 = Long-Term Oven Aging, 100°C, 2 days

Table 6.5 (continued). Modulus data for aggregate RD

Asphalt	Aging Method	% Air Voids	Modulus Values (ksi)			
			Diametral		Triaxial	
			Before	After	Before	After
AAF	LPO 85	8.9	795	1193	763	1393
	LPO 85	8.9	857	1244	1009	1818
	LPO 60	9	703	1034	998	1588
	LPO 60	8.6	704	862	806	1359
	LTOA 85	9.2	807	1072	1066	1342
	LTOA 85	8.3	786	1068	1036	1538
	LTOA 100	8.9	754	1100	871	919
	LTOA 100	8.9	706	1119	1127	1796
	NONE	9.6	493	—	609	—
	NONE	8.9	526	—	700	—
	NONE	8.8	564	—	850	—
AAG	LPO 85	8.6	991	1147	1194	1588
	LPO 85	8.8	1101	1162	1380	2298
	LPO 60	7.7	1002	1312	1178	1570
	LPO 60	8.7	854	1201	1162	1598
	LTOA 85	8.5	917	1108	1264	1617
	LTOA 85	8.4	893	1161	1186	1277
	LTOA 100	8.4	791	1015	1116	1266
	LTOA 100	8.5	745	1105	1215	1272
	NONE	8	608	—	1040	—
	NONE	8.4	551	—	733	—
	NONE	8	552	—	975	—
AAK	LPO 85	7.8	544	977	507	1039
	LPO 85	8.2	545	782	672	1065
	LPO 60	8	538	721	556	745
	LPO 60	8	567	804	638	1104
	LTOA 85	7.6	527	761	690	1062
	LTOA 85	8.8	336	650	302	1120
	LTOA 100	7.7	507	900	646	842
	LTOA 100	7.2	516	890	723	1066
	NONE	9.3	343	—	391	—
	NONE	8.3	482	—	436	—
	NONE	7.7	493	—	536	—
AAM	LPO 85	8.8	437	629	536	793
	LPO 85	8.2	509	703	556	668
	LPO 60	8.3	406	571	605	882
	LPO 60	8.3	446	616	476	807
	LTOA 85	7.3	458	638	510	807
	LTOA 85	8	459	710	593	809
	LTOA 100	8.2	410	648	546	696
	LTOA 100	8.6	458	639	518	840
	NONE	5.5	438	—	485	—
	NONE	8.6	407	—	391	—
	NONE	7.9	518	—	469	—

Table 6.6. Modulus data for aggregate RH

Asphalt	Aging Method	% Air Voids	Modulus Values (ksi)			
			Diametral		Triaxial	
			Before	After	Before	After
AAA	LPO 85	8.2	211	572	295	805
	LPO 85	8.4	193	504	350	802
	LPO 60	8	233	367	434	600
	LPO 60	8.1	270	414	373	442
	LTOA 85	9.5	225	405	357	780
	LTOA 85	8.7	221	412	295	583
	LTOA 100	9	219	475	270	570
	LTOA 100	8.6	216	499	295	455
	NONE	8	152	—	230	—
	NONE	8.8	153	—	225	—
	NONE	7.9	164	—	236	—
AAB	LPO 85	8.8	311	479	281	541
	LPO 85	10.6	244	385	275	539
	LPO 60	8.5	276	490	306	605
	LPO 60	8.9	256	330	356	539
	LTOA 85	8.8	313	419	351	567
	LTOA 85	8.4	289	445	363	655
	LTOA 100	7.6	360	454	564	562
	LTOA 100	8	348	451	425	434
	NONE	8.8	160	—	165	—
	NONE	7.8	191	—	260	—
	NONE	7.5	216	—	305	—
AAC	LPO 85	8.3	290	505	271	589
	LPO 85	8.5	313	487	288	520
	LPO 60	8.4	264	374	242	373
	LPO 60	7.8	307	375	310	449
	LTOA 85	8.8	286	403	319	507
	LTOA 85	8.4	272	387	364	439
	LTOA 100	6.8	419	453	493	521
	LTOA 100	6.8	413	455	618	548
	NONE	7.5	176	—	200	—
	NONE	7.7	163	—	220	—
	NONE	8	161	—	210	—
AAD	LPO 85	6.3	252	553	272	573
	LPO 85	8.4	317	616	401	826
	LPO 60	8.9	229	316	295	522
	LPO 60	7.3	261	309	237	408
	LTOA 85	8	227	385	317	613
	LTOA 85	7.8	278	435	184	283
	LTOA 100	6.6	256	348	307	513
	LTOA 100	6.9	240	390	261	567
	NONE	6.2	197	—	167	—
	NONE	6.9	162	—	240	—
	NONE	5.6	174	—	255	—

NONE = No Aging
LPO 60 = Low Pressure Oxidation, 60°C, 5 days
LPO 85 = Low Pressure Oxidation, 85°C, 5 days
LTOA 85 = Long-Term Oven Aging, 85°C, 5 days
LTOA 100 = Long-Term Oven Aging, 100°C, 2 days

Table 6.6 (continued). Modulus data for aggregate RH

Asphalt	Aging Method	% Air Voids	Modulus Values (ksi)			
			Diametral		Triaxial	
			Before	After	Before	After
AAF	LPO 85	6.9	677	982	656	1206
	LPO 85	8	864	1089	1158	1705
	LPO 60	7.4	889	1041	874	896
	LPO 60	8	816	903	790	986
	LTOA 85	6.6	776	918	720	1128
	LTOA 85	7.2	762	862	742	1260
	LTOA 100	7.5	775	855	787	1004
	LTOA 100	7.5	700	935	689	932
	NONE	7.2	617	—	855	—
	NONE	7.2	603	—	665	—
	NONE	6.5	673	—	864	—
AAG	LPO 85	9.4	643	912	615	1133
	LPO 85	10.3	610	886	627	1020
	LPO 60	10.2	624	964	925	1102
	LPO 60	10.1	617	837	967	1034
	LTOA 85	8.9	858	1260	982	1303
	LTOA 85	8.4	727	1001	1012	1246
	LTOA 100	—	—	—	—	—
	LTOA 100	—	—	—	—	—
	NONE	8.9	483	—	641	—
	NONE	8.5	511	—	709	—
	NONE	8.6	608	—	663	—
AAK	LPO 85	8.5	506	735	593	904
	LPO 85	8.2	430	700	594	904
	LPO 60	8.8	453	592	607	845
	LPO 60	8.1	400	543	453	710
	LTOA 85	7.6	502	571	517	847
	LTOA 85	8.3	421	453	453	764
	LTOA 100	8	371	646	753	1018
	LTOA 100	7.1	443	626	531	667
	NONE	7.5	250	—	353	—
	NONE	6.9	274	—	303	—
	NONE	6.8	277	—	377	—
AAM	LPO 85	6.8	432	563	430	747
	LPO 85	7.4	382	606	583	818
	LPO 60	7.1	408	521	537	721
	LPO 60	7.2	365	467	530	620
	LTOA 85	6.6	411	479	500	705
	LTOA 85	6.5	411	545	485	779
	LTOA 100	7.1	416	560	467	541
	LTOA 100	7	429	576	517	546
	NONE	5.8	319	—	478	—
	NONE	5.1	349	—	624	—
	NONE	4.6	338	—	666	—

Table 6.7. Modulus data for aggregate RJ

Asphalt	Aging Method	% Air Voids	Modulus Values (ksi)			
			Diametral		Triaxial	
			Before	After	Before	After
AAA	LPO 85	8.2	211	572	295	805
	LPO 85	8.4	193	504	350	802
	LPO 60	8	233	367	434	600
	LPO 60	8.1	270	414	373	442
	LTOA 85	9.5	225	405	357	780
	LTOA 85	8.7	221	412	295	583
	LTOA 100	9	219	475	270	570
	LTOA 100	8.6	216	499	295	455
	NONE	8	152	—	230	—
	NONE	8.8	153	—	225	—
	NONE	7.9	164	—	236	—
AAB	LPO 85	8.7	277	398	357	556
	LPO 85	9	318	521	357	578
	LPO 60	8.8	325	426	284	480
	LPO 60	9.4	292	376	286	588
	LTOA 85	8.6	293	431	344	536
	LTOA 85	9.1	292	455	494	521
	LTOA 100	8.2	335	451	324	536
	LTOA 100	8.2	328	460	373	650
	NONE	7.9	196	—	247	—
	NONE	8.2	209	—	253	—
	NONE	7.5	231	—	235	—
AAC	LPO 85	8.6	267	490	341	843
	LPO 85	7.6	405	594	464	604
	LPO 60	7.8	392	493	478	534
	LPO 60	6.7	440	558	582	651
	LTOA 85	7.2	405	480	439	595
	LTOA 85	8	326	457	589	689
	LTOA 100	8.2	350	431	379	585
	LTOA 100	8.4	345	453	500	636
	NONE	6.4	326	—	376	—
	NONE	6.8	238	—	355	—
	NONE	7	245	—	365	—
AAD	LPO 85	7.7	259	502	445	795
	LPO 85	7.9	265	507	343	780
	LPO 60	7.6	262	375	434	581
	LPO 60	8	299	452	296	548
	LTOA 85	8.4	271	491	420	708
	LTOA 85	7.5	285	476	283	439
	LTOA 100	8.6	317	496	308	651
	LTOA 100	9.2	326	571	481	790
	NONE	7.1	149	—	205	—
	NONE	7.6	136	—	192	—
	NONE	7.6	154	—	214	—

NONE = No Aging
LPO 60 = Low Pressure Oxidation, 60°C, 5 days
LPO 85 = Low Pressure Oxidation, 85°C, 5 days
LTOA 85 = Long-Term Oven Aging, 85°C, 5 days
LTOA 100 = Long-Term Oven Aging, 100°C, 2 days

Table 6.7 (continued). Modulus data for aggregate RJ

Asphalt	Aging Method	% Air Voids	Modulus Values (ksi)			
			Diametral		Triaxial	
			Before	After	Before	After
AAF	LPO 85	8.7	635	1001	802	1186
	LPO 85	8.7	752	1062	798	1025
	LPO 60	7.6	673	849	756	951
	LPO 60	8.9	706	871	926	1117
	LTOA 85	8.3	677	884	988	1123
	LTOA 85	8.4	779	1006	809	988
	LTOA 100	8.4	681	961	711	1251
	LTOA 100	9	712	1061	736	937
	NONE	9	558	—	668	—
	NONE	8.4	575	—	723	—
	NONE	7.8	567	—	802	—
AAG	LPO 85	7.9	620	895	745	1465
	LPO 85	8.1	735	1006	771	1341
	LPO 60	8.1	812	914	853	1268
	LPO 60	8.2	675	810	760	1030
	LTOA 85	7.9	673	785	822	1324
	LTOA 85	7.4	722	857	885	1349
	LTOA 100	8.9	598	821	717	1010
	LTOA 100	7.9	698	939	986	1116
	NONE	7.5	527	—	657	—
	NONE	7.1	535	—	563	—
	NONE	7.2	581	—	640	—
AAK	LPO 85	9.1	403	660	674	1057
	LPO 85	8.4	419	712	512	1066
	LPO 60	9.2	408	574	499	824
	LPO 60	8.5	463	665	460	656
	LTOA 85	8.3	533	862	551	808
	LTOA 85	9.3	562	928	771	1022
	LTOA 100	9.7	354	586	520	808
	LTOA 100	9	450	737	692	972
	NONE	7.9	309	—	473	—
	NONE	7.8	340	—	421	—
	NONE	7.7	347	—	460	—
AAM	LPO 85	7.2	370	548	347	652
	LPO 85	8.2	344	492	602	792
	LPO 60	7.9	367	504	598	734
	LPO 60	7.3	394	529	452	621
	LTOA 85	8.1	437	558	604	813
	LTOA 85	8.3	385	479	480	717
	LTOA 100	7.6	410	442	510	492
	LTOA 100	7.5	356	491	436	519
	NONE	7.3	312	—	422	—
	NONE	6.8	323	—	393	—
	NONE	6.6	343	—	355	—

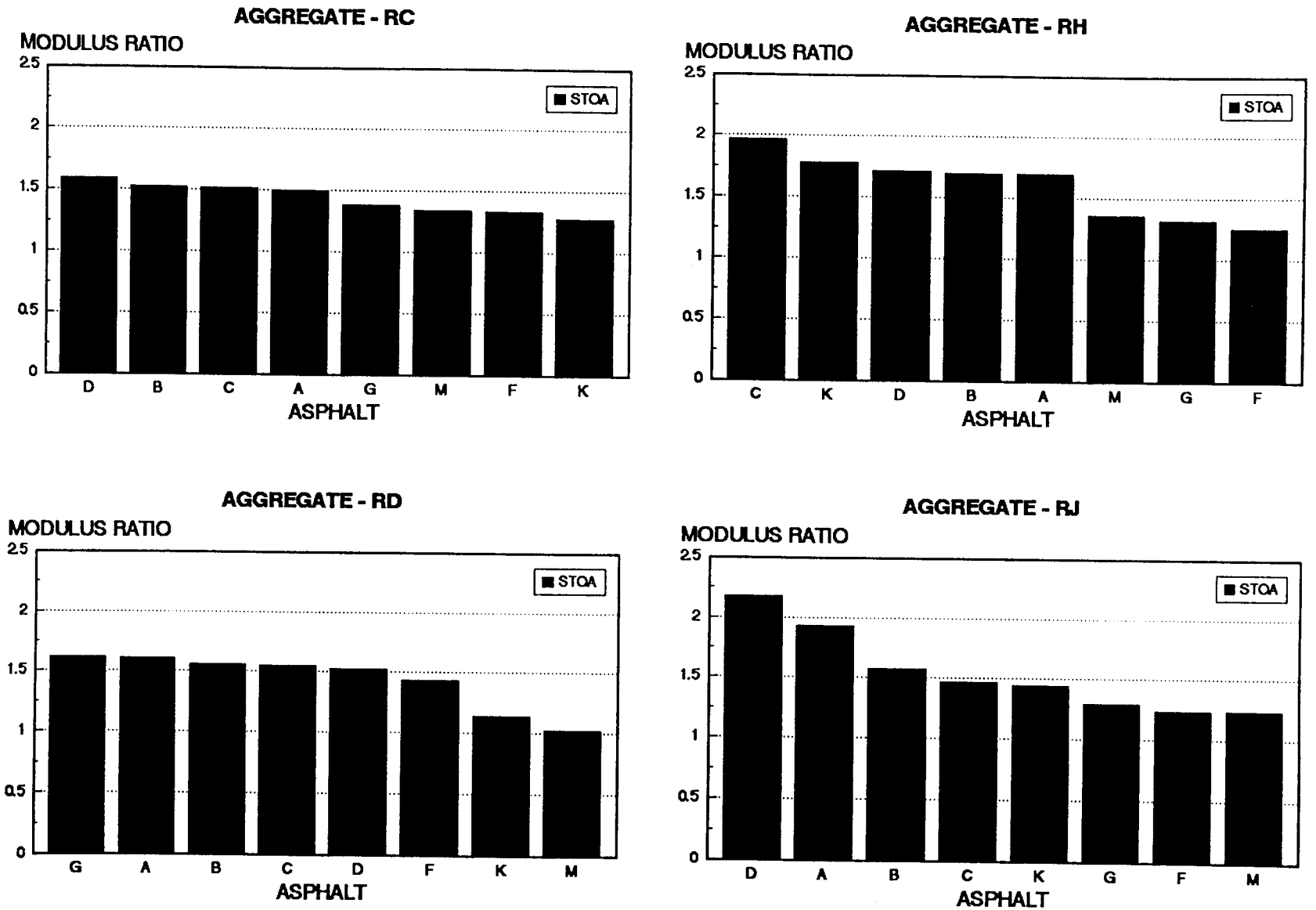

Figure 6.2. Diametral modulus ratio rankings for short-term oven aging

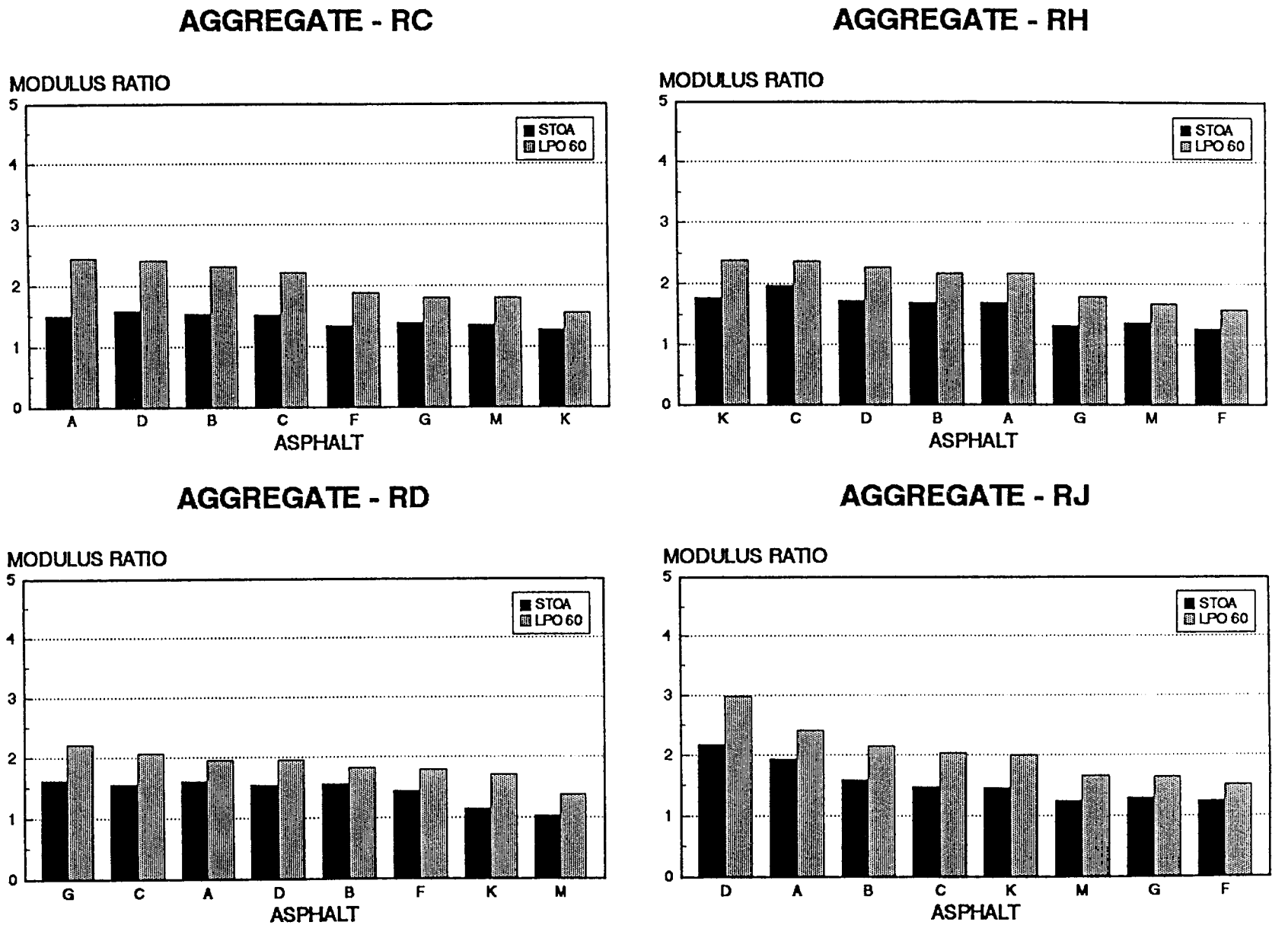

Figure 6.3. Diametral modulus ratio rankings for LPO at 60°C

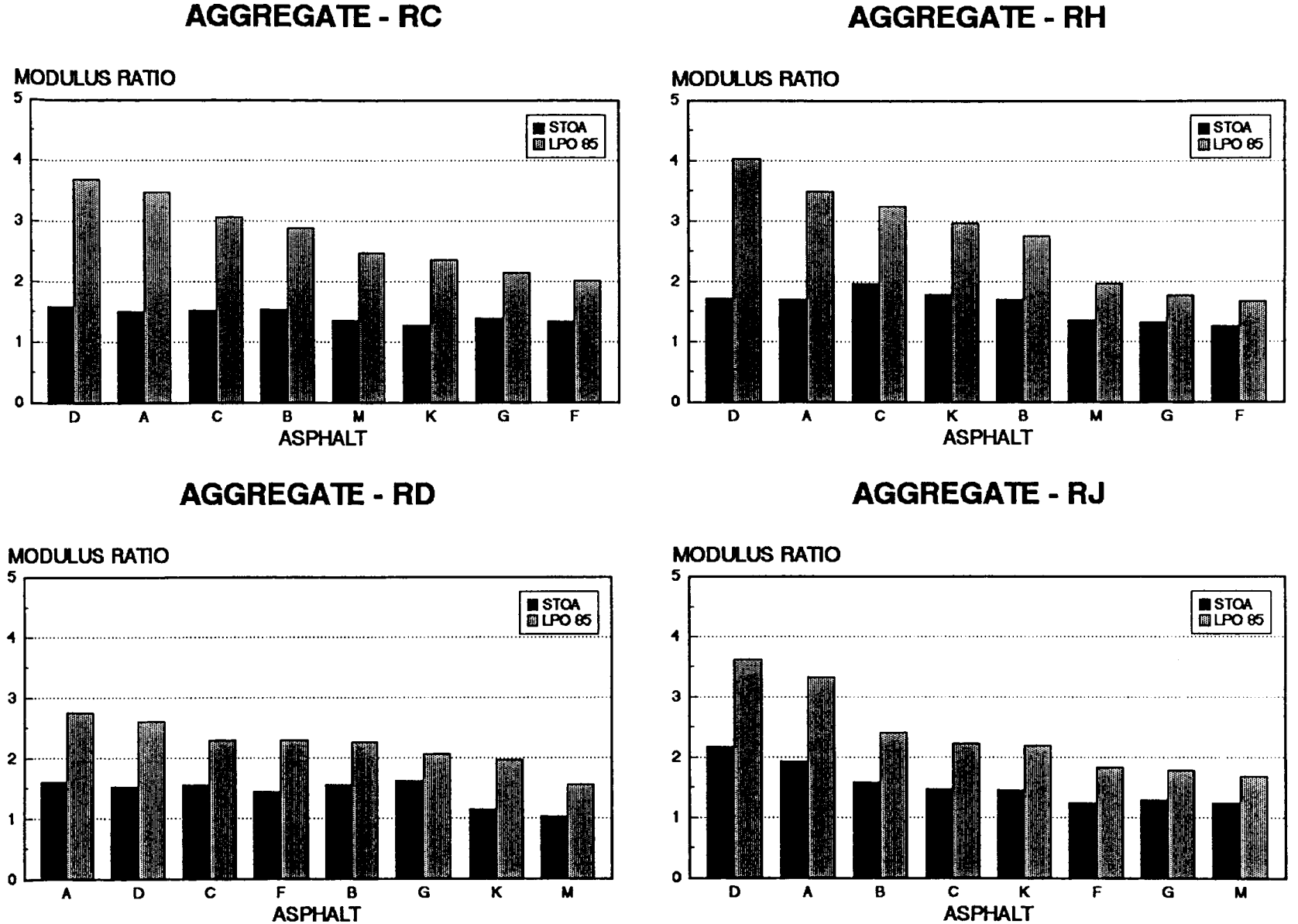

Figure 6.4. Diametral modulus ratio rankings for LPO at 85°C

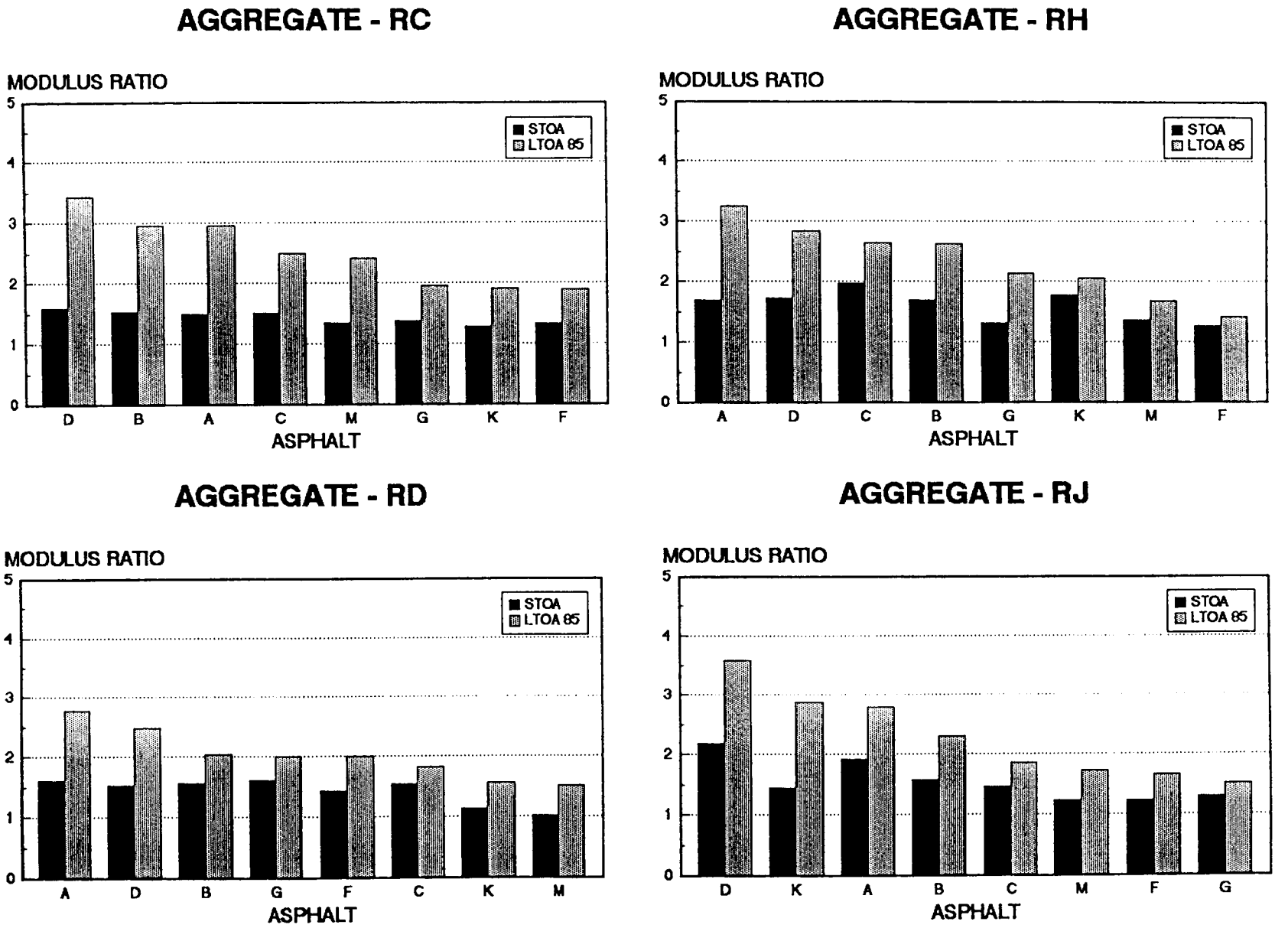

Figure 6.5. Diametral modulus ratio rankings for LTOA at 85°C

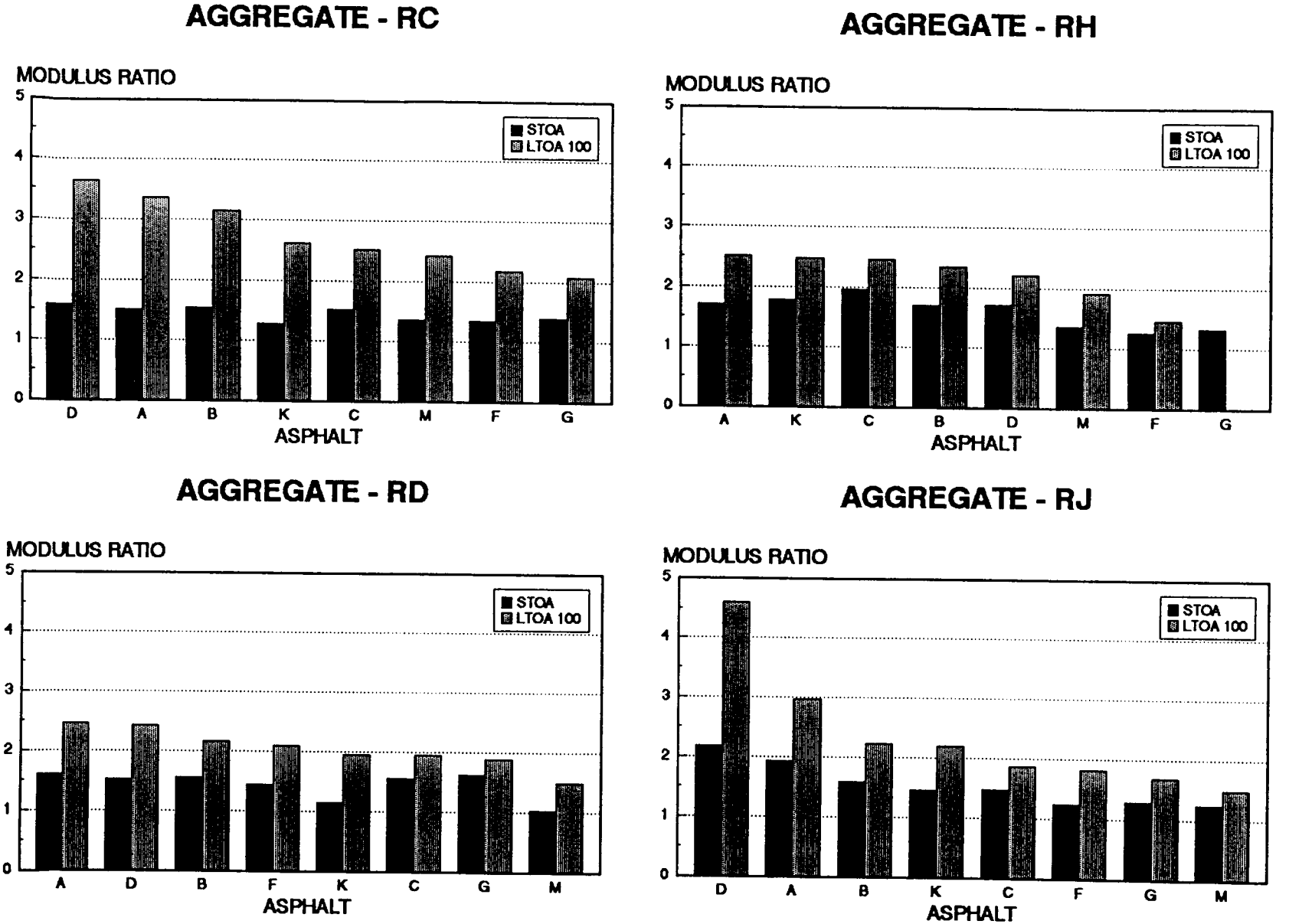

Figure 6.6. Diametral modulus ratio rankings for LTOA at 100°C

Long-Term Aging of Asphalt-Aggregate Mixes

The data for long-term aging, Figures 6.3 through 6.6, support those for short-term aging; that is, they also suggest that aging is aggregate dependent as well as asphalt dependent. Tables 6.9 through 6.12 present the rankings numerically and show where groups of asphalt are statistically similar, again using Waller groupings. Note that there appears to be more differentiation among asphalts following long-term aging, than with short-term aging, and the differentiation becomes more pronounced with the severity of the aging procedure.

Comparison of Mix Aging by Short-Term and Long-Term Aging Methods

The numerical rankings of aging presented in Tables 6.8 through 6.12 are summarized in Table 6.13. Comparison of the rankings resulting from short-term aging with those from long-term aging shows that small movements in the rankings are common. However, using the short-term rankings as a datum, only a few asphalts move more than two places in the rankings, as shown in Table 6.13. These comparisons imply that the LPO aging procedure relates more closely to the short-term aging rankings than the LTOA procedure does. This may be because of the greater potential for damage to the specimen in the LTOA, which could be the cause of the greater variability in LTOA specimens, particularly at 100°C. It should be noted that the short-term aging rankings are based on data from six specimens, whereas those for each set of long-term aged specimens are based on data from only two specimens. Hence, more variability is expected for the long-term aging.

Comparison of Mix Aging with Asphalt Aging

Aging of asphalt cement has been carried out by the SHRP Project A-002A contractor. Data for original (tank), thin-film oven (TFO) aged, and PAV aged asphalt have been presented in several A-002A reports. These routine data have been summarized recently by Christensen and Anderson (1992). As with mix aging data, the asphalt aging data can be used to calculate an aging ratio based on the aged viscosity at 60°C compared with the original viscosity at 60°C. The asphalts can be then ranked in order of aging susceptibility. Table 6.14 shows the routine asphalt data and the calculated viscosity ratios.

Short-Term Aging

Table 6.15 shows rankings for mixes based on short-term aging and the asphalt rankings based on TFO aging. It should be noted that TFO aging is analogous to short-term mix aging and that (as with mix rankings) the difference between some asphalts is not statistically significant. Nevertheless, it is clear that there is little relationship between the mix rankings and the asphalt rankings. The major similarity is that asphalt AAM-1 is one of the two best

Table 6.8. Short-term rankings by aggregate

Aggregate	Ranking															
RC	D	>	B	>	C	>	A	>	G	>	M	>	F	>	K	
	1.59		1.53		1.52		1.58		1.39		1.35		1.34		1.28	
RD	G	>	A	>	B	>	C	>	D	>	F	>	K	>	M	
	1.62		1.61		1.56		1.55		1.53		1.44		1.14		1.03	
RH	C	>	K	>	D	>	B	>	A	>	M	>	G	>	F	
	1.97		1.78		1.72		1.70		1.70		1.36		1.32		1.26	
RJ	D	>	A	>	B	>	C	>	K	>	G	>	F	>	M	
	2.18		1.93		1.58		1.47		1.45		1.30		1.24		1.24	

Note: Waller groupings of statistically similar behavior are identified with underscores.

Table 6.9. Long-term aging by LPO at 60°C—rankings by aggregate

Aggregate	Ranking													
RC	A	>	D	>	B	>	C	>	F	>	G	>	M	>	K
	2.44		2.40		2.31		2.21		1.88		1.80		1.80		1.56
RD	G	>	C	>	A	>	D	>	B	>	F	>	K	>	M
	2.21		2.07		1.95		1.95		1.82		1.78		1.70		1.37
RH	K	>	C	>	D	>	B	>	A	>	G	>	M	>	F
	2.38		2.36		2.26		2.17		2.17		1.79		1.67		1.58
RJ	D	>	A	>	B	>	C	>	K	>	M	>	G	>	F
	2.99		2.40		2.14		2.03		1.99		1.66		1.63		1.51

Note: Waller groupings of statistically similar behavior are identified with underscores.

Table 6.10. Long-term aging by LPO at 85°C—rankings by aggregate

Aggregate	Ranking															
RC	D	>	A	>	C	>	B	>	M	>	K	>	G	>	F	
	3.69		3.47		3.07		2.88		2.47		2.36		2.15		2.01	
RD	A	>	D	>	C	>	F	>	B	>	G	>	K	>	M	
	2.76		2.61		2.30		2.29		2.26		2.07		1.96		1.55	
RH	D	>	A	>	C	>	K	>	B	>	M	>	G	>	F	
	4.03		3.49		3.24		2.97		2.75		1.97		1.77		1.67	
RJ	D	>	A	>	B	>	C	>	K	>	F	>	G	>	M	
	3.63		3.32		2.40		2.23		2.20		1.84		1.78		1.68	

Note: Waller groupings of statistically similar behavior are identified with underscores.

Table 6.11. LTOA at 85°C—rankings by aggregate

Aggregate	Ranking															
RC	D	>	B	>	A	>	C	>	M	>	G	>	K	>	F	
	3.43		2.95		2.95		2.49		2.41		1.96		1.90		1.89	
RD	A	>	D	>	B	>	G	>	F	>	C	>	K	>	M	
	2.78		2.48		2.04		2.01		2.00		1.83		1.56		1.51	
RH	A	>	D	>	C	>	B	>	G	>	K	>	M	>	F	
	3.26		2.84		2.65		2.63		2.13		2.05		1.67		1.41	
RJ	D	>	K	>	A	>	B	>	C	>	M	>	F	>	G	
	3.58		2.88		2.80		2.31		1.86		1.73		1.67		1.52	

Note: Waller groupings of statistically similar behavior are identified with underscores.

Table 6.12. LTOA at 100°C—rankings by aggregate

Aggregate	Ranking																			
RC	D	>	A	>	B	>	K	>	C	>	M	>	F	>	G					
	3.63		3.36		3.14		2.62		2.52		2.42		2.18		2.07					
RD		>	D	>	B	>	F	>	K	>	C	>	G	>	M					
	2.46		2.42		2.16		2.09		1.95		1.95		1.88		1.49					
RH	A	>	K	>	C	>	B	>	D	>	M	>	F		G					
	2.51		2.48		2.45		2.34		2.21		1.91		1.45							
RJ	D	>	A	>	B	>	K	>	C	>	F	>	G	>	M					
	4.59		2.97		2.22		2.19		1.86		1.81		1.68		1.49					

Note: Waller groupings of statistically similar behavior are identified with underscores.

asphalts in both the mix and asphalt short-term aging. A major difference is that asphalt AAK-1 is ranked one of the two worst from asphalt TFO aging and one of the two best if short-term aging with aggregates RC and RD is considered.

Long-Term Aging

Table 6.16 shows the rankings for mixes based on long-term aging by LPO at 85°C and rankings for asphalt developed from the data reported by Christensen and Anderson (1992). Also summarized are rankings developed from data reported by Robertson et al. (1991) for asphalt recovered from "mixes" of single-size fine aggregate and asphalt subjected to pressure aging.

As with the short-term aging comparisons, there is little similarity between the rankings for long-term aging of asphalt mixes and those for asphalt alone. In fact, there is even less similarity, since asphalt AAM-1 appears to have more susceptibility to long-term aging in the PAV than it does in the TFO, relative to the other asphalts, and has moved in the rankings.

There is more similarity between the rankings based on mix aging and those based on the data for fine aggregate mixes developed by the A-002A contractor. However, the rankings are different, as indicated in Table 6.16.

General Discussion

The difference in rankings between mixes and asphalt, based on either short-term or long-term aging data, indicates the need for mix testing to evaluate the aging susceptibility of a mix. Clearly, the aging of the asphalt alone, or in a fine aggregate mix, is not an indicator of how a mix will age. The aggregate influences mix aging, apparently through the chemical interaction of the aggregate and the asphalt. This interaction may be related to adhesion; the greater the adhesion, the greater the mitigation of aging. The mix aging rankings given in Tables 6.9 through 6.12 suggest this hypothesis, since the rankings are similar for the two basic aggregates (RC and RD) and for the two acidic aggregates (RH and RJ). Some of the asphalts rank similarly regardless of the aggregate types, whereas others (such as AAG-1 and AAK-1) behave very differently with different aggregate types. It is known that asphalt AAG-1 was treated with lime in the refining process, and it is therefore reasonable that it would exhibit good adhesion and reduced aging tendency with the acidic aggregates (RH and RJ), as is indicated by the short-term aging data. However, the rankings of asphalt AAG-1 for long-term aging do not appear to be influenced by aggregate type.

Table 6.13. Rankings of asphalt for each aggregate based on diametral modulus ratios and aging method

	Short-Term Oven Aging Aggregate				Low Pressure Oxidation at 60°C				Low Pressure Oxidation at 85°C				Long-Term Oven Aging at 85°C				Long-Term Oven Aging at 100°C			
	RC	RD	RH	RJ	RC	RD	RH	RJ	RC	RD	RH	RJ	RC	RD	RH	RJ	RC	RD	RH	RJ
Worst	D	G	C	D	A	G	K	D	D	A	D	D	D	A	$A_{\uparrow}^{4}$	D	D	A	$A_{\uparrow}^{4}$	D
	B	A	K	A	D	C	C	A	A	$D_{\uparrow}^{3}$	$A_{\uparrow}^{3}$	A	B	$D_{\uparrow}^{3}$	D	$K_{\uparrow}^{3}$	A	$D_{\uparrow}^{3}$	K	A
	C	B	D	B	B	A	D	B	C	C	C	B	A	B	C	A	B	B	C	B
	A	C	B	C	C	D	B	C	B	F	K	C	C	$G_{3}^{\downarrow}$	B	B	$K_{\uparrow}^{4}$	F	B	K
	G	D	A	K	F	B	A	K	M	B	B	K	M	F	G	C	C	K	D	C
	M	F	M	G	G	F	G	M	K	$G_{5}^{\downarrow}$	M	F	G	C	$K_{4}^{\downarrow}$	M	M	C	M	F
	F	K	G	F	M	K	M	G	G	K	G	G	K	K	M	F	F	$G_{6}^{\downarrow}$	F	G
Best	K	M	F	M	K	M	F	F	F	M	F	M	F	M	F	G	$G_{3}^{\downarrow}$	M		M

Note: An underlined cell indicates an asphalt that changes more than two rankings relative to the short-term aging rankings. The arrow and adjacent number indicate the number of places moved and the direction.

Table 6.14. Summary of routine test data for asphalt alone

	Asphalt							
	AAA-1 (150/200)	**AAB-1** (AC-10)	**AAC-1** (AC-8)	**AAD-1** (AR-4000)	**AAF-1** (AC-20)	**AAG-1** (AR-4000)	**AAK-1** (AC-30)	**AAM-1** (AC-20)
ORIGINAL ASPHALT								
Viscosity (60°C) (Poises)	900	1120	710	1140	1750	1950	3320	2040
AGED ASPHALT (THIN-FILM OVENT TEST)								
Viscosity (60°C) (Poises)	2080	2620	1780	3690	4560	3490	10240	4490
Viscoity Ratio (60°C TFO Aged/Original)	2.31	2.34	2.51	3.24	2.61	1.79	3.08	2.20
LONG-TERM AGED (PAV)								
Viscosity (60°C) (Poises)	5380	7110	5170	12000	16250	8140	27300	17150
Viscoity Ratio (60°C TFO Aged/Original)	5.98	6.35	7.28	10.53	9.29	4.71	8.22	8.41

Table 6.15. Comparison of rankings for short-term aging of mixes and asphalts

	Ranking of Asphalt					
	A-003A[a]					A-002A[b]
	Aggregate RC	Aggregate RD	Aggregate RH	Aggregate RJ	Average of A-003A Rankings	No Aggregate
Worst	D	G	C	D	D	D
	B	A	K	A	A	K
	C	B	D	B	C	F
	A	C	B	C	B	C
	G	D	A	K	K	B
	M	F	M	G	G	A
	F	K	G	F	F	M
Best	K	M	F	M	M	G

[a]Based on short-term aging ratios from diametral modulus.
[b]Based on data reported by Christensen and Anderson (1992).

Table 6.16. Comparison of rankings for long-term aging of mixes and asphalts

	Ranking of Asphalts								
	A-003A[a]				A-002A[b]	A-002A[c]		A-002A[d]	
	Aggregate RC	Aggregate RD	Aggregate RH	Aggregate RJ	No Aggregate	Aggregate RD	Aggregate RJ	Aggregate RD	Average of A-003A Rankings
Worst	D	A	D	D	D	F	D	F	D
	A	D	C	A	F	$M^{6}_{\uparrow}$	B	$M^{6}_{\uparrow}$	A
	C	C	A	B	M	D	$F^{3}_{\uparrow}$	C	C
	B	F	C	C	K	C	C	D	B
	M	B	K	K	C	$A^{\downarrow}_{3}$	$M^{3}_{\uparrow}$	G	K
	K	G	M	F	B	K	$A^{\downarrow}_{4}$	$A^{\downarrow}_{4}$	F
	G	K	G	G	A	G	K	$B^{\downarrow}_{3}$	G
Best	F	M	F	M	G	$B^{\downarrow}_{4}$	G	K	M

[a]Based on long-term aging ratios from diametral modulus for LPO aging.
[b]Based on data reported by Christensen and Anderson (1992) for TFO-PAV aging.
[c]Reported in 4th Quarterly Report, 1991, based on PAV aging at 60°C for 144 hours. Prior short-term aging.
[d]Reported in 4th Quarterly Report, 1991. Asphalt alone was subjected to TFO aging before mixing and PAV aging.

Conclusions

The following conclusions can be drawn from the results of this study:

1. The aging of asphalt-aggregate mixes is influenced by both asphalt type and aggregate type.

2. Aging of the asphalt alone, and subsequent testing, does not appear to be an adequate means of predicting mix performance because of the apparent mitigating effect aggregate has on aging.

3. The aging of certain asphalts is strongly mitigated by some aggregates but not by others. This effect appears to be related to the strength of the chemical bonding (adhesion) between the asphalt and aggregate.

4. The short-term aging procedure produces a change in resilient modulus of up to a factor of 2. For a particular aggregate, there is not a statistically significant difference in the aging of certain asphalts. The eight asphalts investigated typically fell into three groups: those with high, medium, and low aging susceptibility.

5. The four long-term aging methods produce somewhat different rankings of aging susceptibility compared with short-term aging procedure and with each other. The differences are partially attributable to variability in the materials, aging process, and testing. However, it appears that the short-term aging procedure does not enable prediction of long-term aging.

6. The LPO long-term aging procedure causes the most aging—and less variability—in the rankings of aging susceptibility, relative to the short-term aging rankings.

7

Validation of Binder Properties Related to Water Sensitivity

Water-sensitivity of asphalt-aggregate mixes is a major problem throughout the United States. Water-related problems can be associated with any of the following:

1. Loss of adhesion between the binder and the aggregate (stripping).
2. Loss of cohesion (or tensile strength) and softening of the binder.
3. Loss of integrity within the aggregate because of the presence of clay in the aggregate.

This chapter presents a summary of the findings of an extensive study to validate the hypothesis of Strategic Highway Research Program (SHRP) contractors A-002A and A-003B related to water sensitivity.

An accelerated rutting test using the LCPC rutting tester at Oregon State University (OSU), here referred to as the OSU wheel tracker, was selected as the primary method to evaluate water sensitivity. However, tests on the same mixes were also conducted using the wheel-rutting tester at SWK/University of Nottingham, here referred to as the SWK/UN wheel tracker, and the Environmental Conditioning System (ECS) developed at OSU. Each test procedure results in a different failure mechanism, but all tests can be used to evaluate the water sensitivity of asphalt-aggregate mixes.

Hypotheses

With a primary purpose of this work being to validate the A-002A hypothesis for water sensitivity, it is necessary to review this hypothesis. This section presents a review of the

A-002A hypothesis prepared in March 1991 (Robertson 1991) as well as a review of the A-003B hypothesis (Curtis et al. 1991).

A-002A

The SHRP A-002A contractor (Western Research Institute) was commissioned to develop predictions for asphalt-aggregate mix performance based on the properties of the binder. Mix performance measures included fatigue, permanent deformation (rutting), aging, thermal cracking, and water sensitivity (in terms of loss of adhesion). Only the predictions for water sensitivity and permanent deformation will be considered in this report; validation of permanent deformation predictions is included here because this work used rutting tests as part of the validation effort.

The ranking of asphalts for permanent deformation is shown in Table 7.1 (Robertson 1991). This ranking is based on preparative size exclusion chromotography (SEC) Fraction I to SEC Fraction II ratios that show a strong correlation with viscoelastic properties of the binder as shown in Figure 7.1. It should be noted that this ranking is based on asphalts that have experienced short-term aging only. The SEC Fraction I is the weight of the nonfluorescent components in the asphalt, whereas the SEC Fraction II is the weight of the fluorescent components. The nonfluorescent components appear to assemble into an elastic matrix, while the fluorescent components form the dispersing phase for the matrix. This dispersing phase does not appear to self-assemble at moderate to high temperatures and therefore is primarily a viscous material. The ratio (SEC Fraction I to SEC Fraction II) provides a measure of the total of the SEC system.

Several studies have demonstrated that loss of adhesion via moisture damage is primarily associated with the aggregate (Curtis et al. 1991; Robertson 1991). The Project A-002A contractor believes that the chemistry of the binder has only a minor effect, at best, on its susceptibility to damage by moisture (Robertson 1991). However, the A-002A contractor formulated a hypothesis, shown in Table 7.2, based on the carbonyl content (with emphasis on the free acid content) as determined by Fourier-transform infrared spectroscopy. Note that aging affects the asphalts differently.

A-003B

The SHRP A-003B contractor (Auburn University) was charged with describing and defining asphalt-aggregate interactions that are sensitive to water. This effort examined three specific areas: (1) evaluation of the specific chemistry of asphalt adsorption onto aggregate using model specimens that are representative of polar functional groups present in asphalts; (2) evaluation of the compatibility of various asphalt-aggregate pairs and their sensitivity to water; and (3) determination of the effect that aggregates treated with saline compounds of differing chemistries have on asphalt-aggregate interactions and water sensitivity (Curtis et al. 1991).

Table 7.1. Rank of high-temperature permanent deformation and rutting by SEC tan δ

Asphalt Type	Resistance
AAM-1 AAK-1 AAE	Excellent
AAS-1 AAH-1 AAD-1 AAB-1 AAW-1 AAJ	Very good
AAA-1 AAN	Good
AAX AAF-1 AAC-1	Fair
AAZ AAV	Poor
AAG-1 ABD	Little or no resistance

Note: After Robertson (1991)

Table 7.2. Rank of moisture damage resistance by infrared spectroscopy of functional groups

New Material		Aged Material	
Asphalt	**Resistance**	**Asphalt**	**Resistance**
AAF-1 AAB-1 AAM-1 AAA-1	Good (no order established)	AAB-1 AAM-1 AAC-1 AAF-1	Good (in order as shown)
AAD-1 AAK-1	Intermediate–good	AAD-1	Intermediate–good
AAG-1	Fair–poor		
ABD	Poor	AAG-1 ABD	Poor

Note: After Robertson (1991)

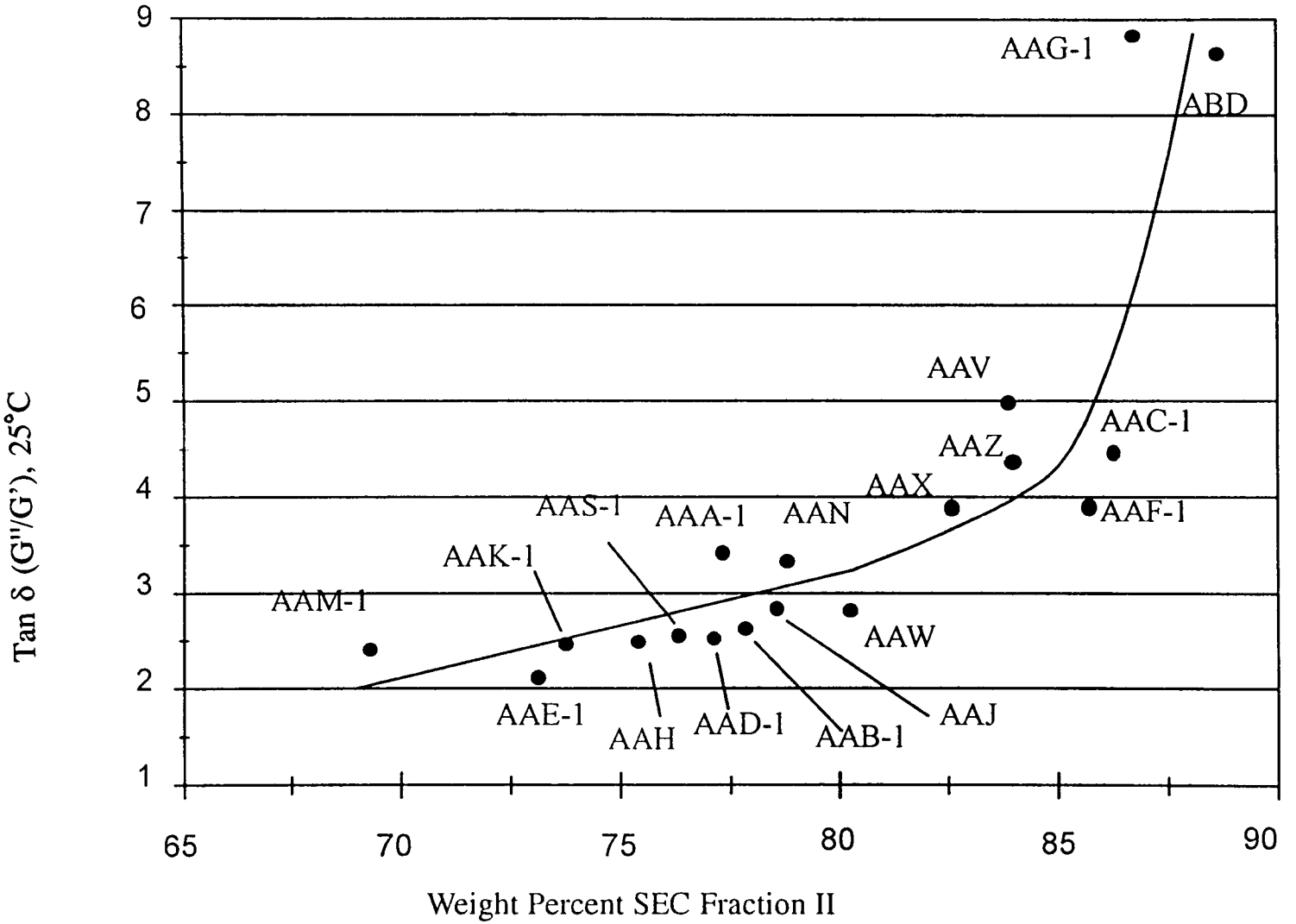

Figure 7.1. Relationship between weight percent SEC Fraction II and tan δ for SHRP asphalts (after Robertson 1991)

The A-003B contractor concluded that the adsorptive behavior of asphalt and asphalt model components on aggregates is highly specific and particularly influenced by the aggregate surface chemistry; the chemistry of the asphalt binder has less influence. Net adsorption tests (NATs), which were used to investigate the compatibility and water sensitivity of asphalt-aggregate pairs, clearly showed that the adsorption behavior of asphalt on aggregate was controlled by the aggregate chemistry. The A-003B researchers found that substantial differences in adsorption and aqueous desorption behavior existed among aggregates, while small and generally insignificant differences existed among asphalts. That is, the differences in adsorption and desorption behavior of one particular asphalt in combination with various aggregates were far in excess of that of one particular aggregate in combination with various asphalts. Table 7.3 shows the net adsorption data obtained by the A-003B contractor during the development of the NAT procedure. The initial amount of asphalt adsorbed before introduction of water gives an indication of the affinity a particular asphalt has for a given aggregate. The net adsorption, or the amount remaining on the surface of the aggregate after aqueous desorption, is an indication of the moisture sensitivity of the asphalt-aggregate pair (Curtis et al. 1991); however, these tests used a diluted solution of asphalt rather than straight asphalt. The results of the NAT (i.e., ranking of aggregates by net adsorption) will be used here to compare with the results obtained by the A-003B and A-003A contractors.

The NAT was used by the A-003B contractors on only a few of the Materials Reference Library (MRL) aggregate-asphalt combinations. Late in the A-003A research program, it was determined that additional NAT results would be beneficial. Accordingly, a subcontract was initiated with the University of Nevada at Reno to test the 32 combinations (8 asphalts, 4 aggregates) that were used in the validation experiment. These results were not available until after this report had been completed. Accordingly, the reader is referred to the report by Scholz et al. (1992).

Experiment Design

The experiment design is shown in Table 7.4. The ECS validation phase was divided into two tasks: (1) lab validation, using the ECS, and (2) field validation, using wheel-tracking tests. The same experiment design was used for both tasks.

The testing program included eight asphalt types and four aggregate types. The conditioning variables considered for this phase of the SHRP project are as shown in Table 7.5 and discussed below:

1. The specimen was preconditioned or saturated with water at 51 mm Hg of vacuum.

2. Temperatures applied during the conditioning cycle were hot (60°C), and freeze (-18°C). Testing for modulus of resilience was conducted at 25°C.

3. The time for each cycle was 6 hr, and each test had three hot cycles and one freeze cycle.

4. Repeated loading was applied during the hot cycles, static load was applied during the freeze cycle.

5. Conditioning of specimens for the ECS and OSU wheel tracker was essentially the same, except that the wheel tracker beams were subjected to all three hot cycles and one freeze cycle before loading.

The response variables included the following:

1. Modulus of resilience—measured after each conditioning cycle.

2. Permeability—measured after each conditioning cycle, to monitor the change in moisture damage susceptibility.

3. Percentage of asphalt coating retained on the aggregate—visually evaluated at the end of the test.

A full-factorial experiment design was used, as shown in Table 7.5. The order of sample preparation was randomized independently for each replicate. The specimens were selected and tested randomly.

Variables Considered

The variables considered in the experiment design include asphalt and aggregate type. Specimen density (air-void content), mix asphalt content, gradation of the aggregate, and test specimen conditioning were all held as constant as possible. Specimen air-void content was "held constant" at 8±1 percent, and each test program employed a conditioning procedure that remained the same for all specimens tested.

Materials

The materials used in the study included the eight core asphalts and four aggregates from the MRL (Tables 2.1 and 2.2).

Specimen Preparation

Specimens were prepared by rolling-wheel compaction. Table 7.6 gives a brief description of the procedure developed at OSU specifically for preparing specimens to be tested in the ECS, the OSU wheel tracker, and the SWK/UN wheel tracker.

Table 7.3. Initial and net adsorption of asphalt on aggregate

Aggregate	Asphalt								
	AAD-1			AAK-1			AAM-1		
	Initial Adsorption	Net Adsorption	Percent Desorption	Initial Adsorption	Net Adsorption	Percent Desorption	Initial Adsorption	Net Adsorption	Percent Desorption
RA	0.18±0.03	0.07	61.5	0.25±0.04	0.18	28.7	0.20±0.18	0.001	99.5
RB	0.85±0.04	0.68	19.1	0.89±0.11	0.73	18.1	0.77±0.03	0.60	22.6
RC	1.9*	1.5	20.0	1.7	1.3	25	1.4	1.2	22
RD	0.73±0.06	0.60	18.5	0.73±0.02	0.59	18.9	0.69±0.09	0.50	30.4
RE	0.98±0.05	0.69	29.7	1.01±0.006	0.61	39.0	0.85±0.02	0.45	47.1
RF	0.90±0.04	0.61	32.2	0.85±0.06	0.52	43.7	0.83±0.05	0.44	47.2
RG	0.70±0.02	0.58	17.8	0.60±0.09	0.42	31.0	0.59±0.02	0.34	42.0
RH	1.3*	1.0	25	1.22	0.94	23	1.2	0.91	24
RJ	0.31±0.003	0.12	60.3	0.34±0.06	0.19	44.0	0.42±0.63	0.21	50.0
RK	1.7*	1.4	17	1.56	1.26	19	1.4	1.2	17
RL	1.4*	1.0	28	1.4	0.99	30	1.2	0.83	28

Note: After Curtis et al. (1991).
*Obtained from isotherm data.

Table 7.4. Experiment design for the water-sensitivity validation

Mix Number	Mix Code	MRL Aggregate	MRL Asphalt	Required Replicate
1	00000	RC	AAA-1	RC & AAA-1
2	10000		AAB-1	
3	01000		AAC-1	
4	11000		AAD-1	
5	00100		AAF-1	
6	10100		AAG-1	
7	01100		AAK-1	RC & AAK-1
8	11100		AAM-1	
9	00010	RD	AAA-1	
10	10010		AAB-1	
11	01010		AAC-1	
12	11010		AAD-1	RD & AAD-1
13	00110		AAF-1	
14	10110		AAG-1	RD & AAG-1
15	01110		AAK-1	
16	11110		AAM-1	
17	00001	RH	AAA-1	
18	10001		AAB-1	
19	01001		AAC-1	
20	11001		AAD-1	RH & AAD-1
21	00101		AAF-1	
22	10101		AAG-1	RH & AAG-1
23	01101		AAK-1	
24	11101		AAM-1	
25	00011	RJ	AAA-1	RJ & AAA-1
26	10011		AAB-1	
27	01011		AAC-1	
28	11011		AAD-1	
29	00111		AAF-1	
30	10111		AAG-1	
31	01111		AAK-1	RJ & AAK-1
32	11111		AAM-1	

Table 7.5. Experiment design of water-sensitivity testing program

Controlled Variable	Level of Treatment 1	2	3	Number of Levels
Asphalt Type				
• Temperature susceptibility				8
• Grade				1
• Content		Optimum		1
Aggregate Type				
• Stripping potential	Low	Medium	2 High	4
• Gradation		Medium		1
Compaction				
• Air-void content (%)			8±1	1
• Permeability			High	1
Testing Compaction Factors				
• Test temperature	3 hot cycles (60°C) + freeze cycle (-18°C)			1
• Load			Repeated	1
• Pressure			High	1
• Fluid			High sat.	1
• Time			6 hr	1
			Total	32

Complete factorial	32
Replicate	32
Total number of samples	64

Response variables:

Initial ECS modulus
Air permeability
ECS resilient modulus after each cycle
Water permeability after each cycle
Visual evaluation, percentage of retained asphalt coating on the aggregate

The specimen preparation process is shown schematically in Figure 7.2. The mixer was a conventional concrete mixer modified to include infrared propane heaters to preheat the mixer bowl as well as to reduce heat loss during mixing. The preheated and preweighed aggregate was added to the mixer, followed by the asphalt. The mix, typically 125 to 132 kg, was mixed in one batch.

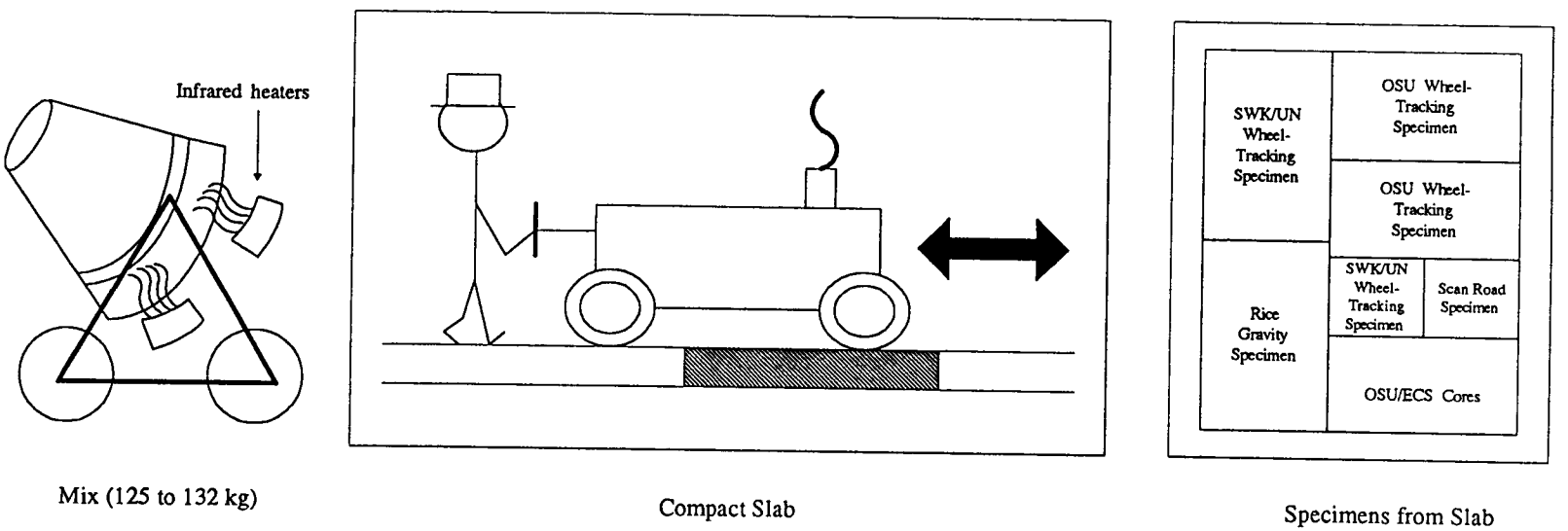

Mix (125 to 132 kg)

Compact Slab

Specimens from Slab

Figure 7.2. Schematic of the specimen preparation process

Table 7.6. Summary of specimen preparation procedure for water-sensitivity validation effort

Step	Description
1	Calculate the quantity of materials (asphalt and aggregate) needed based on the volume of the mold, the theoretical maximum (Rice) specific gravity of the mix, and the desired percent air-void content. Batch weights ranged between 125 to 132 kg at an air-void content of 8±1 percent.
2	Prepare the asphalt and aggregate for mixing.
3	Heat the materials to the mixing temperature for the asphalt (170±20 centistokes). Mixing temperatures ranged between 137°C and 160°C.[c]
4	Mix the asphalt and aggregate for 4 min in a conventional concrete mixer fitted with infrared propane burners and preheated to the mixing temperature for the asphalt.
5	Age the mix at 135°C in a forced-draft oven for 4 hr stirring the mix every hour, to represent the amount of aging that occurs in the mixing plant.
6	Assemble and preheat the compaction mold using infrared heat lamps.
7	Place the mix in the compaction mold and level it using a rake while avoiding segregation of the mix.
8	Compact the mix when it reaches the compaction temperature, using a rolling-wheel compactor until the desired density is obtained. Density is determined from the thickness of the specimen (the only volumetric dimension that can be varied during compaction for a set width and length of slab). Steel channels with depth equal to the thickness of the specimen prevent overcompaction of the mix. Compaction temperatures (based on 630±20 centistokes) ranged between 112°C and 133°C.
9	Allow the compacted mix to cool to room temperature (about 15 hr).
10	Disassemble the mold and remove the slab. Dry-cut (saw) beams[a] for the OSU and SWK/UN wheel trackers. Dry-cut cores[b] for the ECS.

[a]Beams for testing in the OSU wheel tracker were 178 mm wide, 560 mm long, and 100 mm thick.
[b]Cores for testing in the ECS were 100 mm in diameter by 100 mm high.
[c]Temperature-viscosity data were measured on the MRL asphalts for OSU by Oregon Department of Transportation.

After mixing, the asphalt-aggregate mix was placed in a forced-draft oven set to 135°C and short-term aged for 4 hr to simulate the amount of aging that occurs in a batch or drum dryer plant. The mix was stirred once each hour to promote uniform aging.

At the completion of the aging process, the mix was placed in the mold and compacted to a predetermined density using a small steel wheel compactor with tandem rollers (e.g., a roller for compacting sidewalks and bike paths). The compacted slab was then allowed to cool overnight (about 15 hr) after which beam specimens were sawed and core specimens were drilled from the slab (see Figure 7.3). The beams were sawed and the cores were drilled without the use of water to prevent errors in density and void analysis as well as in the initial air-permeability tests.

Testing Methods

Each test program (ECS, OSU wheel tracking, and SWK/UN wheel tracking) employed specimen conditioning in its test procedure, which subjected the specimen to water damage followed by measurement of rutting (OSU and SWK/UN wheel trackers) or the reduction in modulus (ECS). Details on the test methods are given in the report by Scholz et al. (1992).

Results

This section presents the results of the water-sensitivity validation efforts. Included are the results obtained in the ECS and OSU wheel-tracking programs conducted at OSU as well as those obtained in the SWK/UN wheel-tracking program conducted at the University of Nottingham.

ECS Test Program

The mixes tested in the ECS program are summarized in Tables 7.7 through 7.10. As indicated, two tests were conducted on each mix, thus exceeding the minimum requirement of eight repeated tests. Tables 7.7 through 7.10 summarize the ECS test program data for mixes with aggregates RC, RD, RH, and RJ, respectively. These tables include actual data for each mix (including replicate) and the average of the two replicate data sets. For example, two specimens were tested for the RC/AAA-1 mix: A (Specimen 0) and B (Specimen 1). Actual data for both Specimens A and B are shown, and the average of the two is shown in the first block of data.

Test results for the ECS test program are also shown graphically in Figures 7.4 through 7.7. Note that each data point represents the average of two tests and that the line connecting the data points represents the trend in retained resilient modulus (termed ECS-M_R ratio) as a function of conditioning level (each 6-hr block represents a conditioning cycle, with the first three cycles being hot cycles and the last the freeze cycle). That is, the plots show the ratio of conditioned resilient modulus to unconditioned resilient modulus for several conditioning cycles. Thus, the ECS-M_R ratio indicates the amount of water damage sustained by the test specimen, with the dry (and unconditioned) ECS-M_R being the datum.

Figure 7.4 shows the effect of ECS conditioning on all RC mix combinations. After the first cycle, mixes that have good cohesion properties are not affected by ECS conditioning. Mixes susceptible to cohesion loss tend to lose substantial strength after the first cycle. Mixes susceptible to moisture damage through adhesion loss tend to lose strength after the first cycle. Based on observations and water-permeability data, for adhesion loss to occur, additional ECS conditioning (i.e., more cycles) is needed. Figure 7.4 also shows that after one cycle of ECS conditioning, the asphalts form two groups. Three asphalts (AAK-1, AAD-1, and AAC-1) that are at or below 0.9 ECS-M_R ratio[5] are susceptible to moisture

[5]The value of 0.9 was selected only for convenience; no performance indication is implied.

damage and tend to continue losing strength with each cycle. Other asphalts that were not affected by the first cycle tend to maintain the same gradual loss of strength with each cycle. Mix RC/AAF-1 is an exception to these observations, because some mixes tend to be more susceptible to adhesion than cohesion loss; therefore, this mix was not affected by the first cycle as much as the other cycles.

Although the lines of the different asphalts cross, the data emphasize that asphalt type can influence moisture susceptibility. In the fourth (freeze) cycle, all eight mixes lost strength. It was observed in the ECS tests that during the freeze cycle, poor aggregates tend to disintegrate, and this is another moisture damage phenomenon. In aggregate processing and sample preparation, aggregate RC was found to disintegrate easily. Also, aggregate RC tends to absorb moisture. This absorptive character makes it more likely to disintegrate when subjected to a freeze cycle.

Figure 7.5 shows the plot of ECS conditioning's effect on all aggregate RD mixes. RD mix combinations were less susceptible to ECS conditioning. All mixes show a gradual decrease in strength (i.e., good moisture damage resistance). The freeze cycle did not significantly affect the strength of the mixes because RD aggregate is nonabsorptive.

Figure 7.6 is the plot of all RH mixes and shows the wide spread in the data. However, after one cycle, three asphalts had lost more than 10 percent of ECS-M_R ratio (AAF-1, AAK-1, and AAM-1). The other five mixes showed ECS-M_R ratios of 0.9 or better. Each group maintained its set of mixes after each cycle, and both groups of asphalts continue to lose strength very slowly. This emphasizes that the three asphalts mixes that showed ECS-M_R ratios below 0.9 after one cycle exhibited cohesion loss and not much adhesion loss. The five asphalt mixes that had ECS-M_R ratios above 0.9 showed little cohesion or adhesion loss; that is, they were highly resistant to water damage. Throughout the freeze cycle, constant strength was maintained; that is, there was not much moisture damage or aggregate degradation.

Figure 7.7 shows plots for mixes with aggregate RJ, and the same observations that were made for aggregate RC can be made here. Mixes with aggregate RH show significant moisture susceptibility, especially loss in strength after the first cycle. This aggregate has a performance record of being highly susceptible to moisture damage. All mix combinations show a gradual decrease in strength after each conditioning cycle.

OSU Wheel-Tracking Program

As previously mentioned, duplication of tests in the OSU wheel-tracking program exceeded what was required by the experiment design. Table 7.11 lists the mixes tested as well as air-void content and percent saturation data for each mix. The last column in Table 7.11 shows the visual percent stripping for the mixes following testing as cores in the ECS. As indicated, 25 of the 32 mixes were repeated, thus exceeding the minimum requirement of repeating 8 of the tests.

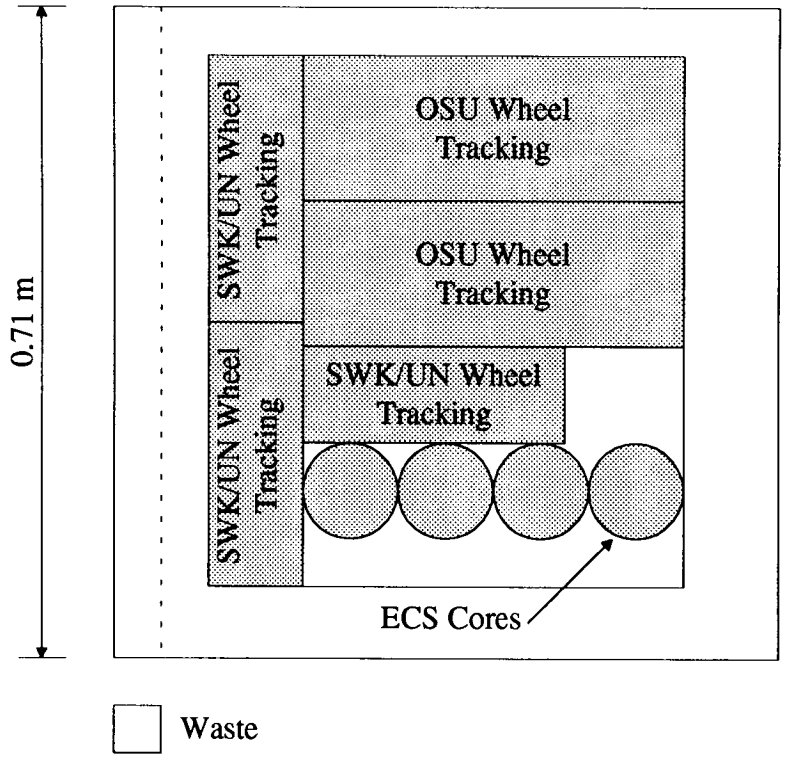

(a) Plan View

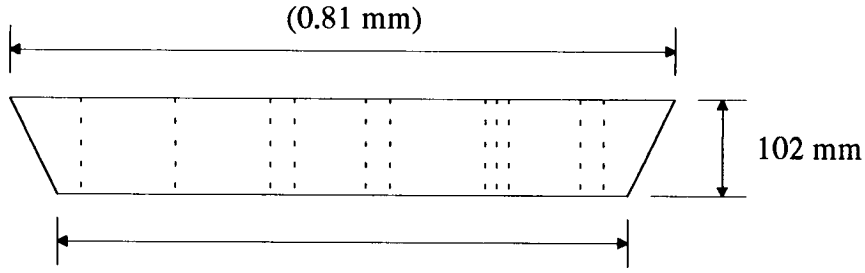

(b) Elevation View

Figure 7.3. Layout of specimens cut from the slab

Table 7.7. Summary of ECS test data for RCS mixes

Asphalt Type	Air Voids (%)	Cycle No.	ECS MR (ksi)	Retained MR Ratio	Water Perm. E-3 cm/s	Retained Perm. Ratio	Stripping Rate
AAA-1	8.7	0	190.0	1.00	4.41	1.00	
	8.7	1	184.0	0.97	3.58	0.81	
	8.7	2	180.0	0.95	2.89	0.66	
	8.7	3	172.5	0.91	2.87	0.65	
	8.7	4	162.5	0.86	2.56	0.58	15.0
AAB-1	9.4	0	252.5	1.00	4.68	1.00	
	9.4	1	245.5	0.97	3.53	0.76	
	9.4	2	228.0	0.90	2.78	0.59	
	9.4	3	226.0	0.90	2.76	0.59	
	9.4	4	206.5	0.82	2.46	0.53	15.0
AAC-1	9.0	0	305.0	1.00	4.96	1.00	
	9.0	1	262.5	0.86	3.69	0.74	
	9.0	2	255.0	0.84	3.20	0.65	
	9.0	3	251.5	0.82	2.71	0.55	
	9.0	4	228.5	0.75	2.28	0.46	20.0
AAD-1	9.0	0	238.0	1.00	1.88	1.00	
	9.0	1	202.0	0.85	2.03	1.08	
	9.0	2	192.5	0.81	1.87	0.99	
	9.0	3	186.0	0.78	1.71	0.91	
	9.0	4	181.0	0.76	1.64	0.87	10.0
AAF-1	8.7	0	485.5	1.00	5.83	1.00	
	8.7	1	168.0	0.96	2.53	0.43	
	8.7	2	423.0	0.87	2.14	0.37	
	8.7	3	385.0	0.79	1.81	0.31	
	8.7	4	374.5	0.77	1.63	0.28	20.0
AAG-1	10.3	0	362.5	1.00	8.97	1.00	
	10.3	1	354.0	0.98	4.99	0.56	
	10.3	2	338.5	0.93	4.12	0.46	
	10.3	3	321.5	0.89	3.47	0.39	
	10.3	4	292.0	0.81	2.27	0.25	20.0
AAK-1	9.3	0	265.0	1.00	7.41	1.00	
	9.3	1	238.0	0.90	4.68	0.63	
	9.3	2	235.8	0.89	4.02	0.54	
	9.3	3	231.0	0.87	3.64	0.49	
	9.3	4	271.8	0.82	3.39	0.46	15.0
AAM-1	10.1	0	255.0	1.00	9.60	1.00	
	10.1	1	245.1	0.96	5.91	0.62	
	10.1	2	236.0	0.93	4.91	0.51	
	10.1	3	235.5	0.92	4.18	0.43	
	10.1	4	226.1	0.89	4.02	0.42	15.0

Table 7.8. Summary of ECS test data for RD mixes

Asphalt Type	Air Voids (%)	Cycle No.	ECS MR (ksi)	Retained MR Ratio	Water Perm. E-3 cm/s	Retained Perm. Ratio	Stripping Rate
AAA-1	8.1	0	187.3	1.00	1.92	1.00	
	8.1	1	183.3	0.98	3.40	1.77	
	8.1	2	179.1	0.96	2.98	1.55	
	8.1	3	176.4	0.94	2.80	1.46	
	8.1	4	174.8	0.93	2.72	1.42	10.0
AAB-1	8.0	0	277.5	1.00	4.81	1.00	
	8.0	1	262.5	0.95	4.69	0.98	
	8.0	2	245.1	0.88	4.13	0.86	
	8.0	3	241.7	0.87	3.96	0.82	
	8.0	4	234.5	0.85	3.56	0.74	5.0
AAC-1	8.6	0	265.0	1.00	9.93	1.00	
	8.6	1	255.0	0.96	7.22	0.73	
	8.6	2	248.5	0.94	6.75	0.68	
	8.6	3	240.2	0.91	6.44	0.65	
	8.6	4	234.8	0.89	6.44	0.65	5.0
AAD-1	9.0	0	206.5	1.00	7.2	1.00	
	9.0	1	201.5	0.98	5.41	0.75	
	9.0	2	182.9	0.89	4.20	0.58	
	9.0	3	174.4	0.84	4.78	0.66	
	9.0	4	174.6	0.85	4.73	0.66	10.0
AAF-1	9.7	0	570.0	1.00	4.38	1.00	
	9.7	1	547.5	0.96	5.80	1.33	
	9.7	2	514.8	0.90	5.52	1.26	
	9.7	3	498.9	0.88	5.21	1.19	
	9.7	4	490.0	0.86	5.04	1.15	10.0
AAG-1	8.2	0	528.0	1.00	1.12	1.00	
	8.2	1	491.7	0.93	2.36	2.10	
	8.2	2	473.5	0.90	2.18	1.94	
	8.2	3	464.9	0.88	2.17	1.93	
	8.2	4	488.1	0.92	2.14	1.91	15.0
AAK-1	8.4	0	290.0	1.00	2.42	1.00	
	8.4	1	274.6	0.95	3.40	1.40	
	8.4	2	271.1	0.93	3.45	1.43	
	8.4	3	270.0	0.93	3.43	1.42	
	8.4	4	276.3	0.95	3.43	1.42	5.0
AAM-1	10.3	0	357.5	1.00	1.45	1.00	
	10.3	1	342.8	0.96	3.06	2.11	
	10.3	2	324.7	0.91	2.55	1.76	
	10.3	3	316.5	0.89	2.79	1.93	
	10.3	4	318.5	0.89	2.81	1.94	5.0

Table 7.9. Summary of ECS test data for RH mixes

Asphalt Type	Air Voids (%)	Cycle No.	ECS MR (ksi)	Retained MR Ratio	Water Perm. E-3 cm/s	Retained Perm. Ratio	Stripping Rate
	8.0	0	126.5	1.00	5.85	1.00	
	8.0	1	119.2	0.94	4.62	0.79	
	8.0	2	113.7	0.90	4.29	0.73	
AAA-1	8.0	3	120.3	0.95	3.46	0.59	
	8.0	4	118.7	0.94	3.78	0.65	7.5
	8.3	0	230.0	1.00	0.06	1.00	
	8.3	1	226.5	0.98	2.50	45.05	
	8.3	2	208.5	0.91	2.09	37.66	
AAB-1	8.3	3	212.5	0.92	2.09	37.66	
	8.3	4	208.5	0.91	1.79	32.25	10.0
	6.9	0	230.5	1.00	0.00		
	6.9	1	252.0	1.09	0.12	1.00	
	6.9	2	269.5	1.17	0.09	0.74	
AAC-1	6.9	3	259.5	1.13	0.07	0.60	
	6.9	4	259.5	1.13	0.06	0.55	10.0
	7.3	0	201.0	1.00	0.00		
	7.3	1	192.0	0.96	1.43	1.00	
	7.3	2	190.0	0.95	1.88	1.32	
AAC-1	7.3	3	185.5	0.92	1.44	1.01	
	7.3	4	184.0	0.92	1.61	1.13	7.5
	7.3	0	564.5	1.00	0.08	1.00	
	7.3	1	471.7	0.84	1.41	17.58	
	7.3	2	431.3	0.76	1.22	15.19	
AAF-1	7.3	3	446.7	0.79	1.16	14.44	
	7.3	4	444.0	0.79	1.14	14.25	10.0
	6.4	0	625.0	1.00	0.05	1.00	
	6.4	1	566.8	0.91	2.33	46.50	
	6.4	2	555.5	0.89	0.13	2.60	
AAG-1	6.4	3	553.4	0.89	0.09	1.80	
	6.4	4	551.4	0.88	0.07	1.30	10.0
	8.0	0	364.5	1.00	1.68	1.00	
	8.0	1	306.5	0.84	2.65	1.57	
	8.0	2	301.0	0.83	2.69	1.60	
AAK-1	8.0	3	287.5	0.79	2.22	1.32	
	8.0	4	284.0	0.78	2.02	1.20	15.0
	7.0	0	415.0	1.00	0.00		
	7.0	1	346.0	0.83	2.29	1.00	
	7.0	2	322.3	0.78	0.14	0.06	
AAM-1	7.0	3	332.5	0.80	1.50	0.65	
	7.0	4	327.2	0.79	1.44	0.63	10.0

Table 7.10. Summary of ECS test data for RJ mixes

Asphalt Type	Air Voids (%)	Cycle No.	ECS MR (ksi)	Retained MR Ratio	Water Perm. E-3 cm/s	Retained Perm. Ratio	Stripping Rate
	8.2	0	145.5	1.00	2.09	1.00	
	8.2	1	135.4	0.93	1.26	0.60	
AAA-1	8.2	2	129.4	0.89	0.94	0.45	
	8.2	3	128.5	0.88	0.34	0.16	
	8.2	4	126.7	0.87	0.08	0.04	7.5
	8.4	0	337.5	1.00	4.54	1.00	
	8.4	1	328.8	0.97	1.66	0.37	
	8.4	2	286.2	0.85	0.54	0.12	
AAB-1	8.4	3	281.7	0.83	0.14	0.03	
	8.4	4	273.1	0.81	0.13	0.03	12.5
	7.2	0	300.0	1.00	4.29	1.00	
	7.2	1	241.5	0.81	3.95	0.92	
	7.2	2	219.5	0.73	3.04	0.71	
AAC-1	7.2	3	212.3	0.71	2.41	0.56	
	7.2	4	209.0	0.70	2.25	0.53	7.5
	7.5	0	185.5	1.00	3.74	1.00	
	7.5	1	157.7	0.85	1.86	0.50	
	7.5	2	148.0	0.80	0.13	0.03	
AAD-1	7.5	3	145.5	0.79	0.11	0.03	
	7.5	4	138.9	0.75	0.08	0.02	10.0
	8.5	0	426.3	1.00	1.87	1.00	
	8.5	1	424.0	0.99	0.88	0.47	
	8.5	2	406.4	0.95	0.71	0.38	
AAF-1	8.5	3	385.2	0.90	0.31	0.17	
	8.5	4	355.0	0.83	0.04	0.02	20.0
	8.8	0	352.5	1.00	5.85	1.00	
	8.8	1	302.6	0.86	2.73	0.47	
	8.8	2	264.9	0.75	2.35	0.40	
AAG-1	8.8	3	236.6	0.67	2.09	0.36	
	8.8	4	240.6	0.68	1.98	0.34	10.0
	8.5	0	265.0	1.00	4.22	1.00	
	8.5	1	218.6	0.82	3.71	0.88	
	8.5	2	214.2	0.81	3.34	0.79	
AAK-1	8.5	3	203.1	0.77	3.19	0.76	
	8.5	4	213.0	0.80	3.37	0.80	5.0
	8.6	0	299.0	1.00	2.43	1.00	
	8.6	1	272.8	0.91	2.14	0.88	
	8.6	2	260.7	0.87	2.01	0.83	
AAM-1	8.6	3	245.9	0.82	1.60	0.66	
	8.6	4	234.1	0.78	0.87	0.36	12.5

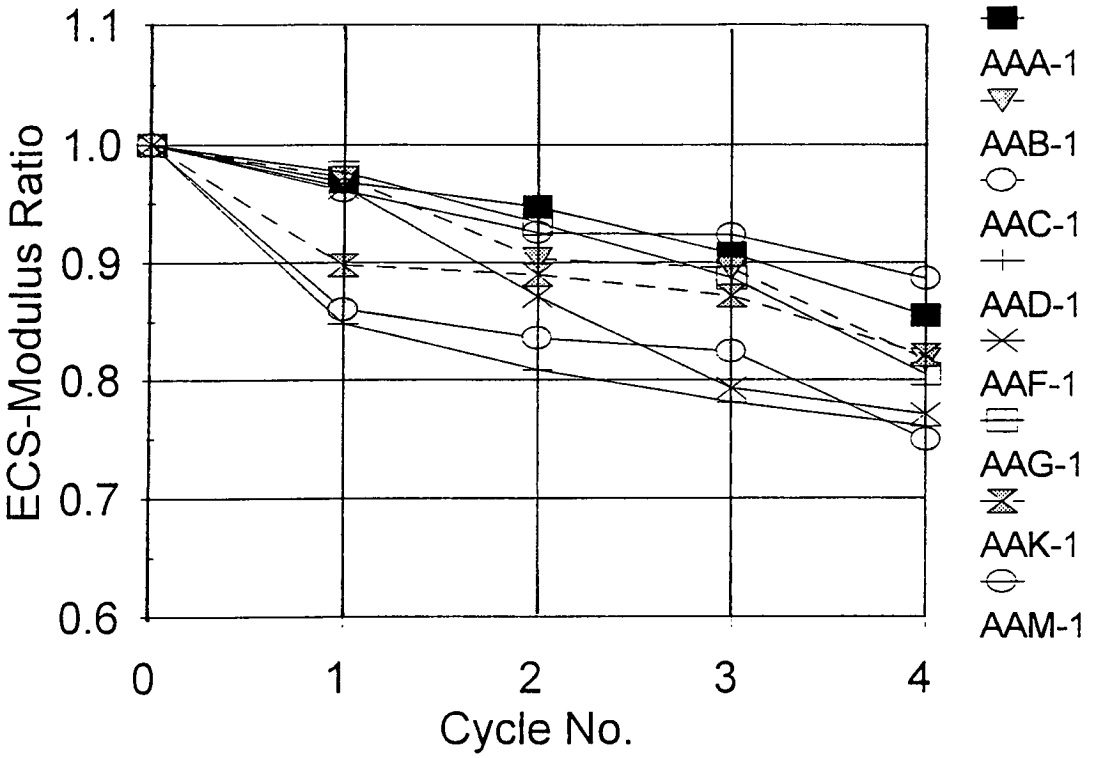

Figure 7.4. ECS test results for mixes with aggregate RC

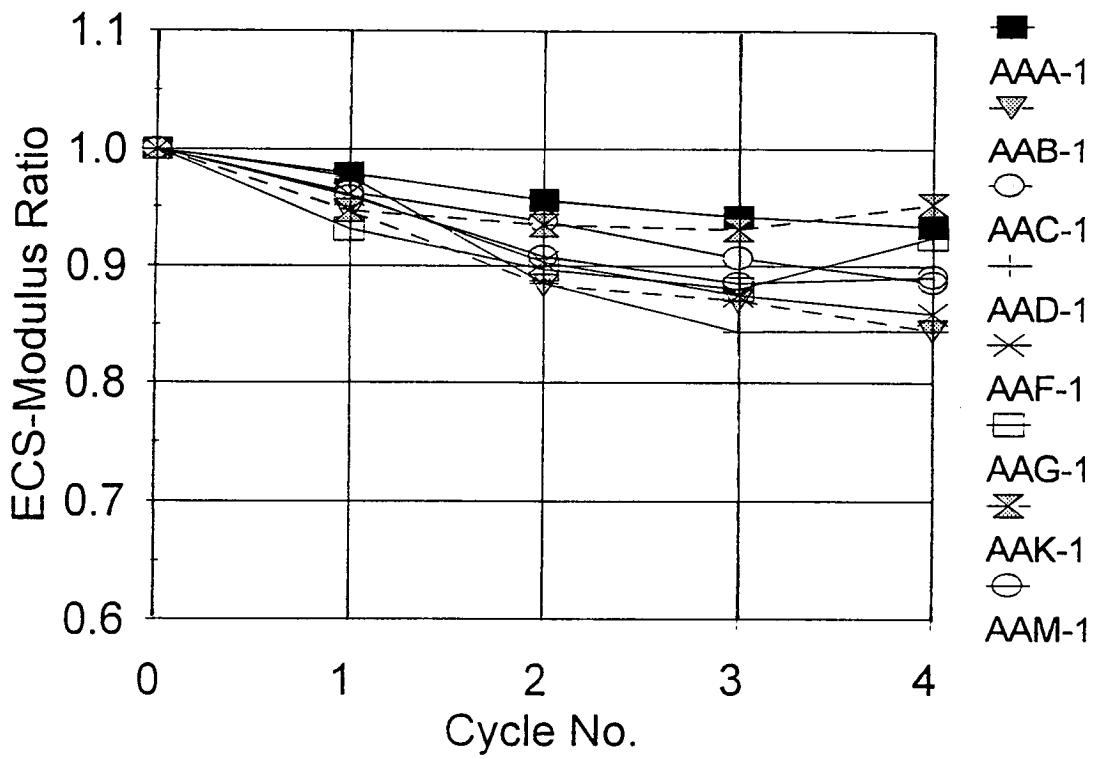

Figure 7.5. ECS test results for mixes with aggregate RD

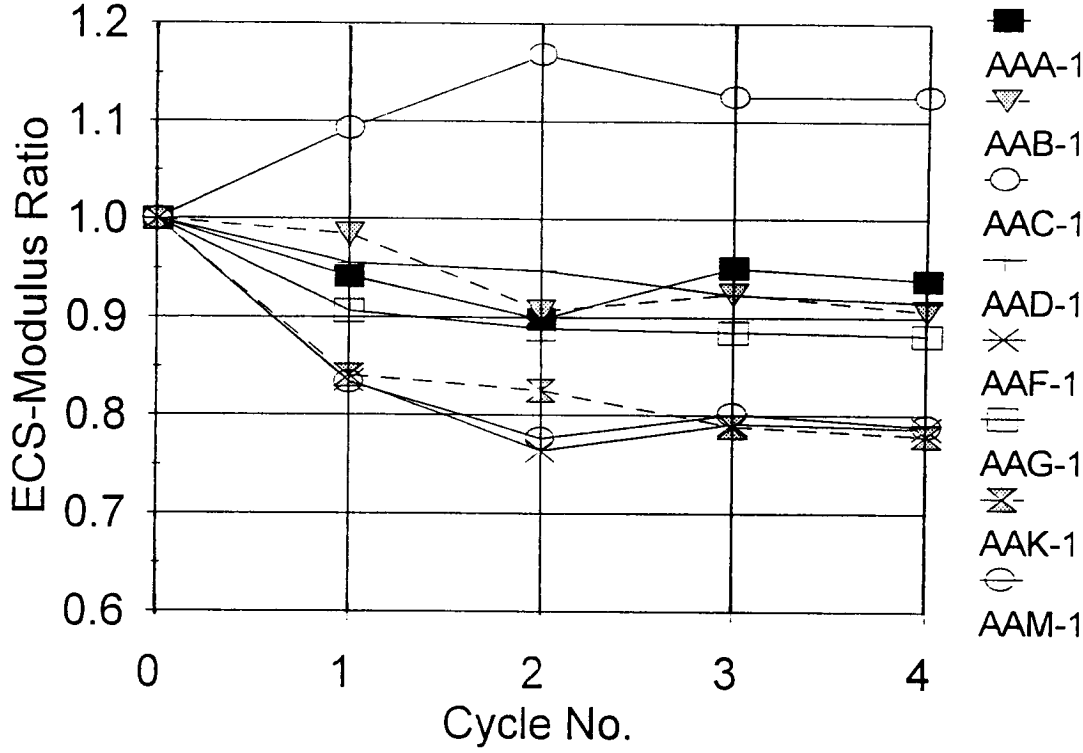

Figure 7.6. ECS test results for mixes with aggregate RH

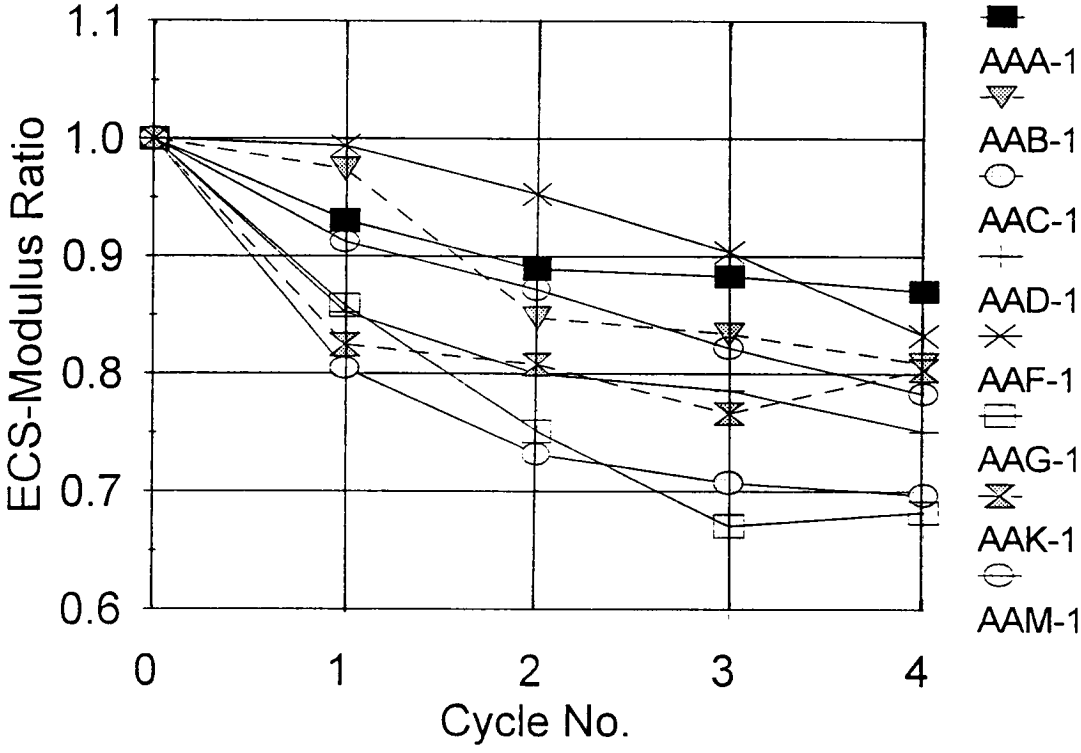

Figure 7.7. ECS test results for mixes with aggregate RJ

The OSU wheel-tracking test results are summarized in Table 7.12. Note that an average value for the rut depth was used where the mix was replicated (i.e., the result tabulated for a replicated mix is the average of the two tests performed on the mix). Graphs of the data are shown in Figures 7.8 through 7.11. These plots indicate that with three of the four aggregates, mixes containing asphalts AAA-1 and AAC-1 performed the worst, and mixes containing asphalts AAK-1 and AAM-1 performed the best in terms of rut resistance.

SWK/UN Wheel-Tracking Program

The test results for the SWK/UN wheel-tracking program are shown in Table 7.13. Note that the SWK/UN contractor has reported a time to failure in hours, where failure is defined as a sudden and significant increase in plastic deformation. A "pass" is reported if the specimen does not experience failure within 7 days of testing (about 500,000 wheel passes). Also included in Table 7.13 are void contents of the "parent" beam and test specimen as well as the percent saturation of the test specimen. The parent beam is the oversized beam fabricated at OSU and sent to SWK/UN, where it was cut to the test specimen dimensions. The 10 columns on the right side of the table show the time in hours to attain 1, 2, 3, 4, 5, 6, 7, 8, 9, and 10 mm of deformation.

Analysis of Results

This section presents an analysis of the results and includes a description of the statistical analyses for the ECS, OSU wheel-tracking, and SWK/UN wheel-tracking test programs as well as the performance rankings of the materials as determined by each program. Also presented is a comparison of the performance rankings for each program with those proposed by the A-002A and A-003B contractors, including a discussion of the results and comparisons.

Statistical Analysis

Each program included testing of 32 asphalt-aggregate mixes according to the experiment design presented earlier. The set of 40 tests (32 mixes plus 8 repeated tests) was designed primarily to identify the water sensitivity of the mixes using either rutting (OSU and SWK/UN wheel tracking) or reduction in modulus (ECS) as the objective function. The test program provides information to rank the relative performance of the eight asphalts and four aggregates, thus enabling a comparison of results provided by the A-002A, A-003A, and A-003B contractors.

Table 7.11. Mixes tested in the OSU wheel-tracking program

Mix Number	Aggregate Type	Asphalt Type	Mix Code*	Sample ID	Percent Voids	Percent Saturation	Percent Stripping
1	RC	AAA-1	00000	RR0	7.1	33	25
1		AAA-1	00000	RR1	7.8	55	40
2		AAB-1	10000	RR0	6.9	63	5.0
2		AAB-1	10000	RR1	6.9	73	25
3		AAC-1	01000	RR0	7.7	64	---
3		AAC-1	01000	RR1	7.8	59	30
4		AAD-1	11000	RR0	8.0	65	0.0
4		ADD-1	11000	RR1	7.4	60	30
5		AAF-1	00100	RR0	7.6	92	5.0
5		AAF-1	00100	RR1	7.7	66	17.5
6		AAG-1	10100	RR6	7.9	72	0.0
7		AAK-1	01100	RR0	7.8	79	5.0
7		AAK-1	01100	RR1	8.9	61	5.0
8		AAM-1	11100	RR0	7.7	73	0.0
8		AAM-1	11100	RR1	8.0	47	5.0
9	RD	AAA-1	00010	RR2	8.2	52	---
9		AAA-1	00010	RR3	8.0	60	5.0
10		AAB-1	10010	RR2	8.7	45	15
10		AAB-1	10010	RR3	8.4	52	17.5
11		AAC-1	01010	RR2	8.9	40	5.0
12		AAD-1	11010	RR0	8.4	57	---
12		AAD-1	11010	RR1	8.6	56	---
13		AAF-1	00110	RR0	9.0	56	---
13		AAF-1	00110	RR1	8.6	49	10
14		AAG-1	10110	RR2	8.7	61	5.0
14		AAG-1	10110	RR3	8.6	61	0.0
15		AAK-1	01110	RR2	8.1	51	---
15		AAK-1	01110	RR3	9.0	63	5.0
16		AAM-1	11110	RR1	8.6	44	---

Table 7.11 (continued). Mixes tested in OSU wheel-tracking program

Mix Number	Aggregate Type	Asphalt Type	Mix Code*	Sample ID	Percent Voids	Percent Saturation	Percent Stripping
17	RH	AAA-1	00001	RR4	8.2	54	0.0
17		AAA-1	00001	RR5	7.5	63	12.5
18		AAB-1	10001	RR3	8.8	42	10
19		AAC-1	01001	RR1	6.9	44	7.5
19		AAC-1	01001	RR3	6.9	32	5.0
20		AAD-1	11001	RR0	7.6	46	15
20		AAD-1	11001	RR1	7.8	56	5.0
21		AAF-1	00101	RR0	8.7	40	30
21		AAF-1	00101	RR1	8.5	57	0.0
22		AAG-1	10101	RR4	8.7	65	45
22		AAG-1	10101	RR5	8.7	61	35
23		AAK-1	01101	RR0	8.7	43	7.5
23		AAK-1	01101	RR1	8.8	46	7.5
24		AAM-1	11101	RR0	7.7	71	5.0
24		AAM-1	11101	RR1	7.7	38	2.5
25	RJ	AAA-1	00011	RR2	8.4	53	---
25		AAA-1	00011	RR3	8.4	55	---
26		AAB-1	10011	RR2	7.7	80	5.0
26		AAB-1	10011	RR3	7.7	55	---
27		AAC-1	01011	RR7	9.0	63	25
28		AAD-1	11011	RR0	7.2	57	7.5
28		AAD-1	11011	RR1	7.4	66	---
29		AAF-1	00111	RR0	8.1	57	---
29		AAF-1	00111	RR1	8.0	41	---
30		AAG-1	10111	RR4	8.4	53	70
31		AAK-1	01111	RR0	7.2	47	---
31		AAK-1	01111	RR1	7.1	50	---
32		AAM-1	11111	RR3	9.2	54	---

*The mix code is an accounting system established to distinguish among the 32 asphalt-aggregate combinations (see Table 7.4).

Table 7.12. Rut depths for the OSU wheel-tracking program

Wheel Passes	Rut Depth (mm)							
	AAA-1	AAB-1	AAC-1	AAD-1	AAF-1	AAG-1	AAK-1	AAM-1
Aggregate RC								
0	0.00	0.00	0.00	0.00	0.00	0.00	0.00	0.00
200	2.38	1.54	2.14	2.19	2.22	1.98	1.30	2.08
500	4.29	2.51	3.65	3.42	3.19	3.00	2.17	3.15
1,000	6.10	3.89	4.99	4.99	4.52	4.09	2.72	4.47
2,000	8.06	5.21	6.88	5.59	6.32	5.06	4.48	5.65
5,000	12.16	7.69	12.29	6.98	8.28	6.65	6.05	7.55
10,000	24.00*	10.83	36.00*	9.87	10.72	9.82	10.17	9.53
Aggregate RD								
0	0.00	0.00	0.00	0.00	0.00	0.00	0.00	0.00
200	1.03	0.74	1.22	0.77	0.47	0.62	0.39	1.04
500	1.72	1.66	2.47	1.66	1.42	1.52	0.92	1.58
1,000	2.22	2.67	3.12	2.54	2.13	2.43	1.32	2.17
2,000	3.68	3.77	4.35	4.07	3.33	3.99	2.12	3.32
5,000	5.23	5.68	5.91	5.97	4.96	7.08	3.70	4.56
10,000	6.16	6.84	7.16	7.18	6.31	9.47	4.90	5.19
Aggregate RH								
0	0.00	0.00	0.00	0.00	0.00	0.00	0.00	0.00
200	1.05	0.63	1.19	0.78	0.80	1.22	0.47	0.95
500	1.86	1.31	1.72	1.42	1.62	2.26	0.93	1.33
1,000	2.88	1.90	2.63	2.26	1.62	3.06	1.05	1.72
2,000	4.69	3.41	3.71	3.66	3.2	4.22	2.20	2.62
5,000	6.98	5.87	6.40	5.75	5.58	6.09	3.99	4.41
10,000	8.82	7.88	8.68	7.51	7.96	7.70	6.07	6.27
Aggregate RJ								
0	0.00	0.00	0.00	0.00	0.00	0.00	0.00	0.00
200	0.65	0.49	0.75	0.65	0.60	1.11	0.46	0.59
500	1.58	1.04	2.18	1.25	1.40	2.43	1.16	0.95
1,000	2.52	1.99	3.16	1.71	1.77	3.14	1.59	1.28
2,000	4.42	3.00	4.43	2.49	2.59	4.36	2.48	1.96
5,000	6.62	3.94	6.91	3.74	4.25	5.81	3.39	2.59
10,000	8.30	4.92	8.79	5.53	6.23	8.65	4.32	2.65

*Estimated rut depth.

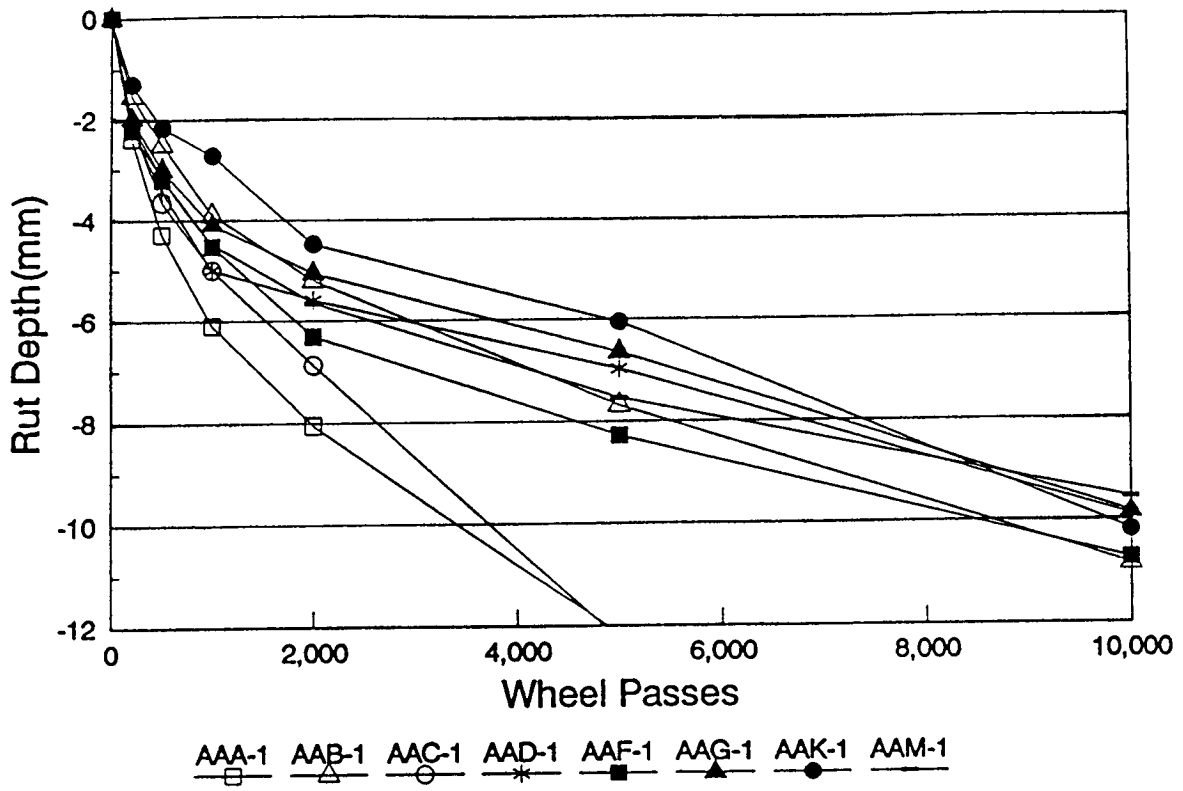

Figure 7.8. OSU wheel-tracking test results for mixes with aggregate RC

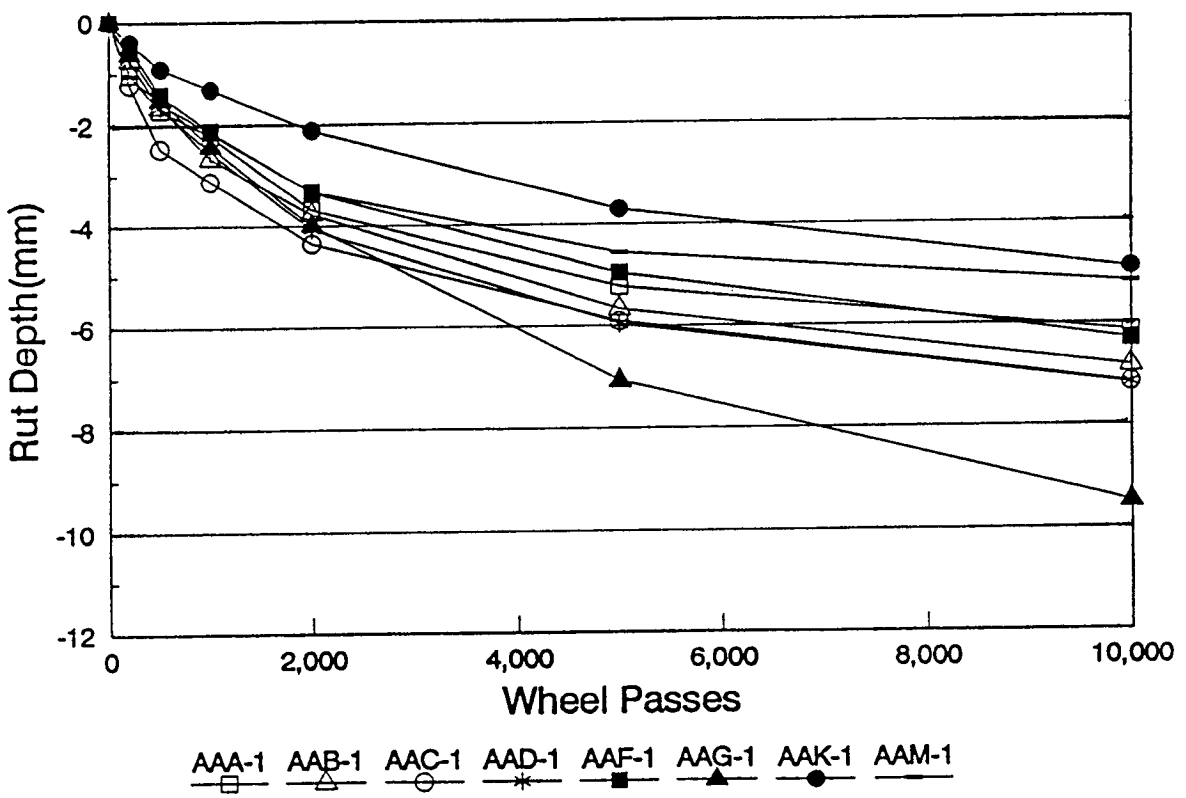

Figure 7.9. OSU wheel-tracking test results for mixes with aggregate RD

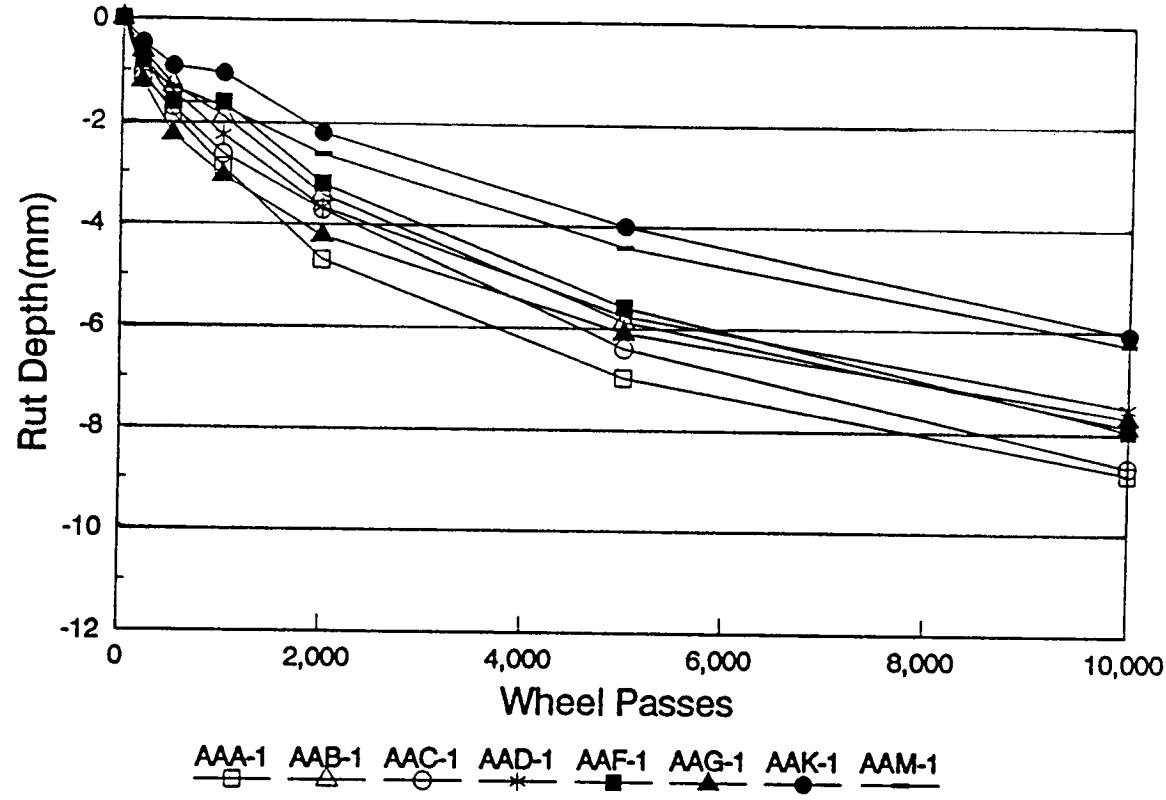

Figure 7.10. OSU wheel-tracking test results for mixes with aggregate RH

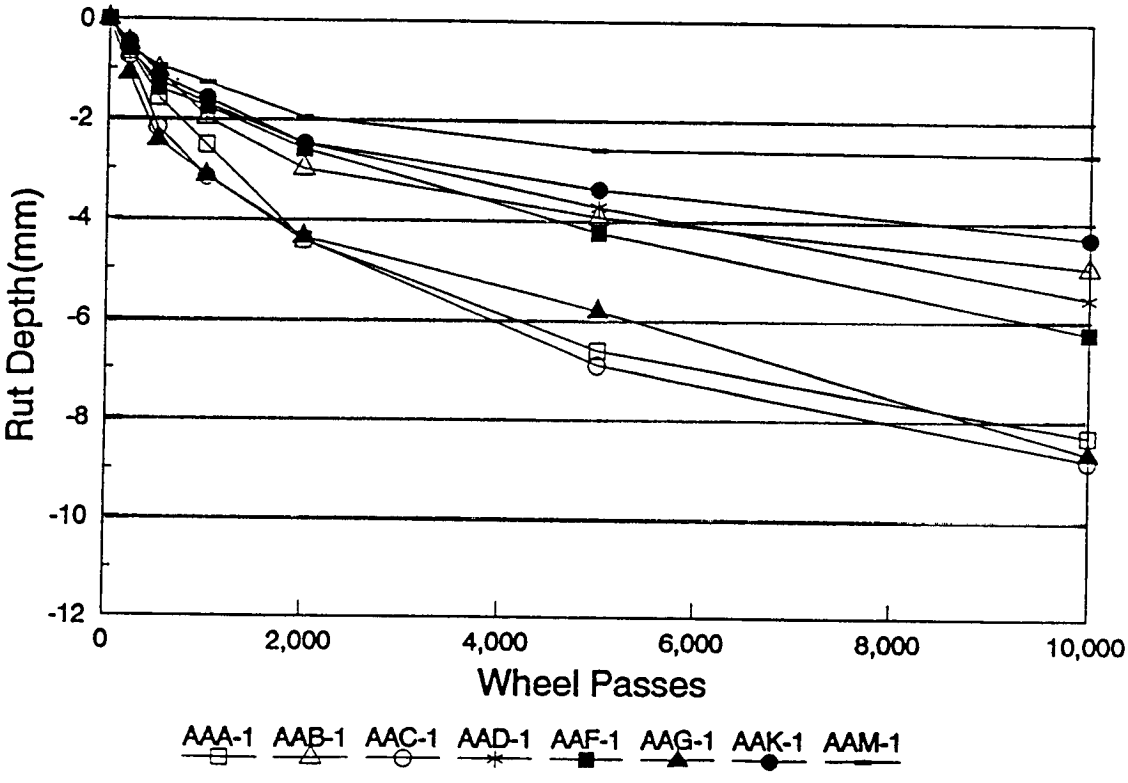

Figure 7.11. OSU wheel-tracking test results for mixes with aggregate RJ

Table 7.13. SWK/UN wheel-tracking test results

Mix No.	Aggregate type	Asphalt Type	Mix Code[a]	Sample ID	Void Content of Beam[b] (%)	Void Content of Specimen[c] (%)	Percent Saturation of Test Specimen	Time to Failure[d] (hr)	Time (hr) to Deformation (mm)									
									1	2	3	4	5	6	7	8	9	10
1	RC	AAA-1	00000	RW1	7.0	8.4	64.8	pass	0.5	64.0	--	--	--	--	--	--	--	--
1		AAA-1	00000	RW0	8.6	11.5	84.7	5	0.5	0.5	1.0	2.0	3.0	4.5	5.5	7.0	8.0	8.5
2		AAB-1	10000	RW1	8.9	12.4	72.9	58	0.5	26.0	56.0	62.0	78.0	87.0	91.0	--	--	--
3		AAC-1	01000	RW0	8.0	11.7	69.0	24	0.5	1.0	3.0	5.5	10.5	16.5	24.0	24.5	25.0	25.5
4		AAD-1	11000	RW0	8.8	11.4	95.8	pass	0.5	10.0	--	--	--	--	--	--	--	--
5		AAF-1	00100	RW1	9.0	10.9	90.0	165	0.5	3.0	26.0	54.0	70.0	98.0	163.0	164.0	165.0	165.0
6		AAG-1	10100	RW5	9.2	12.8	70.0	10	3.0	8.5	10.0	10.0	10.0	10.0	10.0	10.5	10.5	11.0
7		AAK-1	01100	RW2	8.8	9.2	56.4	pass	6.0	--	--	--	--	--	--	--	--	--
7		AAK-1	01100	RW3	8.3	9.4	66.0	pass	2.0	--	--	--	--	--	--	--	--	--
8		AAM-1	11100	RW0	8.9	12.1	75.4	pass	0.5	13.0	--	--	--	--	--	--	--	--
9	RD	AAA-1	00010	RW1	9.0	8.5	51.9	pass	20.0	--	--	--	--	--	--	--	--	--
9		AAA-1	00010	RW0	6.3	4.3	30.5	pass	30.0	--	--	--	--	--	--	--	--	--
10		AAB-1	10010	FW3	9.1	8.9	67.9	pass	1.0	--	--	--	--	--	--	--	--	--
11		AAC-1	01010	RW1	7.0	11.1	65.4	6	0.5	1.5	1.5	5.5	6.0	6.0	6.5	6.5	7.0	7.5
12		AAD-1	11010	RW0	8.7	8.0	51.4	pass	--	--	--	--	--	--	--	--	--	--
12		AAD-1	11010	RW1	8.7	7.6	54.4	pass	0.5	30	3.0	--	--	--	--	--	--	--
13		AAF-1	00110	RW1	8.9	8.2	42.4	pass	--	--	--	--	--	--	--	--	--	--
14		AAG-1	10110	RW1	7.0	6.0	73.3	pass	13.0	--	--	--	--	--	--	--	--	--
14		AAG-1	10110	RW0	7.0	5.8	42.9	pass	0.5	6.0	6.0	--	--	--	--	--	--	--
15		AAK-1	01110	RW3	8.9	8.4	55.5	pass	--	--	--	--	--	--	--	--	--	--
15		AAK-1	01110	RW1	6.4	7.6	35.7	pass	20.0	--	--	--	--	--	--	--	--	--
16		AAM-1	11110	RW0	9.0	10.2	49.4	pass	0.5	6.0	6.0	--	--	--	--	--	--	--
17	RH	AAA-1	00001	RW5	8.0	9.0	77.3	pass	0.5		--	--	--	--	--	--	--	--
18		AAB-1	10001	RW5	10.4	12.1	64.2	pass	4.0		--	--	--	--	--	--	--	--
19		AAC-1	01001	RW0	7.5	9.2	24.3	54	2.0		49.5	50.0	51.0	54.0	54.0	55.0	55.5	56.5
20		AAD-1	11011	RW0	7.9	10.8	55.6	56	0.5		55.0	56.0	56.5	57.0	57.0	57.5	57.5	58.0
20		AAD-1	11001	RW3	9.9	12.4	81.1	14	0.5		12.5	13.5	13.5	15.5	15.5	15.5	16.0	16.5
21		AAF-1	00101	RW1	8.1	9.8	39.1	13	0.5		13.0	14.0	14.0	14.0	14.0	14.5	14.5	15.0
22		AAG-1	10101	RW5	7.9	10.6	44.4	90	3.0		81.0	86.0	86.5	93.0	93.0	94.0	95.0	95.9
22		AAG-1	10101	RW4	9.5	12.3	74.3	26	7.0		24.0	25.5	26.0	26.0	26.0	26.0	26.5	27.0
23		AAK-1	01101	RW0	8.4	9.3	92.0	pass	5.0		--	--	--	--	--	--	--	--
24		AAM-1	11101	RW0	7.0	8.1	76.2	pass	0.5		--	--	--	--	--	--	--	--

Table 7.13 (continued). SWK/UN wheel-tracking test results

Mix No.	Aggregate type	Asphalt Type	Mix Code[a]	Sample ID	Void Content of Beam[b] (%)	Void Content of Specimen[c] (%)	Percent Saturation of Test Specimen	Time to Failure[d] (hr)	Time (hr) to Deformation (mm)									
									1	2	3	4	5	6	7	8	9	10
25	RJ	AAA-1	00011	RW0	9.0	10.6	58.4	10	4.0	7.0	9.0	10.0	10.5	11.0	11.0	11.0	11.0	11.5
25		AAA-1	00011	RW1	7.9	8.3	50.3	20	0.5	4.0	16.0	19.0	20.0	21.0	21.5	21.5	22.0	22.0
26		AAB-1	10011	RW0	11.7	14.0	82.5	3.0	0.5	2.0	3.0	3.0	3.5	3.5	3.5	3.5	4.0	4.0
27		AAC-1	01011	RW0	12.8	9.2	74.3	9.5	0.5	2.0	3.0	4.0	5.5	8.5	8.8	9.0	9.0	9.5
28		AAD-1	11011	RW0	7.1	8.4	41.9	17	3.0	7.5	9.0	9.5	10.5	13.0	13.0	15.0	17.0	17.0
29		AAF-1	00111	RW0	8.0	8.2	38.4	2.0	1.5	2.0	2.5	3.5	5.0	6.0	6.0	6.0	6.5	6.5
30		AAG-1	10111	RW0	9.9	9.7	75.0	6.0	1.5	5.0	6.5	7.0	7.5	9.0	9.5	9.5	9.5	9.5
31		AAK-1	01111	RW3	9.5	11.6	84.4	45	1.0	28.0	36.5	38.5	41.5	44.5	46.0	46.0	47.0	47.5
31		AAK-1	01111	RW1	99	11.2	83.0	15	0.5	1.0	4.0	6.0	10.5	15.0	15.0	15.0	15.5	16.0
32		AAM-1	11111	RW0	11.0	11.7	63.6	67	0.5	6.0	57.0	64.5	65.4	67.0	67.0	67.0	67.0	67.0

[a]The mix code is an accounting system established to distinguish among the 32 asphalt-aggreage combintaions (see Table 7.11).
[b]Void content of the beam fabricated at OSU and sawed by SWK/UN.
[c]Void content of the test specimen sawed by sWK/un from the beam fabricated at OSU.
[d]Determined by a sudden and significant increase in plastic deformation. A pass is recorded if the specimen does not fail within 7 days (about 500,000 wheel passes).

ECS Test Results

The analysis of the ECS test results employed a generalized linear model (GLM) procedure to investigate the significance of the effects of all the variables and their interactions on ECS-M_R ratio (the dependent variable). The GLM procedure is one of several statistical methods used in the SAS program and makes use of the method of least squares to fit GLMs. One of the statistical methods available in the GLM is an analysis of variance for unbalanced data like those used in the ECS analysis.

Analyses were performed on the results obtained after each conditioning cycle (i.e., after 1, 2, 3, and 4 cycles of conditioning). The analyses used an iterative approach. First, a model was used in which ECS-M_R ratio was related to all the variables—asphalt type, aggregate type, air-void content, water permeability, air permeability, initial water permeability, initial modulus, and asphalt-aggregate interactions (Table 7.14). Applying a Type III hypothesis, the least significant variables were removed from the model one at a time. Table 7.15 shows the results of each iteration; an X for a variable means that the variable was not significant at this level and was eliminated from the model in the next iteration. The final model that best represents the effect of asphalt type, aggregate type, initial modulus, and asphalt-aggregate interactions is shown Table 7.16.

This analysis does not mean that all variables eliminated do not contribute to the results of the ECS. Another observation that can be made is that initial air permeability is significant after three cycles. This means that initial air permeability influences the outcome of ECS test results. The most important observation from this analysis is that the asphalt-aggregate interaction is highly significant (i.e., the susceptibility of one aggregate depends on the type of asphalt, and vice versa).

OSU Wheel-Tracking Test Results

The analysis of the OSU wheel-tracking test results also employed a GLM procedure to investigate the significance of the effects of asphalt type, aggregate type, air-void content, percent stripping, and asphalt-aggregate interaction on the rut depth developed after 5000 wheel passes in the OSU wheel tracker. The results of the analysis are provided in Table 7.17. Initial analysis has shown that aggregate-asphalt interaction has no effect on rut depth developed at 5000 wheel passes. The analysis does show a very high correlation between rut depth at 5000 wheel passes and stripping rate, asphalt type, aggregate type, and air-void content at a 95 percent confidence level.

SWK/UN Wheel-Tracking Test Results

The statistical analysis of the SWK/UN wheel-tracking tests used a Bayesian "survival analysis" with time (to failure) distributed as a Weibull random variable. The Weibull model employed a shape factor (C) of 2 (i.e., skewed to the right), a minimum value (A) of 0

(which seemed appropriate, since the smallest observed time to failure was 2 hr and A must be less than the smallest observation), and a scale parameter (B) as follows:

$$B = e^{-\left(\frac{AV-8}{B_{AV(i)}}\right)} B_{ASPH(j)(k)};\ AV > 8$$

$$B = B_{ASPH(j)} B_{AGGR(k)};\ AV \leq 8$$

where:

AV = air-void content of the test specimen, percent
$B_{AV}(i)$ = weighting for air-void content, with values of 6, 7, 8, 9, or 10
$B_{ASPH}(j)$ = weighting for asphalt type, with values of 2, 6, 10, 14, or 18
$B_{AGGR}(k)$ = weighting for aggregate type, with values of 2, 6, 10, 14, or 18

As shown, the scale parameter is a multiplicative function of asphalt type, aggregate type, and air-void content, with the contribution from air-void content decreasing exponentially for values greater than 8 percent and having no contribution (i.e., equal to unity) for air-void contents less than or equal to 8 percent. It is through the shape parameter (B) that these factors have their effect on the distribution of time to failure.

The SWK/UN wheel tracking data were tested to determine the probability (Pr) of the time to failure (T) being less than or equal to some reasonable time value (in this case 7 days of testing). The test is mathematically represented as follows:

$$Pr\ (T \leq t^*) = 1 - e^{-\left(\frac{t^*-A}{B}\right)C}$$

where:

A = minimum allowed time value (0 in this case)
B = scale parameter as previously defined
C = shape factor (2 in this case)
t* = predetermined cutoff time value (7 days in this case)

The above analysis method allows the ranking of asphalt types and aggregate types while giving some importance to the air-void content of the test specimen, provided it is greater than 8 percent (i.e., air-void contents greater than 8 percent were considered detrimental to the probability of the specimen surviving beyond 7 days, with exponentially increasing detriment the farther away the specimen was from 8 percent air-void content).

Table 7.14. Variables considered in the analyses of the ECS test results

Variable	Type	Levels
Aggregate type (AGGR)	Class	RC, RD, RM, RJ
Asphalt type (ASPH)	Class	AAA-1, AAB-1, AAC-1, AAD-1, AAF-1, AAG-1, AAK-1, AAM-1
Time (cycle number)	Class	6, 12, 18, 24 hr (1, 2, 3, 4 cycles)
Air-void content (AVOID)	Covariant	8±1.5 percent
Water permeability (WK)	Covariant	0.0 ≈ 12.0 E-3 cm/s
Water permeability ratio (WKR)	Covariant	0.03 ≈ 15.0
Initial air permeability (AK)	Covariant	0.0 ≈ 20.0 E-5 cm/s
Initial water permeability (WK0)	Covariant	0.0 ≈ 12.0 E-3 cm/s
Initial modulus	Covariant	100 ≈ 700 lb/m^2
ECS-M_R ratio	Independent	0.6 ≈ 1.1

Table 7.15. An overview of the ECS statistical analyses

Interation 1					
Variable	Cycle No.				
	1	2	3	4	
Aggregate	Y	Y	X	Y	
Asphalt	X	Y	Y	Y	
Air Voids	X	X	X	X	↵
Water Perm.	X	X	X	X	
Water Perm. Ratio	X	X	X	X	
Air Perm	X	X	Y	X	
Initial Water Perm.	X	Y	X	X	
Initial Modulus	Y	Y	Y	Y	
Aggregate*Asphalt	Y	Y	Y	Y	

Iteration 3					
Variable	Cycle No.				
	1	2	3	4	
Aggregate	Y	Y	X	Y	
Asphalt	Y	Y	Y	Y	
Water Perm.	X	X	X	X	↵
Air Perm.	X	X	Y	X	
Initial Water Perm.	X	Y	X	X	
Initial Modulus	Y	Y	Y	Y	
Aggregate*Asphalt	Y	Y	Y	Y	

Iteration 5					
Variable	Cycle No.				
	1	2	3	4	
Aggregate	Y	Y	Y	Y	
Asphalt	Y	Y	Y	Y	
Initial Water Perm.	X	Y	X	X	↵
Initial Modulus	Y	Y	Y	Y	
Aggregate*Asphalt	Y	Y	Y	Y	

Iteration 2					
Variable	Cycle No.				
	1	2	3	4	
Aggregate	Y	Y	X	X	
Asphalt	Y	Y	Y	Y	
Water Perm.	Y	X	X	X	
Water Perm. Ratio	X	X	X	X	↵
Air Perm.	X	X	Y	Y	
Initial Water Perm.	X	Y	X	X	
Initial Modulus	Y	Y	Y	Y	
Aggregate*Asphalt	Y	Y	Y	Y	

Iteration 4					
Variable	Cycle No.				
	1	2	3	4	
Aggregate	Y	Y	Y	Y	
Asphalt	Y	Y	Y	Y	
Air Perm.	X	X	Y	X	↵
Initial Water Perm.	Y	Y	X	X	
Initial Modulus	Y	Y	Y	Y	
Aggregate*Asphalt	Y	Y	Y	Y	

Iteration 6					
Variable	Cycle No.				
	1	2	3	4	
Aggregate	Y	Y	Y	Y	
Asphalt	Y	Y	Y	Y	
Initial Modulus	Y	Y	Y	Y	
Aggregate*Asphalt	Y	Y	Y	Y	

Note: X means the variable was not significant at 0.05 level. Y means the variable was significant at 0.05 level. ↵ means eliminate this variable.

Table 7.16. GLM analysis of the ECS results for asphalt and aggregate type

Class Variables	Levels	Values
AGGR	4	RC, RD, RH, RJ
ASPH	8	AAA-1, AAB-1, AAC-1, AAD-1, AAF-1, AAG-1 AAK-1, AAM-1

Time = 6
Model: R^2 = 0.79, CV = 4.88, ECS-M_R ratio mean = 0.93

Source of Error	Degrees of Freedom	Type III Sum of Squares	F Values	Probability of $F > F_{critical}$
AGGR	3	0.03275601	5.35	0.0037
ASPH	7	0.04715846	3.30	0.0079
MR0	1	0.00894455	4.38	0.0433
AGGR*ASPH	21	0.14340240	3.34	0.0007

Time = 12
Model: R^2 = 0.85, CV = 5.22, ECS-M_R ratio mean = 0.88

Source of Error	Degrees of Freedom	Type III Sum of Squares	F Values	Probability of $F > F_{critical}$
AGGR	3	0.07121460	11.13	0.0001
ASPH	7	0.04083428	2.73	0.0216
MR0	1	0.02653206	12.44	0.0011
AGGR*ASPH	21	0.25769088	5.75	0.0001

Time = 18
Model: R^2 = 0.81, CV = 6.21, ECS M_R ratio mean = 0.86

Source of Error	Degrees of Freedom	Type III Sum of Squares	F Values	Probability of $F > F_{critical}$
AGGR	3	0.10603905	12.28	0.0001
ASPH	7	0.04310104	2.14	0.0634
MR0	1	0.00825944	2.87	0.0987
AGGR*ASPH	21	0.23901440	3.95	0.0001

Time = 24
Model: R^2 = 0.89, CV = 4.65, ECS-M_R ratio mean = 0.84

Source of Error	Degrees of Freedom	Type III Sum of Squares	F Values	Probability of $F > F_{critical}$
AGGR	3	0.15659618	33.88	0.0001
ASPH	7	0.02909552	2.70	0.0231
MR0	1	0.00953970	6.19	0.0175
AGGR*ASPH	21	0.23805089	7.36	0.0001

Table 7.17. GLM analysis of the OSU wheel tracking test results

Class	Levels	Values
AGGR	4	RC, RD, RH, RJ
ASPH	8	AAA-1, AAB-1, AAC-1, AAD-1, AAF-1, AAG-1 AAK-1, AAM-1

Source of Error	Degrees of Freedom	Type III Sum of Squares	F Values	Probability of $F > F_{critical}$
AGGR	3	142.94961295	29.86	0.0001
ASPH	7	70.99560815	6.36	0.0001
AV2[a]	1	8.79590144	5.51	0.0234
STRIPPING[b]	1	10.82167482	6.78	0.0125

[a]AV2 is air-void content of LCPC cores taken from the rutted beam after OSU wheel tracking.
[b]STRIPPING is degree of stripping by visual evaluation of broken specimen after the OSU wheel-tracking test.

Table 7.18. Bayesian survival analysis of the SWK/UN test results

Mix Component	Probability of Attaining a Score of					Expected Score*
	2	6	10	14	18	
Asphalts						
AAA-1	0.0000	0.0225	0.6351	0.2743	0.0681	11.55
AAB-1	0.0000	0.0047	0.3004	0.4293	0.2655	13.82
AAC-1	0.0188	0.9135	0.0606	0.0061	0.0010	6.23
AAD-1	0.0000	0.0000	0.1382	0.4934	0.3683	14.92
AAF-1	0.0000	0.0914	0.5258	0.2806	0.1022	11.57
AAG-1	0.0000	0.7532	0.2252	0.0197	0.0020	7.08
AAK-1	0.0000	0.0000	0.0006	0.1961	0.8032	17.21
AAM-1	0.0000	0.0000	0.0005	0.0143	0.9852	17.94
Aggregates						
RC	0.0000	0.0000	0.0948	0.5035	0.4017	15.23
RD	0.0000	0.0000	0.0526	0.6212	0.3262	15.09
RH	0.0000	0.0006	0.4745	0.3930	0.1318	12.62
RJ	0.9862	0.0138	0.0000	0.0000	0.0000	2.06

*Expected score = $\Sigma(\text{Probability})_i(\text{Score})_i$; i = 2, 6, 10, 14, 18.

Table 7.19. Performance ranking of aggregates based on ECS test

Aggregate	Modulus Ratio LSMEAN	Aggregate	Modulus Ratio LSMEAN
	First hot cycle		Second hot cycle
RD	0.952	RD	0.911
RC	0.931	RH	0.897
RH	0.921	RC	0.889
RJ	0.899	RJ	0.840
	Third hot cycle		Freeze cycle
RH	0.897	RD	0.897
RD	0.892	RH	0.889
RC	0.860	RC	0.811
RJ	0.801	RJ	0.783

The results of the analysis are shown in Table 7.18. The table lists for each asphalt and aggregate the probabilities of attaining scores of 2, 6, 10, 14, and 18 (a range of scores that embraces the whole of the data set) and the expected score for the mix components. The expected score is computed by multiplying the probabilities by their respective scores and then summing the values. Higher expected scores indicate a greater probability of obtaining a pass (i.e., not failing after 7 days of testing) in the SWK/UN wheel tracker.

Thus, as indicated, asphalts AAM-1 and AAK-1 and aggregates RC and RD performed the best, while asphalts AAC-1 and AAG-1 and aggregate RJ performed the worst.

Performance Ranking

In addition to investigating which independent variables influence the dependent variable for each test program, the test results were analyzed with the objective of ranking the materials (asphalts and aggregates) in terms of rutting resistance (OSU wheel tracking and SWK/UN wheel tracking) and resistance to reduction in modulus (ECS) of moisture-damaged mixes. This section presents the performance rankings of the materials obtained from the analyses of the ECS, OSU wheel-tracking, and SWK/UN wheel-tracking test results.

Aggregates

The analysis of the ECS test program results shows the interaction of asphalt type and aggregate type to be significant. Thus, ranking the results by aggregate type is inappropriate; however, aggregate ranking is presented in Table 7.19 and should be interpreted with caution.

The analysis of the OSU wheel-tracking program results shows the interaction of asphalt type and aggregate type to be not significant. Thus, in this case, ranking the results by aggregate is appropriate. The performance ranking of aggregates (based on least squares means) for the OSU wheel-tracking program is listed in Table 7.20. The analysis shows that aggregate RJ performs the best and aggregate RC the worst. The performance ranking of aggregates based on SWK/UN wheel-tracking test results is listed in Table 7.21. The ranking indicates that aggregates RC and RD are good performers and aggregate RJ performs poorly.

Table 7.20. Performance ranking of aggregates (OSU wheel-tracking program)

Aggregate	Least-squares means	Homogenous Groups*	Performance Ranking
RJ	4.456875	A	Good
RD	5.384375	B	Intermediate
RH	5.653125	B	
RC	8.475375	C	Poor

*Groups with the same letter designation are not significantly different.

Table 7.21. Performance ranking of aggregates (SWK/UN wheel-tracking program)

Aggregate	Least-squares means	Homogenous Groups*	Performance Ranking
RC	15.23	A	Good
RD	15.09	A	
RH	12.62	B	Intermediate
RJ	2.06	C	Poor

*Groups with the same letter designation are not significantly different.

Asphalts

The analysis of results for the ECS test program shows the interaction of asphalt type and aggregate type to be significant. Although ranking the results by asphalt type is inappropriate, the data are shown in Table 7.22. The analysis of results for the OSU wheel-tracking program shows that the effect of the asphalt-aggregate interaction is not significant. Thus, a ranking by asphalt type can be accomplished. The performance ranking of asphalts (based on least-squares means) for the OSU wheel-tracking program is listed in Table 7.23; the performance ranking of asphalts based on the SWK/UN wheel-tracking test results is listed in Table 7.24.

Table 7.22. Performance ranking of asphalt based on ECS test

Asphalt	Modulus Ratio LSMEAN	Performance Ranking	Asphalt	Modulus Ratio LSMEAN	Performance Ranking
	First hot cycle			Second hot cycle	
AAB-1	0.968	1	AAC-1	0.924	1
AAA-1	0.956	2	AAA-1	0.922	2
AAC-1	0.934	4	AAB-1	0.895	3
AAF-1	0.926	5	AAG-1	0.874	4
AAG-1	0.923	5	AAM-1	0.867	5
AAD-1	0.910	6	AAF-1	0.865	6
AAM-1	0.910	7	AAK-1	0.865	7
AAK-1	0.880	8	AAD-1	0.861	8
	Third hot cycle			Freeze cycle	
AAA-1	0.921	1	AAA-1	0.901	1
AAB-1	0.894	2	AAC-1	0.868	2
AAC-1	0.894	3	AAB-1	0.851	3
AAM-1	0.855	4	AAK-1	0.846	4
AAK-1	0.840	5	AAM-1	0.831	5
AAD-1	0.834	6	AAG-1	0.825	6
AAF-1	0.834	7	AAD-1	0.816	7
AAG-1	0.828	8	AAF-1	0.809	8

Table 7.23. Performance ranking of asphalts (OSU wheel-tracking program)

Asphalt	Least-squares means	Homogenous Groups*	Performance ranking
AAK-1	4.28125	A	Good
AAM-1	4.77750	AB	Good
AAD-1	5.60875	BC	Intermediate
AAF-1	5.76625	BC	Intermediate
AAB-1	5.79375	BC	Intermediate
AAG-1	6.40500	C	Poor
AAA-1	7.38625	C	Poor
AAC-1	7.87750	C	Poor

*Groups with the same letter designation are not significantly different.

Table 7.24. Performance ranking of asphalts (SWK/UN wheel-tracking program)

Asphalt	Expected Score	Homogenous Group*	Performance Ranking
AAM-1	17.94	A	Very good
AAK-1	17.21	A	
AAD-1	14.92	B	Good
AAB-1	13.82	B	
AAF-1	11.57	C	Fair
AAA-1	11.55	C	
AAG-1	7.08	D	Poor
AAC-1	6.23	D	

*Groups with the same letter designation are not significantly different.

Mix

The statistical analysis of the ECS results shows that asphalt-aggregate interaction is significant at a 95 percent confidence level. This conclusion would reject any rankings by asphalt type only or aggregate type only. To say that aggregate RD performs much better than RJ in moisture susceptibility, a single common asphalt would need to be matched with each aggregate. The statistical analysis of OSU wheel-tracking results has shown that there are no asphalt-aggregate interactions, so it would be inappropriate to include rankings based on mixes here. Table 7.25 shows ECS ranking based on ECS-M_R ratio after each cycle; the mixes are ranked from 1 to 32.

Table 7.25. Ranking of 32 mixes after each ECS cycle

Aggregate	Asphalt	ECS M_R LSMEAN	Performance Ranking	Aggregate	Asphalt	ECS M_R LSMEAN	Performance Ranking
First hot cycle				Second hot cycle			
RH	AAC-1	1.090	1	RH	AAC-1	1.170	1
RJ	AAF-1	0.993	2	RJ	AAF-1	0.957	2
RH	AAB-1	0.985	3	RD	AAA-1	0.953	3
RD	AAA-1	0.980	4	RH	AAD-1	0.950	4
RD	AAD-1	0.975	5	RC	AAA-1	0.945	5
RC	AAG-1	0.975	6	RD	AAC-1	0.940	6
RC	AAB-1	0.970	7	RC	AAG-1	0.935	7
RC	AAA-1	0.970	8	RD	AAK-1	0.935	8
RD	AAC-1	0.965	9	RC	AAM-1	0.920	9
RJ	AAB-1	0.965	10	RD	AAM-1	0.915	10
RC	AAF-1	0.965	11	RC	AAB-1	0.905	11
RC	AAM-1	0.960	12	RH	AAB-1	0.905	12
RD	AAM-1	0.960	13	RD	AAB-1	0.903	13
RH	AAD-1	0.955	14	RH	AAA-1	0.900	14
RD	AAK-1	0.950	15	RD	AAG-1	0.897	15
RD	AAB-1	0.950	16	RJ	AAA-1	0.890	16
RH	AAA-1	0.940	17	RH	AAG-1	0.890	17
RJ	AAA-1	0.935	18	RD	AAD-1	0.885	18
RD	AAG-1	0.930	19	RC	AAK-1	0.885	19
RJ	AAM-1	0.915	20	RJ	AAM-1	0.875	20
RD	AAF-1	0.907	21	RC	AAF-1	0.870	21
RJ	AAG-1	0.905	22	RJ	AAB-1	0.865	22
RC	AAK-1	0.895	23	RD	AAF-1	0.857	23
RJ	AAG-1	0.880	24	RC	AAC-1	0.840	24
RC	AAC-1	0.865	25	RH	AAK-1	0.830	25
RJ	AAD-1	0.860	26	RC	AAD-1	0.810	26
RC	AAD-1	0.850	27	RJ	AAK-1	0.810	27
RH	AAK-1	0.845	28	RJ	AAD-1	0.800	28
RH	AAF-1	0.840	29	RH	AAF-1	0.775	29
RJ	AAK-1	0.830	30	RJ	AAG-1	0.775	30
RJ	AAC-1	0.815	31	RH	AAM-1	0.757	31
RH	AAM-1	0.807	32	RJ	AAC-1	0.745	32

Table 7.25 (continued). Ranking of 32 mixes after each ECS cycle

Aggregate	Asphalt	ECS M_R LSMEAN	Performance Ranking	Aggregate	Asphalt	ECS M_R LSMEAN	Performance Ranking
Third hot cycle				Freeze cycle			
RH	AAC-1	1.125	1	RH	AAC-1	1.125	1
RH	AAA-1	0.950	2	RD	AAK-1	0.955	2
RD	AAA-1	0.943	3	RH	AAA-1	0.940	3
RD	AAK-1	0.930	4	RD	AAA-1	0.933	4
RH	AAB-1	0.925	5	RD	AAG-1	0.927	5
RC	AAM-1	0.920	6	RH	AAB-1	0.910	6
RH	AAD-1	0.915	7	RH	AAD-1	0.910	7
RD	AAB-1	0.907	8	RD	AAM-1	0.890	8
RC	AAA-1	0.905	9	RD	AAC-1	0.885	9
RD	AAC-1	0.905	10	RC	AAM-1	0.885	10
RJ	AAF-1	0.903	11	RH	AAG-1	0.880	11
RC	AAB-1	0.895	12	RJ	AAA-1	0.870	12
RD	AAM-1	0.895	13	RC	AAA-1	0.860	13
RC	AAG-1	0.885	14	RD	AAB-1	0.860	14
RJ	AAA-1	0.885	15	RD	AAD-1	0.845	15
RH	AAG-1	0.885	16	RC	AAK-1	0.840	16
RD	AAG-1	0.873	17	RJ	AAF-1	0.840	17
RC	AAK-1	0.870	18	RD	AAF-1	0.830	18
RJ	AAB-1	0.850	19	RJ	AAB-1	0.820	19
RD	AAD-1	0.845	20	RC	AAB-1	0.815	20
RD	AAF-1	0.837	21	RC	AAG-1	0.810	21
RC	AAC-1	0.830	22	RJ	AAK-1	0.805	22
RJ	AAM-1	0.825	23	RH	AAF-1	0.795	23
RH	AAF-1	0.800	24	RH	AAK-1	0.785	24
RH	AAK-1	0.795	25	RJ	AAM-1	0.785	25
RC	AAF-1	0.795	26	RC	AAF-1	0.770	26
RJ	AAD-1	0.795	27	RH	AAM-1	0.763	27
RH	AAM-1	0.780	28	RC	AAD-1	0.760	28
RC	AAD-1	0.780	29	RJ	AAD-1	0.750	29
RJ	AAK-1	0.765	30	RC	AAC-1	0.750	30
RJ	AAC-1	0.715	31	RJ	AAC-1	0.710	31
RJ	AAG-1	0.670	32	RJ	AAG-1	0.685	32

Table 7.25 shows no breakdown between the poor (moisture-susceptible) and good aggregates, nor between the poor and good asphalts. However, it shows the breakdown between moisture-susceptible mixes and moisture-damage-resistant mixes. After each cycle, mixes that were moisture susceptible progressively lost strength, but mixes that were least susceptible to moisture damage maintained about the same strength. Table 7.25 shows that mixes that performed well after one cycle did not maintain the same ranking with respect to other mixes (see Figure 7.12). Finally, one should note that the range of data presented in Table 7.25 is very small; that is, ECS-M_R ratios of all 32 mixes vary between 1.12 and 0.685 and probably do not represent the wider range expected from field mixes; *this is somewhat limiting in terms of validation.*

Comparison with A-002A and A-003B Results

This section compares the results obtained in the A-003A study with the A-002A and A-003B results pertaining to moisture sensitivity and permanent deformation. The rankings of aggregates from A-002A, A-003A, and A-003B contractors are summarized in Table 7.26. It is evident that good agreement exists between the SWK/UN wheel-tracking results and the A-003B net adsorption results. However, the OSU wheel-tracking results do not match those of the other two tests.

Table 7.26. Summary of aggregate rankings

	Water Sensitivity	Rutting	
Performance Ranking	**A-003B (Net Adsorption)**	**A-003A (OSU Wheel Tracking)**	**A-003A (SWK/UN Wheel Tracking)**
Good	RD	RJ	RC, RD
Intermediate	RC, RH	RD, RH	RH
Poor	RJ	RC	RJ

The rankings of asphalts from the A-002A, A-003A, and A-003B contractors are shown in Table 7.27. Good agreement exists among the SWK/UN wheel-tracking results, the OSU wheel-tracking results, and the A-002A predictions for permanent deformation. Thus, it appears that the wheel-tracking test results (OSU and SWK/UN) validate the predictions made by the SEC tan δ tests proposed by A-002A.

However, there is little agreement among the wheel-tracking test results and the predictions for the water sensitivity of the binder made by the A-002A and A-003B contractors. And since both wheel-tracking tests indicate similar rankings that closely match the predicted ranking for permanent deformation, it appears that either the wheel-tracking tests are poor indicators of water sensitivity of the binder or that the net adsorption test (A-003B) and the Fourier-transformation infrared spectroscopy (FTIR) test (A-002A) are not appropriate for

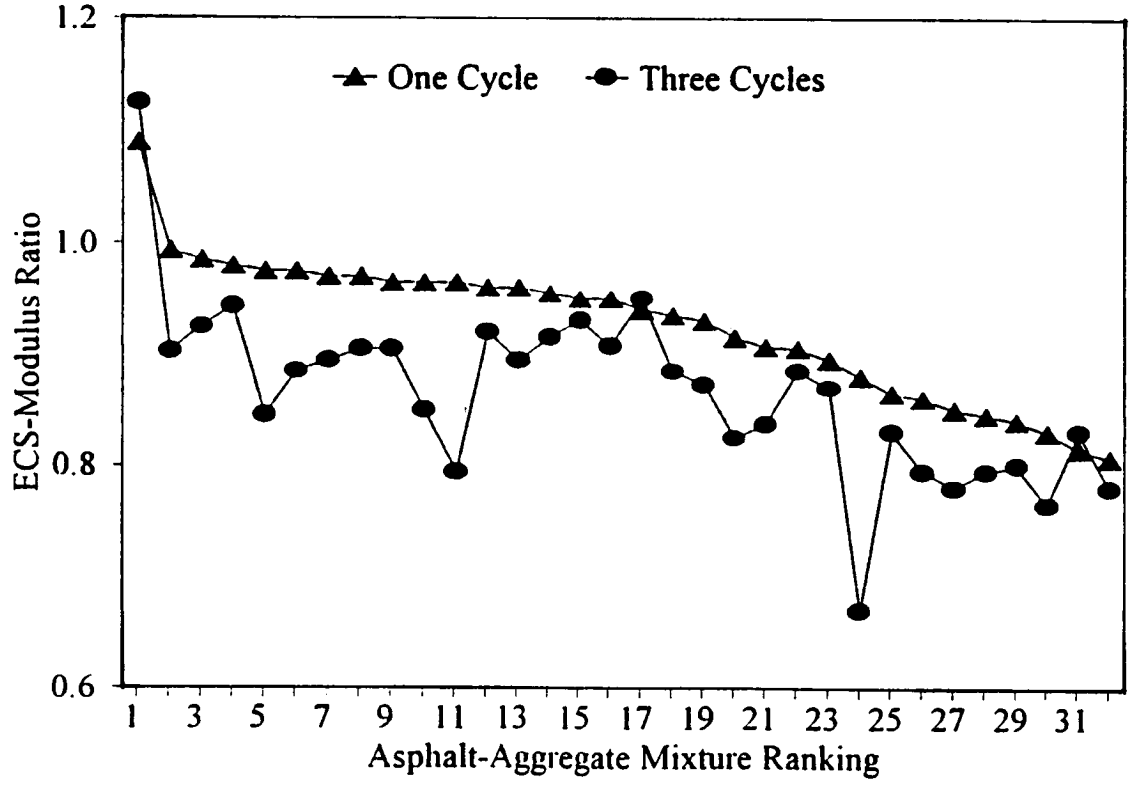

Figure 7.12. Ranking of 32 mixes after one and three cycles

Table 7.27. Summary of asphalt rankings

	Water Sensitivity		Permanent Deformation		
Performance Ranking	**A-002A**	**A-003B**	**A-002A**	**A-003A (OSU)**	**A-003A (SWK/UN)**
Good	AAF-1	AAD-1	AAM-1	AAK-1	AAM-1
	AAB-1		AAK-1	AAM-1	AAK-1
	AAM-1				
	AAA-1		AAD-1	AAD-1	AAD-1
			AAB-1	AAF-1	AAB-1
	AAD-1	AAK-1		AAB-1	
	AAK-1				AAF-1
			AAA-1	AAG-1	AAA-1
	AAG-1	AAM-1	AAF-1	AAA-1	
			AAC-1	AAC-1	AAG-1
Poor			AAG-1		AAC-1

predicting the water sensitivity of the binder. It is appropriate to point out that the original performance predictions for water sensitivity proposed by the A-002A contractors were very tentative and were later withdrawn (i.e., there is no hypothesis for water-sensitivity prediction by A-002A).

The ECS data were not used in the above comparison because the ECS measures change in resilience, rather than permanent deformation as measured in the wheel-tracking tests.

Discussion of Specifications

One of the goals of the ECS test development was to establish specifications. The appropriate limits for specifications should be based on field performance. The validation testing covered in this report includes only MRL materials with no direct link to field projects. Therefore, the consideration of specifications will be deferred until after completion of the testing of materials from field projects (i.e., actual pavements already constructed) (Allen and Terrel 1992).

Conclusions and Recommendations

Conclusions

The testing results and analysis presented appear to warrant the following conclusions:

1. Performance ranking of mixes by asphalt type or aggregate type alone cannot be made for the ECS test results because of the significant interaction between

asphalt and aggregate. Water sensitivity in the ECS is significant for pairs of asphalts and aggregates.

2. The OSU wheel-tracking test results indicate that aggregate RJ is a good performer, aggregate RC is a poor performer, and aggregates RD and RH are intermediate performers in terms of rut resistance. The SWK/UN wheel-tracking test results indicate that aggregates RC and RD are good performers (with practically no difference between the two), aggregate RH is an intermediate performer, and aggregate RJ is a poor performer. The significant differences between the results of the two test methods may be attributed to the differences in testing methods, test apparatus, specimen size, specimen environment during testing, and other factors. However, the results of the SWK/UN wheel-tracking test appear generally to validate the predictions proposed by the net adsorption test (A-003B), while those of the OSU wheel-tracking test do not. Thus, it would appear that the OSU wheel-tracking test may not be appropriate for evaluating aggregate type as it pertains to water sensitivity.

3. The SEC tests proposed by the A-002A contractor appear to adequately predict the performance of asphalt type in terms of rutting potential, as evidenced by close agreement with the asphalt rankings from the OSU wheel-tracking and SWK/UN wheel-tracking tests. There is almost perfect agreement between A-002A predictions and the SWK/UN results.

4. Predictions of the water sensitivity of the binder as proposed by the A-002A FTIR test and the A-003B net adsorption test show little or no correlation with wheel-tracking tests on the mix. There is very good to excellent correlation among the wheel-tracking tests and the A-002A predictions for permanent deformation, but it would appear that the FTIR test and the net adsorption test are poor indicators of the moisture sensitivity of the binder.

Recommendations

From the results of this research, it is evident that some of the test procedures used were not appropriate for evaluating water sensitivity of mixes. Therefore, several recommendations can be made for improved comparisons in future research:

1. The ECS should be used to evaluate specific pairs (asphalt-aggregate combinations) only.

2. If water sensitivity is important in the OSU wheel-tracking tests, both dry and water-conditioned specimens should be tested. This approach will provide a ratio of wet to dry rutting (and possibly other failures) similar to that for ECS.

3. An improved method of water conditioning needs to be developed for the large beam specimens used in the OSU wheel tracker. The method used in this project was slow and cumbersome, and the thoroughness of wetting or conditioning was uncertain.

8

Conclusions and Recommendations

The information in this report has attempted to summarize the results of the A-003A contractor's efforts to validate the findings and recommendations of the A-002A contractor regarding the influence of asphalt on the five properties incorporated in the asphalt research program of Strategic Highway Research Program (SHRP).

Additional validation efforts are under way or planned for a Stage II type activity. Texas A&M, as part of its SHRP Project A-005 contract, is attempting to validate results using information from selected general pavement studies sites with results expected as part of its final report. Post-SHRP validation is also planned using SPS-9 pavement sections as part of the ongoing long-term pavement performance program managed by the Federal Highway Administration.

Statistical analyses have been used to help evaluate the relative influence of the material properties on designated response variables. Analysis of variance (ANOVA), generalized linear models, and several methods of grouping and ranking have been used, depending on the experiment designs and the character of the data, all on advice of project statisticians. A Type I null hypothesis with an α (rejection region) of 0.05 has been used in each analysis unless otherwise indicated. Although a significance level of 0.05 was used to test the hypothesis, in many cases the actual level was less than 0.01 for the main effects of asphalt source, aggregate type, and air-void content, indicating a highly significant level of rejection for the null hypothesis, or that there is a very high probability that the main effects are, in fact, influencing the response variable.

Overall, the findings to date are encouraging for fatigue and thermal cracking but less encouraging for permanent deformation. No specific properties have been associated with aging and water sensitivity in the SHRP asphalt binder specifications. The specifications do stipulate that the tests for rheological properties will be made with tank, short-term aging, or long-term aging, depending on the performance requirements. The results of the A-003A research indicate that asphalt properties, as well as aggregate properties, will influence the effect of both aging and water sensitivity, underscoring that these effects should be evaluated in the asphalt-aggregate mix to be confident of their effects on pavement performance.

The recommendations stemming from this validation effort relate primarily to post-SHRP activities.

Conclusions

Fatigue

Validation of the A-002A recommendations for fatigue is based on the use of the flexural fatigue test method performed in the controlled-strain mode of loading. The asphalt binder property recommended for inclusion in the SHRP asphalt binder specifications is a maximum value for the loss modulus ($G^* \sin \delta$) of the long-term aged asphalt when tested at a specific temperature and time of loading, the temperature being dependent on the geographic region in which the binder will be used.

As part of the A-003A investigation, an effort was also made to evaluate other rheological properties reported by the A-002A contractor, such as complex shear modulus (G^*), shear storage modulus ($G^* \cos \delta$), and loss tangent (loss modulus divided by the storage modulus).

The analysis of variance, used to determine the significance of main effects and interactions at a 0.05 level, indicated that asphalt type, aggregate type, and air-void content influence fatigue properties. In addition, the interactions of aggregate and asphalt types, asphalt type and air-void content, and aggregate type and air-void content were also significant at the same level. In order not to confuse the analysis and evaluations of the role of the asphalt, separate analyses were made for each combination of aggregate type and air-void content, with asphalt type being the main influencing variable.

Conclusions from this study to define the influence of asphalt properties on fatigue are summarized as follows:

1. According to the ANOVA, asphalt type, aggregate type, and air-void content significantly affect the fatigue properties of asphalt-aggregate mixes. In addition, the interactions between asphalt source, aggregate type, and air-void content were shown to be significant.

2. The relationships for the rheological properties of the asphalt binder versus flexural stiffness and versus fatigue life—based on maximum tensile strain—were very strong. There was also a good relationship between fatigue life, based on dissipated energy, and asphalt properties. However, this relationship was not as strong as that based on tensile strain, suggesting that fatigue response based on tensile strain would be the preferred method to evaluate the influence of asphalt properties. Both fatigue relationships were affected by some combinations of aggregate type and air-void content and in particular by one combination of aggregate type and air-void content. This suggests that caution must be exercised in any attempt to predict fatigue

properties from correlations with asphalt properties alone. Nevertheless, it would appear that reasonably good estimates of fatigue properties can be made from the rheological properties of the asphalt for mix containing conventional dense-grained aggregates.

3. The asphalt properties of G* sin δ, G*, and G* cos δ all result in equivalent influence with regard to mix fatigue response.

4. Overall, asphalt binder properties play an important role in the fatigue response of the asphalt-aggregate mixes. However, other mix characteristics can also have a significant impact. In important design situations, mix fatigue testing should be performed to increase the reliability of the estimates of pavement fatigue cracking.

Permanent Deformation

The A-002A binder properties were validated by means of permanent deformation tests on specimens of asphalt-aggregate mixes in a wheel-tracking testing device at the University of Nottingham and by repeated-load simple shear tests at The University of California at Berkeley using the Universal Test Machine (UTM).

The asphalt binder property recommended for inclusion in the SHRP asphalt binder specifications is a minimum value of G*/sin δ obtained from testing the rolling thin-film oven test residue at a maximum temperature associated with the geographic region where the binder will be used. In addition to comparisons with G*/sin δ, the A-003A contractor also made an effort to evaluate other rheological properties reported by the A-002A contractor, such as complex shear modulus (G*), shear storage modulus (G* cos δ), and shear loss modulus (G* sin δ).

Wheel-Tracking Tests

The results of the ANOVA for the wheel-tracking tests indicated that asphalt type, aggregate type, and air-void content significantly affect the rutting response of asphalt-aggregate mixes. Aggregate type was the major factor influencing permanent deformation response. Interactions of asphalt type with aggregate type, asphalt type with air-void content, and aggregate type with air-void content were also indicated to be significant at the 0.05 level or lower. Because of the interaction between asphalt and aggregate types, the evaluation of mix response to rutting was evaluated separately for each combination of aggregate type and air-void content.

Correlations between the rheological properties of the asphalt binder and rutting response were relatively poor as determined from the coefficients of determination, R^2; however, trends with asphalt binder properties were indicated by the regression lines for the various combinations of asphalt type, aggregate type, and air-void content.

The overall conclusions based on the data obtained from the wheel-tracking tests are summarized as follows:

1. The parameter G*/sin δ is not a reliable predictor of rutting potential, nor were any of the other rheological properties included in this investigation.

2. Aggregate type and air-void content appear to have a greater influence on the rutting response in the wheel-tracking test than do asphalt binder properties.

3. In spite of the problems associated with correlations, it was possible to rank the asphalts according to their relative performance in the wheel-tracking device.

4. The University of Nottingham wheel-tracking device has limitations that could make evaluations difficult; for example, (1) the wheel-tracking tests were performed at 40°C, which may not be high enough to accelerate rutting under the loading device; (2) the magnitude of the rutting, especially for the better-performing specimens, was small, making it difficult to reliably separate the response to loads; and (3) while the wheel-tracking test equipment is considered useful, it is relatively small. The surface area of each specimen used for the wheel-tracking tests was 32,000 mm^2, which could exaggerate the boundary effects.

Laboratory Shear Testing

Conclusions from the repeated-load simple shear tests under controlled conditions in the laboratory are summarized as follows:

1. Results of the ANOVA indicated that asphalt source, aggregate type, and air-void content significantly affected test results. Based on the contribution to the sum of squares from the ANOVA, the most significant effect was that of the aggregate, followed by air-void content, and then asphalt characteristics. The relatively small influence of the asphalt could help explain why it was difficult in the wheel-tracking test to associate asphalt properties with performance.

2. Although the relationship is rather weak, partly because the scatter in the data, there is some indication that asphalt binder properties G*/sin δ, G*, and G* sin δ do influence the cumulative shear response observed in this testing program.

3. While not a part of the A-002A validation effort, the results of the laboratory permanent deformation tests do indicate that the relationship between asphalt properties and permanent deformation is not strong enough to use such relationships to predict rutting. Accordingly, testing and analysis are critical for permanent deformation evaluation for a particular mix and environment.

Thermal Cracking

Validation of the A-002A asphalt binder properties for thermal cracking was based on the use of the thermal stress restrained-specimen test (TSRST).

The properties of the long-term aged asphalt binder recommended for inclusion in the SHRP specifications include creep stiffness, m value, and failure strain. A maximum value is stipulated for creep stiffness as a function of the test temperature associated with the 14 grades of asphalt binder included in the specifications, A minimum m value, which is the slope of log stiffness versus the log time curve at 60 sec loading time, is specified as a function the grade of binder properties.

In addition to these properties, correlations between the TSRST results were made with specific properties of the asphalt such as penetration at 15°C after short-term and long-term aging and with the Fraass brittle point (temperature).

Based on the use of the TSRST, the following conclusions can be formulated:

1. Thermal cracking properties of asphalt-aggregate mixes are significantly influenced by the asphalt type, aggregate type, degree of aging and air-void content in the mix. The interaction between asphalt type and degree of aging is also significant.

2. Fracture temperature is primarily affected by asphalt type and degree of aging.

3. Fracture temperature increases with aging of the asphalt in the mix.

4. A ranking of mix fracture temperature compares well with A-002A ranking of the asphalts based on the fundamental properties of the asphalt as described above (i.e., creep stiffness, m value, and failure strain).

5. The results of the TSRST correlate well with penetration values for tank, short-term aged, and long-term aged asphalts.

6. The results of the TSRST correlate reasonably well with the Fraass brittle point (temperature) for both short-term and long-term aged asphalts.

7. The TSRST method of evaluating low-temperature properties of asphalt-aggregate mixes provides a direct measure of thermal cracking tendencies and could be used as the basis for mix design and for specifications.

Aging

The aging investigation was required to address both short-term aging and long-term aging. For purposes of this investigation, short-term aging is defined as aging during construction

(mixing and placing) and for approximately 1 year of the service life. Long-term aging is defined as being representative of conditions after 3 to 5 years of service life. For most practical purposes, the effects of aging will generally approach an asymptotic condition after about 5 years.

The method selected for short-term aging consists of curing asphalt-aggregate mixes in a forced- draft oven at 135°C for 4 hr, after which the material is compacted into an appropriately sized specimen for the determination of its dynamic and resilient modulus. These results are then compared with similar test values with no aging.

Two methods have been used to simulate long-term aging of the compacted specimens. One involves a continuation of the use of the forced-draft oven and requires an additional curing period of 5 days at 85°C before modulus testing. An alternative procedure uses a low-pressure oxidation apparatus to accomplish the aging. The findings from both methods are the same.

Based on the tests developed by the A-003A investigators for short-term and long-term aging, the following conclusions can be formulated:

1. The aging of asphalt-aggregate mixes is influenced by the properties of the asphalt and the aggregate and the interaction of the two.

2. Aging of the asphalt alone does not appear to be an adequate measure of the aging of the mix.

3. The short-term aging procedure produces a change in the resilient modulus by up to a factor of 2.

4. The asphalts included in the aging study can be grouped into three categories based on mix aging tendencies, which does reflect some grouping of aging properties as a function of asphalt source.

5. Long-term aging cannot be predicted from short-term aging.

6. Methods for simulating both short-term and long-term aging of mixes have been developed and are feasible for use in mix design procedures to facilitate both short-term and long-term performance predictions.

Water Sensitivity

For this task, the A-003A contractor was to develop a test method to evaluate the water sensitivity of asphalt-aggregate mixes and to determine how aggregates of different types and asphalts from different sources would influence water sensitivity. A test system was developed to evaluate the major factors influencing water sensitivity. The Environmental Conditioning System (ECS) was developed to condition specimens to reflect the effects of

water, humidity, temperature cycling (hot and cold), and dynamic loading to simulate traffic. Response variables used to measure water sensitivity include permeability, modulus and modulus ratios, and stripping (by visual observation of conditioned specimens after modulus testing).

The validity of the ECS system and further validation of the influence of asphalt on water sensitivity was evaluated by two wheel-tracking devices. One such device, at Oregon State University (OSU), was a special modification of the LCPC wheel-tracking device. A second device was available for use at the University of Nottingham by the SWK subcontractor. The response variable for each of the wheel-tracking devices was a measurement of permanent deformation due to repeated applications of a wheel load.

The A-200A contractor specific recommendations provided regarding the relationship between the physical properties of asphalt and water sensitivity. A proposed ranking of asphalts, based on the state of knowledge, tended to indicate that water sensitivity was more related to the aggregate than to the asphalt. For this reason four aggregates were included in this testing program rather than the two used in the other programs.

The conclusions from the ECS and wheel-tracking testing programs are summarized as follows:

1. The ECS procedure provides a new method for evaluating water sensitivity of asphalt-aggregate mixes that is significantly influenced by the properties of the aggregate and the interaction of the aggregate and asphalt and is only slightly less sensitive to the properties of the asphalt.

2. The ECS method is capable of comparing or ranking mixes with regard to their water sensitivity based on measurements of fundamental properties such as stiffness modulus.

3. Results of tests made with two different wheel-tracking devices do not always provide comparable results with regard to the rutting response variable and the source of asphalt or aggregate. The significant difference between the two devices is probably due to test methods, configuration, and procedures used to condition the specimens. Since the procedures are essentially empirical, it is not surprising that different results are obtained. The results of the SWK/UN wheel-tracking device generally agree with the net adsorption test developed by A-003B, while those of the OSU device do not. Thus, based on this comparison, the OSU modification to the LCPC device may not be appropriate for evaluating asphalt-aggregate compatibility in the presence of water.

4. The SEC tan δ a test proposed by A-002A appears to adequately predict the performance of asphalt type in terms of rutting potential as evidenced by close agreement with the asphalt rankings from the OSU wheel-tracking and SWK/UN wheel-tracking tests. There is almost perfect agreement between A-002A predictions and the SWK/UN results. The SEC procedure is not used as a specification requirement; however, the correlations do suggest that a

useful chemical property can be identified and could be used to evaluate asphalts for rutting.

5. The ECS has been shown to be sufficiently sensitive to water damage to detect the effects of water in terms of saturation level, conditioning temperature, and air-void content.

Recommendations

The recommendations for each of the validation efforts are the same: to continue to investigate the validity of the relationships between proposed asphalt properties and performance of asphalt-aggregate mixes. Based on the analyses presented in this report, the validation effort should not be restricted to a single asphalt binder property, since several showed promise depending on the attribute under consideration.

Eventually, field validation will be required, especially true for aging, water sensitivity, and thermal cracking, since laboratory simulations are difficult. It must be recognized that field validation using in-service pavement sections requires good planning and extensive data on traffic, temperature, aging (for thermal cracking), and the occurrence of damage (change in properties) and distress (cracking or rutting) in or on the pavement. In all probability, many sections will be required to minimize the effects of random errors. For fatigue and permanent deformation, and to a lesser degree thermal cracking, the analysis will be more difficult because of the interactions with the pavement structure.

For fatigue and permanent deformation, improved laboratory scale models can be developed that will allow validations to be made quickly and for less cost than field tests. Also, the role of the asphalt mix will not be confounded by the character of the supporting layers, variations in traffic loads, and changes in temperature, rainfall, and other conditions.

Fatigue cracking in asphalt pavements is likely to be affected by the pavement structure—that is, the level of strain or amount of dissipated energy in the asphalt concrete caused by wheel loads. The A-003A contractor has attempted to simulate the structural affects by analyzing two pavement structures with interpretations as to the occurrence of damage to the asphalt-concrete and the relationship between damage and $G^* \sin \delta$. This analysis suggests that the structural effects are significant and, in fact, the relationships may be reversed when considering in situ performance. Specifically, the analysis indicates that the performance improves with increasing values of $G^* \sin \delta$ and that the specification should stipulate a minimum, not a maximum, value for this property. Further evaluation of this characteristic should be made before finalizing the specification for the asphalt binder.

9

References

Ab-Wahab, Y., C. A. Bell, and D. Sosnovske (1993). Evaluation of asphalt-aggregate mixture aging by dynamic mechanical analysis. In Conference on SHRP Asphalt Research, Transportation Research Record No. 1386, pp. 22-30.

Allen, W., and R. L. Terrel (1992). Field validation of the environmental conditioning system (ECS). Technical memorandum TM-OSU-A-003A-92-12. Final report to the Strategic Highway Research Program, Washington, DC.

Bell, C. A., Y. Ab-Wahab, M. E. Cristi, and D. Sosnovske (1992). Selection of laboratory aging procedures for asphalt-aggregate mixes. Technical memorandum TM-OSU-A-003A-02-27. Final report to the Strategic Highway Research Program, Washington, DC.

California Department of Transportation (1984). Methods for recommending optimum bitumen content. Test Method 367. Sacramento, California.

Christensen, D., and D. Anderson (1992). Interpretation of dynamic mechanical analysis test data for paving grade asphalt cements. Journal of the Association of Asphalt Paving Technologists 61:67-116.

Coplantz, J., and A. A. Tayebali (1992). Statistical analysis of flexural fatigue validation testing. Technical memorandum TM-ARE-A-003A-92-2. Prepared for SHRP Project A-003A, Asphalt Research Program, Institute of Transportation Studies, University of California, Berkeley.

Curtis, C. W., K. E. Ensley, and J. Epps (1991). SHRP A-003B fundamental properties of asphalt-aggregate interactions including adhesion and absorption. Final report for SHRP Project A-003B.

Federal Highway Administration (1985). ELSYM5 computer program. Washington, DC.

Gibb, J. M., P. S. Pell, and S. F. Brown (1991). An evaluation of the wheel-tracking test as a means of assessing resistance to permanent deformation. Prepared for SHRP Project A-003A, Asphalt Research Program, Institute for Transportation Studies, University of California at Berkeley.

Harvey, J. (1991). Asphalt concrete specimen preparation protocol—SHRP asphalt project A-003A. Technical memorandum TM-UCB-A-003A-91-2. Prepared at Institute for Transportation Studies, University of California, Berkeley.

Jung, D.-H., and T. S. Vinson (1992). Validation of A-002A findings for low temperature cracking. Technical memorandum TM-OSU-A-003A-02-13. Final summary report for Strategic Highway Research Program, Washington, DC.

Paulsen, G., and J. Sousa (1992). Statistical analysis of permanent deformation validation testing. Technical memorandum TM-ARE-A-003A-92-3. Prepared for SHRP Project A-003A, Asphalt Research Program, Institute of Transportation Studies, University of California, Berkeley.

Petersen, J. C., R. E. Robertson, J. F. Branthaver, and D. A. Anderson (1992). SHRP A-002A binder characterization and evaluation—Draft final report. Volumes 1, 2, 3, and 4. Draft final report prepared for SHRP Project A-002A.

Robertson, R. E., J. F. Branthaver, D. A. Anderson, and J. C. Peterson (1991). Binder characterization and evaluation. Quarterly report prepared for SHRP Project A-002A, June.

Robertson, R. (1991). Quarterly report for SHRP contract A-002A. SHRP, Project A-002A, December.

SAS Institute Inc. (1991a). SAS/STAT user's guide. Release 6.03. Cary, NC.

SAS Institute Inc. (1991b). SAS language guide for personal computers. Release 6.03. Cary, NC.

Scholz, T. V., R. L. Terrel, A. Al-Joaib, and J. Bea (1992). Validation of the SHRP A-002A hypothesis for water sensitivity. Technical memorandum TM-OSU-A-003A-92-20. Final report for Strategic Highway Research Program, Washington, DC.

Strategic Highway Research Program (1991). The SHRP materials reference library asphalt cement: A concise data compilation. Publication No. SHRP-A-645, Strategic Highway Research Program, National Research Council, Washington, DC.

Sousa, J. B., et al. (1993). Permanent deformation response of apshalt-aggregate mixes. Technical memorandum TM-UCB-A-003A-93-4. Prepared at Institute of Transportation Studies, University of California at Berkeley.

Tayebali, A. A., et al. (1993). Fatigue response of asphalt-aggregate mixes. Technical memorandum TM-UCB-A-003A-93-3. Prepared at Institute of Transportation Studies, University of California at Berkeley.

University of California at Berkeley, Oregon State University, and Austin Research Engineers, Inc. (1993). Accelerated performance tests for asphalt-aggregate mixes and their mix design/analysis system. Technical memorandum TM-UCB-A-003A-93-7. Prepared at Institute of Transportation Studies, University of California at Berkeley.

Waller, R. A., and K. E. Kemp (1976). Computations of Bayesian t-values for multiple comparisons. Journal of Statistical Computation and Simulation 75:169-72.